Thermogelling Materials for Topical Drug Delivery

Peter James Haddow

Submitted to the University of Hertfordshire in Partial Fulfilment of the requirements to the degree of Doctor of Philosophy

November 2020

Acknowledgements

List of Figures

List of Tables

Abbreviations

LCST	Lower critical solution temperature
UCST	Upper critical solution temperature
PNIPAM	Poly(N-isopropyl acrylamide)
PDEA	Poly(N,N-diethyl acrylamide)
PDEGMEMA	Poly(diethylene glycol methyl ether methacrylate)
PDMAEMA	Poly(2-(N-dimethylamino)ethyl methacrylate)
PEG	Poly(ethylene glycol)
PPG	Poly(propylene glycol)
CP	Cloud Point
MOE	Molecular Operating Environment
BiBB	α-Bromoisobutyryl bromide
DMAP	4-dimethylaminopyridine
Me6TREN	Tris[2-(dimethylamino)ethyl]amine
Bpy	Bipyridine
PMDETA	N,N,N',N'',N''-Pentamethyldiethylenetriamine
MeOH	Methanol
EtOH	Ethanol
iPa	Isopropyl alcohol
THF	Tetrahydrofuran
DMF	N-dimethylformamide
DLS	Dynamic light scattering
SANS	Small angle neutron scattering
LDH	Lactate dehydrogenase
MTS	3-(4,5-dimethylthiazol-2-yl)-5-(3-carboxymethoxyphenyl)-2-(4-sulfophenyl)-2H-tetrazolium
OSS	Oscillatory stress sweep
OFS	Oscillatory frequency sweep

Research Outputs

Papers:

1. P. Haddow, W. J. McAuley, S. B. Kirton and M. T. Cook, Poly(N-isopropyl acrylamide)–poly(ethylene glycol)–poly(N-isopropyl acrylamide) as a thermoreversible gelator for topical administration, Materials Advances, 2020, 1, 371-386.
2. Polymers exhibiting lower critical solution temperatures as a route to thermoreversible gelators for healthcare accepted for publication in Advanced Functional Materials.
3. The influence of LCST exhibiting polymer type (A) on the thermogellation properties of ABA triblock copolymers with PEG (B) in preparation.

Oral conference presentations:

1. P. Haddow, W. J. McAuley, S. B. Kirton and M. T. Cook, ABA thermogelling triblock copolymers - London Polymer Group, University of Kent, 2019.
2. P. Haddow, W. J. McAuley, S. B. Kirton and M. T. Cook, ABA thermogelling triblock copolymers – School of life and medical sciences annual research conference, University of Hertfordshire, 2019.

Poster conference presentations:

1. P. Haddow, W. J. McAuley, S. B. Kirton and M. T. Cook, A novel QSPR for the prediction of polymeric LCSTs in aqueous solution, School of life and medical sciences annual research conference, University of Hertfordshire, 2017.
2. P. Haddow, W. J. McAuley, S. B. Kirton and M. T. Cook, The influence of LCST polymer type on the thermogellation of ABA triblock copolymers, School of life and medical sciences annual research conference, University of Hertfordshire, 2018.
3. P. Haddow, W. J. McAuley, S. B. Kirton and M. T. Cook, The influence of LCST polymer type on the thermogellation of ABA triblock copolymers, London Polymer Group, Kings College London, 2018.
4. P. Haddow, W. J. McAuley, S. B. Kirton and M. T. Cook, Thermoresponsive Gelators from ABA Triblock Copolymers, The 14th International Conference on Polymer Chemistry, Aston University, Birmingham, 2019.
5. P. Haddow, W. J. McAuley, S. B. Kirton and M. T. Cook, Thermoresponsive Gelators from ABA Triblock Copolymers, Chemical Nanoscience and Nanotech conference, University of East Anglia, 2019.

Contents

Abstract

This thesis describes the synthesis and characterisation of thermogelling materials and their evaluation as topical drug delivery excipients. Thermogelling materials are polymers which transition from solution to gel when heated above a critical temperature. For topical administration, these materials offer the benefit of easy application via an applicator and allow for enhanced retention and prolonged drug delivery in the gel state when warmed by the body. A review of the literature highlighted that poloxamer 407 is the most studied thermogelling polymer for drug delivery. However, these gels are typically weak as a result of their shear thinning behaviour and exhibit poor mucoadhesion as well as rapid dissolution. Alternate thermogelling materials within the literature are block copolymers containing a component which become insoluble in aqueous solution with an increase in temperature, also known as a lower critical solution temperature (LCST). For example, ABA copolymers of poly(N-isopropyl acrylamide) (PNIPAM) (A) (LCST = 32 °C) and PEG (B) exhibit thermogelling behaviour. Unfortunately, there are only a small number of polymers which exhibit LCSTs between 25 and 37 °C, required for topical drug delivery applications. Therefore, the first results chapter discusses the development of quantitative structure property relationships (QSPRs) with the aim of guiding the development of novel LCST exhibiting polymers. The best model derived in this work had a training set r^2 of 0.56, training q^2 of 0.35 and test r^2 of 0.17, indicating this model not able to adequately predict LCST to within the narrow temperature range required for topical drug delivery applications. Guided by the literature, PNIPAM, poly(N,N-diethyl acrylamide) poly(2-N-dimethylamino)ethyl methacrylate) and poly(diethylene glycol methyl ether methacrylate) were used to synthesise novel ABA triblock copolymers with LCST exhibiting arms (A) and a central poly(ethylene glycol) (B) block. These were synthesised to target molecular weights of 10-4-10, 20-4-20, 10-10-10 and 20-10-20 kDa. Following successful synthesis, the phase behaviour of these polymers was investigated in aqueous solution. All triblock copolymers were found to increase in viscosity with temperature at 20 % (w/v). The mechanism by which this gelation occurs was investigated by DLS and SANS, which highlighted these materials form polymer micelles which in concentrated solution interact, resulting in a gel. Some correlation was observed where smaller micelles formed more viscous gels, which is evaluated against existing theories governing the rheology of disperse systems. SANS indicated that the smaller aggregates are spherical micelles whereas larger structures are cylindrical in nature, negatively impacting the ability to form a gel. Two triblock copolymers were taken forward for further study, PNIPAM10-PEG10-PNIPAM10 and PDEA20-PEG10-PDEA20, based on the strengths of the gels formed and their biocompatibility. The rheology, mucoadhesion and stability of these polymers were found to offer advantages over

poloxamer 407, indicating that both may have application in topical drug delivery. The solubility and release of progesterone and tenofovir disoproxil fumarate was investigated for all three polymers, as exemplar hydrophobic and hydrophilic drugs relevant to vaginal drug delivery. Sustained release over 140 h and 24 h was achieved for progesterone and tenofovir disoproxil fumarate from both synthetic thermogelling materials, respectively, prolonging delivery relative to poloxamer. Thus, these materials are attractive as novel thermogelling materials for topical drug delivery.

Chapter One: General Introduction

[1.1] Thesis Introduction

The aim of this project is to identify, synthesize and evaluate novel thermogelling materials for topical drug delivery. Thermogelling materials are aqueous polymer solutions that change from a solution to a gel with an increase in temperature.[1] These thermogelling materials could be administered topically to either the skin or mucosal membranes and if the temperature at which gelation occurs (Tgel) is below the temperature of the site of application, the formulation would transition to a retentive gel state. Traditional topical medicines typically come in the form of creams, gels, ointments or lotions which can be messy to apply and often require reapplication every 4-6 hours.[2] The thermogelling materials aim to have enhanced retention at the site of application, prolonging therapeutic effect, with the benefit of easy administration via an applicator or spray device. These materials may also allow for sustained delivery of therapeutics, which combined with effective retention may reduce the need for reapplication, aiming to improve patient experience of therapies. This project has been proposed as there are a limited number of thermogelling materials, and those reported have drawbacks for topical drug delivery. These materials are reviewed in chapter 2.

The most studied thermogelling polymer is poloxamer 407, an ABA block copolymer of polyethylene glycol (PEG) (A) and polypropylene glycol (B).[3] Poloxamer 407 gels typically exhibit rapid dissolution, low mucoadhesion, and a high dependence of gelation temperature on concentration, leading to mild dilution in physiological fluids triggering an elevation in Tgel to above the temperature of the body and thus a reverse gel to solution transition.[4] Due to these factors poloxamer 407 formulations can have relatively short retention times which results in frequent reapplications to allow for a sustained exposure of drug.[4] Novel thermogelling materials must be demonstrated to improve upon the properties of poloxamer 407 to warrant their use as thermogelling excipients where the expense of translation is high. These thermogelling materials may be developed using temperature responsive polymers which exhibit a lower critical solution temperature (LCST). LCST exhibiting polymers phase separate from aqueous solution upon an increase in temperature and can be used in copolymers to translate this phase change to a gelation. Thermogelling materials may be prepared using LCST exhibiting polymers reported in the literature or novel polymers designed using *in silico* methods.

Computational predictive models may be used to guide the development of novel materials by predicting physical properties without lengthy and costly synthesis. There are an abundance of predictive computational models described within the literature which include the use of quantitative structure activity relationships (QSAR), quantitative structure property relationships

(QSPR) and artificial neural networks (ANN) in the identification of novel materials with specific properties. These models use computationally derived physicochemical properties to predict a desired property. Specifically, there are two studies which have proven QSPR models may be used to predict the LCSTs of polymers in organic solution.[5,6] Therefore, this may be possible for polymers in aqueous solution. Chapter 3 assessed this possibility by developing databases of LCST exhibiting homopolymers and designing QSPR models with the aim of predicting novel thermoresponsive polymers.

Chapter 4 concerns the selection of LCST exhibiting homopolymers based on transition temperature and predicted safety profile, followed by their synthesis. Following the identification of successful synthetic procedures, these were used to develop ABA triblock copolymers with LCST exhibiting "A" blocks and PEG "B" blocks to be used as candidate thermogelling materials. Triblock copolymers were selected for synthesis as they are known to form stronger gels than diblock copolymers.[7] All materials were extensively characterised by NMR spectroscopy and gel-permeation chromatography to ensure pure and well-defined polymers.

Chapter 5 then discusses the solution properties of the ABA triblock copolymers synthesised in chapter 4 in order to evaluate potential thermogelling behaviour. Rheology was used to characterise the thermogelling properties of these triblock copolymers in solution, as the changes in viscosity may be determined as a function of temperature. Currently, the mechanism by which thermogelling block copolymers form gels is insufficiently understood to guide the rational development of novel materials with high performance. Thus, the solution properties were also probed by dynamic light scattering and preliminary small-angle neutron scattering studies. This chapter aimed to identify polymers which may be used as thermogelling drug delivery excipients and provide an insight into nanoscale behaviour. The ABA copolymers where then streamlined based on their cytotoxicity and rheological performance to identify two candidate thermogelling materials.

Chapter 6 concerns the further development and evaluation of the two thermogelling materials. Properties such as gelation temperature, gel strength, gelation time, resistance to shear stress, dissolution time and mucoadhesion were evaluated to identify target sites and evaluate the potential of the materials in topical drug delivery. These performance tests were also conducted on poloxamer 407 to act as a comparator material.

Lastly, chapter 7 investigated the ability for these thermogelling materials to solubilise relatively hydrophilic and hydrophobic therapeutics relevant to topical drug delivery. For a therapeutic effect to be possible the drug must be in aqueous solution, therefore, hydrophilic drugs are preferred. However, most drugs are poorly water soluble. Therefore, solubility enhancement of poorly water

soluble drugs is an ideal characteristic for these materials to have.[8–10] To this end, the solubility of both drug types will be investigated. Following this, the release kinetics of these drugs was investigated to understand how long these materials may be able to deliver their dose.

The final chapter, chapter 8, consists of a general conclusions and future work. These general conclusions contextualise the work presented in this thesis and their meaning in the wider literature. The future work highlights areas which are still unknown and may be probed further given the findings of this thesis.

[1.2] References

1   M. H. Park, M. K. Joo, B. G. Choi and B. Jeong, *Biodegradable thermogels*, American Chemical Society, 2012, vol. 45.

2   X. Tan, S. R. Feldman, J. Chang and R. Balkrishnan, *Expert Opin. Drug Deliv.*, 2012, **9**, 1263–1271.

3   G. Dumortier, J. L. Grossiord, F. Agnely and J. C. Chaumeil, *Pharm. Res.*, 2006, **23**, 2709–2728.

4   M. A. Abou-Shamat, J. Calvo-Castro, J. L. Stair and M. T. Cook, *Macromol. Chem. Phys.*, 2019, **220**, 18–25.

5   J. Xu, L. Liu, W. Xu, S. Zhao and D. Zuo, *J. Mol. Graph. Model.*, 2007, **26**, 352–359.

6   G. Melagraki, A. Afantitis, H. Sarimveis, P. A. Koutentis, J. Markopoulos and O. Igglessi-Markopoulou, *J. Mol. Model.*, 2007, **13**, 55–64.

7   H. H. Lin and Y. L. Cheng, *Macromolecules*, 2001, **34**, 3710–3715.

8   E. K. S. de Melo, T. P. de Araujo, J. W. V. da Silva, S. C. C. Chagas, D. C. G. Bedor, D. P. de Santana and L. B. Leal, *Brazilian J. Pharm. Sci.*, 2017, **53**, 1–5.

9   L. L. Wang, W. S. Zheng, S. H. Chen and X. Q. Fang, *PLoS One*, 2013, **8**, 717–726.

10   J. Suksiriworapong, T. Rungvimolsin, A. A-Gomol, V. B. Junyaprasert and D. Chantasart, *AAPS PharmSciTech*, 2014, **15**, 52–64.

Chapter Two: A Literature Review of Lower Critical Solution Temperature Exhibiting Polymers and their use in the Synthesis of Thermogelling Materials

[2.1] Introduction

Thermogelling materials are polymer solutions which transition to a gel state upon an increase in temperature, undergoing the reverse transition upon cooling. These thermogelling materials have enabled ground-breaking discoveries in fields including: protein and peptide delivery,[1] drug delivery,[2,3] gene delivery,[4] tissue engineering[5] and cell culture[6]. Thermogelling materials are also being explored for 3D printing.[7] Research into drug delivery using thermogelling materials has gained interest in recent years due to advantages they may offer over traditional drug delivery vehicles. Thermogelling materials are advantageous in drug delivery as the dosage form is a free-flowing fluid below a critical temperature so can pass through an applicator,[8] and subsequently form a gel upon contact with the body's heat that can offer enhanced retention and prolonged drug delivery at the target site.[9] This, in turn, would allow for reduced dosing frequency, enhanced efficacy, and localisation of delivery.

Typically, there are two classes of thermogelling material; those which rely upon a hydrophilic/hydrophobic balance and those which consist of a temperature responsive polymer block covalently bound to a hydrophilic component. The first class of thermogelling material which rely on a hydrophilic/hydrophobic balance include Pluronics (poly(ethylene oxide)–*b*–poly(propylene oxide)–*b*–poly(ethylene oxide))[10] and poly(ethylene oxide)–*b*–poly(lactic-co-glycolic acid) (PLGA) containing block copolymers.[11] The second class of thermogelling material require a temperature responsive polymer component. There are two classes of temperature responsive polymer, those which exhibit a "lower critical solution temperature" (LCST) and those which exhibit an "upper critical solution temperature" (UCST). LCST-exhibiting blocks may impart sol-gel transition with warming, where UCST exhibiting polymers are expected to undergo the reverse transition i.e gel to sol, and thus are excluded from this review. There are existing reviews which may be referred to for information related to UCST systems.[12]

[2.1.1] Thermodynamics of the LCST

The LCST is the critical temperature above which components in a mixture are no longer miscible.[13] The precipitation temperature, or "cloud point" is physically identified by a transition from a clear polymer solution to a turbid one, which is an indicator of the polymer surpassing an LCST.[14] Polymer precipitation at the LCST is an entropically driven process [15] and can be described using the equation for ideal mixing[16] (Equation 2.1).

$$\text{Equation 2.1: } \Delta G_{mix} = \Delta H_{mix} - T\Delta S_{mix}$$

The spontaneous process of dissolution of a simple solute such as sodium chloride in water is characterised by a negative change in the Gibbs free energy of mixing (ΔG_{mix}).[17] The sodium and chloride ions become hydrated by water molecules, breaking the cation-anion interactions and forming water-ion interactions, which results in an enthalpy change (ΔH_{mix}).[18] To accompany the change in enthalpy, there is also a change in entropy (ΔS_{mix}) which in most ideal dissolution processes is positive, showing an increase in disorder.[19] A negative value of ΔG_{mix} may be achieved due to the enthalpic or entropic processes, the latter of which are dependent upon temperature.

Using classical thermodynamics in the case of polymer dissolution in water, water-water and intra- and inter- molecular polymer-polymer bonds are broken, and water-polymer intermolecular bonds are formed, resulting a change in ΔH_{mix}.[18] When a polymer is dissolved there is also a ΔS_{mix}, which may be negative under certain conditions. Polymers which exhibit a negative ΔS_{mix} when mixed with water have ordered layers of solvent molecules around the polymer chains, which may be entropically unfavourable in cases where the polymer solid is inherently disordered.[20] For a polymer to exhibit an LCST in aqueous solution, the ΔS_{mix} of dissolution must be negative, as well as the ΔH_{mix}. Upon surpassing a critical temperature known as the "spinodal point", the ΔG_{mix} changes from negative to positive, making the mixing of polymer and water disfavoured resulting in demixing to a two-phase system.[21] The temperature at which the two-phase system is formed is known as the LCST[22] (Figure 2.1). There are three types of LCST demixing reported: where the LCST is dependent on molecular weight and not concentration (Type I), where the LCST is dependent on concentration regardless of molecular weight (Type II) and the LCST is dependent on both molecular weight and concentration (Type III).[23]
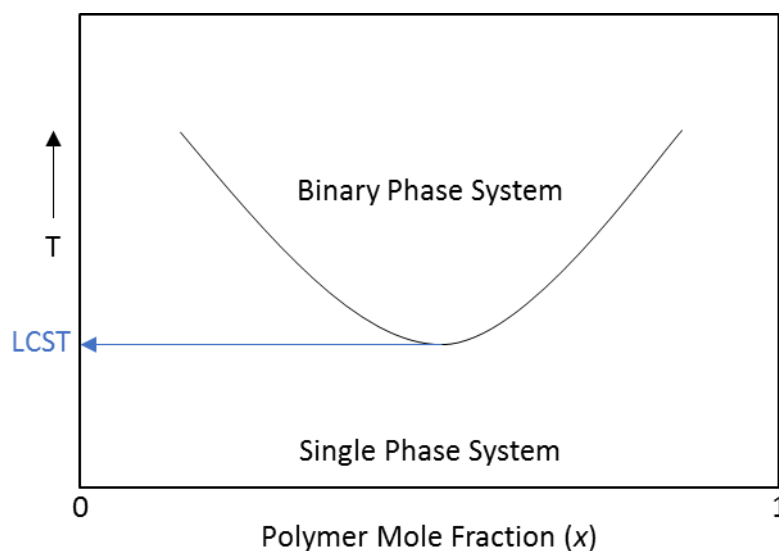
Figure 2.1: A phase diagram exhibiting the typical solution behaviour of LCST exhibiting polymers.

It should be noted that the thermodynamics of dissolution for simple solutes in aqueous solution does not always hold true for polymer solutions. For polymeric solutions where there is a greater difference between the molecular sizes of the solute and solvent, Flory-Huggins theory is applicable. Flory-Huggins theory is a lattice model which incorporates the number of polymer-solvent interactions when calculating the ΔG_{mix}.[24] This theory takes into account the great dissimilarity between the molecular sizes of polymers and the solvent in solution. Flory-Huggins calculates ΔG_{mix} from the gas constant (R), the number of moles of the solvent (n_1) and polymer (n_2), the volume fraction of the solvent (v_1) and polymer (v_2), and the chi parameter (χ), also known as the Flory-Huggins interaction parameter (Equation 2.2). The chi parameter considers the energy required to intersperse the polymer and solvent molecules in the solution. LCST behaviour is often accounted for in this theory by variation in chi with temperature.[17]

$$\text{Equation 2.2: } \Delta G_{mix} = RT[n_1 \ln v_1 + n_2 \ln v_2 + n_1 v_2 \chi]$$

[2.1.2] Structure and Physical Properties of Thermogelling Materials

Thermogelling materials may be produced from block copolymers containing a temperature-responsive block and at least one hydrophilic block. Thermogelling materials may be di-, tri-, tetra-, or star-shaped block copolymers, with the latter two geometries are reported in only a small number of publications. Thermogelling di-block copolymers typically consist of an LCST-exhibiting component and a hydrophilic polymer (Figure 2.2A).[25] Tri-block copolymers can have ABA, BAB, ABC or BAC structures where the A block is temperature responsive and the B and C blocks can be either hydrophilic or hydrophobic (Figure 2.2B & 2.2C).[26] Tetra-block copolymers are block copolymers containing four blocks of polymer, where all four blocks can be different, or up to two blocks can be present twice. Common architectures are ABCD, ABCB or BACB, where any block can be either temperature responsive, hydrophobic or hydrophilic in nature.[27] Star-shaped thermogelling block copolymers have three or more temperature-responsive arms, and usually contain a central branched hydrophilic polymer, such as poly(ethylene glycol) (PEG) (Figure 2.2D).[28] Both tetra- and star-shaped thermogelling block copolymers are less common within the literature compared to di- and tri-block copolymers, due to their complex structures and properties as well as the relatively high cost of star-shaped starting macroinitiators. Thermogelling graft copolymers have been reported,[29] and consist of a linear synthetic or natural polymer backbone which may be hydrophilic or temperature responsive in nature, which is grafted with a temperature responsive component (Figure 2.3E). Heating any form of thermogelling material past a critical temperature results in sol-gel transition, caused by overall increase in hydrophobic character above the LCST.[30]
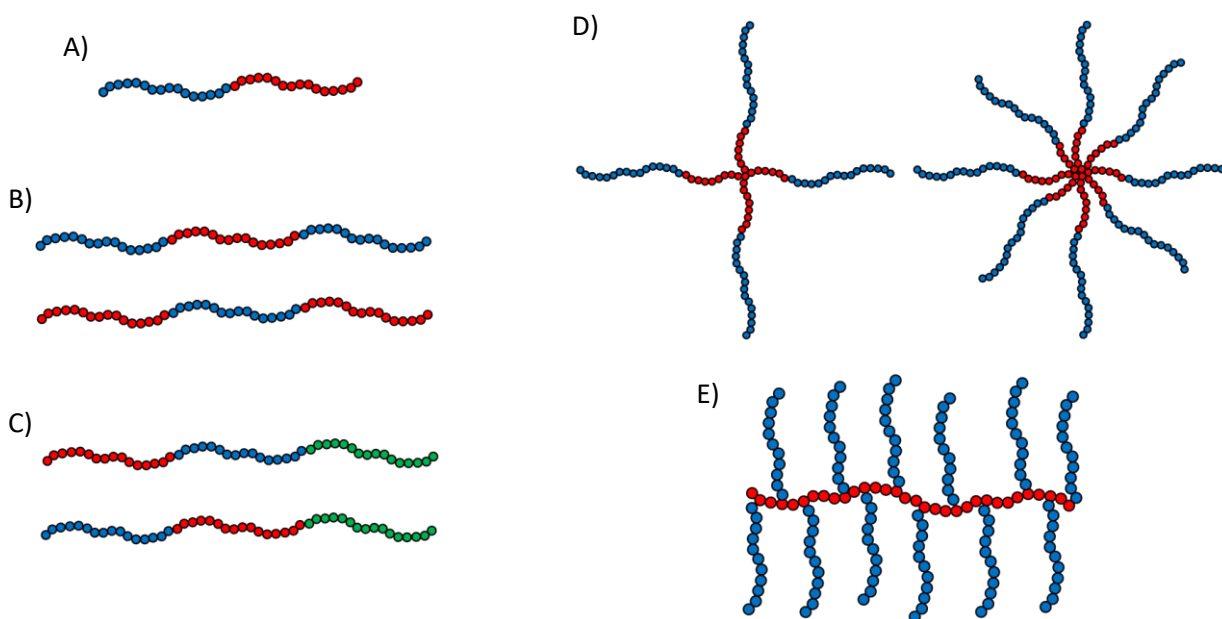
Figure 2. 2: Polymer geometries used in the construction of thermogelling materials A) diblock B) ABA and BAB tri-block C) ABC and BAC tri-block D) 4 and 8 arm star shaped and E) graft copolymers, where red, blue, and green designated chemically distinct polymer moieties.

Thermogelling materials require both a critical concentration and temperature to exhibit a sol-gel transition.[31] Block copolymers which contain an LCST exhibiting polymer are proposed to form gels by self-assembly into micellar structures, which may pack or undergo a conformational change,[32] and/or by physical polymer entanglements between thermoresponsive components above the LCST[33,34] (Figure 2.3). The formation of a gel via micellar packing can be modelled using hard-sphere crystallisation.[35] In order to form a gel via micellar packing, the phase volume of micelles must surpass a critical point.[36] Packing may occur in either a liquid crystalline or amorphous manner, giving rise to a gel state. For example, spherical micelles may pack into face-centred cubic mesophases.[37] Micelles have also been reported to undergo a conformational change upon from spherical to worm-like, due to an increase in temperature. These worm-like micelles can become intertwined and result in the formation of a mesophase gel.[38] Block copolymers with more than one temperature responsive block are reported to not only form micelles, but also form physical entanglements when above a critical temperature. These physical entanglements may anchor micelles together as described by Semenov et al.[32] Semenov's theory is that "telechelic" polymer chains with hydrophilic centres and hydrophobic termini form gels by the formation of "flower-like" micelles, within which the polymer acts as a "loop", which are associated by unimer "bridges" (Figure 2.3b). In cases where LCST-exhibiting blocks flank a hydrophilic core, heating above the LCST results in the copolymer behaving as a telechelic chain.
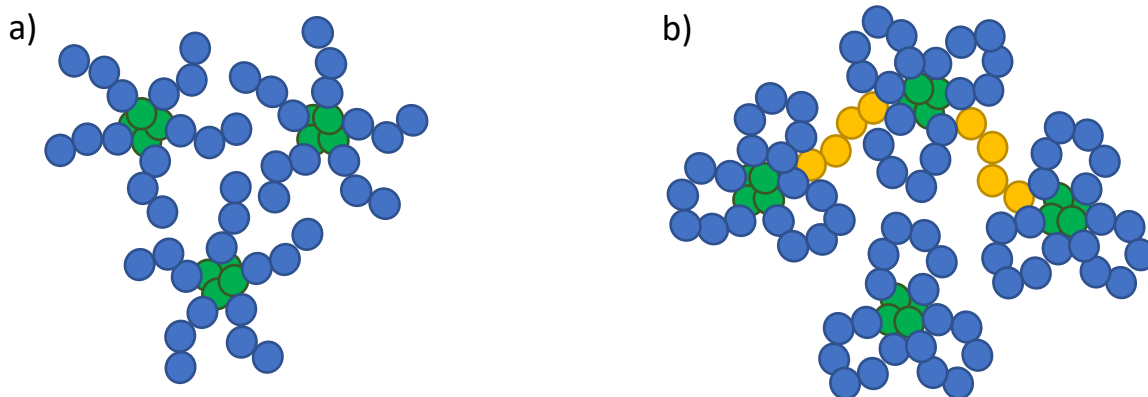
Figure 2. 3: Schematic representation of a) the formation of packed micelles when an aqueous solution of diblock thermogelling polymer is increased past a critical temperature and b) the formation of bridged flower-like micelles when the temperature of an aqueous solution of tri-block thermogelling polymer is increased past a critical temperature. The hydrophilic, temperature responsive and bridging (hydrophilic) polymers are shown in blue, green and yellow respectively.

[2.2] Poloxamer

Poloxamers, also known as Synperonics (Croda), Pluronics (BASF) and Kolliphor (BASF), are ABA tri-block copolymer of PEG (A) and poly(propylene glycol) (PPG) (B). Poloxamers exhibit surfactant like properties due to their amphiphilic structure, which makes them ideal for cosmetic and pharmaceutical applications. There are two poloxamers which exhibit thermogelling behaviour, poloxamer 188 and 407. The gelation temperatures of poloxamer 188 and 407 in 20 % w/v solution occur above 50 and around 25 °C, respectively.[39] Due to the physiologically relevant gelation temperature of poloxamer 407, it has been widely investigated as an *in situ* thermogelling drug delivery vehicle. Poloxamer 407 contains 101 and 56 repeat units of PEG and PPG respectively (Figure 2.4).[40]
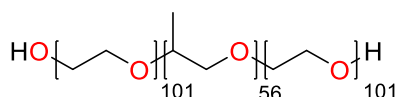
Figure 2. 4: The molecular structure of poloxamer 407.

[2.2.1] The Gelation Mechanism of Poloxamer 407

Within the literature, the solution behaviour of Poloxamer 407 has been characterised using techniques including dynamic light scattering (DLS),[41] cryogenic transition electron microscopy (cryo-TEM)[42] and small angle neutron scattering (SANS).[43] Such techniques have concluded that in aqueous solution poloxamer 407 exists as both solubilised chains and micelles in equilibrium. The micelles form due to aggregation of the hydrophobic PPG chains to reduce contact with water molecules. When the temperature is increased the equilibrium shifts to a large volume fraction of micelles as the PPG chains become increasingly desolvated. The aggregation of poloxamer 407 into micelles results in face-centred cubic packing which results in the formation of a gel (Figure 2.5).[44]
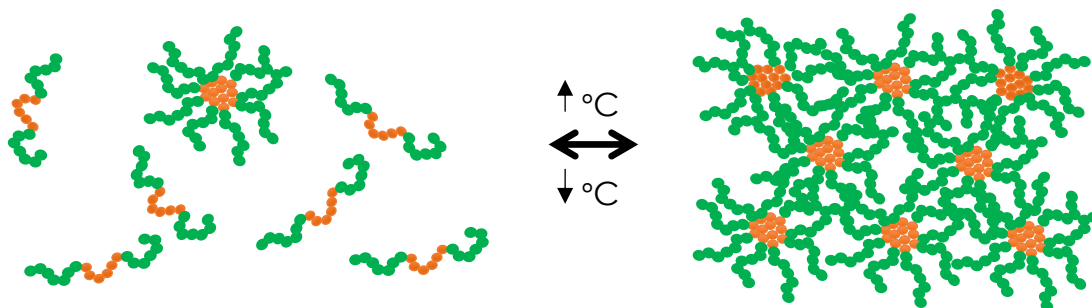
Figure 2. 5: The gelation mechanism of Poloxamer 407 in aqueous solution. An increase in temperature results in an increase in the volume of micelles present, which pack to form a gel. These micelles consist of a hydrophobic PPG core (orange) and a hydrophilic PEG corona (green).

[2.2.2] Solution Properties of Poloxamer 407

The solution properties of Poloxamer 407 have been thoroughly investigated throughout the literature. DLS studies of Poloxamer 407 have found the critical micellization concentration of Poloxamer 407 at room temperature to occur between 0.12 to 2.00 % w/v.[41,45–48] Specifically Wanka et al found that increasing the temperature of the solution to 42 °C results in a decrease in the critical micelle concentration from 0.7 to 0.005 % w/v.[47] In addition to this, Alexandridis et al found that increasing the polymer concentration results in a reduced micellization temperature from 35.5 to 19.5 °C when the concentration was increased from 0.01 to 5.00 % w/v.[46] Cryo-TEM studies have confirmed the structure of these aggregates formed by poloxamer 407 to be spherical in nature with a hydrodynamic radius between 5-7 nm (Figure 2.6).[49,50] Mortensen and Talmon performed SANS experiments of poloxamer 407 in dueterated water, which also identified spherical micelles with a 5 nm diameter.[49]
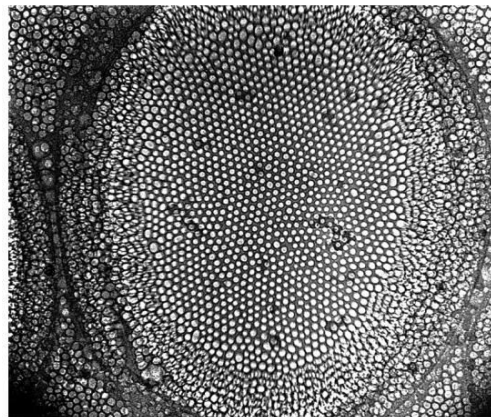
100 nm

Figure 2. 6: A cryo-TEM image from Lam (1999) of the micelles formed by poloxamer 407 in aqueous solution.

When Poloxamer 407 is in solution above a critical concentration, an increase in temperature can result in a solution to gel transition. There have been many studies in the literature which characterise the effect of Poloxamer 407 concentration on the gelation properties. One such study found that Poloxamer 407 does not form a gel below concentrations of 12.6 % w/v.[51] The study also found that the gelation temperature falls with an increase in poloxamer 407 concentration but the gel strength increases, which is in agreement with other literature studies.[52–55] The decrease in gelation temperature is reported to be due to a greater overall number of polymer chains, as a result of which, the increase in temperature to reach the critical phase volume of micelles required to form a gel is lower.[56] As such, less heat energy is required to form enough micelles to reach the critical phase volume for a solution to gel transition to occur. As for the gel strength, this may be ascertained using rheology. The rheology of thermogelling materials is investigated by exploring parameters such viscosity and storage (G') and loss (G'') moduli, with temperature. Poloxamer 407 solutions which exhibit thermogelling behaviour show a sharp increase in viscosity, G' and G'' upon surpassing a critical temperature, an example of which is shown in Figure 6.7. The gel strength, as investigated by rheology at a strain amplitude of 0.1 %, has been shown to increase from 17 to 25 MPa when the poloxamer 407 concentration is increased from 16 to 19 % (w/v).[51] This is as a result of denser micelle packing above a critical temperature, as previously discussed.[57]
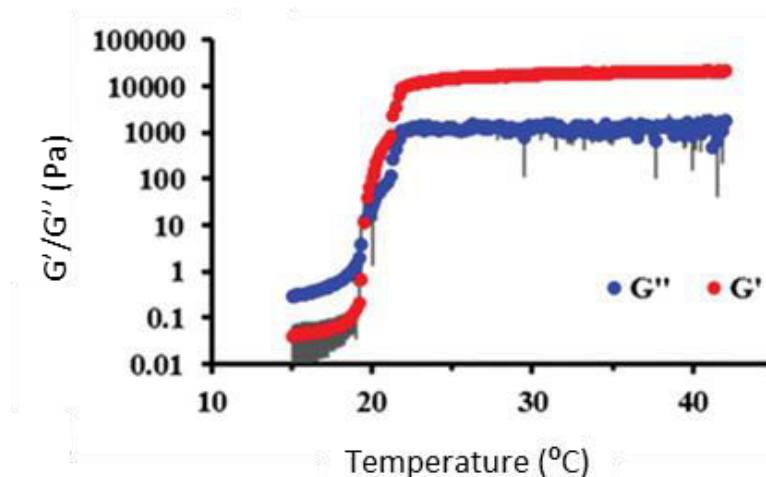
Figure 2. 7: A temperature ramp rheogram of a 20 % (w/v) aqueous solution of poloxamer 407 where both G' (red) and G'' (blue) sharply increase upon surpassing a critical temperature.[37]

The gelation properties of poloxamer 407 maybe modified using additives such as salts, polar organic solvents, additional polymers and the inclusion of therapeutic agents. The inclusion of salts in poloxamer 407 formulations has been shown to result in a reduced micellization temperature and as such a reduced gelation temperature.[58–60] In comparison to micellization, the effect of salts on the gel strength is less often studied. One study by Yong (2001) found that including sodium chloride into poloxamer 407 gels results in an increased gel strength and bio-adhesive force.[39] The bio-adhesive force increases for salt containing dosage forms as a result of an increase in formulation ionic strength, which allows for a greater degree of interaction between physiological mucins and the polymer present.[61] Formulations often include alcohols for their bactericidal and preservative properties, and thus the effect of organic alcohols on the solution properties of poloxamer 407 have been investigated in the literature. Two studies have found that alcohols such as methanol and ethanol increase the micellization temperature of poloxamer 407 in solution and in turn increase the gelation temperature.[62,63]

The thermogelling properties of poloxamer 407 have also been studied in polymer blends. Polymers such as poloxamer 188,[64,65] poly(vinyl alcohol)[66,67] and Carbopol[68–70] have been included in thermogelling poloxamer 407 formulations. Zhang et al and Al Khateb et al found that poloxamer 407 and 188 blends result in stronger gels and an increase in gelling temperature when the poloxamer 188 content increases.[64,65] For example, Zhang et al showed the gelation temperature of formulations containing 20 % w/w poloxamer 407 increased from 29.6 ± 0.1 to 31.7 ± 0.3 °C, when the poloxamer 188 concentration was increased from 5 to 10 % w/w.[64] In addition to this, a

formulation of 24 % w/w poloxamer 407 exhibited a viscosity of 6.15 Pa.s, while a blend of poloxamer 407 and 188 at 24 and 10 % w/w, respectively, formed a gel with a viscosity of 11.86 Pa.s. In the case of PVA blends, Bercea et al found the gelation temperature increased from 20.1 to 36.7 °C for formulations of 20 % poloxamer and 15 and 5 % poloxamer and PVA, respectively.[67] Typically, poloxamer 407 formulations below a critical concentration of 15 % w/v do not exhibit thermogelling behaviour. Thus, the PVA must enhance this thermogelling behaviour. The mechanism of this is not discussed, but this may be due to enhanced micelle interactions caused by bridging of PVA molecules. This increase in gelation temperature is accompanied by a decrease in gel strength from 10597 to 2000 Pa at 37 °C. This may be as a result of a decrease in the number/strength of interactions between poloxamer 407 chains, leading to a decrease in viscosity[51] Carbopols are high molecular weight poly(acrylic acids) (PAAs) cross-linked with allyl sucrose or allyl pentaerythritol.[71] The gelation temperature of 20 % w/w poloxamer 407 formulations has been shown to fall from 25.44 ± 0.12 to 21.84 ± 0.37 with the addition of 0.25 % w/w Carbopol 934P, while the gel strength remained consistent around ca. 15000 Pa.[72] The gelation temperature fell as a result of fewer water molecules present to hydrate the poloxamer 407 polymers, resulting in a reduced gelation temperature. The gel strength, however, was not significantly impacted, indicating the micelle packing at elevated temperature is not compromised by the presence of Carbopol.[70] Additional studies also add that Carbopol enhances the bio-adhesive nature of poloxamer 407 formulations. For example, one study found the adhesion of 20 % poloxamer 407 formulations increased from 20 to 100 gf (gram force) when the Carbopol was increased from 0.5 to 3 % w/w.[68] This is expected, as Carbopol is a well-known bio-adhesive polymer, which can interact with mucins due to the charged nature of the PAA.[73]

In formulation development, the effect of therapeutic agent on the formulation properties must be investigated. There have been several studies which investigate the effect of active pharmaceutical ingredient (API) on the gelation temperature and gel strength of thermogelling poloxamer formulations. In addition to this, the release kinetics of the therapeutic compounds has also been investigated. APIs such as vancomycin,[58] lidocaine,[52] fentanyl,[53] triamcinolone acetonide,[74,75] fluorouracil,[54] adriamycin,[54] capsaicin,[55] arginine vasopressin[76] and insulin[77] have been investigated. All of these therapeutic agents except vancomycin and arginine vasopressin are considered to be hydrophobic in nature. Vancomycin (2 % w/v) was found to not significantly change the gelation temperature and gel strength of 20 % w/v poloxamer 407 formulations. The gelation temperatures and gel strengths of the vancomycin containing formulations and pure poloxamer formulations were 12.7 and 12.9 °C and 23580 and 24606 Pa, respectively. Alongside this, both vancomycin and arginine vasopressin formulations exhibited a sustained release over 12 h. When analysing

hydrophobic therapeutics, their solubility is enhanced in poloxamer 407 formulations when compared to pure water. The enhanced solubility is due to dissolution of the drug to the core of the poloxamer 407 micelles.[78] Incorporation of hydrophobic therapeutics, such as piroxicam (0 and 4.0 %), have been shown to reduce the viscosity of poloxamer 407 gels from ca. 8000 mPas to ca. 4000 mPas.[79] The therapeutics partition between the aqueous media and the core of the micelle. Solubilisation into the core of the micelle may increase their size and reduce their packing density while, solubilisation of the therapeutics to the extra-micellar water may increase the distance between the micelles, resulting in fewer micellar-micellar interactions. Both of these are suggested to contribute to a decrease in the degree of hydrogen bonding between micelles and a reduction in gel strength.[79]Although the viscosity of the poloxamer 407 gels was found to decrease, the complete release of piroxicam reached ca. 60 % after 48 hours. This is significantly longer than the release which has been reported for hydrophilic therapeutics such as vancomycin.

Overall, poloxamer 407 is an attractive thermogelling material for topical drug delivery as a result of its low viscosity at room temperature and sharp transition to viscous gel when reaching physiologically relevant temperatures (i.e. ca. 37 °C). As a result of this property, poloxamer 407 can be applied via a syringe or an applicator to achieve *in situ* gelation at the target site. These formulations have also been found to allow dissolution of hydrophilic therapeutics and enhance the solubility of poorly-water soluble drugs. In addition to this, poloxamer 407 gels also offer prolonged release of both hydrophilic and hydrophobic therapeutics. As much as poloxamer thermogels may be attractive, there are still some drawbacks to using this as a drug delivery vehicle. Poloxamer 407 gels offer weak mechanical strength[39] as a result of the shear thinning character,[80] rapid dissolution[81] and weak mucoadhesion.[82] As a result of this, poloxamer 407 gels offer poor residence times as shown when a meloxicam containing gel was completely eroded after 360 min.[83,84]

Novel thermogelling materials may offer the favourable characteristics which are shown by poloxamer 407 gels, principally low viscosity at room temperature with a transition to a viscous gel at body temperature. In addition to this, novel thermogelling materials may be designed to offer enhanced mechanical strength, dissolution times and mucoadhesion when compared to poloxamer 407 formulations, developing advanced materials with improved performance. This may allow for enhanced residence times and prolonged drug delivery, enabling new healthcare technologies. The current state of these novel thermogelling materials will now be discussed.

[2.3] Novel thermogelling materials

[2.3.1] Poly(N-isopropyl acrylamide) and related poly(acrylamide)-based thermogelling materials

The most well studied LCST exhibiting polymer is poly(N-isopropyl acrylamide) (PNIPAM) as it possess an LCST at ca. 32 °C in aqueous solution.[85] The temperature at which the LCST occurs makes PNIPAM ideal for the development of thermogelling materials for many biomedical applications including drug delivery, as it sits between room and body temperature. The LCST of PNIPAM is independent of changes in molecular weight but may be modulated by a few degrees by varying the concentration of the polymer in solution.[86] The LCST may be drastically reduced using 'salting out' agents from the Hofmeister series.[87] Ions of the Hofmeister series compete with the polymer for water molecules, and as such fewer water molecules are free to solvate the polymer.[88] This results in a fewer polymer-water bonds which results in a lower energy requirement to induce polymer precipitation. The disadvantage of using PNIPAM to develop thermogelling materials is the potential for toxicity. PNIPAM has been reported to be cytotoxic to smooth muscle cells and fibroblasts, but not to bovine aortic endothelial cells or vero cells.[89,90] Thus, the cytotoxicity of PNIPAM is dependent upon the cell type used. As a result of this, PNIPAM has a limited number of target sites as such is not found on the inactive ingredients database,[91] indicating it is not approved by the FDA. Therefore, this polymer may not be safe for use in the development of thermogelling materials for biomedical applications.

Di-block copolymers containing PNIPAM are reported in the literature. These studies discuss the preparation of AB block copolymers with PNIPAM A blocks and B block of PEG,[92–95] poly(O-allyl-α-D-glucose) (POAG),[96] poly(methyl methacrylate)[97] (PMMA) and PAA.[98] These block copolymers were found to form aggregates with an increase in temperature past the LCST of PNIPAM. A PNIPAM-*b*-PEG block copolymer was found to form aggregates upon surpassing the LCST of PNIPAM with a hydrodynamic diameter of ca. 80 nm.[92] The micellization temperature of PNIPAM-*b*-PEG diblock copolymers has been found to fall from 34 to 31 °C with an increase in PNIPAM molecular weight from 3.8 to 6.2 kDa.[94] To the best of our knowledge there is only one report on the rheology of a PNIPAM containing di-block copolymer. This is a PNIPAM-PEG di-block copolymer where both blocks have molecular weights of 2 kDa. This di-block copolymer was found to be a free-flowing clear solution at 25 °C and transitioned to a turbid viscous gel at 37 °C with a gel strength of 480 ± 70 Pa.[95] This di-block copolymer was also found to have an oscillatory yield stress of 690 ± 90 Pa. The only PNIPAM thermogelling block copolymer, identified by tube inversion, to be investigated for drug release is that of PNIPAM-POAG.[96] The release of methylene blue from the injected PNIPAM-POAG

thermogelling copolymer was found to plateaux at ca. 80% after 60 h, indicating a controlled release.

There are many more studies on thermogelling PNIPAM tri-block copolymers. There are reports in the literature of the synthesis of ABA tri-block copolymers where the A block is PNIPAM and the B block has been PEG,[95,99–102] poly(vinyl pyrrolidone) (PVP)[103] or poly(N,N-dimethylacrylamide) (PDMA).[104,105] All of these block copolymers exist as free polymers in solution below the LCST of PNIPAM. Above the LCST of PNIPAM, these polymers transition to form aggregates which, in the case of PEG, have been proven to be either flower-like micelles[106] or fractals.[107] The ABA tri-block copolymer of PNIPAM (A) and PDMA (B) with molecular weights of 6 and 10.5 kDa, respectively. This polymer was found to transition from a free-flowing fluid to a viscous gel upon surpassing ca. 45 °C. Increasing the polymer concentration from 10 to 20 % w/v increased the gel strength from ca. 100 to 1000 Pa and the gelation temperature fell from ca. 60 to 50 °C. In the case of the PNIPAM-*b*-PVP-*b*-PNIPAM tri-block copolymers, the study found increasing the molecular weight of the PNIPAM blocks from 11 to 26 kDa decreased the gelation temperature from ca. 27 to 23 °C for a 20 % w/v polymer solution.[103] The study also found the minimal concentration for gelation was lower for the polymer with the largest molecular weight (i.e. 48 kDa polymer formed a gel above 30 % w/v while the 71 kDa polymer formed a gel above 20 % w/v). This study also found that at elevated temperature the complete release of Rhodamine B, a model drug with a LogP of 1.95,[108] was achieved after 60 hours at 37 °C, while at 25 °C, complete release was observed after 15 hours. The most investigated PNIPAM thermogelling block copolymer is PNIPAM-*b*-PEG-*b*-PNIPAM. Lin and Cheng found a PNIPAM-*b*-PEG-*b*-PNIPAM block copolymer with 4.6 kDa PEG and 1.9 kDa PNIPAM blocks transitioned from a free-flowing solution to a viscous gel upon an increase in temperature.[95] At 37 °C, a 20 % w/v aqueous solution formed a gel with a gel strength of 2000 ± 200 Pa and an oscillatory yield stress of 430 ± 50 Pa. The most comprehensive studies of PNIPAM-*b*-PEG-*b*-PNIPAM thermogelling tri-block copolymers was performed by Teodorescu et al., where both PEG and PNIPAM molecular weights were varied in addition to the polymer concentration.[99] The study found that increasing the PEG molecular weight from 1 to 4 kDa resulted in an increase in transition temperature from ca. 34 to 40 °C and the gels formed exhibited fewer signs of syneresis. Conversely, increasing the PNIPAM molecular weight from 5 to 30 kDa decreased the transition temperature from ca 42 to 34 °C while also increasing the gel strength from 0.01 to 1000 MPa (Figure 2.8). Larger polymers were found to form gels at lower concentrations, which is in agreement with Cong (2014).[99,103]
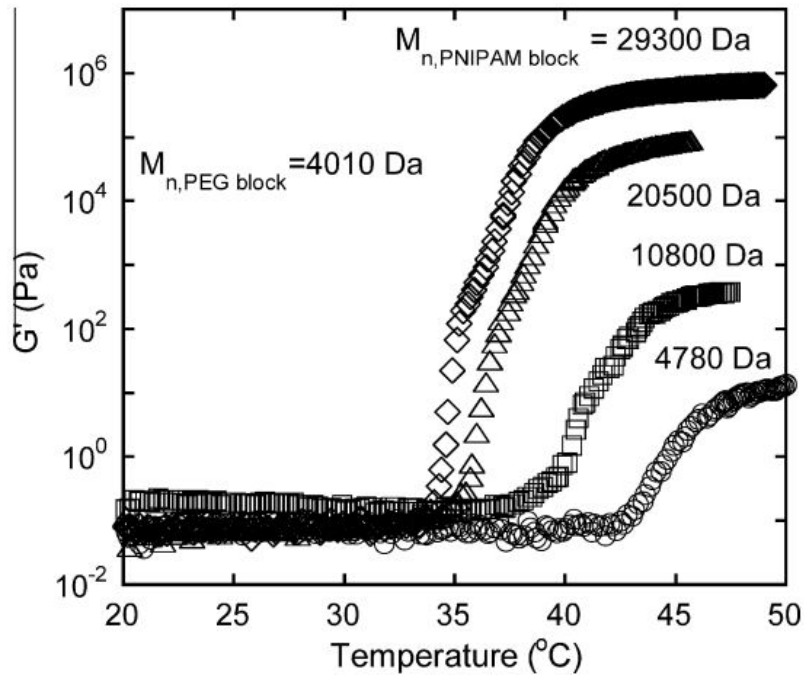
Figure 2. 8: The change in gel strength and gelation temperature shown by Teodorescu et al. of the PNIPAM-PEG-PNIPAM triblock copolymers when the PNIPAM molecular weight was increased from 5 to 30 kDa.

Although there has been extensive work investigating the gelation of PNIPAM-*b*-PEG-*b*-PNIPAM tri-block copolymers, the release kinetics of therapeutics has not been reported. In addition to ABA containing tri-block copolymers, an ABC tri-block copolymer of poly(methyl methacrylate) (PMMA) (A), poly(2-(N-(dimethylamino) ethyl methacrylate) (PDMAEMA) (B) and PNIPAM (C) has been reported.[109] Block copolymers of this type, in 3 % w/v aqueous solution, were found to form gels in pHs < 7.0 upon an increase in temperature, while in pHs > 7.0 a precipitate was formed. Upon an increase in temperature, with pH < 7.0, the PNIPAM blocks aggregate and the polymer forms a network in the aqueous solution with two localised areas of PMMA and PNIPAM. These two localised areas are then bridged by protonated PDMAEMA chains, which results in the formation of a gel. In the case of pH > 7.0, continual increases in temperature causes micelle agglomeration due to desolvation of the PDMAEMA block, resulting in a precipitate rather than a gel. The 3 % w/v tri-block copolymer in a pH 4.0 solution was found to form a gel with a strength of ca. 100 Pa when at 50 °C and yielded at a strain of 18 %.

There are cases where PNIPAM has been used to synthesise thermogelling materials with more complex architectures, such as star shaped[95,100] and graft copolymers.[110] The first report of star

shaped PNIPAM containing block copolymers was by Lin and Cheng, where both 4 and 8 arm block copolymers of PNIPAM and a central PEG were prepared.[95] Solutions of 20 % w/v 4 arm and 8 arm star shaped PNIPAM and PEG copolymers were found to have gel strengths of 2500 ± 200 and 1050 ± 150 Pa respectively, at 37 °C. In addition to this, the star shaped block copolymers were found to have oscillatory yield stresses of 860 ± 80 and 200 ± 30 Pa, respectively. This indicates that the increase in number of temperature responsive arms resulted in a weaker gel that was less resistant to shear forces. The reason or this was not commented on, but it may be due to a decrease in packing efficiency of the aggregates for at elevated temperature. Another study by Teodorescu et al. prepared 4 arm PNIPAM-*b*-PEG copolymers with a central PEG and four PNIPAM arms.[100] This study found as the PNIPAM molecular weight was increased from 5 to 10 kDa, for example, the gelation temperature decreased from 41 to 36 °C while the gel strength increased from ca. 1000 to 10000 Pa. Increasing the PEG molecular weight from 2 to 6 kDa increased the gelation temperature from 35 to 37 °C. A thermogelling copolymer of chitosan grafted with PNIPAM is described in the literature.[110] This polymer was found to increase in viscosity ca. 29 °C and reach a gel with a viscosity of ~ 400 Pas.

There are other LCST exhibiting poly(acrylamides) which have been used to synthesise thermogelling block copolymers, but these have been investigated to a lesser extent when compared to PNIPAM. One such polymer is poly(N,N-diethyl acrylamide) (PDEA), which exhibits an LCST between 25-36 °C,[111] which is dependent on both concentration and molecular weight.[112] An ABA tri-block copolymer of PDEA (A) and poly(acrylic acid) (PAA) (B) has been prepared and the thermogelling properties investigated.[113] The PDEA-*b*-PAA-*b*-PDEA tri-block copolymer was found to form aggregates upon surpassing 40 °C and subsequently formed a gel above 60 °C in 3 % w/v aqueous solution with a viscosity of 10000 Pas.

[2.3.2] Poly(N-vinyl caprolactam)-based thermogelling materials

Poly(N-vinyl caprolactam) (PNVCl) is a potential alternative to temperature responsive materials such as PNIPAM, due its LCST between 30 and 32 °C.[114] In addition to this, PNVCl is a component of Soluplus (Figure 2.9), a pharmaceutical grade graft copolymer excipient and as such is attractive for use in the development of thermogelling materials.[26,115,116,117] PNVCL exhibits type I demixing, where the LCST is solely dependent on polymer molecular weight and decreases as molecular weight is increased.[118] The draw-back of this polymer is the difficulty to polymerise the N-vinyl caprolactam monomer in a controlled manner.[119] This is as a result of the poor radical stability present in the monomer during polymerisation. The radical is particularly unstable because there are no chemical functionalities present which may stabilise the radical via conjugation. Whereas, for monomer such

as PNIPAM, the carbonyl of the amide may stabilise the radical by conjugation, allowing for longer radical residence time and a controlled polymerisation.
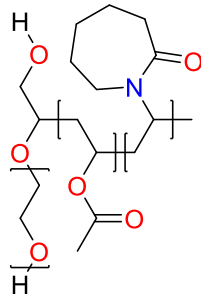
Figure 2. 9: The chemical structure of the graft copolymer Soluplus.

To date, articles describing thermogelling di-block copolymers containing PNVCl have not been published. There is however, a study which prepared tri-block copolymers of PNVCl-*b*-PEG-*b*-PNVCl and investigated the effect of block molecular weight on the gelation properties.[120] For a 20 % w/v triblock copolymer with a PEG molecular weight of 4 kDa, increasing the molecular weight of PNVCl block from 3.6 to 22.5 kDa decreased the gelation temperature from 47 to 37 °C while simultaneously increasing the gel strength from ca. 1 to 1000 kPa. Increasing the PEG molecular weight from 2 to 10 kDa however, increased the gelation temperature from 38 to 41 °C while not compromising the strength of the gel (Figure 2.10).
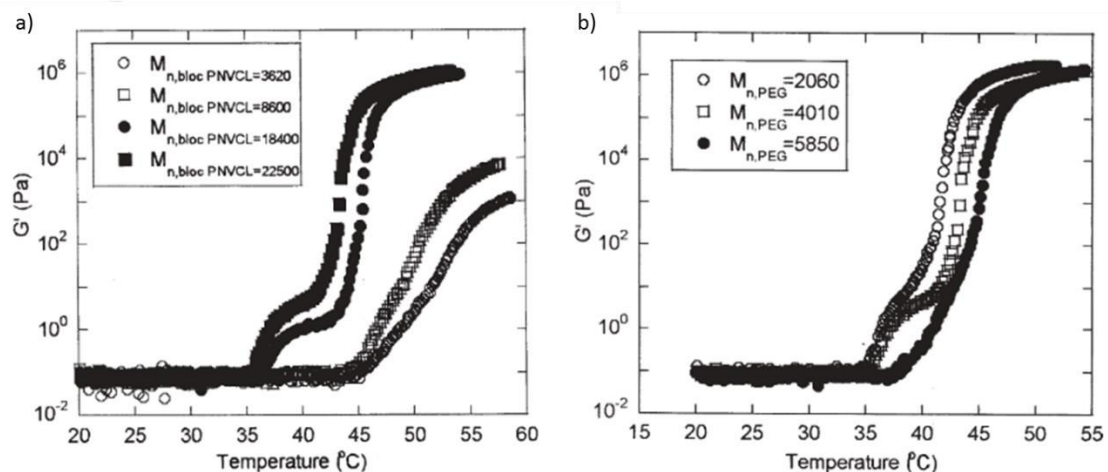
Figure 2. 10: The increase in gel strength with an increase in PNVCl block length (a) and the increase in gelation temperature with an increase in PEG length (B) for PNVCl-b-PEG-b-PNVCl tri-block copolymers.

Soluplus is a pharmaceutical grade excipient with a graft copolymer structure of PNVCl-poly(vinyl acetate)-PEG. The thermogelling properties of Soluplus in water, ethanol and water, a range of phosphate buffered saline solutions and sodium chloride solutions has been studied.[121] The Soluplus solutions with concentrations greater than 20 % were found to form gels with G' maxima greater than ca. 500 Pa. Increasing the concentration of Soluplus from 20 to 40 % resulted in a decrease in gelation temperature from 40 to 37.5 °C. Preparing the same Soluplus formulations in 25 % ethanol:water mixtures led to a decrease in G' maxima to ca. 10 Pa and prevented the formation of a gel (G' > G''). The gelation properties were unaffected by changes in pH from 7 to 4 but the gelation temperature was found to be decreased to 28.9 from 40 °C upon dissolution in 1M NaCl. Sodium chloride is a member of the Hofmeister series and can induce a 'salting out' effect upon the polymer, which presents itself as a reduction in gelation temperature.[121]

[2.3.3] Poly(2-(N-dimethylamino) ethyl methacrylate), poly(oligoethylene glycol (meth)acrylates) and related poly((meth)acrylate)-based thermogelling materials

[2.3.3.1] Poly(2-(N-dimethylamino) ethyl methacrylate)-based materials

Poly(2-(N-dimethylamino) ethyl methacrylate) (PDMAEMA) has become a popular polymer to be used in the development of smart stimuli responsive materials, due to its response to both pH and temperature in aqueous solution.[122] PDMAEMA is known to exhibit an LCST in aqueous solution between 32.2 – 46.4 °C which is dependent on both molecular weight[123] and concentration, where increasing both either independently or simultaneously leads to a decrease in the LCST.[124] Thus, the temperature at which gelation occurs for PDMAEMA-containing thermogelling materials may be tuned to a physiologically relevant temperature. In addition to this, PDMAEMA is a component of Eudragit® E100 (Figure 2.11), a pharmaceutical grade excipient found on the FDA inactive ingredients database[91] which has been used in targeted drug delivery.[125] There are numerous reports within the literature which discuss the synthesis and characterisation of PDMAEMA thermogelling copolymers, but only a handful of these investigate the reversible thermogelation of the polymer in aqueous solution.
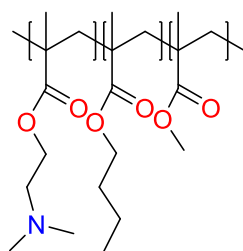
Figure 2. 11: The chemical structure of the pharmaceutical grade excipient Eudragit E100.

To date, no reports of thermogelling PDMAEMA di-block or ABA tri-block copolymers have been found in the literature however, there are reports of thermogelling ABC tri-block copolymers, mostly reported by Georgiou and co-workers. One of these studies was a PMMA-*b*-PDMAEMA-*b*-PNIPAM ABC tri-block copolymer which is shown above in section [2.3.1]. There is another report of a thermogelling ABC tri-block copolymer of poly((ethylene glycol)methyl methacrylate) (PEGMA), poly(n-butyl methacrylate) (PBuMA) and PDMAEMA.[126] This study maintained an ABC tri-block copolymer architecture but varied the ratios of DMAEMA and BuMA as well as their positions within the polymer. The study found all polymers formed aggregates below the LCST of PDMAEMA with average hydrodynamic diameters between 6 and 38 nm. The study showed all polymers in 20 % w/v aqueous solution increased in viscosity with an increase in temperature to ca. 100 Pa. The transition temperature at which this increase in viscosity occurred decreased from ca. 45 to 40 °C when the PDMAEMA degree of polymerisation was increased from 24 to 30. The study also found that when the BuMA block was in the centre of the ABC tri-block copolymer, the critical concentration for gel formation was lower. For example, PEGMA-*b*-PDMAEMA-*b*-BuMA gelled above 30 % w/v while PDEGMA-*b*-BuMA-*b*-PDMAEMA gelled above 20 % w/v. In addition to this, another study found increasing the BuMA molecular weight for a PEGMA-*b*-BuMA-*b*-PDMAEMA copolymer increased the gel strength from 100 to 1000 Pa.[127] The same constituent blocks have been used to synthesise 9 thermogelling tetra-block copolymers (Figure 2.12).[128] Polymers which contained two PDMAEMA blocks formed gels with a strength of ca. 1000 Pa while those with two BuMA blocks formed gels with a strength ca. 100 Pa, which experienced synerisis with increasing temperature. To date, there have not been any studies which investigate the release of therapeutics from thermogelling PDMAEMA block copolymers.
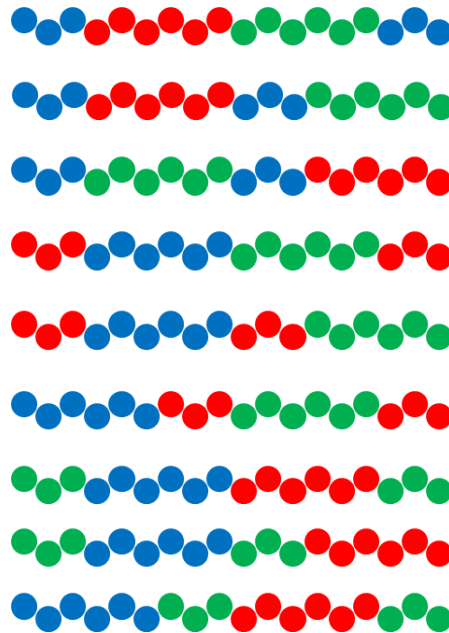
Figure 2. 12: The 9 tetra-block copolymer architectures synthesised using PEGMA (blue), BuMA (red) and PDMAEMA (green).

[2.3.3.1] Poly(oligoethylene glycol (meth)acrylates)

Poly(oligoethylene glycol (meth)acrylates) (POEG(M)As) have gained interest in the development of thermogelling materials due to their range of LCSTs and similarity in structure to the biocompatible polymer PEG. POEGAs have LCSTs ranging from 16.5 to 75.0 °C, which is dependent on the length of the PEG chain on the monomer structure (Figure 2.13).[129,130] This increase in LCST is as a result of the increased hydrophilicity when increasing length of PEG.[130] The POEGAs which have been used to develop thermogelling materials are poly(diethylene glycol ethyl ether acrylate) (PDEGEEA), poly(diethylene glycol methyl ether methacrylate) (PDEGMEMA) and poly(triethylene glycol methyl ether methacrylate) (PTEGMEMA) due to their LCSTs of 16.5, 26 and 52 °C, respectively. The LCSTs of these three polymers are known to be independent of both molecular weight and concentration.[131,132]

16.5 °C   26.0 °C   36.0 °C   45.0 °C   52.0 °C   64.0 °C   75.0 °C

Increasing Hydrophilicity
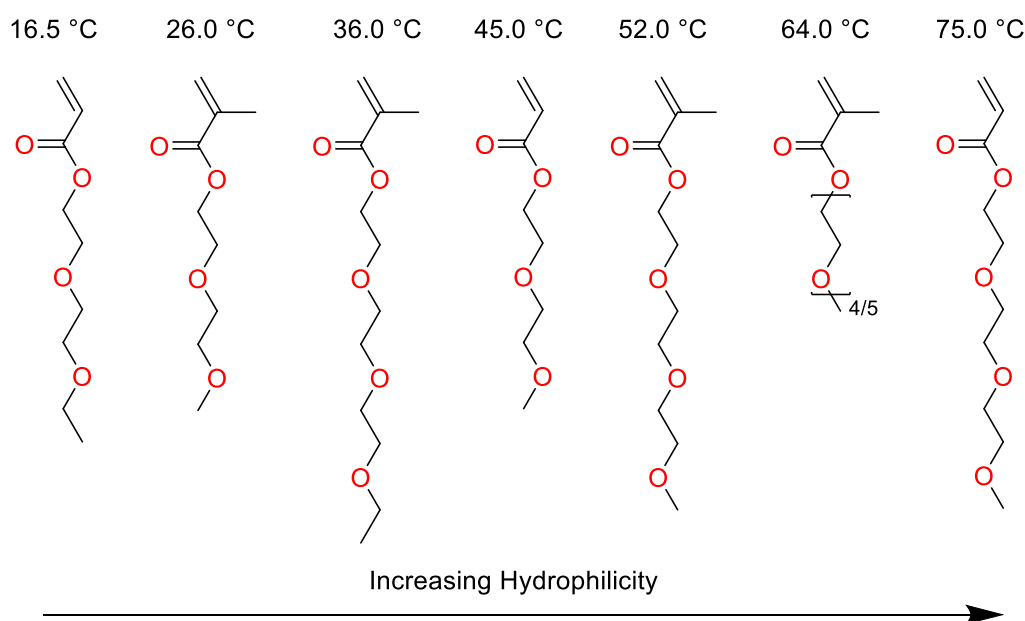
Figure 2. 13: The structures and reported LCSTs of the polymers synthesised from oligoethylene glycol (meth)acrylates.

There is only one report from the literature which describes the synthesis and characterisation of a thermogelling PEOGA containing di-block copolymer. This was a di-block copolymer of PDEGMEMA-*b*-(PTEGMEMA-*co*-PAA) which in 25 % w/v aqueous solution formed gels with a G′ maxima ca. 1000 Pa, but these were only stable between 30 and 45 °C.[133] This gel was found to be resistant to strain amplitudes below 4 %, and the gel yielded above strains of 10 %. In the case of thermogelling tri-block copolymers, there is one study which prepared ABA tri-block copolymers of PDEGEEA-*co*-POEGMA (A) and PEG (B), where the POEGMA monomer contained 9 PEG repeat units.[134] The study found that increasing the PDEGEEA-co-POEGMA degree of polymerisation from 50 to 200, while maintaining 5 % POEGMA, decreased the gelation temperature from 42 to 27 °C, while the gel strength remained constant at ca. 100 Pa. In addition to this, increasing the percent of POEGMA from 0 to 10 % increased the gelation temperature from 19 to 56 °C without altering the strength of the gel. Another key finding from this study was the influence of the PEG central block, which when the molecular weight was increased from 4 to 10 kDa, the gelation temperature fell from 38 to 28 °C, while increasing the gel strength from ca. 10 to 1000. There is one example in the literature of a thermogelling PEOGA containing star shaped block copolymer with a central PEG block and random copolymers of PDEGMEMA and POEGMA with 8 PEG repeat units.[135] This star shaped block copolymer formed a gel with a viscosity of ca. 40 Pa at 38 °C in 25 % w/v aqueous solution. The study found that the gelation temperature fell by ca. 5 °C when using phosphate buffered saline as a

solvent, but the viscosity was not compromised, which is as a result of a salting out effect. To date, studies have not been found which discuss the release of therapeutics from thermogelling POEGA containing block copolymers.

[2.4] Applications of Thermogelling Materials

Poloxamer 407 thermogels have been reported for a variety of uses such as 3D printing,[136,137] depots for tissue regeneration and drug delivery[138,139] and drug delivery to topical sites.[140,141] Therefore, novel thermogelling materials may also have applications in these areas, where polymer design allows for the development of bespoke materials of particular chemical functionality and physical behaviour. One industry which may take advantage of this is 3D printing, which may be used in the manufacture of materials for the aerospace, automotive, building, food and electronic industries.[142] Poloxamer 407 has previously been 3D printed to produce vaginal disks which can carry paclitaxel and rapamycin for the treatment of ovarian cancer bearing mice.[136] These were found to be therapeutically effective and preventative of postsurgical peritoneal adhesion. Both the *in situ* gelling formulation and 3D printed disk were found to exhibit prolonged release, where 80 % and 60 % release of the loaded rapamycin and paclitaxel was achieved after 24 hours, respectively. To replicate their *in vivo* action after implantation, the disks were immersed in 10 mL of PBS and were found to transition from a solid disk to a gel after 40 minutes. The study did not investigate whether the gels formed by the disks and solution were identical but did assume they were. Therefore, if the gels are identical, the formulation residence time, when compared to the solution to gel formulation may only be increased by 40 minutes. Thus, the additional steps and costs required in the manufacturing process may be unnecessary when the compared to the solution to gel poloxamer 407 formulation. In addition to this, PNIPAM grafted hyaluronan with methyl acrylated hyaluronan have been 3D printed to produce scaffolds for the encapsulation and growth of chondrocytes.[143] These cells were found to be viable and as such this polymer may be used to culture a wide range of cell types. In order to maintain the solidity of these scaffold, cross-linking by UV radiation is required. This radiation may be harmful to the cells being cultured, thus limiting their potential applications. Novel thermogelling materials should aim to achieve this prolonged fidelity without the need for harsh cross-linking conditions.

Thermogelling materials may be administered parenterally to produce *in situ* tissue regenerating and drug delivery depots.[144] These gels require long residence times to allow for cell proliferation and tissue growth or prolonged drug delivery.[145] Injected poloxamer gels are known to remain at the injected site for ca. 24 hours which is not ideal for tissue regeneration or long term drug delivery,

where residence may be required for years.[146] Typically, LCST containing *in situ* gelators for tissue regeneration and drug delivery are covalently cross-linked polymers.[147] These polymers are believed to offer greater retention times due to their cross-linked nature but may be difficult to inject due to their greater viscosity even at lower temperatures when compared to non-covalently bonded polymers.[148] Thus, there is a paucity of studies which investigate LCST containing block copolymers as *in situ* tissue regenerators and drug delivery depots. A series of papers by the Matsuda group discuss the preparation of a series of PNIPAM-grafted gelatin copolymers and their tissue regeneration properties investigated.[149–151] This group found that the PNIPAM-gelatin graft copolymers spontaneously formed a smooth muscle cell incorporated 3D gel scaffold at 37 $^{\circ}$C. These cells were distributed throughout the 3D matrix and were successfully cultured for 14 days to yield a tissue.[150,151] Smooth muscle cells were the only cell type investigated in these studies, and the cytotoxicity of PNIPAM is known the be dependent upon cell line.[89] Thus, it is unknown whether these scaffolds may be used to culture alternative tissues.

Poloxamer 407 is the most widely reported thermogelling materials to be investigated for the topical administration of drugs. One study explored the release of etoricoxib and paracetamol from a thermogel consisting of chitosan grafted with PNVCl.[152] An increase in temperature from 25 to 39 °C caused a triggered release of both therapeutics which reached 20 and 100 % release after 3 hours at the respective temperatures (Figure 2.14). Neither the cause of this triggered release or the mechanical properties of the gels were investigated. Particularly, the mechanical properties are of importance when translating such formulations to pharmaceutical applications, as weak gels may offer short residence times. Another study discussed the preparation of chitosan grafted with PNIPAM as a thermogelling ocular drug delivery formulation containing timolol maleate.[153] The *in vivo* studies found the chitosan-g-PNIPAM copolymer delivered ca. 25 µg/ml into the aqueous humor after 10 min, while a conventional eyedrop released ca. 20 µg/ml. This was attributed to the increase in viscosity of the thermogelling formulation which allows for enhanced retention. Although the formulation was found to increase the retention, mechanical properties such as resistance to shear were not investigated, which would allow for a more comprehensive understanding of the formulations.
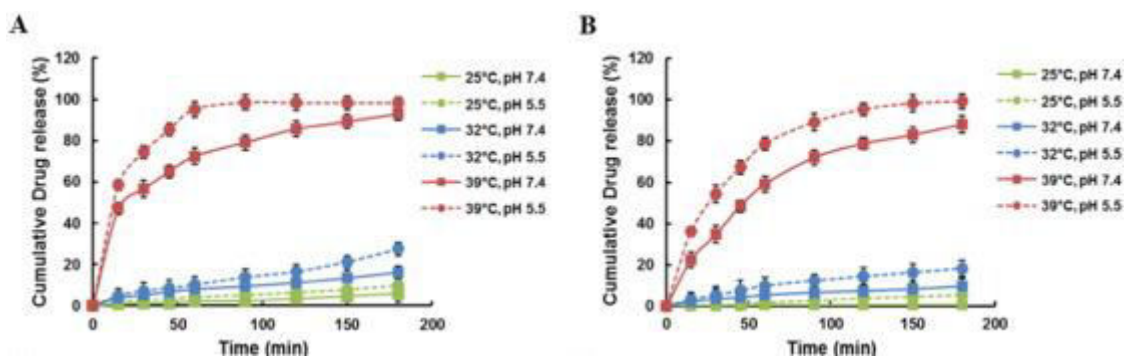
Figure 2. 14: The triggered release of A) etoricoxib and B) paracetamol from the chitosan grafted PNVCl formulation.[152]

Compared to topical drug delivery, the release of therapeutics from parenteral thermogelling drug delivery systems has been investigated to a greater extent. The release of relatively lipophilic drugs and non-therapeutic molecules has been investigated in the literature from novel thermogelling block copolymers. These include paclitaxel,[154] methylene blue[96] and rhodamine[103] which exhibit LogPs of 3.96,[155] 0.75[156] and 1.95,[108] respectively. The release of paclitaxel from what is described as a 'micelle shedding' *in situ* thermogelling formulation containing a PNIPAM-PEG-PNIPAM triblock copolymer has also been investigated.[154] This formulation was found to be give sustained release over 48 hours, but this was investigated in water at 40 °C and in bovine serum at 37 °C. Neither of these conditions are relevant to the delivery of the paclitaxel in humans as the aqueous media was above the physiological range and bovine serum may is not representative of human physiological fluids. The release of methylene blue from a PNIPAM-*b*-POAG copolymer was found to reach 80 % release after 120 hours (Figure 2.15). This release, however, exhibits an initial burst of 50 % after 20 hours, and the final 20 % of methylene blue was not liberated from the gel. A similar trend was observed for the release of methylene blue and rhodamine from thermogelling formulations which used PtBA-*b*-PDMA-*b*-PNIPAM and PNIPAM-*b*-PVP-*b*-PNIPAM, respectively, where 100 % release was achieved after 30 hours.[96,103,157] The reduced release at elevated temperature is suggested to be as a result of an increase in viscosity which hinders the diffusion of drug from the gel matrix. The release of bovine serum albumin (BSA), as a model drug, from a novel poly(2-(N-diethylamino)ethyl methacrylate)-co-PDEGMEMA-co-OEGMA)-*b*-PEG-*b*-poly(2-(N-diethylamino)ethyl methacrylate)-co-PDEGMEMA-co-OEGMA) thermogel has also been investigated.[158] BSA is an water-soluble protein,[159] which is commonly used in cell culture experiments, and may be used to promote tissue regeneration.[160] The release was found to be hindered upon an increase in temperature from 32 to 43 °C, where 20 % release was achieved after 10 and 60 min, respectively.[158] At lower temperatures a micellar gel is not formed, and the copolymer chains are separated in solution, allowing for a rapid

BSA release. Upon an increase in temperature a micellar gel is reported to form, and this creates a tortuous path for the release of BSA, resulting in a slower release. Both studies offer promising candidates as thermogelling formulations for sustained drug delivery. These studies, however, fail to characterise the rheological properties of gels, which may impact their ability to be used as drug delivery formulations. Properties such as resistance to shear stress, dissolution time and polymer stability were not investigated in aqueous media or physiologically relevant fluid. Thus, there is a bridge to gap in the literature between preparation of thermogelling formulations and their translation into pharmaceutical products.
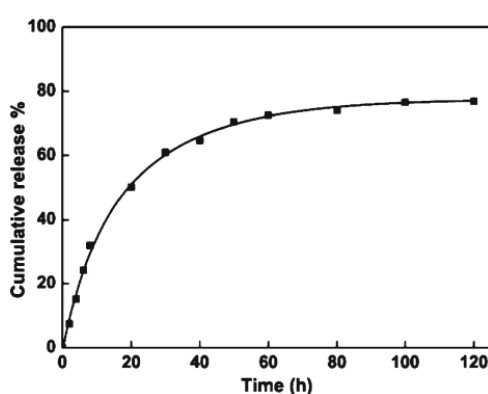
Figure 2. 15: The release of methylene blue from a PNIPAM-b-POAG copolymer over the course of 120 hours.[96]

[2.5.1] Applications of Thermogelling Materials in Topical Drug Delivery

Thermogelling materials may be applicable to the delivery of therapeutics to bodily surfaces, where the formation of a viscous gel may enhance retention and allow for a prolonged localised effect. These thermogels may be applied via an applicator or to the hand and then applied to the afflicted area, where a retentive gel is formed. Currently, these materials are known to prolong the release of therapeutics[161] which may allow for gradual permeating to through the topical membrane or treat afflictions on the surface. In addition to this, these materials may act as a barrier, where for example, anti-retrovirals may be loaded into the formulation and thus prevent the transmission of HIV during sexual intercourse.[162] However, there is a limited number of studies which investigate these materials for topical drug delivery.

[2.5] Conclusions

This literature review has aimed to highlight research concerning thermogelling materials and their applications in drug delivery. Poloxamer 407 has been extensively investigated as a thermogelling drug delivery excipient for both hydrophobic and hydrophilic therapeutics. The literature has identified that the gelation properties of poloxamer 407 may be tuned by varying the polymer concentration, including additives or by preparing co-polymer solutions. These materials can achieve sustained drug release over the course of a few hours, but this is dependent on the residence time of the gel. This residence time is typically short, due to shear thinning character, weak mucoadhesion and prompt dissolution. Furthermore, the high dependence of gelation temperature on concentration means that any uptake of water *in* vivo may result in a rapid gel-to-solution transition, reducing retention.[163] Thus, novel thermogelling systems are required to generate next-generation materials with enhanced performance.

PNIPAM has been investigated in the development of thermogelling materials, significantly more than any other type of LCST exhibiting polymer. Factors including architecture, block molecular weight, additives and polymer concentration, may be used to tune the gelation properties of LCST exhibiting thermogelling materials. In terms of block copolymer architecture, for PNIPAM containing thermogelling materials, increasing the number of temperature responsive blocks results in a stronger gel (i.e. di-blocks typically form weaker gels than tri-block and star shaped block copolymers). The molecular weight of each block can have a profound effect on the gelation, where increasing both blocks can lead to an increase in gel strength. However, increasing the LCST block molecular weight decreases the gelation temperature, while if the remaining block is hydrophilic, the gelation temperature increases. Lastly, increasing the polymer concentration and including additives such as sodium chloride can reduce the gelation temperature without compromising the gel strength. This information may be used to guide the development of novel thermogelling materials with specific gelation characteristics. In addition, this review has highlighted that LCST exhibiting polymers other than PNIPAM may follow the same trends as observed in PNIPAM thermogelling materials. Thus, there is potential to develop novel thermogelling materials with tailored gelation properties using LCST exhibiting polymers which may be safer than PNIPAM and exhibit gelation at a physiologically relevant temperature.

A critical failure of the literature is that the performance of novel thermogelling materials is rarely demonstrated to be superior to existing excipients. Of the literature reviewed, only two tri-block polymers, PNIPAM-b-PEG-b-PNIPAM and PNVCl-b-PEG-b-PNVCl, have been found to form gels which are as strong as those formed by poloxamer 407.[120,164] However, even these studies do not directly

compare the thermogelling materials rheologically, and this comparison was made between publications. The comparison is also only made at a single frequency, which does not describe the true rheological behaviour. Furthermore, comparison to poloxamer 407 in pharmaceutical performance tests was not conducted. Gelation characteristics such as gelation time, resistance to shear stress and mucoadhesion are important features to evaluate when preparing formulations for topical drug delivery.[165] These features may be used to determine the possible target sites that these formulations may be appropriate for. In order to translate these materials into pharmaceutical applications, toxicity, stability and *in vivo* performance testing must also be completed.[166] Thus, there is a need to develop novel thermogelling materials which show beneficial properties in comparison to poloxamer 407 to justify this cost of translating new technologies.

[2.6] References

1   L. E. Bromberg and E. S. Ron, *Adv. Drug Deliv. Rev.*, 1998, **31**, 197–221.

2   L. Yu and J. Ding, *Chem. Soc. Rev.*, 2008, **37**, 1473–1481.

3   C. M. Caramella, S. Rossi, F. Ferrari, M. C. Bonferoni and G. Sandri, *Adv. Drug Deliv. Rev.*, 2015, **92**, 39–52.

4   M. Karimi, A. Ghasemi, P. Sahandi Zangabad, R. Rahighi, S. M. Moosavi Basri, H. Mirshekari, M. Amiri, Z. Shafaei Pishabad, A. Aslani, M. Bozorgomid, D. Ghosh, A. Beyzavi, A. Vaseghi, A. R. Aref, L. Haghani, S. Bahrami and M. R. Hamblin, *Chem. Soc. Rev.*, 2016, **45**, 1457–1501.

5   J. D. Kretlow, L. Klouda and A. G. Mikos, *Adv. Drug Deliv. Rev.*, 2007, **59**, 263–273.

6   M. Patel, H. J. Lee, S. Park, Y. Kim and B. Jeong, *Biomaterials*, 2018, **159**, 91–107.

7   A. Chiappone, E. Fantino, I. Roppolo, M. Lorusso, D. Manfredi, P. Fino, C. F. Pirri and F. Calignano, *ACS Appl. Mater. Interfaces*, 2016, **8**, 5627–5633.

8   L. Zhang, W. Shen, J. Luan, D. Yang, G. Wei, L. Yu, W. Lu and J. Ding, *Acta Biomater.*, 2015, **23**, 271–281.

9   S. Lakkadwala, S. Nguyen, J. Nesamony, A. S. Narang and S. H. Boddu, in *Excipient Applications in Formulation Design and Drug Delivery*, Wolters Kluwer -- Medknow Publications, 2015, vol. 77, pp. 169–199.

10   T. M. Krupka and A. A. Exner, *Int. J. Hyperth.*, 2011, **27**, 663–671.

11   L. Yu, T. Ci, S. Zhou, W. Zeng and J. Ding, *Biomater. Sci.*, 2013, **1**, 411–420.

12   S. Agarwal and J. Seuring, *Macromol. Rapid Commun.*, 2012, **33**, 1898–1920.

13   Q. Zhang, C. Weber, U. S. Schubert and R. Hoogenboom, *Mater. Horizons*, 2017, **4**, 109–116.

14   A. Gandhi, A. Paul, S. O. Sen, K. K. Sen, K. Sen Kumar and K. K. Sen, *Asian J. Pharm. Sci.*, 2015, **10**, 99–107.

15   P. Paricaud, A. Galindo and G. Jackson, *Mol. Phys.*, 2003, **101**, 2575–2600.

16   M. Hasegawa, in *Treatise on Process Metallurgy*, Elsevier Ltd., 2013, vol. 1, pp. 527–556.

17   J. S. Higgins, J. E. G. Lipson and R. P. White, *Philos. Trans. R. Soc. A Math. Phys. Eng. Sci.*, 2010, **368**, 1009–1025.

18   G. D. Smith and D. Bedrov, *J. Phys. Chem. B*, 2003, **107**, 3095–3097.

19   R. L. Montgomery, R. A. Melaugh, C. C. Lau, G. H. Meier, R. T. Grow and F. D. Rossini, *J. Chem. Eng. Data*, 1978, **23**, 245–249.

20   H. W. Kammer, *Acta Polym.*, 1991, **42**, 571–576.

21   J. Heyda, S. Soll, J. Yuan and J. Dzubiella, *Macromolecules*, 2014, **47**, 2096–2102.

22   J. C. Meredith and E. J. Amis, *Macromol. Chem. Phys.*, 2000, **201**, 733–739.

23   K. Van Durme, G. Van Assche and B. Van Mele, *Macromolecules*, 2004, **37**, 9596–9605.

24   P. J. Flory, *J. Chem. Phys.*, 1942, **10**, 51–61.

25   B. Yeon, M. H. Park, H. J. Moon, S.-J. J. Kim, Y. W. Cheon and B. Jeong, *Biomacromolecules*,

2013, **14**, 3256–3266.

26 S. S. Liow, A. A. Karim and X. J. Loh, *MRS Bull.*, 2016, **41**, 557–564.

27 A. P. Constantinou, N. F. Sam-Soon, D. R. Carroll and T. K. Georgiou, *Macromolecules*, 2018, **51**, 7019–7031.

28 P. Zou, J. Suo, L. Nie and S. Feng, *J. Mater. Chem.*, 2012, **22**, 6316–6326.

29 S. S. Liow, Q. Dou, D. Kai, A. A. Karim, K. Zhang, F. Xu and X. J. Loh, *Thermogels: In Situ Gelling Biomaterial*, American Chemical Society, 2016, vol. 2.

30 Z. Li, Z. Zhang, K. L. Liu, X. Ni and J. Li, *Biomacromolecules*, 2012, **13**, 3977–3989.

31 L. Klouda and A. Mikos, *Eur. J. Pharm. Biopharm.*, 2008, **68**, 34–45.

32 A. N. Semenov, J. F. Joanny and A. R. Khokhlov, *Macromolecules*, 1995, **28**, 1066–1075.

33 B. Jeong, S. W. Kim and Y. H. Bae, *Adv. Drug Deliv. Rev.*, 2012, **64**, 154–162.

34 H. Cho and G. S. Kwon, *J. Drug Target.*, 2014, **22**, 669–677.

35 J. Zhu, M. Li, R. Rogers, W. Meyer, R. H. Ottewill, W. B. Russel and P. M. Chaikin, *Nature*, 1997, **387**, 883–885.

36 K. Shi, Y. L. Wang, Y. Qu, J. F. Liao, B. Y. Chu, H. P. Zhang, F. Luo and Z. Y. Qian, *Sci. Rep.*, 2016, **6**, 56–62.

37 M. A. Abou-Shamat, J. Calvo-Castro, J. L. Stair and M. T. Cook, *Macromol. Chem. Phys.*, 2019, **220**, 18–25.

38 A. Blanazs, R. Verber, O. O. Mykhaylyk, A. J. Ryan, J. Z. Heath, C. W. I. Douglas and S. P. Armes, *J. Am. Chem. Soc.*, 2012, **134**, 9741–9748.

39 C. S. Yong, J. S. Choi, Q. Z. Quan, J. D. Rhee, C. K. Kim, S. J. Lim, K. M. Kim, P. S. Oh and H. G. Choi, *Int. J. Pharm.*, 2001, **226**, 195–205.

40 Y. Qiu, S. K. Hamilton and J. Temenoff, in *Injectable Biomaterials: Science and Applications*, Woodhead Publishing, 2011, pp. 61–91.

41 D. R. Perinelli, M. Cespi, S. Pucciarelli, L. Casettari, G. F. Palmieri and G. Bonacucina, *Colloids Surfaces A Physicochem. Eng. Asp.*, 2013, **436**, 123–129.

42 J. Lai, J. Chen, Y. Lu, J. Sun, F. Hu, Z. Yin and W. Wu, *AAPS PharmSciTech*, 2009, **10**, 960–966.

43 Y. Han, S. K. Ahn, Z. Zhang, G. S. Smith and C. Do, *J. Vis. Exp.*, 2016, **112**, 10–16.

44 A. Cabana, A. Aït-Kadi and J. Juhász, *J. Colloid Interface Sci.*, 1997, **190**, 307–312.

45 P. R. Desai, N. J. Jain, R. K. Sharma and P. Bahadur, *Colloids Surfaces A Physicochem. Eng. Asp.*, 2001, **178**, 57–69.

46 P. Alexandridis, J. F. Holzwarth and T. A. Hatton, *Macromolecules*, 1994, **27**, 2414–2425.

47 G. Wanka, H. Hoffmann and W. Ulbricht, *Macromolecules*, 1994, **27**, 4145–4159.

48 P. K. Sharma and S. R. Bhatia, *Int. J. Pharm.*, 2004, **278**, 361–377.

49 K. Mortensen and Y. Talmon, *Macromolecules*, 1995, **28**, 8829–8834.

50 Y. M. Lam, N. Grigorieff and G. Goldbeck-Wood, *Phys. Chem. Chem. Phys.*, 1999, **1**, 3331–3334.

51   A. Fakhari, M. Corcoran and A. Schwarz, *Heliyon*, 2017, **3**, 2–8.

52   E. J. Ricci, L. O. Lunardi, D. M. A. Nanclares and J. M. Marchetti, *Int. J. Pharm.*, 2005, **288**, 235–244.

53   J. Liaw and Y. C. Lin, *J. Control. Release*, 2000, **68**, 273–282.

54   S. Miyazaki, S. Takeuchi, C. Yokouchi and M. Takada, *Chem. Pharm. Bull. (Tokyo).*, 1984, **32**, 4205–4208.

55   Y. Y. Wang, C. T. Hong, W. T. Chiu and J. Y. Fang, *Int. J. Pharm.*, 2001, **224**, 89–104.

56   G. G. Pereira, F. A. Dimer, S. S. Guterres, C. P. Kechinski, J. E. Granada and N. S. M. Cardozo, *Quim. Nova*, 2013, **36**, 1121–1125.

57   G. Dumortier, J. L. Grossiord, F. Agnely and J. C. Chaumeil, *Pharm. Res.*, 2006, **23**, 2709–2728.

58   M. L. Veyries, G. Couarraze, S. Geiger, F. Agnely, L. Massias, B. Kunzli, F. Faurisson and B. Rouveix, *Int. J. Pharm.*, 1999, **192**, 183–193.

59   B. C. Anderson, S. M. Cox, A. V. Ambardekar and S. K. Mallapragada, *J. Pharm. Sci.*, 2002, **91**, 180–188.

60   P. Alexandridis and J. F. Holzwarth, *Langmuir*, 1997, **13**, 6074–6081.

61   E. C. Veerman, M. Valentijn-Benz and A. V. Nieuw Amerongen, *J. Biol. Buccale*, 1989, **17**, 297–306.

62   P. Alexandridis and Y. Lin, *Macromolecules*, 2000, **33**, 5574–5587.

63   C. Chaibundit, N. M. P. S. Ricardo, N. M. P. S. Ricardo, C. A. Muryn, M. B. Madec, S. G. Yeates and C. Booth, *J. Colloid Interface Sci.*, 2010, **351**, 190–196.

64   K. Zhang, X. Shi, X. Lin, C. Yao, L. Shen and Y. Feng, *Drug Deliv.*, 2015, **22**, 375–382.

65   K. Al Khateb, E. K. Ozhmukhametova, M. N. Mussin, S. K. Seilkhanov, T. K. Rakhypbekov, W. M. Lau and V. V. Khutoryanskiy, *Int. J. Pharm.*, 2016, **502**, 70–79.

66   M. Bercea, S. Morariu, L. E. Nita and R. N. Darie, *Polym. - Plast. Technol. Eng.*, 2014, **53**, 1354–1361.

67   M. Bercea, L. E. Nita, S. Morariu and A. Chiriac, *Rev. Roum. Chim.*, 2015, **60**, 787–795.

68   S. C. Shin, J. Y. Kim and I. J. Oh, *Drug Dev. Ind. Pharm.*, 2000, **26**, 307–312.

69   F. Cao, X. Zhang and Q. Ping, *Drug Deliv.*, 2010, **17**, 500–507.

70   J. Chen, R. Zhou, L. Li, B. Li, X. Zhang and J. Su, *Molecules*, 2013, **18**, 12415–12425.

71   J. Brady, T. Drig, P. I. Lee and J. X. Li, in *Developing Solid Oral Dosage Forms: Pharmaceutical Theory and Practice: Second Edition*, Elsevier Inc., 2017, pp. 181–223.

72   D. S. Jones, M. L. Bruschi, O. de Freitas, M. P. D. Gremião, E. H. G. Lara and G. P. Andrews, *Int. J. Pharm.*, 2009, **372**, 49–58.

73   K. Bera, B. Mazumder and J. Khanam, *AAPS PharmSciTech*, 2016, **17**, 743–756.

74   S. C. Shin and J. Y. Kim, *Eur. J. Pharm. Biopharm.*, 2000, **50**, 217–220.

75   M. V. L. B. Bentley, J. M. Marchetti, N. Ricardo, Z. Ali-Abi and J. H. Collett, *Int. J. Pharm.*, 1999, **193**, 49–55.

76 V. Nair and R. Panchagnula, *Pharmacol. Res.*, 2003, **47**, 555–62.

77 O. Pillai and R. Panchagnula, *J. Control. Release*, 2003, **89**, 127–140.

78 E. Giuliano, D. Paolino, M. Fresta and D. Cosco, *Medicines*, 2018, **6**, 7.

79 J. J. Xuan, P. Balakrishnan, D. H. Oh, W. H. Yeo, S. M. Park, C. S. Yong and H. G. Choi, *Int. J. Pharm.*, 2010, **395**, 317–323.

80 G. Niu, F. Du, L. Song, H. Zhang, J. Yang, H. Cao, Y. Zheng, Z. Yang, G. Wang, H. Yang and S. Zhu, *J. Control. Release*, 2009, **138**, 49–56.

81 M. Bhowmik, P. Kumari, G. Sarkar, M. K. Bain, B. Bhowmick, M. M. R. Mollick, D. Mondal, D. Maity, D. Rana, D. Bhattacharjee and D. Chattopadhyay, *Int. J. Biol. Macromol.*, 2013, **62**, 117–123.

82 C. He, S. W. Kim and D. S. Lee, *J. Control. Release*, 2008, **127**, 189–207.

83 O. Inal and E. A. Yapar, *Indian J. Pharm. Sci.*, 2013, **75**, 700–706.

84 S. Van Hemelryck, J. Dewulf, H. Niekus, M. van Heerden, B. Ingelse, R. Holm, E. Mannaert and P. Langguth, *Int. J. Pharm. X*, 2019, **1**, 10–26.

85 K. Jain, R. Vedarajan, M. Watanabe, M. Ishikiriyama and N. Matsumi, *Polym. Chem.*, 2015, **6**, 6819–6825.

86 K. C. Tam, X. Y. Wu and R. H. Pelton, *J. Polym. Sci. Part A Polym. Chem.*, 1993, **31**, 963–969.

87 Y. Zhang, S. Furyk, L. B. Sagle, Y. Cho, D. E. Bergbreiter and P. S. Cremer, *J. Phys. Chem. C*, 2007, **111**, 8916–8924.

88 H. Du, R. Wickramasinghe and X. Qian, *J. Phys. Chem. B*, 2010, **114**, 16594–16604.

89 M. A. Cooperstein and H. E. Canavan, *Biointerphases*, 2013, **8**, 19–25.

90 H. Vihola, A. Laukkanen, L. Valtola, H. Tenhu and J. Hirvonen, *Biomaterials*, 2005, **26**, 3055–3064.

91 FDA, Inactive Ingredient Search for Approved Drug Products, https://www.accessdata.fda.gov/scripts/cder/iig/index.cfm, (accessed 26 January 2020).

92 W. Zhang, L. Shi, K. Wu and Y. An, *Macromolecules*, 2005, **38**, 5743–5747.

93 S. Qin, Y. Geng, D. E. Discher and S. Yang, *Adv. Mater.*, 2006, **18**, 2905–2909.

94 R. Motokawa, K. Morishita, S. Koizumi, T. Nakahira and M. Annaka, *Macromolecules*, 2005, **38**, 5748–5760.

95 H. H. Lin and Y. L. Cheng, *Macromolecules*, 2001, **34**, 3710–3715.

96 Y. Tang, S. Zhang, M. Wang, J. Zhu, T. Sun and G. Jiang, *J. Polym. Res.*, 2014, **21**, 390.

97 L. P. Wang, Y. P. Wang, X. W. Pei and B. Peng, *React. Funct. Polym.*, 2008, **68**, 649–655.

98 X. Liu, S. Luo, J. Ye and C. Wu, *Macromolecules*, 2012, **45**, 4830–4838.

99 M. Teodorescu, I. Negru, P. O. Stanescu, C. Drghici, A. Lungu and A. Sârbu, *React. Funct. Polym.*, 2010, **70**, 790–797.

100 M. Teodorescu, I. Negru, P. O. Stanescu, C. Drăghici, A. Lungu and A. Sârbu, *J. Macromol. Sci. Part A Pure Appl. Chem.*, 2011, **48**, 177–185.

101   M. Sahn, T. Yildirim, M. Dirauf, C. Weber, P. Sungur, S. Hoeppener and U. S. Schubert, *Macromolecules*, 2016, **49**, 7257–7267.

102   L. Ioan, M. Teodorescu, P. O. Stənescu, C. Drəghici, A. Zaharia, A. Sârbu and S. Stoleriu, *J. Macromol. Sci. Part B Phys.*, 2015, **54**, 316–328.

103   H. Cong, J. Li, L. Li and S. Zheng, *Eur. Polym. J.*, 2014, **61**, 23–32.

104   Z. Ge, Y. Zhou, Z. Tong and S. Liu, *Langmuir*, 2011, **27**, 1143–1151.

105   S. E. Kirkland, R. M. Hensarling, S. D. McConaughy, Y. Guo, W. L. Jarrett and C. L. McCormick, *Biomacromolecules*, 2008, **9**, 481–486.

106   A. J. De Graaf, K. W. M. Boere, J. Kemmink, R. G. Fokkink, C. F. Van Nostrum, D. T. S. Rijkers, J. Van Der Gucht, H. Wienk, M. Baldus, E. Mastrobattista, T. Vermonden and W. E. Hennink, *Langmuir*, 2011, **27**, 9843–9848.

107   M. T. Cook, S. K. Filippov and V. V. Khutoryanskiy, *Colloid Polym. Sci.*, 2017, **295**, 1351–1358.

108   N. D. PubChem, Rhodamine B, https://pubchem.ncbi.nlm.nih.gov/compound/Rhodamine-B#section=Solubility, (accessed 10 May 2020).

109   Y. Huang, P. Yong, Y. Chen, Y. Gao, W. Xu, Y. Lv, L. Yang, R. L. Reis, R. P. Pirraco and J. Chen, *RSC Adv.*, 2017, **7**, 28711–28722.

110   J. P. Chen and T. H. Cheng, *Macromol. Biosci.*, 2006, **6**, 1026–1039.

111   D. G. Lessard, M. Ousalem and X. X. Zhu, *Can. J. Chem.*, 2011, **79**, 1870–1874.

112   L. Hou and P. Wu, *Soft Matter*, 2014, **10**, 3578–3586.

113   S. A. Angelopoulos and C. Tsitsilianis, *Macromol. Chem. Phys.*, 2006, **207**, 2188–2194.

114   N. A. Cortez-Lemus and A. Licea-Claverie, *Prog. Polym. Sci.*, 2016, **53**, 1–51.

115   X. Liang, V. Kozlovskaya, C. P. Cox, Y. Wang, M. Saeed and E. Kharlampieva, *J. Polym. Sci. Part A Polym. Chem.*, 2014, **52**, 2725–2737.

116   M. Prabaharan, J. J. Grailer, D. A. Steeber and S. Gong, *Macromol. Biosci.*, 2009, **9**, 744–753.

117   U. Paaver, I. Tamm, I. Laidmäe, A. Lust, K. Kirsimäe, P. Veski, K. Kogermann and J. Heinämäki, *Biomed Res. Int.*, 2014, **2014**, 789765.

118   E. Goethals, S. Verbrugghe, F. Meeussen, H. Berghmans, E. Nies and F. Du Prez, *Polymer (Guildf).*, 2002, **41**, 8597–8602.

119   A. C. Serra, J. R. Góis, J. F. J. Coelho, A. V Popov and J. R. C. Costa, *RSC Adv.*, 2016, **6**, 16996–17007.

120   I. Negru, M. Teodorescu, P. O. Stanescu, C. Draghici, A. Lungu and A. Sarbu, *Mater. Plast.*, 2010, **47**, 35–41.

121   I. Salah, M. A. Shamat and M. T. Cook, *J. Appl. Polym. Sci.*, 2019, **136**, 46915–46922.

122   F. Taktak, *Afyon Kocatepe Univ. J. Sci. Eng.*, 2016, **16**, 68–75.

123   M. Mohammadi, M. Salami-Kalajahi, H. Roghani-Mamaqani and M. Golshan, *Int. J. Polym. Mater. Polym. Biomater.*, 2017, **66**, 455–461.

124   V. Bütün, S. . P. Armes and N. . C. Billingham, *Polymer (Guildf).*, 2001, **42**, 5993–6008.

125   M. Joshi, *Int. J. Curr. Pharm. Res.*, 2013, **5**, 58–62.

126   M. A. Ward and T. K. Georgiou, *J. Polym. Sci. Part A Polym. Chem.*, 2010, **48**, 775–783.

127   I. J. Gomez, B. Arnaiz, M. Cacioppo, F. Arcudi and M. Prato, *J. Mater. Chem. B*, 2018, **6**, 1–3.

128   A. P. Constantinou, N. F. Sam-Soon, D. R. Carroll and T. K. Georgiou, *Macromolecules*, 2018, **51**, 7019–7031.

129   G. Vancoillie, D. Frank and R. Hoogenboom, *Prog. Polym. Sci.*, 2014, **39**, 1074–1095.

130   J. F. Lutz, *J. Polym. Sci. Part A Polym. Chem.*, 2008, **46**, 3459–3470.

131   S. Han, M. Hagiwara and T. Ishizone, *Macromolecules*, 2003, **36**, 8312–8319.

132   J. F. Lutz, K. Weichenhan, Ö. Akdemir and A. Hoth, *Macromolecules*, 2007, **40**, 2503–2508.

133   N. Jin, H. Zhang, S. Jin, M. D. Dadmun and B. Zhao, *J. Phys. Chem. B*, 2012, **116**, 3125–3137.

134   I. Negru, M. Teodorescu, P. O. Stănescu, C. Drăghici, A. Lungu and A. Sârbu, *Soft Mater.*, 2013, **11**, 149–156.

135   N. Badi and J.-F. F. Lutz, *J. Control. Release*, 2009, **140**, 224–229.

136   H. Cho, U. Jammalamadaka, K. Tappa, C. Egbulefu, J. Prior, R. Tang and S. Achilefu, *Mol. Pharm.*, 2019, **16**, 552–560.

137   W. Kempin, V. Domsta, G. Grathoff, I. Brecht, B. Semmling, S. Tillmann, W. Weitschies and A. Seidlitz, *Pharm. Res.*, 2018, **35**, 1–12.

138   Y. Z. Zhao, X. Jiang, J. Xiao, Q. Lin, W. Z. Yu, F. R. Tian, K. L. Mao, W. Yang, H. L. Wong and C. T. Lu, *Acta Biomater.*, 2016, **29**, 71–80.

139   J. F. Pan, N. H. Liu, H. Sun and F. Xu, *PLoS One*, 2014, **9**, 10–26.

140   D. R. Devi, P. Sandhya and B. N. V. Hari, *J. Pharm. Sci. Res.*, 2013, **5**, 159–165.

141   L. Mayol, F. Quaglia, A. Borzacchiello, L. Ambrosio and M. I. L. Rotonda, *Eur. J. Pharm. Biopharm.*, 2008, **70**, 199–206.

142   W. Zhu, J. G. Ock, X. Ma, W. Li and S. Chen, in *3D Bioprinting and Nanotechnology in Tissue Engineering and Regenerative Medicine*, Elsevier Inc., 2015, pp. 25–55.

143   M. Kesti, M. Müller, J. Becher, M. Schnabelrauch, M. D'Este, D. Eglin and M. Zenobi-Wong, *Acta Biomater.*, 2015, **11**, 162–172.

144   M. Kharkar and A. Kloxin, *Injectable Hydrogels for Cell Delivery and Tissue Regeneration*, 2015.

145   H. J. Moon, D. Y. Ko, M. H. Park, M. K. Joo and B. Jeong, *Chem. Soc. Rev.*, 2012, **41**, 4860–4883.

146   M. H. Park, M. K. Joo, B. G. Choi and B. Jeong, *Biodegradable thermogels*, American Chemical Society, 2012, vol. 45.

147   A. Alexander, Ajazuddin, J. Khan, S. S. S. Saraf and S. S. S. Saraf, *Eur. J. Pharm. Biopharm.*, 2014, **88**, 575–585.

148   R. Parhi, *Adv. Pharm. Bull.*, 2017, **7**, 515–530.

149   S. Ohya and T. Matsuda, *J. Biomater. Sci. Polym. Ed.*, 2005, **16**, 809–827.

150   T. Matsuda, *J. Biomater. Sci. Polym. Ed.*, 2004, **15**, 947–955.

151   S. Ohya, S. Kidoaki and T. Matsuda, *Biomaterials*, 2005, **26**, 3105–3111.

152   S. Indulekha, P. Arunkumar, D. Bahadur and R. Srivastava, *Mater. Sci. Eng. C*, 2016, **62**, 113–122.

153   Y. Cao, C. Zhang, W. Shen, Z. Cheng, L. (Lucy) Yu and Q. Ping, *J. Control. Release*, 2007, **120**, 186–194.

154   A. J. De Graaf, I. I. Azevedo Próspero Dos Santos, E. H. E. Pieters, D. T. S. Rijkers, C. F. Van Nostrum, T. Vermonden, R. J. Kok, W. E. Hennink and E. Mastrobattista, *J. Control. Release*, 2012, **162**, 582–590.

155   M. S. Surapaneni, S. K. Das and N. G. Das, *ISRN Pharmacol.*, 2012, **2**, 10–30.

156   N. D. PubChem, Methylene blue, https://pubchem.ncbi.nlm.nih.gov/compound/Methylene-blue#section=Vapor-Pressure, (accessed 10 May 2020).

157   Y. Chen, Y. Gao, L. P. Da Silva, R. P. Pirraco, M. Ma, L. Yang, R. L. Reis and J. Chen, *Polym. Chem.*, 2018, **9**, 4063–4072.

158   Y. Han, S. Liu, H. Mao, L. Tian and W. Ning, *Polymers (Basel).*, 2016, **8**, 367.

159   M. A. Masuelli, *Adv. Phys. Chem.*, 2013, **2013**, 1–8.

160   B. B. Crow and K. D. Nelson, *Biopolymers*, 2006, **81**, 419–427.

161   M. Mora-Pereira, E. M. Abarca, S. Duran, W. Ravis, R. J. McMullen, B. M. Fischer, Y. H. P. Lee and A. A. Wooldridge, *BMC Vet. Res.*, 2020, **16**, 115.

162   M.-D. Veiga-Ochoa, R. Ruiz-Caro, R. Cazorla-Luna, A. Martín-Illana and F. Notario-Pérez, in *Advances in HIV and AIDS Control*, IntechOpen, 2018.

163   K. Edsman, J. Carlfors and R. Petersson, *Eur. J. Pharm. Sci.*, 1998, **6**, 105–112.

164   M. Teodorescu, I. Negru, P. O. Stanescu, C. Drăghici, A. Lungu and A. Sârbu, *React. Funct. Polym.*, 2010, **70**, 790–797.

165   S. C. R. Gandra, S. Nguyen, S. Nazzal, A. Alayoubi, R. Jung and J. Nesamony, *Pharm. Dev. Technol.*, 2015, **20**, 41–49.

166   WHO, Good manufacturing practices: supplementary guidelines for the manufacture of pharmaceutical excipients, https://www.who.int/medicines/areas/quality_safety/quality_assurance/SupplementaryGMPPharmaceuticalExcipientsTRS885Annex5.pdf, (accessed 3 May 2020).

Chapter Three: Development of a Quantitative Structure-Property Relationship Model to Predict the Cloud Points of Poly(acrylate)s and Poly(acrylamide)s in Aqueous Solution.

[3.1] Introduction

This chapter focuses on the development of *in silico* models to predict the cloud point (CP) of polymers which exhibit a lower critical solution temperature (LCST) in aqueous solution. Temperature responsive polymers can be physically characterised by a transition from a clear solution to a turbid one upon an increase in temperature. The temperature at which this transition occurs is known as the cloud point (CP). The LCST and CP are related as the LCST is the lowest temperature at which a CP exists. The experimental determination of the LCST and CP requires synthesis of the corresponding polymer and characterisation using techniques such as ultraviolet-visible (UV) light spectroscopy, dynamic light scattering or by observing a transition from a clear solution to a turbid one. Computational models may offer a cost-effective method and a time saving alternative to these laboratory experiments. Also, these models may provide new information to guide the development of novel polymers which exhibit LCSTs and CPs.

There are two computational models described in the literature which aim to predict the LCSTs of homopolymers.[1,2] These two computational models are both quantitative structure-property relationship models (QSPRs) that use computationally calculated physicochemical properties, or "descriptors", derived from chemical structures to build regression models for the prediction of a desired property. A dataset of polymers and their corresponding LCST in a variety of organic solvents were used to build these models. In both cases, the dataset was split into a training and test set which represented ca. 80 and 20 % of the dataset respectively. The training set was then used to construct the two models (Equations 1a and 1b), and these models were used to predict the LCST of the compounds in the test set.

Equation 1a:

$$\text{LCST} = -166.975 + 53.901 \times \text{X3v(sol)} + 36.305 \times \text{X4v(sol)} - 26.060 \times \text{TII(poly)} + 218.370 \times \text{IVDM(sol)} - 6.420 \times \text{TIC2(sol)} - 89.700 \times \text{Jhete(poly)} + 136.480 \times \text{IC2(sol)} + 148.520 \times \text{BIC2(polY)} + 35.922 \times \text{Jhetv(sol)} - 44.559 \times \text{IVDE(sol)}$$

Equation 1b:

$$\text{LCST} = 33.0 \text{ X DPLL(sol)} - 39.8 \times {}^3\chi^{SG} + 47.3 \times \text{Rad} - 92.1 \times \text{DPLL(poly)} + 95.7 \times \text{ShpC} + 41.4 \times {}^3\chi_p + 0.0371 \times \text{ElcE} - 99.1 \times \text{HOMO} + 32.2 \times \text{SDeg} - 860.7$$

The predictiveness of such models is typically evaluated using the R-squared (r^2) correlation coefficient between the predicted LCSTs and experimental LCSTs of both the training and test set. To compliment this, a parameter known as the q^2 is also used to test model robustness. The q^2 is calculated by leave-one-out cross validation.[3] This entails removal of a data point in the training set and recalculating the r^2. The q^2 is the average of all correlation coefficients after each data point is removed one by one. If the q^2 is considerably less than training r^2 when all data points are present, the training set is highly dependent on the data present. As such, the model may not be generalisable to molecules not used in the development of the model. Typically, models are deemed predictive, robust and generalisable if both the training r^2 and test r^2 values are above 0.6 and the q^2 is above 0.5.[4]
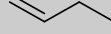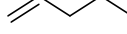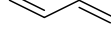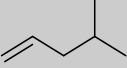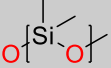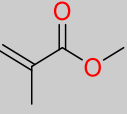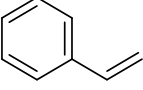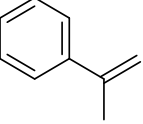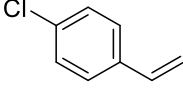
The two models from the literature yielded training r^2 values of 0.8874 (a) and 0.8860 (b), training q^2 values of 0.8658 (a) and 0.8546 (b) and test r^2 values of 0.8016 (a) and 0.8738 (b). Thus, given the criteria above, both models were deemed predictive, robust and generalisable. Both models used properties relating to the solvent and polymer, to predict LCSTs within a range of polymer and solvent mixtures. The descriptors used in both models were topological in nature, calculated based on the atom-atom connectivity within the molecule. The descriptors used in the models described in the literature and their definitions are given in Table 3.1.

Table 3. 1: The definition of the descriptors used in the two QSPR models from the literature given above as Equations 1a and 1b.

Equation 1a		Equation 1b	
Descriptor	**Definition**	**Descriptor**	**Definition**
X3v (Sol)	Valence connectivity index chi-3[5]	**DPLL (Sol)**	Dipole length of the solvent[6]
X4v (Sol)	Valence connectivity index chi-4[5]	$^3\chi^{SG}$	Polymer third order connectivity index contributed by the side groups[7]
TII (Poly)	First Mohar index[8]	**Rad**	Radius[9]
IVDM (Sol)	Mean information content on the vertex degree magnitude[10]	**DPLL (Poly)**	Dipole length of the polymer[6]
TIC2 (Sol)	Total information content index[11]	**SDeg**	Sum of degrees[10]
Jhete (Poly)	Balaban-type index from electronegativity weighted distance matrix[12]	$^3\chi_p$	Solvent third-order connectivity index[7]
IC2 (Sol)	Information content index (neighbourhood symmetry of two-order)[13]	**ElcE**	Total electronic energy given in electron volt at 0 °C[1]
BIC2 (Poly)	Bond information content (neighbourhood symmetry of two-order)[13]	**HOMO**	Energy of the highest occupied molecular orbital[14]
Jhetv (Sol)	Balaban-type index from van der Waals weighted distance matrix[12]	**ShpC**	Shape coefficient (diameter-rad)/rad, where diameter is the maximum such value for all atoms and is held by the most outlying atoms. [15]
IVDE (Sol)	Mean information content on the vertex degree equality[10]		

These solvent and polymer descriptors may be calculated for monomers, which when polymerised, exhibit LCSTs in aqueous solution. However, the two QSPR models described in the literature were built using a dataset of 12 monomers which when polymerised may exhibit an LCST in 66 solvents, not including water.[1,2] Also, the chemical structures of the monomers from the literature (Table 3.2), with the exception of methyl methacrylate, are significantly different to the monomers, which when polymerised, exhibit LCSTs in aqueous solution. For example, this dataset contained monomers which are hydrophobic unsaturated alkenes (e.g. ethylene and propylene) while the majority of polymers which exhibit LCSTs in aqueous solution are similar to N-isopropyl acrylamide, a water-soluble unsaturated acrylamide. In addition to this, the training set used to build the models only contained four reported LCSTs between the water limited range of 0-100 °C due to freezing and boiling, respectively. Therefore, monomers which exhibit LCSTs in aqueous solution are expected to lie outside of the applicability domain of the models described in the literature. As a result of this, these model were deemed inappropriate for the prediction of LCSTs in aqueous solution.

Table 3. 2: The chemical structures and names of the monomers used to build the two QSPR models from literature which aim to predict polymer LCST in organic solvents.

Monomer name and structure		
Ethylene	Propylene	But-1-ene
Isobutylene	Pent-1-ene	1,3-Butadiene
4-Methylpent-1-ene	Dimethylsiloxane	Methyl methacrylate
Styrene	a-Methylstyrene	p-Chlorostyrene

Within the literature, there are many reports of polymers which exhibit LCSTs and CPs in water, such as poly(N-vinyl caprolactam), poly(N-isopropyl acrylamide) and poly(2-(N-dimethylamino)ethyl methacrylate). There are numerous reports of the construction of predictive and robust QSPR models using literature derived databases.[16–18] These models require the structure of the molecules and the variable which is to be predicted. In the case of LCST exhibiting polymers in aqueous solution, generally CPs are reported rather than the more specific LCST. Thus, a database of these polymers and their CPs in aqueous solution can be created and predictive computational models may be derived. These models may be capable of predicting the CPs of novel polymers in aqueous solution. Also, descriptors specific to characterising the CP transition in aqueous solution may be identified.

A QSPR model has not previously been designed to predict the CPs of homopolymers in aqueous solution. As such, this research aims to develop a robust and generalisable predictive model for the prediction of CPs in aqueous solution, using a literature derived dataset. Were such a model developed, it could be used to identify the next generation of novel thermoresponsive homopolymers. These homopolymers may lead to new materials for use in drug delivery, cell culture, tissue engineering and 3D printing.

[3.2] Aims and objectives

The aim of this chapter was to develop a QSPR model which was capable of predicting the CPs of novel temperature-responsive homopolymers in aqueous solution. The aim was explored with the following objectives:

- The literature was searched in order to build a dataset of polymers which exhibit CPs in aqueous solution, including the temperature at which the transition occurs.

- The dataset was split into a training and test set and molecular and polymer descriptors were calculated for all monomers in the dataset.

- QSPR models were built using the training set and the descriptors which correlated strongly to CP.

- The QSPR models were evaluated by predicting the CPs of the test set molecules and investigating the training r^2, training q^2 and test r^2.

- Candidate polymers not used to build the QSPR models were selected, synthesised, characterised.

- The QSPR model which performed best was then used to predict the CP of the synthesised polymers and these were compared to the experimental values.

[3.3] Computational software, materials and methods

QSPR models were built using the Molecular Operating Environment (MOE)[19] (Canada). Tanimoto Coefficients were calculated using OpenBabel[20] (US). Molecular clustering was performed using LibMCS by ChemAxon (US).

2-hydroxyethyl 2-bromoisobutyrate (95 %), Copper (I) Bromide (98 %), N,N,N',N'',N''-Pentamethyldiethylenetriamine (PMDETA) (99 %), N-(3-methoxypropyl)acrylamide (95 %), 4-acryloylmorpholine (97 %), N-(hydroxymethyl)acrylamide solution (48 % in H_2O), N-[3-(dimethylamino)propyl]methacrylamide (99 %), N-hydroxyethyl acrylamide (97 %), tetrahydrofuran (THF) (99.9 %) and 2-propanol (99.5 %) were purchased from Sigma-Aldrich (UK) and used without further purification. Me_6TREN (99 %) was purchased from Alfa Aesar (UK) and used without further purification. Dimethylformamide (DMF) (99 %) was purchased from Fischer Scientific (UK) and used without further purification. Dialysis membrane with molecular weight cut-off (MWCO) of 3.5 kDa was purchased from Medicell Membranes (UK) was hydrated for 30 min in deionised water prior to use. EasiVial mixed poly(methyl methacrylate) (PMMA) gel permeation chromatography (GPC) standards, were purchased from Agilent (UK) and reconstituted in 1 mL DMF with 0.1 % LiBr.

[3.4] Methods

[3.4.1] Development of the QSPR model to predict the CP of temperature responsive polymers in aqueous solution

[3.4.1.1] Dataset development

The dataset of CP exhibiting polymers was identified by searching the literature with the term ("LCST" or "lower critical solution temperature") and "poly*". This term was used on Scopus, then PubMed and finally Google Scholar. Polymers were only selected for inclusion if a CP was given with a published concentration and molecular weight determined by either gel permeation chromatography (GPC) or nuclear magnetic resonance spectroscopy (NMR). The constituent monomer (mCP) of the CP exhibiting polymer was used to develop the QSPR models. The dataset of mCPs from the literature was designated dataset A. The mCPs were "washed" using the wash function of MOE at pH 7.0 to identify monomers which are likely to be protonated in neutral aqueous solution.

[3.4.1.2] Identification of the training and test sets

In QSPR modelling, the model predictability has been proven to be strongly dependent on the structural similarity between the training and test sets, where structurally similar sets perform better than dissimilar sets.[21] To this end, Tanimoto coefficients were used to split the dataset into the training and test sets. Tanimoto coefficients are a measure of pairwise structural similarity, which are calculated using molecules in the form of bit strings (i.e. 0 and 1 digits). The similarity is calculated by identifying the number of bit similarities (c) in the bit strings of two molecules and relating this to the total number of bits present in molecules A (a) and B (b) (Equation 3.2).[22] Tanimoto coefficients range from $0 - 1$, where 1 are two chemicals which are structurally identical.

$$\text{Equation 3.2: Tanimoto Coefficient} = \frac{c}{a + b - c}$$

Considering this, the individual Tanimoto coefficients for each monomer in the dataset were calculated when compared to the remaining monomers in the dataset (i.e. for each monomer in a dataset of 43 molecules, 42 Tanimoto coefficients were calculated). These Tanimoto coefficients for each individual monomer were then averaged and used as a ranking system for assigning molecules to the training and test sets. The mCPs in the dataset were organised in order of increasing CP and

sorted into groups which represented CPs within the ranges of 11-20, 21-30, 31-40, 41-50, 51-60, 61-70 and 71-80 °C.[23] To ensure the test set was representative of the spread of the entire dataset, 20 % of each CP group with the greatest average Tanimoto coefficient were selected for the test set, and the remaining monomers formed the training set.[24] Finally, the training set also contained the upper and lower boundary of CP values found in the dataset.[25]

Following the splitting of the dataset into the training and test sets, a Shapiro-Wilks normality test was performed to ensure the training set was normally distributed (Equation 3.3). Shapiro-Wilks normality test is calculated from constants generated from covariances, variances and means of the sample size (a_i), the ordered random sample values ($x_{(i)}$), the values in the dataset (x_i) and the mean ($\bar{x}$).[26] If a training set is not normally distributed, the model will not able to predict the CP outside of the normal distribution range. This would place limitations upon any predictive model developed.

$$\text{Equation 3.3: } W = \frac{\left(\sum_{i=1}^{n} a_i x_{(i)}\right)^2}{\sum_{i=1}^{n} (x_i - \bar{x})^2}$$

[3.4.1.3] Molecular and polymer descriptor calculation and selection

All 426 molecular descriptors and all 40 polymer descriptors were calculated from MOE[19] for the training set. To prevent giving too much weight to the variables that exhibit high variation ranges due to their units, all descriptors were standardized in Excel to ensure the magnitude of all the descriptors was the same (Equation 3.4). The data was standardised using the selected data point (X_i), the mean (μ) and the standard deviation (σ).

$$\text{Equation 3.4: Standardized Descriptor} = \frac{X_i - \mu}{\sigma}$$

The Pearson correlation of all standardized descriptors to the CPs of the training set were calculated (Equation 3.5). Pearson correlation is calculated using the values in the x and y datasets and the average of each dataset ($\bar{x}$ or $\bar{y}$).

$$\text{Equation 3.5: Pearson Correlation} = \frac{\sum (x - \bar{x})(y - \bar{y})}{\sqrt{\sum (x - \bar{x})^2 \sum (y - \bar{y})^2}}$$

Descriptors which correlated to the CP with correlation coefficients greater than an absolute value of 0.4 were taken forward for further investigation. A Grubbs test (Equation 3.6) was used to determine if any outliers were present within the individual descriptors. Descriptors which contained a significant outlier (P < 0.05), resulted in the removal of the outlying monomer from the data set. Grubbs outliers are calculated using the data point (Y_i), the mean (Y) and the standard deviation (s).

$$\text{Equation 3.6: Grubbs outlier} = \frac{\max\limits_{i=1,\dots,N} |Y_i - Y|}{s}$$

The collinearity (correlation to one another) of the remaining descriptors was used to further narrow the number of descriptors to be used in the construction of QSPR models. Collinear descriptors with correlation coefficients greater than an absolute value of 0.7 were identified, and the descriptor which correlated to the CP least was removed. Following this, the descriptors were iteratively removed in order of increasing relative importance. The relative importance is the ratio of each descriptors correlation coefficient to the largest correlation coefficient i.e. on a scale of 0 to 1. Descriptors which have low relative importance contribute less to the explanation of the variance in the dataset. In this case, having a lesser impact upon the calculation of the CP within the training set.

[3.4.1.4] QSPR model validation

The robustness of the QSPR models was evaluated using leave-one-out cross validation (q^2) (Equation 3.7). The q^2 of the training set QSPR regression line is calculated using the experimental value (y_{exp}), the predicted value (y_{pred}) and the average experimental value (y_{mean}).[27] The calculation is performed by removing each point from the training set, one by one, and recalculating the r^2. The q^2 is then calculated by averaging the r^2 for each instance where a point is removed. Generally, it is accepted that the q^2 should be as close to the training r^2 as possible for the model to be robust.[28] Significant differences in the r^2 and q^2 would indicate a highly variable training set, which will result in a model which is not robust.[29]

$$\text{Equation 3.7: } q^2 = 1 - \frac{\sum_{i-1}^{n}(y_{exp} - y_{pred})^2}{\sum_{i=1}^{n}(y_{exp} - y_{mean})^2}$$

[3.4.1.5] Removal of structurally dissimilar monomers from dataset A

To iteratively improve the QSPR model, mCPs which were structurally dissimilar to the remaining dataset was identified and removed. In order to do this, mCPs with average Tanimoto coefficients less than 0.3 were removed. The new dataset, designated dataset B, was then split into the training and test set as described in [3.4.1.2] and new QSPR models were developed using the approach outlined in sections [3.4.1.3] and [3.4.1.4].

[3.4.1.6] Clustering and Selection of monomers to test the QSPR model

To test the derived QSPR models, 48 commercially available monomers which are not reported to exhibit LCSTs were identified (Appendix; Table A.3). The 48 monomers formed a dataset which was designated dataset C. The monomers of dataset C were clustered by hierarchical clustering using LibMCS by ChemAxon (US). A representative, known as the medoid, from each cluster was identified by selecting the monomer with the greatest average Tanimoto coefficient when compared to the remaining molecules in the cluster. If the medoid of a cluster contained a halogen atom, the cluster was rejected from testing as the selected route of synthesis may result in branched polymers, which the models may not be applicable for. The remaining medoids were then synthesised to a target number-average molecular weight (Mn) of 10 kDa as described below in section [3.3.2.1], and the CP was investigated at 100 mg/mL as described in section [3.3.2.4].

[3.4.2] Synthesis of homopolymers

[3.4.2.1] Synthesis of 10 kDa homopolymers

In a general synthesis, the monomer (Table 3.3), Me_6TREN (80 µL, 300 µmol) and 2-hydroxyethyl 2-bromoisobutyrate (43 µL, 300 µmol) were dissolved in deionised water (20 mL) in a sealed round-bottom flask (Table 3.1). Copper (I) bromide (43 mg, 300 µmol) was placed in a separate flask, which was then sealed. Both flasks were degassed with nitrogen for 30 mins. After degassing, the reaction mixture in water was added to the copper (I) bromide using a degassed syringe and was allowed to stir for 48 h. After 48 h the solutions were concentrated *In Vacuo*, dispersed in THF (10 mL) and passed through neutral alumina. The THF was then removed *In Vacuo* and the resulting product was dissolved in deionised water (50 mL) and dialysed using cellulose dialysis membrane MWCO of 3.5 kDa for 48 h, with regular changing of the dialysis water. The aqueous solutions were then freeze dried.

Table 3.3: The amount of monomer used to synthesise 10 kDa polymers using the monomers identified from the clustering exercise.

Polymer	Monomer (Quantity)
Poly(4-acryloyl morpholine)	4-Acryloyl morpholine (2.67 mL, 21 mmol)
Poly(hydroxyethyl acrylamide)	Hydroxyethyl acrylamide (2.70 mL, 26 mmol)
Poly(hydroxymethyl acrylamide)	Hydroxymethyl acrylamide (5.58 mL, 30 mmol)
Poly(N-([3-(Dimethylamino)propyl]methacrylamide))	N-([3-(Dimethylamino)propyl]methacrylamide) (3.19 mL, 17.6 mmol)
Poly(N-(3-Methoxypropyl)acrylamide)	N-(3-Methoxypropyl)acrylamide (2.93 mL, 21 mmol)

[3.4.2.3] Polymer characterisation

The purified polymers were fully characterised by ^{1}H nuclear magnetic resonance (NMR) spectroscopy, Fourier-transform infra-red (FTIR) spectroscopy and GPC. FTIR spectroscopy was performed on a Perkin Elmer Fourier Transform Infra-red Spectrometer Frontier with a Perkin Elmer Universal ATR Sample Accessory. A wavelength range of 650-4000 cm^{-1} was used with a resolution of 4 cm^{-1}. The instrument was cleaned with isopropyl alcohol before and after use.

^{1}H NMR was performed on an Oxford Instrument ECA600 600 MHz NMR spectrometer with Delta 4.3.6 software. All sampled were measured in D$_2$O unless otherwise stated. All spectra were analysed using MNOVA by Mestrelab (Spain).

Molecular weights were determined using an Agilent 12600 Infinity II GPC equipped with a refractive index (RI) detector. A Phenomenex Phenogel 10 μm 10E5 Å GPC column ran DMF with 0.1 % LiBr as an eluent, at a flow rate of 0.4 mL/min with both the column and detector held at 30 °C. The GPC was calibrated with Agilent Easivial PMMA standards with molecular weights ranging from 370 to 364000 Da (Figure 3.1).
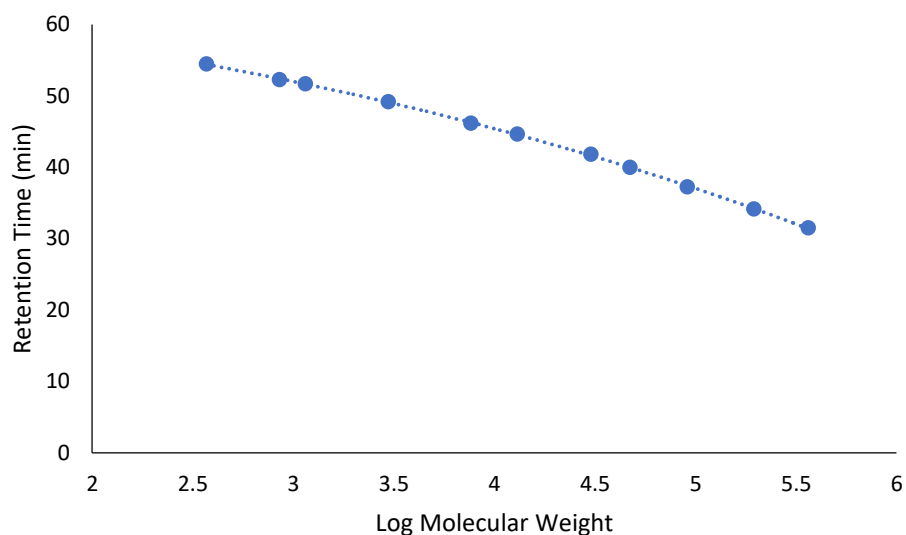
Figure 3.1: The 3rd order narrow calibration polynomial curve of the GPC using Agilent (PMMA) standards.

[3.4.2.4] Identification of the synthetic polymer's CPs

The synthesised polymers were investigated for a CP by preparing 1 mL of 100 mg/mL aqueous polymer solution. The polymer solutions were prepared in sample vials and refrigerated for 24 h. After storage, the vial was immersed in a water bath for 1 min set to 25 °C. If the solution did not go turbid after 1 min, the water bath temperature was increased by 5 °C and equilibrated for 5 min. Following this, the vial was immersed for 1 min again and the solution observed. This was repeated until either the solution became turbid or the water bath reached 95 °C. If a CP was detected the water bath temperature was reduced to the 5 °C increment below which the CP was observed. The water bath was then increased by 1 °C increments and at each increment the polymer solution was immersed for 1 min. The temperature at which the solution became turbid was noted as the cloud point.[30] This was performed in triplicate, and the data presented as a mean ± standard deviation.

[3.5] Results and discussion

[3.5.1] Development of a molecular dataset from CP-exhibiting polymers
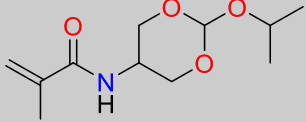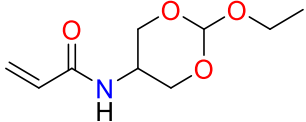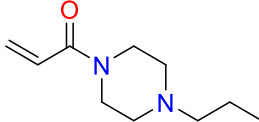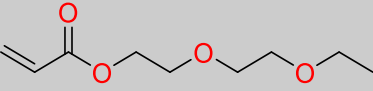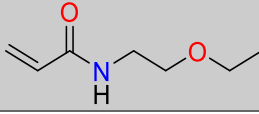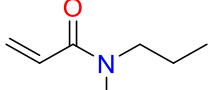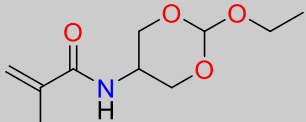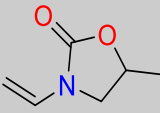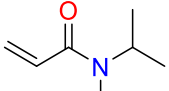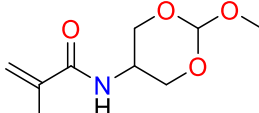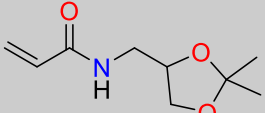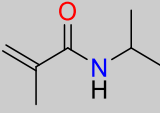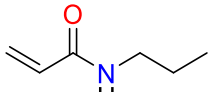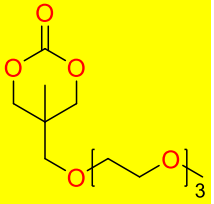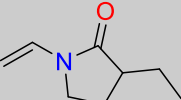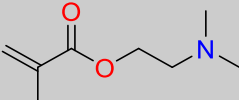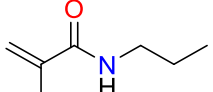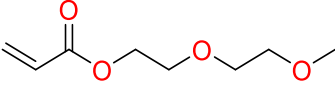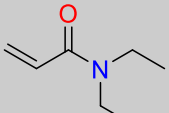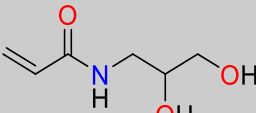
Dataset A, constructed from literature sources, contained 53 mCPs. The quality of QSPR models depends on the dataset used to construct them,[31] and to ensure the quality of the dataset was maximised, only polymers from the literature with reported ^{1}H NMR and GPC characterisation were included in the final dataset. Thus, the number of mCPs in dataset A was reduced from 53 to 45. Table 3.4 shows the 45 mCPs.
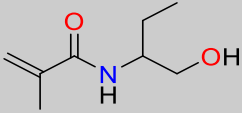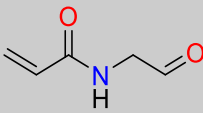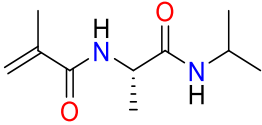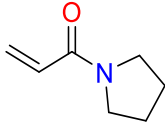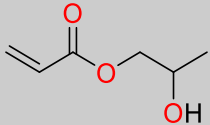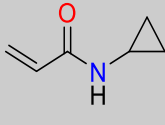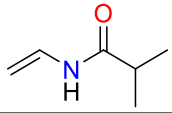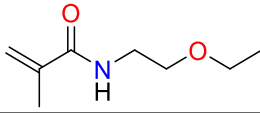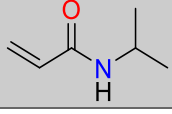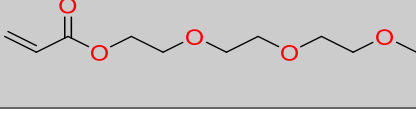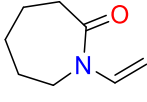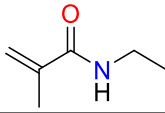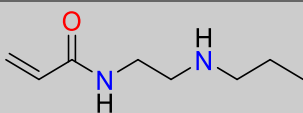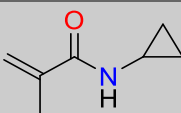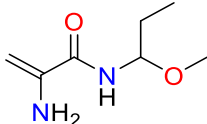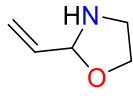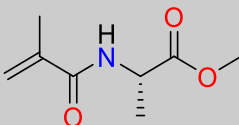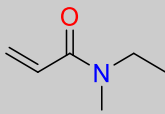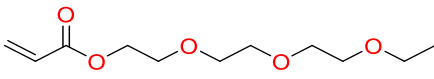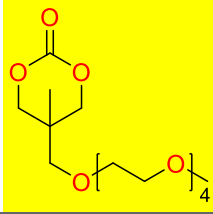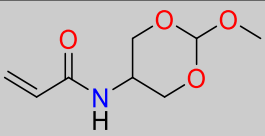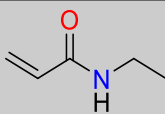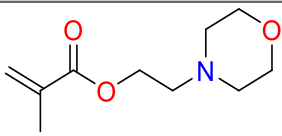
The next criteria for quality control was to screen the structure of the monomer in terms of the technique required to polymerise them. For example, monomers which may be polymerised by radical polymerisation require structures with unsaturated groups. While those which polymerise by condensation polymerisation rely upon the reaction between functionalities such as acyl chlorides and amines. Such variety in functionalities may increase the applicability domain of the QSPR model, which is ideal for a QSPR model. However, there must be enough structural representation of each type of functionality to allow for an accurate prediction.

The dataset of 45 monomers consisted of 43 unsaturated monomers which may only be polymerised by radical polymerisation and 2 which may be polymerised by ring-opening polymerisation. Thus, the 2 structurally different monomers were removed because there was not enough structural representation of this type of monomer. If these monomers were to be included, there would be added noise which would impact the regression of the descriptors to the CP. The monomers which were removed are highlighted in yellow in Table 3.3, the remaining 43 non-highlighted were used to develop QSPR models.

Table 3. 4: Dataset A of mCPs and temperature, in degrees Celsius, at which the CP occurs. Monomers highlighted in yellow were removed from the dataset.

Structure	CP (°C)	Structure	CP (°C)
	11.5[32]		37.0[33]
	12.0[32]		37.0[34]
	16.5[35]		38.0[36]
	19.8[37]		40.0[38]
	21.9[32]		40.0[38]
	22.3[39]		40.6[40]
	23.0[41]		41.2[38]
	25.0[42]		43.0[43]
	27.0[44]		43.2[45]
	28.0[38]		45.0[46]
	28.4[47]		46.0[48]

Structure	CP (°C)	Structure	CP (°C)
	30.0[49]		48.0[48]
	30.0[50]		48.0[38]
	31.7[35]		49.0[42]
	32.0[51]		50.0[36]
	32.0[52]		56.0[53]
	34.0[54]		58.0[42]
	35.0[48]		59.0[42]
	35.0[48]		62.0[55]
	35.0[50]		70.0[56]
	36.0[57]		72.0[43]
	36.3[32]		79.5[56]
	36.3[45]		

[3.5.2] Development of a QSPR model using dataset A

[3.5.2.1] Identification of the training and test sets from dataset A

Figure 3.2 shows the distribution of monomers in the whole dataset (dataset A), training set and test set. This distribution of both the training and test sets are representative of the distribution of dataset A as a whole. The normality of the data distribution in dataset A, training set and test set was investigated using a Shapiro-Wilks test.[58] Dataset A and the training set were found to be distribution were found to have P values of < 0.01, while the test set had a P value of < 0.05. The larger the degree of normal distribution, the larger the CP range the QSPR model may be predictive over. Therefore, the normal distribution to 99 % observed by the training set was deemed acceptable.
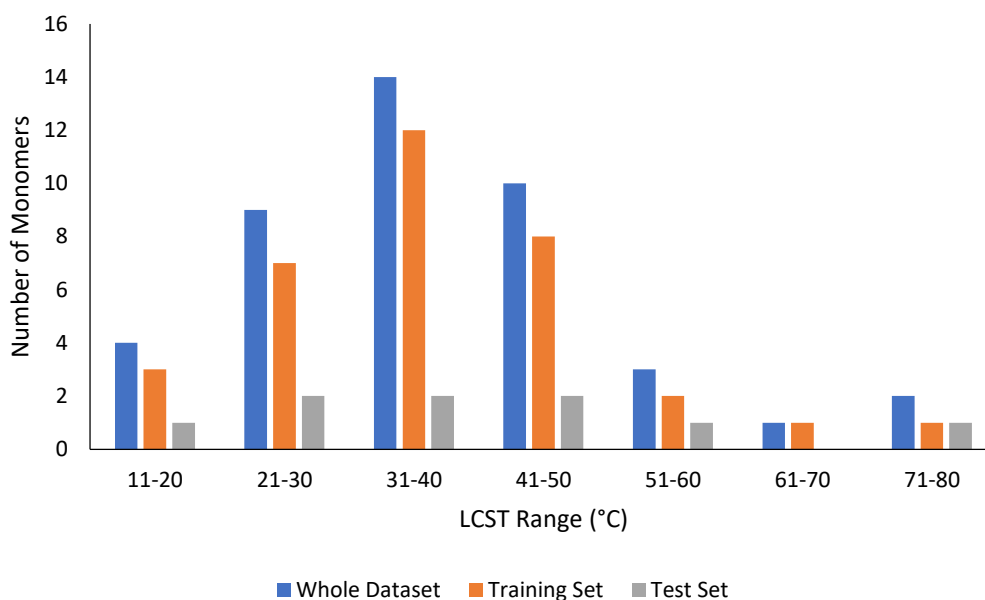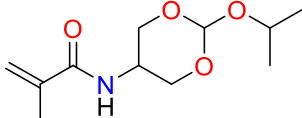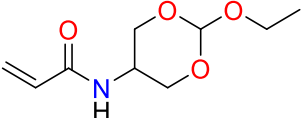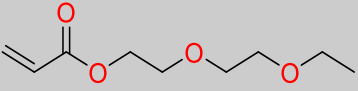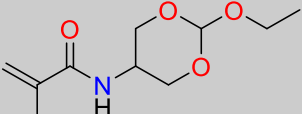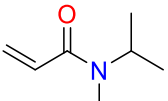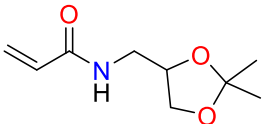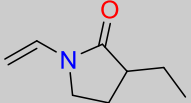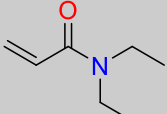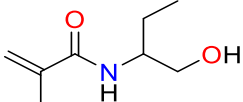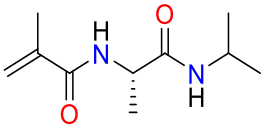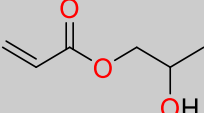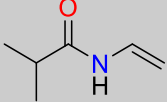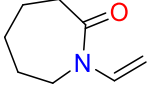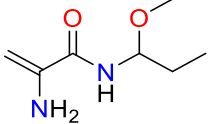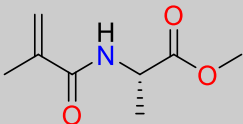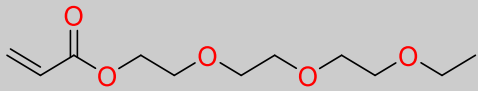
Figure 3.2: The distribution of all 43 mCPs (Blue) in dataset A, the training set (Orange) and test set (Grey) classified by their CP.

The percent split of the entire dataset was 79 and 21 % for the training and test sets respectively. Thus, the training set and test set contained 34 and 9 molecules respectively. The training and test molecules are shown in Table 3.5.

Table 3.5: The names and structures of the compounds in the training and test sets used to construct the initial QSPR model from dataset A.

Name and structure of compound
Training Set

N-(2-isopropoxy-1,3-dioxan-5-yl)methacrylamide

N-(2-ethoxy-1,3-dioxan-5-yl)acrylamide

2-(2-ethoxyethoxy)ethyl acrylate

N-(2-ethoxy-1,3-dioxan-5-yl)methacrylamide

N-isopropyl-N-methylacrylamide

N-((2,2-dimethyl-1,3-dioxolan-4-yl)methyl)acrylamide

3-ethyl-1-vinylpyrrolidin-2-one

N,N-diethylacrylamide

N-(1-hydroxybutan-2-yl)methacrylamide

(S)-N-(1-(isopropylamino)-1-oxopropan-2-yl)methacrylamide

2-hydroxypropyl acrylate

N-vinylisobutyramide

N-vinyl caprolactam

2-amino-N-(1-methoxypropyl)acrylamide

methyl methacryloyl-L-alaninate

2-(2-(2-ethoxyethoxy)ethoxy)ethyl acrylate
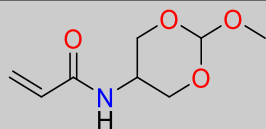
N-(2-methoxy-1,3-dioxan-5-yl)acrylamide
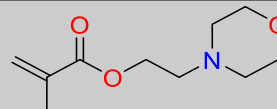
2-morpholinoethyl methacrylate
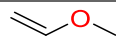
methoxyethene
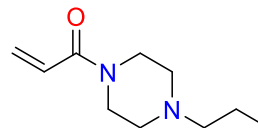
1-(4-propylpiperazin-1-yl)prop-2-en-1-one
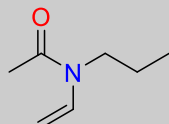
N-propyl-N-vinylacetamide
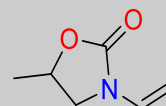
5-methyl-3-vinyloxazolidin-2-one
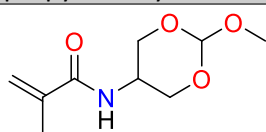
N-(2-methoxy-1,3-dioxan-5-yl)methacrylamide
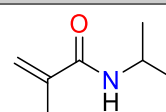
N-isopropylmethacrylamide
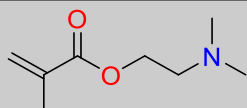
2-(dimethylamino)ethyl methacrylate
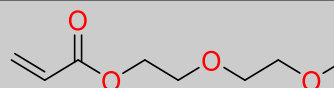
2-(2-methoxyethoxy)ethyl acrylate
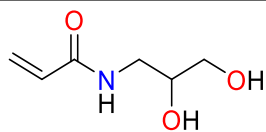
N-(2,3-dihydroxypropyl)acrylamide
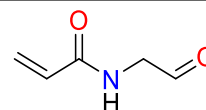
N-(2-oxoethyl)acrylamide
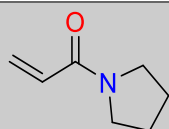
1-(pyrrolidin-1-yl)prop-2-en-1-one
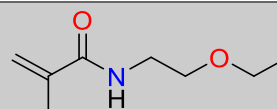
N-(2-ethoxyethyl)methacrylamide
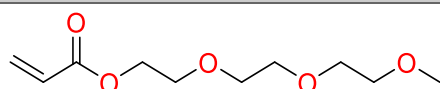
2-(2-(2-methoxyethoxy)ethoxy)ethyl acrylate
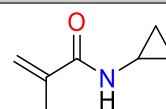
N-cyclopropylmethacrylamide
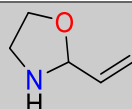
2-vinyloxazolidine
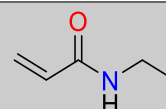
N-ethylacrylamide
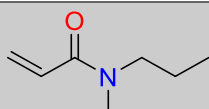
Test Set

N-methyl-N-propylacrylamide
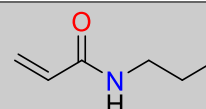
N-propylacrylamide
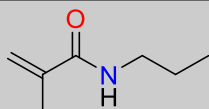
Test Set	
N-propylmethacrylamide	N-isopropylacrylamide
N-(2-(propylamino)ethyl)acrylamide	N-(2-ethoxyethyl)acrylamide
N-cyclopropylacrylamide	N-ethylmethacrylamide
N-ethyl-N-methylacrylamide	
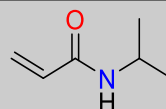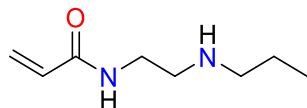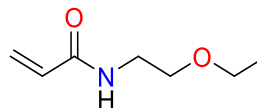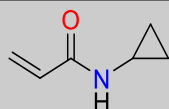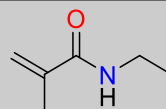
[3.5.2.2] Descriptor selection

All molecular and polymer descriptors available in MOE[19] were calculated for the training set and correlated to the corresponding polymer CP. Of all calculated descriptors, 11 molecular descriptors were found to correlate to the CP with correlations above an absolute value of 0.4 (Appendix; Table A.1). None of these 11 descriptors were found to contain values that were significant outliers according to Grubb's test. The collinearity of these 11 descriptors was investigated by pairwise testing, which resulted in the number of descriptors reducing from 11 to 3. In attempt to build the most robust models possible, the pairs of descriptors which exhibited collinearity had the one removed which had a weaker correlation to the CP. The 3 descriptors taken forward for model development are shown below in Table 3.6.

Table 3.6: The molecular descriptors identified as non-collinear from the training set of the whole dataset with their description, type, Pearson correlation to the CP and relative importance.

Descriptor	Description	Type	Correlation to CP	Relative Importance
DipoleY	The y component of the dipole moment	Electronic	-0.40	0.66
WeinerPol	Weiner polarity number	Steric	-0.46	0.52
Q_VSA_PNEG	Total negative polar van der Waals surface area	Lipophilic/Steric	-0.50	1.00

Molecular descriptors are commonly categorised into three subgroups, those which describe lipophilic, steric or electronic properties of the molecule.[59] These subgroups are not always mutually exclusive, as there are descriptors which may describe properties relating to more than one group. All subgroups of molecular descriptor were represented by the 3 descriptors in table 3.6.

The dipoleY descriptor provides information relating to the distribution of charge across the monomer and as such is an electronic descriptor. DipoleY has previously been reported in the development of a QSPR with the aim of predicting the CP of non-ionic surfactants, although the importance of this descriptor was not investigated.[60] In this case, the negative correlation of -0.40 between dipoleY and CP indicates monomers with larger dipoles result in polymers with CP at lower temperatures. Thus, it is theorised that the magnitude of this dipole moment may impact upon the structure the polymer takes when in aqueous solution. If the dipole moment favours polymer-polymer interactions, there may be fewer water-polymer bonds which is expected to result in a reduced CP. This may result in a greater change in enthalpy of mixing and thus a more ordered system. A more ordered system would require less energy (i.e. lower temperature) to change the Gibbs free energy of mixing from negative to positive resulting in precipitation.

Q_VSA_PNEG is the total polar negative van der Waals surface area and thus is a lipophilic/steric descriptor. CASA- has not previously been used to explain the solubility of molecules, but Q_VSA_PNEG has. The total polar negative van der Waals surface area has been reported to be positively correlated to the solubility of proteins in polar media.[61] For the descriptors identified in this report, polymer solubility is being assessed and as a result the correlation may be different. The Q_VSA_PNEG descriptor was negatively correlated to the CP, which suggests monomers with low negative surface areas polymerise to yield polymers with CPs at elevated temperatures. Upon dissolution, these polymers may form structures with ordered water molecules at the surface as the polymer is expected to arrange to maximise the contact area between the water and the negative

van der Waals surface area. As such, these polymer solutions may require a greater degree of heat to release the ordered water and induce precipitation.

The final descriptor is the Wiener polarity number (WeinerPol) was found to increase with a decreasing CP, with a correlation coefficient of -0.46. WeinerPol is a topological descriptor which provides information on how atoms in a molecule are connected to one another, and as such is classified as a steric descriptor. Specifically, WeinerPol is the number of atoms which are separated by at least 3 edges (i.e. 3 atoms). The correlation between WeinerPol and CP indicates larger monomers, when polymerised, result in polymers with lower CPs. For example, N-(2-isopropoxy-1,3-dioxan-5-yl)methacrylamide has a WeinerPol of 19 and a CP of 11.5 °C, while N-ethylacrylamide has a WeinerPol of 5 and a CP of 79.5 °C. To date, WeinerPol has not previously been used in the prediction of solubility. Therefore, it is hypothesised that polymers synthesised from larger monomers may exhibit more hydrophobic character and are less soluble in aqueous media. Thus, the energy required to induce precipitation is reduced for monomers with a greater WeinerPol.

Two QSPR models were developed using the 3 descriptors identified above. The first model included all descriptors, and then the second model contained only dipoleY and Q_VSA_PNEG, as WeinerPol was deemed less important by the computational software MOE.[19] The 2 QSPR model equations are given below as Equations 3.5a and b.

<u>a) 2 Descriptor Model:</u>

$$CP = 38.49706 - 4.12597 \times dipoleY - 6.22309 \times Q\_VSA\_PNEG - 3.22228 \times WeinerPol$$

<u>b) 1 Descriptor Model:</u>

$$CP = 38.49706 - 5.44566 \times dipoleY - 7.22107 \times Q\_VSA\_PNEG$$

When evaluating the models as a whole, the negative correlation coefficients exhibited by all descriptors indicate these are penalty terms. In addition to this, Q_VSA_PNEG exhibit the greatest correlation coefficient and as such can be considered more important when explaining the variation in CP within the training set. Q_VSA_PNEG is a steric/lipophilic descriptor, indicating that these properties are dominant over electronic properties. Thus, in order for a polymer to exhibit an LCST at reduced temperature, the monomer will be more lipophilic.

[3.5.2.3] Testing the QSPR models built using dataset A

The QSPR models above were evaluated in terms of predictivity, robustness and generalisability using the training r^2, training q^2 and test r^2 values, respectively (Table 3.7). For a QSPR model to be classified as predictive and robust, the training r^2 should ideally be greater than 0.6 and the training q^2 should be within 0.3 of the training r^2.[62] The test r^2 however should be as close to training r^2 but not greater than it otherwise the model is at risk of being overfitted. An overfitted model is one which contains more descriptors than can be justified by the data, which adds noise to the prediction. Using fewer descriptors than recommended reduces the risk of overfitting as noise is less likely to be used in the model.

Table 3. 7: The training r^2, training q^2 and test r^2 of the three QSPR models 1-A and 1-B built using dataset A.

Model Code	Number of Descriptors in the Model	Training r^2	Training q^2	Test r^2
1-A	3	0.40	0.23	0.02
1-B	2	0.37	0.26	0.01

Both models are not ideal for the use as a predictive model, given the low training r^2, training q^2 and test r^2 which indicate that the model is not predictive, robust or generalisable. The best model of the two was model 1-A, due to it observing the greatest training r^2 and test r^2.

To understand why these models performed poorly, the accuracy of the individual predictions observed for molecules in the training and tests for dataset A were evaluated by investigating the deviation of the predicted CP from the experimental value (Table 3.8). In this study CPs which were predicted greater than an absolute value of 10 °C from their experimental value were identified for investigation. This deviation was selected due to the limited range at which aqueous CPs may exist. For the training set, 12 of the 34 molecules present exhibited a difference in experimental and predicted CPs which was greater than an absolute value of 10 °C. These 12 molecules belong to three types of substructures present within the dataset; those with cyclic structures in the pendant group (5), those which contain PEG-like chains (3) and acrylamides (4). Of the 5 monomers incorrectly predicted with cyclic pendant groups consisted of 2 acrylamides, 2 N-vinyl monomers and one cyclic vinyl monomer. In the training set there were 6 acrylamides with cyclic groups, 3 N-vinyl monomers with cyclic groups and the single cyclic vinyl monomer. Thus, the failure of N-vinyl monomers and single cyclic vinyl monomer are as a result of a lack of structural representation within the training a set. The 2 acrylamides with cyclic groups, however, lie at the extremes of the
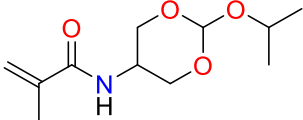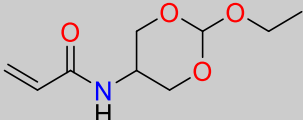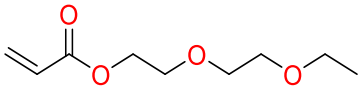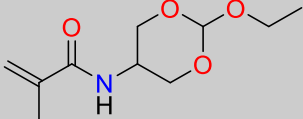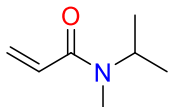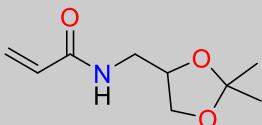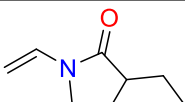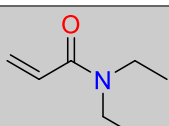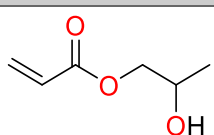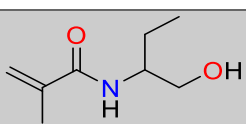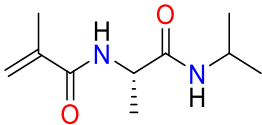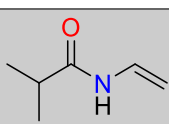
dataset, below 20 and above 40 °C. These two failures are thought to be as a result of a lack of structural representation at these two points in the data set.

The three monomers with PEG-like chains which were inaccurately predicted in the data set were 2-(2-ethoxyethoxy)ethyl acrylate, methoxyethene and 2-(2-(2-methoxyethoxy)ethoxy)ethyl acrylate. These types of monomer make up 5 of 34 monomers present in the training set, and those which were wrongly predicted were randomly distributed throughout the dataset. As such, their incorrect predictions are thought to be as a result of structural underrepresentation within the training set.
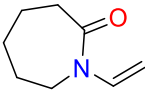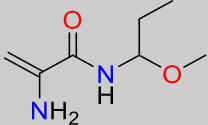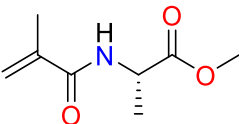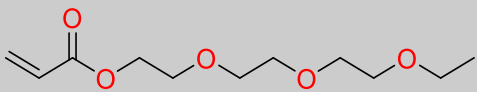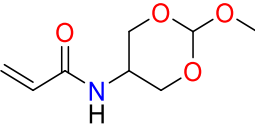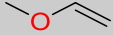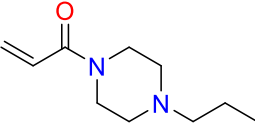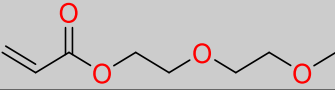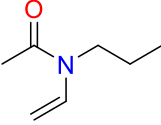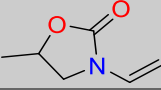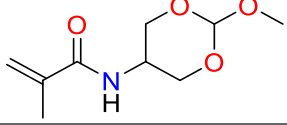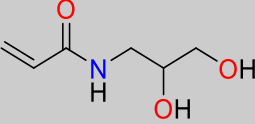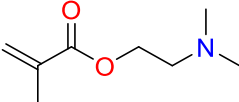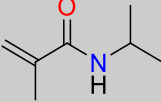
The acrylamide monomers which were predicted incorrectly, with a difference greater than 10 °C, were N-isopropyl-N-methylacrylamide, (S)-N-(1-(isopropylamino)-1-oxopropan-2-yl)methacrylamide N-isopropylmethacrylamide and N-ethylacrylamide with reported CPs of 22.3, 30.0, 48.0 and 79.5 °C, respectively. Given the fact that these are acrylamides, and acrylamides made up 21 of the 34 monomers in the training set, these were expected to be predicted accurately. The incorrect CP prediction for N-isopropyl-N-methylacrylamide may be as a result of underrepresentation of this type of monomer below 28.6 °C, as out of seven monomers below this point, only one was an acrylamide. In the case of (S)-N-(1-(isopropylamino)-1-oxopropan-2-yl)methacrylamide, the prediction may have been false due to the structural complexity of the monomer, as there are only two monomers in the dataset which show a second amide functionality present. This is likely to not be enough information to allow for an accurate prediction. For N-isopropylmethacrylamide and N-ethylacrylamide, their failure is thought to be as a result structural underrepresentation above 48 °C, as there were only 9 monomers which cover the CPs from 48 to 79.5 °C.
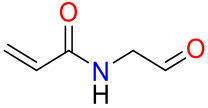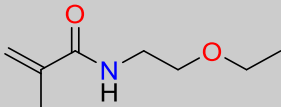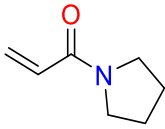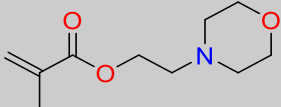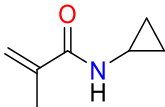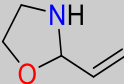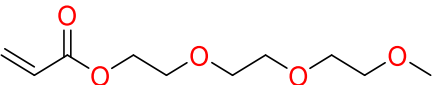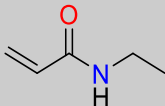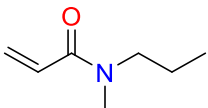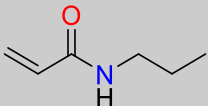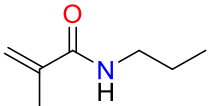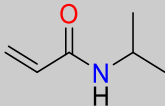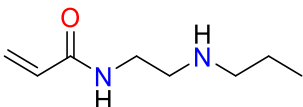
In terms of the test set, monomers which exhibited a reported CP between 28.0 and 58.0 °C were predicted accurately with a difference less than an absolute value of 10 °C. The inaccurate prediction outside of this range is expected to be as a result of underrepresentation of CPs either less than 28.0 °C or greater than 58.0 °C. The two incorrectly predicted monomers with experimental CPs below 28.0 °C were N-propylacrylamide and N-propylmethacrylamide, both of which are structurally very similar. In the training set, below 28.0 °C there was only 1 N-alkyl acrylamide out of 7 monomers therefore, monomers like N-propylacrylamide and N-propylmethacrylamide are underrepresented. Above 58.0 °C in the test set, N-ethylmethacrylamide and N-ethyl-N-methacrylamide were the only monomers present with experimental CPs of 58.0 and 70.0 °C, respectively. These incorrect predictions were likely to be as a result of underrepresentation of CPs above 50.0 °C within the training set, as there was only 7 monomers present in to represent the 50 to 80 °C range. As such, these monomers were not expected to be predicted correctly due to a lack of information available.
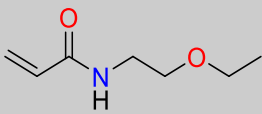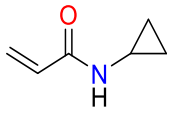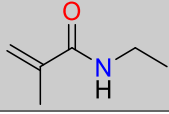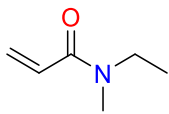
Table 3. 8: The structures, experimental CP, predicted CP using QSPR model 1-B and the absolute difference between these for the training and test sets derived from dataset A.

Training Set			
Monomer Structure	Experimental CP (°C)	Predicted CP (°C)	Difference (°C)
	11.5	17.7	6.2
	12.0	24.8	12.8
	16.5	37.8	21.3
	18.8	22.8	4.0
	22.3	36.3	14.0
	23.0	31.7	8.7
	27.0	42.8	15.8
	28.6	35.9	7.3
	29.5	38.6	9.1
	30.0	29.1	-0.9
	30.0	14.7	-15.3
	32.0	36.4	4.4

Training Set			
Monomer Structure	Experimental CP (°C)	Predicted CP (°C)	Difference (°C)
	34.0	47.1	13.1
	35.0	33.6	-1.4
	35.0	28.0	-7.0
	36.0	37.1	1.1
	36.3	32.5	-3.8
	37.0	59.1	22.1
	37.0	38.1	1.1
	38.0	45.6	7.6
	40.0	37.7	-2.3
	40.0	45.8	5.8
	40.6	30.5	-10.1
	46.0	42.8	-3.2
	46.4	48.8	2.4
	48.0	37.4	-10.6

Training Set			
Monomer Structure	**Experimental CP (°C)**	**Predicted CP (°C)**	**Difference (°C)**
	48.0	43.2	-4.8
	50.0	42.9	-7.1
	51.5	51.5	0.0
	53.4	43.9	-9.5
	59.0	52.1	-6.9
	62.0	50.5	-11.5
	75.0	44.9	-30.1
	79.5	47.3	-32.2

Test Set			
Monomer Structure	**Experimental CP (°C)**	**Predicted CP (°C)**	**Difference (°C)**
	19.8	27.8	8.0
	23.2	45.5	22.3
	28.0	40.9	12.9
	32.0	30.5	-1.5
	35.0	35.1	0.1
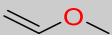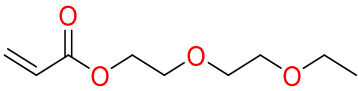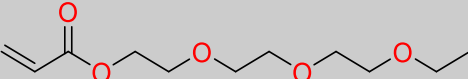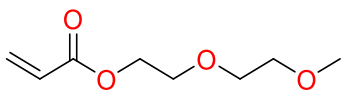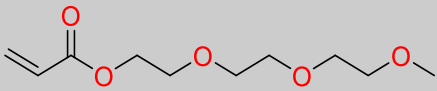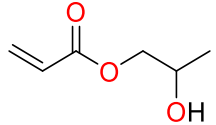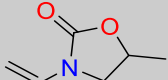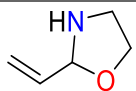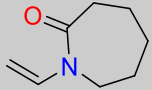
Test Set			
Monomer Structure	Experimental CP (°C)	Predicted CP (°C)	Difference (°C)
	38.0	37.6	-0.4
	49.0	55.2	6.2
	58.0	43.5	-14.5
	70.0	30.4	-39.6

[3.5.3] Development of a QSPR model using dataset B

[3.5.3.1] Optimisation of dataset A

None of the models derived above in section [3.5.2] were predictive or generalisable. The greatest training r^2 achieved was 0.40, which indicates the model is capable of explaining 40 % of the variance in the CPs. In attempt to increase the predictability and generalisability of the QSPR model, monomers which were identified as structurally dissimilar were removed from dataset A.[63] Nine monomers had an average pairwise Tanimoto coefficient less than 0.3 and were subsequently removed from dataset A (Table 3.9). The dataset was reduced from 43 mCPs to 34, and was named dataset B. The monomers removed from dataset A belong to two main classes of monomer; those with oligoethylene glycol chains and those with cyclic structures. These included many of the monomers which were predicted incorrectly as shown above in Table 3.8, so their inaccurate prediction may have been as a result of structural dissimilarity. Removal of structurally different molecules from a dataset may improve the QSPR model by removing noise from both the training and test set which may negatively impact the model predictability.[4] The trade off in achieving improved prediction is that the applicability domain of the model is reduced, as less functionalities are present.

Table 3. 9: The molecules which were identified as structurally dissimilar (average Tanimoto < 0.3) to the remaining dataset and were consequently removed from the dataset.

Molecule	Average Tanimoto
	0.08
	0.25
	0.25
	0.25
	0.25
	0.25
	0.27
	0.28
	0.29

[3.5.3.2] Identification of the training and test sets from dataset B

Figure 3.4 shows the distribution of the data in dataset B, and the training and test sets identified from this dataset. Dataset B and the resulting training set and test set were all found to be normally distributed with confidence intervals of $P < 0.10$, $P < 0.05$ and $P < 0.01$, respectively.
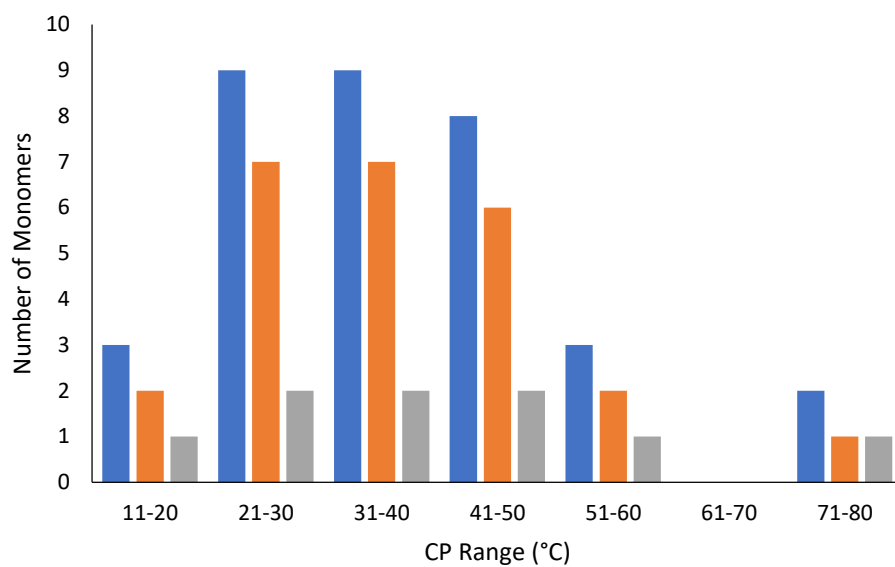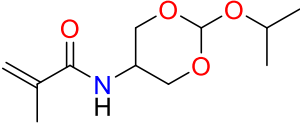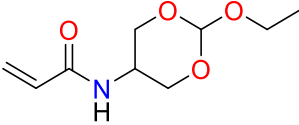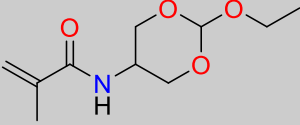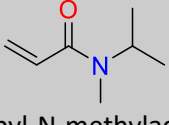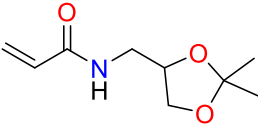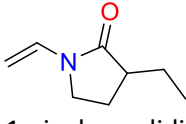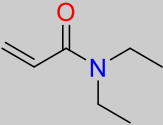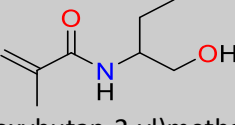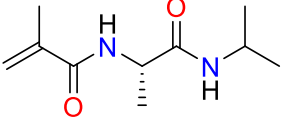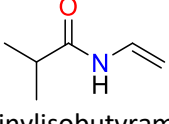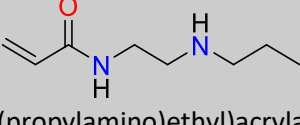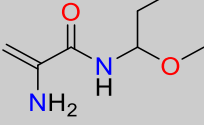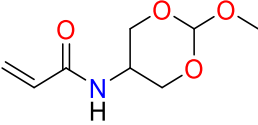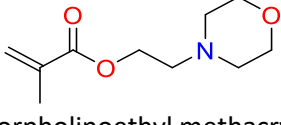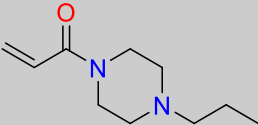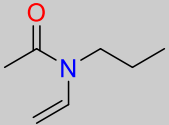
Figure 3.3: The distribution of the remaining 34 monomers (Blue) in dataset B, the training set (Orange) and test set (Grey) classified by their CP.

The percent split of the entire date set was 74 and 26 % for the training and test sets respectively. Thus, the training set and test set contained 25 and 9 molecules respectively. The training and test molecules are shown in Table 3.10.

Table 3. 10: The names and structures of the compounds in the training and test sets used to construct the QSPR model using dataset B.

Name and structure of compound
Training Set

N-(2-isopropoxy-1,3-dioxan-5-yl)methacrylamide

N-(2-ethoxy-1,3-dioxan-5-yl)acrylamide

N-(2-ethoxy-1,3-dioxan-5-yl)methacrylamide

N-isopropyl-N-methylacrylamide

N-((2,2-dimethyl-1,3-dioxolan-4-yl)methyl)acrylamide

3-ethyl-1-vinylpyrrolidin-2-one

N,N-diethylacrylamide

N-(1-hydroxybutan-2-yl)methacrylamide

(S)-N-(1-(isopropylamino)-1-oxopropan-2-yl)methacrylamide

N-vinylisobutyramide

N-(2-(propylamino)ethyl)acrylamide

2-amino-N-(1-methoxypropyl)acrylamide

N-(2-methoxy-1,3-dioxan-5-yl)acrylamide

2-morpholinoethyl methacrylate

1-(4-propylpiperazin-1-yl)prop-2-en-1-one

N-propyl-N-vinylacetamide

Training Set
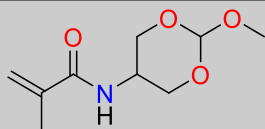
N-(2-methoxy-1,3-dioxan-5-yl)methacrylamide
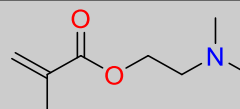
2-(dimethylamino)ethyl methacrylate
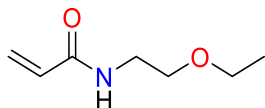
N-(2-ethoxyethyl)acrylamide
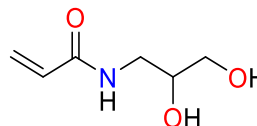
N-(2,3-dihydroxypropyl)acrylamide
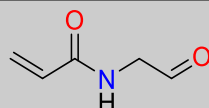
N-(2-oxoethyl)acrylamide
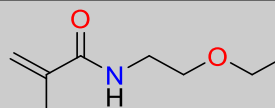
N-(2-ethoxyethyl)methacrylamide
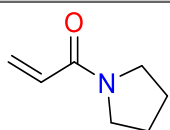
1-(pyrrolidin-1-yl)prop-2-en-1-one
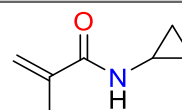
N-cyclopropylmethacrylamide
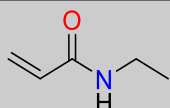
N-ethylacrylamide

Test Set
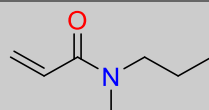
N-methyl-N-propylacrylamide
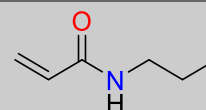
N-propylacrylamide
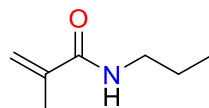
N-propylmethacrylamide

N-isopropylacrylamide
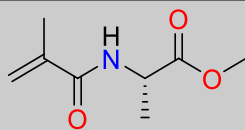
methyl methacryloyl-L-alaninate
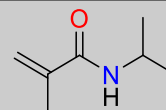
N-isopropylmethacrylamide
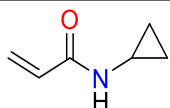
N-cyclopropylacrylamide
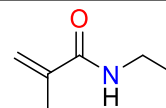
N-ethylmethacrylamide
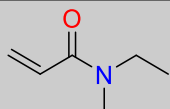
N-ethyl-N-methylacrylamide

[3.5.3.3] Descriptor selection

The molecular and polymer descriptors for dataset B were correlated to the CPs of the molecules without those which were identified as structurally dissimilar. No polymer descriptors were found to correlate to the CP whereas, the number of molecular descriptors with a correlation to CP greater than an absolute value of 0.4 increased from 11 to 105 (Appendix; Table A.2). The increase in the number of correlated descriptors indicated the removal of monomers which were structurally dissimilar may have removed unwanted noise from the data. Grubbs outlier test on the individual descriptor values found none of the 105 descriptors contained a significant outlier. The collinearity of the 104 standardized descriptors was investigated and were subsequently reduced from 104 to 8, which did not exhibit collinearity. Due to the size of the training set, a maximum number of 5 descriptors could be used in the QSPR model, otherwise the data was at risk of being overfitted.[4] Therefore, the 3 descriptors which had the lowest relative importance were removed leaving the 5 most important descriptors to be used to build QSPR models (Table 3.11).

Table 3. 11: The molecular descriptors identified as non-collinear from the training set of dataset B with their description, type, Pearson correlation to the CP and relative importance.

Descriptor	Description	Type	Correlation to CP	Relative Importance
GCUT_PEOE_3	Partial equalization of orbital electronegativities	Electronic	-0.59	0.82
h_emd_C	Sum of hydrogen bond donor strengths of carbon atoms	Lipophilic	-0.47	0.29
Q_RPC-	Relative negative partial charge	Electronic	0.63	0.43
Q_VSA_PNEG	Total negative polar van der Waals surface area	Steric/Lipophilic	-0.57	1.00
Std_dim3	Standard dimension 3	Steric	-0.62	0.32

Between the two datasets, Q_VSA_PNEG is the only descriptor which is common to both. Upon the removal of structurally dissimilar monomers, the absolute correlation to CP increased from 0.50 to 0.57. This is a result of removing structurally dissimilar monomers from the dataset, which were adding noise to the correlation of this descriptor. Upon removing those structurally dissimilar monomers, new descriptors GCUT_PEOE_3, h_emd_c, Q_RPC- and std_dim3 emerged with a correlation to the CP above an absolute value of 0.4.

Given that 5 descriptors were identified, 4 QSPR models were produced where the number of descriptors was reduced sequentially from 5 to 2 by removing the least important descriptor (Equations 3.6a, b, c and d). Descriptors including GCUT_PEOE_3, h_emd_c, Q_VSA_PNEG and std_dim3 exhibit negative correlation coefficients and are thus penalty terms in the prediction of the CP. Conversely, Q_RPC- exhibit positive correlation coefficients and as such are not a penalty term.

GCUT_PEOE_3 is an electronic descriptor which represents the electrostatic interactions present on the monomer and are calculated using distance between the atoms. GCUT_PEOE_3 was negatively correlated to the CP, with correlation coefficients of -0.59. Thus, as the degree of electrostatic interactions falls, the CP increases. The electrostatic interactions are thought to be important as polymers with a greater number of electrostatic interactions are expected to readily solvate in water[64] and in turn, result in a greater change in the enthalpy of mixing. The change in enthalpy of mixing is proportional to the number and strength of monomer-solvent interactions within each polymer chain.[65] The more electrostatic interactions present, the more hydrophilic a polymer is, which is expected to result in a CP at elevated temperature.

The next newly identified descriptor was h_emd_c, which represents the sum of hydrogen bond donor strengths of carbon atoms. This descriptor was negatively correlated to the CP with a correlation coefficient of -0.47. This indicates that as the number of hydrogen bond donor strengths of carbon atoms increases the CP decreases. Monomers which contain a larger number of hydrogen bond donors may form a larger number of inter-molecular interactions and a reduced number of polymer-water bonds. Therefore, the energy required to induce precipitation in these monomers may be reduced, resulting a CP at a lower temperature.

The descriptor with the greatest correlation to CP was Q_RPC-, with a correlation coefficient of 0.63. Q_RPC- is the relative negative partial charge of the monomer and was found to be positively correlated to the CP. Thus, as the relative negative partial charge increases the CP increases. This is likely as a result of an increased number of monomer-water interactions which may require a greater degree of energy to break and induce precipitation resulting in a CP.

Std_dim3 is a steric descriptor which found to correlate to the CP with a correlation coefficient of -0.62, as such std_dim3 decreases as the CP increases. This shows that molecules in the dataset which are larger result in polymers with CPs at lower temperatures. These molecules which are larger, typically contain a larger number of electronegative atoms. This is expected to result in more intra-molecular interactions and less water-polymer interaction which may account for the reduce CPs.

a) 5 Descriptor Model:

CP = 36.96 - 4.44437 × GCUT_PEOE_3 – 1.57874 × h_emd_C + 2.33541 × Q_RPC- - 5.39675 × Q_VSA_PNEG – 1.70216 × std_dim3

b) 4 Descriptor Model:

CP = 36.96 – 4.99731 × GCUT_PEOE_3 + 3.27384 × Q_RPC- - 5.08580 × Q_VSA_PNEG – 1.59768 × std_dim3

c) 3 Descriptor Model:

CP = 36.96 – 5.64442 × GCUT_PEOE_3 + 3.27656 × Q_RPC- - 6.03649 × Q_VSA_PNEG

d) 2 Descriptor Model:

CP = 36.96 – 7.48905 × GCUT_PEOE_3 – 7.09904 × Q_VSA_PNEG

[3.5.3.4] Testing the QSPR models built using dataset B

The models built from dataset B was investigated in the same way as the models developed for dataset A. The training r^2s and q^2s as well as the test r^2s were investigated for the four QSPR models (Table 3.12). The removal of the structurally dissimilar monomers resulted in an increase in the training r^2 as the noise introduced by these monomers was removed, indicating a greater predictability. In addition to this, the training q^2 was improved, thus resulting in a more robust model. In contrast to this, the test r^2 did not significantly vary with the removal of descriptors.

Table 3. 12: The training r^2, training q^2 and test r^2 of the four QSPR models developed using the dataset B.

Model Code	Number of Descriptors	Training r^2	Training q^2	Test r^2
2-A	5	0.59	0.20	0.11
2-B	4	0.59	0.23	0.14
2-C	3	0.58	0.35	0.16
2-D	2	0.56	0.35	0.17

The most robust model was 2-D with 2-descriptors. The four-descriptor model had a training r^2 of 0.56, training q^2 of 0.35 and test r^2 of 0.17. This model contained descriptors across all three types of descriptor in attempt to produce a robust model. But, due to the low test r^2, the model is not generalisable for the prediction of the CP of polymers not used in its construction. The correlation of the training set and test set of model 2-D are shown below in Figure 3.5 a and b.
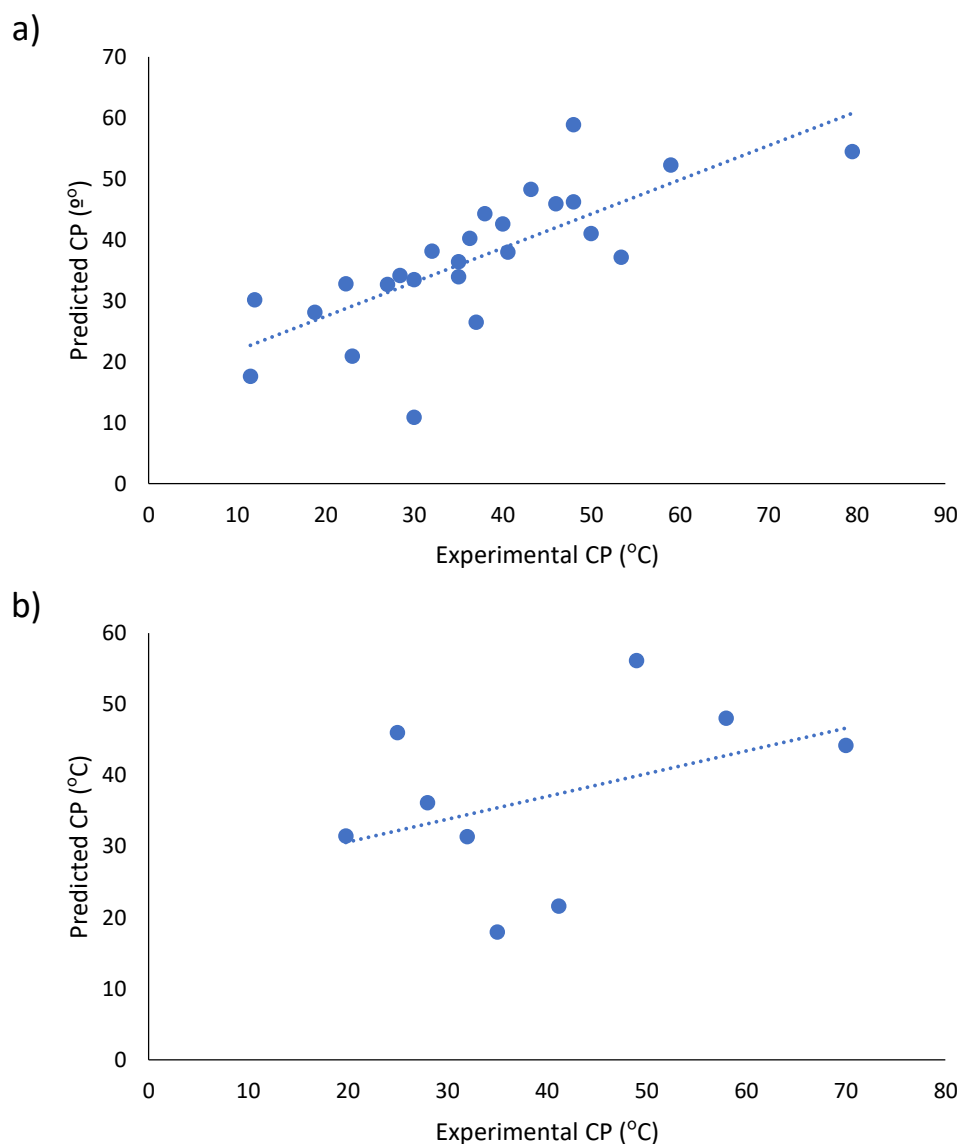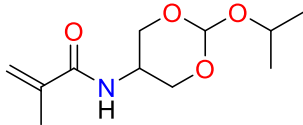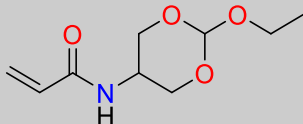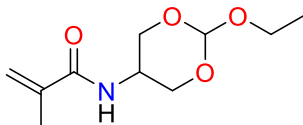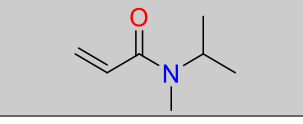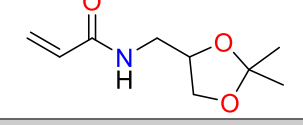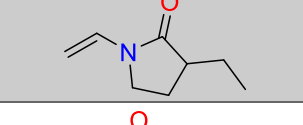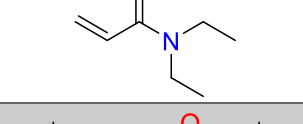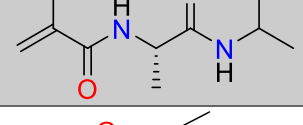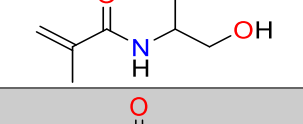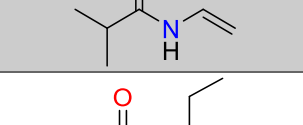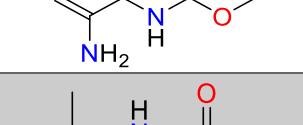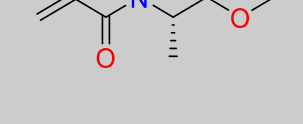
Figure 3. 4: The correlation graphs indicating the performance of the 4-descriptor QSPR model 2-D. a) The training set plot of the predicted vs experimental CP values according to the QSPR model (r^2 = 0.56). b) The test set plot of the predicted vs experimental CP values according to the QSPR model (r^2 = 0.17).
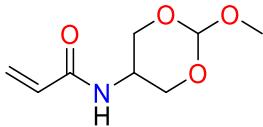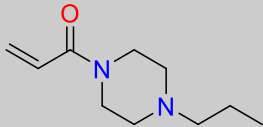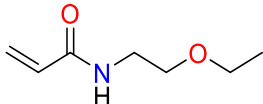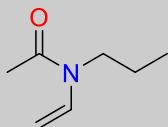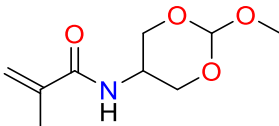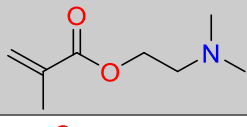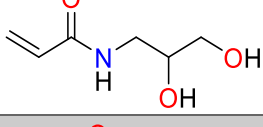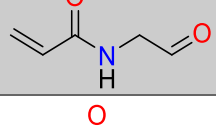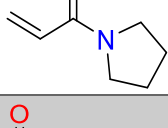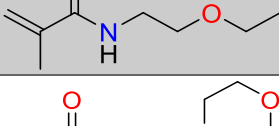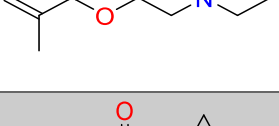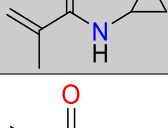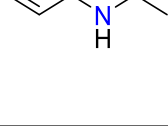
When comparing the the QSPR models produced using dataset B to those using the dataset A, the maximum training r^2 value increases from 0.40 to 0.59 and the training q^2 maximum value increases from 0.26 to 0.35 indicating both the predictability and robustness of the model has improved. Also, the test r^2 values increased from 0.02 to 0.17, indicating the generalisability of the model has improved. The two sets of models were built using the same method and as such the differences in r^2's and q^2 must be due to the difference between the datasets used to build the models.
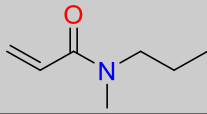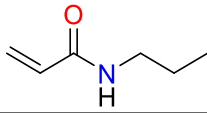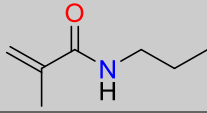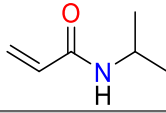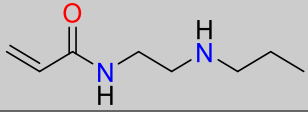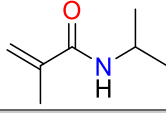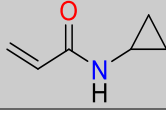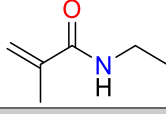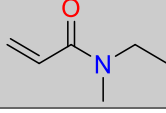
Upon investigating the predictions of each monomer one by one it is clear to see why the r^2 of the training set and test set improved (Table 3.13). In the training set, the number of predictions which were greater than an absolute value of 10 °C from the experimental value decreased from 12 to 7 after the removal of structurally dissimilar monomers. This is in agreement with the improved training set r^2. This result was expected as the monomers which were structurally dissimilar were adding noise to the data set. The monomers in which were not accurately predicted came from two classes of monomer within the training set, acrylamides and those with cyclic structures. Those acrylamides which were predicted wrongly were N-isopropyl-N-methylacrylamide, (S)-N-(1-(isopropylamino)-1-oxopropan-2-yl)methacrylamide, N-(2-oxoethyl)acrylamide and N-ethylacrylamide. N-isopropyl-N-methylacrylamide and N-ethylacrylamide were likely predicted wrong because of the lack of structural representation at their points in the data set. N-isopropyl-N-methylacrylamide is the only N-alkyl acrylamide with a reported CP below 22.3 °C out of 4 monomers with CPs below this temperature. N-ethylacrylamide is the monomer with the largest reported CP in the data set, and this too was likely predicted wrong as a result of a lack of structural representation at the highest extreme of the training set. (S)-N-(1-(isopropylamino)-1-oxopropan-2-yl)methacrylamide and N-(2-oxoethyl)acrylamide however, reside in the middle of the training set. These were predicted wrongly because they contain a second amide functionality and an aldehyde group, respectively. These groups are unique to these two monomers so may prevent their accurate prediction. For those which contain cyclic groups, these are randomly distributed throughout the training set, thus their inaccurate predictions may be as a result a lack of structural representation. In the training set of 25 monomers 10 contain cyclic structures, which may not include enough structural diversity to allow for an accurate prediction.

In terms of the test set, the monomers with a larger difference between the predicted and experimental CP are randomly distributed throughout the set. This suggests that the training set does not contain enough information to allow for an accurate prediction in the test set. The test set primarily consists of N-alkyl acrylamides, while the training set contains 6 N-alkyl acrylamides. Therefore, there may not be enough structural information provided in the training set to allow for an accurate prediction in the test set.

Table 3. 13: The structures, experimental CP, predicted CP from model 2-B and absolute difference between these for the training and test sets derived from dataset B.

Training Set			
Structure	**Experimental CP (°C)**	**Predicted CP (°C)**	**Difference (°C)**
	11.5	17.6	6.1
	12.0	30.1	18.1
	18.8	28.1	9.3
	22.3	32.7	10.4
	23.0	20.9	-2.1
	27.0	32.6	5.6
	28.4	34.1	5.7
	30.0	10.9	-19.1
	30.0	33.4	3.4
	32.0	38.1	6.1
	35.0	36.4	1.4
	35.0	33.9	-1.1

Training Set			
Structure	**Experimental CP (°C)**	**Predicted CP (°C)**	**Difference (°C)**
	36.3	40.2	3.9
	37.0	26.4	-10.6
	38.0	44.3	6.3
	40.0	42.6	2.6
	40.6	37.9	-2.7
	43.2	48.2	5.0
	46.0	45.9	-0.1
	48.0	58.8	10.8
	48.0	46.2	-1.8
	50.0	41.0	-9.0
	53.4	37.1	-16.3
	59.0	52.2	-6.8
	79.5	54.4	-25.1

Test Set			
Structure	**Experimental CP (°C)**	**Predicted CP (°C)**	**Difference (°C)**
	19.8	31.4	11.6
	25.0	46.0	21.0
	28.0	36.1	8.1
	32.0	31.3	-0.7
	35.0	17.9	-17.1
	41.2	21.6	-19.6
	49.0	56.1	7.1
	58.0	48.0	-10.0
	70.0	44.2	-25.8

Dataset B improved upon the training r^2, training q^2 and test r^2 observed by the models produced using data set A. The structurally dissimilar monomers were clouding the descriptor correlations with noise, which will directly impact their use in the prediction of the predictor variable. Unfortunately, these models were not predictive or generalisable enough to allow for an accurate prediction, which may be as a result of such a small data set. Regardless of this, these models may provide relevant information to guide the temperature at which a polymer may exhibit a CP. As such, QSPR model 2-D was selected to predict the CPs of polymers, using their monomer structure, which were not included in the construction of the models (Equation 3.8). The descriptors identified for QSPR equation 2-D were predicted, standardized and used to predict the CP of each polymer.

$$\text{Equation 3.8: } CP = 36.96 - 7.48905 \times GCUT\_PEOE\_3 - 7.09904 \times Q\_VSA\_PNEG$$
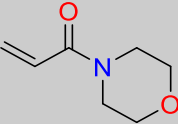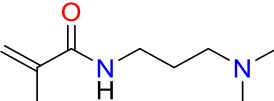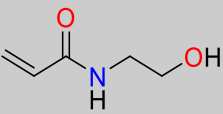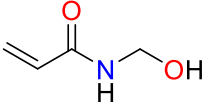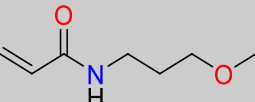
[3.5.4] Evaluating the predictability and generalisability of QSPR model 1-B using acrylamides and acrylates not used to construct the model

[3.5.4.1] Identification and clustering of commercially available acrylamide and acrylates

To further test the validity of the model, CPs were predicted from monomers which were not used to build the QSPR models. To identify these monomers, Sigma-Aldrich was searched for monomers which may be polymerised by radical polymerisation. To this end, a database of 48 commercially available monomers which were not used to build the QSPR models was identified, and designated dataset C (Appendix; Table A. 1). The 48 monomers of dataset C were clustered based on chemical similarity which resulted in 13 clusters. Following the clustering exercise, the monomer which best represented the chemical structure of each cluster, the "medoid", was identified from the average Tanimoto coefficient. Thus 13 representative monomers were identified to test QSPR model 2-B. The 13 monomers were narrowed in number by removing those with halogen atoms. Monomers which contain halogen atoms such as fluorine[66], chlorine[67] and bromine[68] in the side chain exhibit chain-transfer when polymerised by atom-transfer radical polymerisation (ATRP).[69] The model was built using monomers which are polymerised to yield linear temperature responsive polymers and may not be applicable in the prediction of the CP of branched polymers. The removal of monomers with halogen atoms reduced the number of test monomers from 13 to five (Table 3.14).

The structural similarity of the 5 medoids to the molecular structures found in the training set used to build QSPR model 2-B was evaluated using average Tanimoto coefficients. The average Tanimoto coefficients of the medoids (Table 3.14) lie between the 0.08 and 0.53, which are the minimum and maximum observed in the training set used to build the model. As such, these structures are applicable for the QSPR model.

Table 3. 14: The names, chemical structures and average Tanimoto coefficients of the selected medoid monomers when compared to the training set used to build QSPR model 2-B.

Monomer Name	Monomer Structure	Average Tanimoto Coefficient
4-Acryloyl Morpholine		0.40
3-(N-dimethylamino)propyl methacrylamide		0.39
Hydroxyethyl acrylamide		0.42
Hydroxymethyl acrylamide		0.32
N-(3-Methoxypropyl)acrylamide		0.41

[3.5.4.2] Experimental identification of the CP of the polymerised medoids

The CP of temperature responsive polymers can be varied by a few degrees Celsius (~ 2 °C) by altering their polymer molecular weight and/or concentration.[70,71] Therefore, the medoid monomers were polymerised to target 10 kDa and the CP investigated in 100 mg/mL aqueous solution to standardise the approach. This molecular weight and concentration were selected as the most well-known CP exhibiting polymer, poly(N-isopropyl acrylamide), exhibits an CP c.a. 32 °C for 10 kDa polymer and at concentrations of 100 mg/mL and above.[72]

^{1}H NMR, FTIR spectroscopy and GPC were used to confirm the synthesis of the polymers. ^{1}H NMR spectroscopy confirmed the synthesis of all 5 polymers due to three observations. These observations were i) the disappearance of the vinyl protons between 4.5 and 6.5 ppm, ii) broadening of the remaining proton peaks in the polymer spectrum and iii) the presence of two new broad peaks representing the newly formed polymer backbone. In all polymerisations these characteristics were observed (Figures 3.9a, 3.10a, 3.11a, 3.12a and 3.13a). In the case of FTIR spectroscopy, similar criteria were used to confirm successful polymerisation for all monomers. These criteria were the observation of change in the peak which represents the vinyl group between the monomer and polymer FTIR spectra. Vinyl, carbonyl and amides typically exhibit stretching between 1500 – 1800 cm^{-1}, as such, when comparing the spectra of the monomer to the polymer, the number of peaks in

this range was noted. Polymerisation was deemed successful when the number of peaks in this range decreased by 1, indicating the vinyl group was no longer present. The FTIR spectra of the 5 monomers and polymers are given in Figures 3.7b, 3.8b, 3.9b, 3.10b and 3.11b.

The GPC traces of each polymer is shown in Figure 3.6 confirms the formation of a polymer with a single population of number average molecular weights (Mns). The elution times vary significantly because of the extreme variation in polymer structure.[73] The GPC was calibrated with a series of standards of a single type of polymer, resulting in a narrow calibration. Such calibrations are not fully representative of the true Mn, and are used to approximate the molecular weight, relative to the standard used. Regardless of this, the PDI may be ascertained, which provides an indication to the variety of Mns present in a polymer sample. The PDI of each polymer is given in Table 3.12.
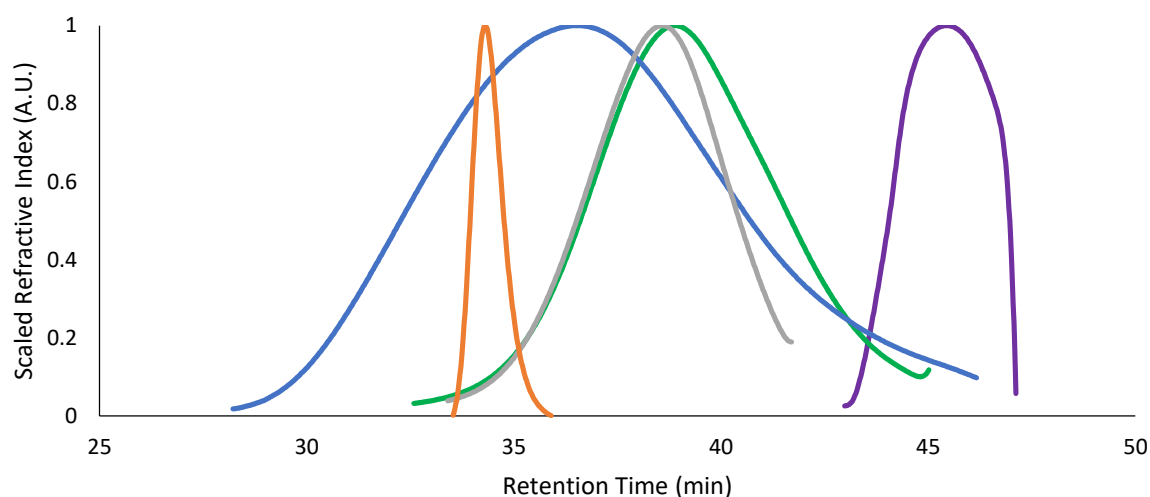
Figure 3. 5: The GPC traces of the 10 kDa poly(4-acryloyl morpholine) (green), poly(3-(N-dimethylamino)propyl methacrylamide) (blue), poly(N-hydroxyethyl acrylamide) (orange), poly(N-hydroxymethyl acrylamide) (purple) and poly(N-(3-Methoxypropyl)acrylamide) (grey) which were synthesised in this work.

^{1}H NMR was used to calculate Mn without approximation to a standard. The ratio of the initiator peaks to those of the polymer backbone allows for the degree of polymerisation to be calculated, and as such the Mn may be predicted. The Mn as given by ^{1}H NMR are also given in Table 3.15.

Table 3. 15: The Mn in Da of the synthesised polymers as determined by GPC and ^{1}H NMR and PDI of the polymers as determined by GPC.

Polymer	GPC Mn (Da)	PDI	^{1}H NMR Mn (Da)
Poly(4-acryloyl morpholine)	46072	1.47	10023
Poly(3-(N-dimethylamino)propyl methacrylamide)	64189	2.13	7232
Poly(N-hydroxyethyl acrylamide)	8512	1.04	10016
Poly(N-hydroxymethyl acrylamide)	9667	1.08	8708
Poly(N-(3-Methoxypropyl)acrylamide)	29329	1.87	9753

The CP of the synthesised polymers were predicted using QSPR model 2-C (Table 3.16). The synthesised polymers were then studied to identify if a CP was exhibited in 100 mg/mL aqueous solution. Given the chemical structures of the 5 medoid monomers and their similarity to the monomers in the training set, all 5 monomers were expected to polymerise to yield a CP exhibiting polymer. The only polymer found to exhibit a CP in aqueous solution between 25 and 95 °C was poly(N-(3-methoxypropyl)acrylamide) which had a CP of 76.4 ± 0.3 °C. This CP was greater than the predicted value of 37.0 °C.

Table 3. 16: The predicted and experimental CPs of the 5 synthesised homopolymers.

Monomer Name	Predicted CP (°C)	Experimental CP (°C)
4-Acryloyl Morpholine	34.8	N/A
N-([3-(Dimethylamino)propyl]methacrylamide)	37.3	N/A
Hydroxyethyl acrylamide	34.4	N/A
Hydroxymethyl acrylamide	39.7	N/A
N-(3-Methoxypropyl)acrylamide	38.5	76.4 ± 0.3

There are several possible reasons as to why the model is not predictive enough to determine the CPs of polymers in aqueous solution. One of which is the quality of the dataset used to build the model. Every attempt was made to ensure the dataset was the best it could be for the development of the QSPR model. Unfortunately, the CP can be determined using many different methods including by eye, FTIR spectroscopy and dynamic light scattering.[74] This variety in the method of CP identification may negatively impact the reliability of the data, which will directly impact any QSPR model built using them. Another possible reason for the inaccuracy of the model may be due to the dataset size used to build the model. Unfortunately, this is something which cannot be overcome

until novel CP exhibiting polymers are identified and published. Also, the monomer structures used to build the QSPR models may not be representative enough of the polymer structure to allow for an accurate prediction. Polymer descriptors were predicted for each entry into the dataset but, these were not found to be correlated to the CP and were disregarded. Molecular descriptors may have been more applicable but, the computational power required to perform the calculations to predict these was not available. Thus, such descriptors could not be calculated for the polymer, so the monomer structure was used. Another issue is the prediction of CPs for polymers which are synthesised from monomers that are structurally like the molecules present in the training set. A stated above, the five monomers had average Tanimoto coefficients within the range of those observed by the training set. Thus, these polymers were expected to exhibit CP behaviour in aqueous solution, but only one did. Thus, the model may not be sufficiently predictive to guide development of novel temperature responsive polymers.

In order to further improve QSPR model 2-B, there a few options which may be considered. Firstly, a binary system may be introduced which would screen the monomers prior to calculating the CP. The binary system would include a yes/no screen and would reject monomers which are not expected to exhibit a CP. Such a screen may be based on the chemical similarity to molecules in the training set. For example, molecules with an average Tanimoto coefficient less than a threshold value would be rejected from prediction of the CP. In addition to this, the monomers identified from the literature could be synthesised to target the same molecular weight and their CPs investigated at the same concentration. This would highlight any data which is not correct and eliminate the variation in CP which occurs as a result of molecular weight and concentration. Another, more computationally expensive, way of improving the model would be build the polymers and calculate the molecular descriptors for each one. This could not be done in this case, as the computational power required was not available.

[3.6] Conclusions

The research presented in this chapter details the development of a novel QSPR model designed to predict the CP of temperature responsive polymers from the structure of their constituent monomers. From the literature, a dataset of 53 monomers which exhibit CPs in aqueous solution was built. This dataset was streamlined in terms of polymerisation route and reported characterisation. The most predictive and generalisable QSPR model was derived a dataset of 34 acrylamides and acrylates, using dataset B. This model had a training r^2 of 0.56, training q^2 of 0.35 and a test r^2 of 0.17. This model contained the molecular descriptors GCUT_PEOE_3 and Q_VSA_PNEG which represent the electronic, lipophilic and steric characteristics of the monomers in the training dataset. Due to the small dataset, this model was not predictive or generalisable so may not be able to predict the CP of novel polymers, but these identified descriptors may be used to guide the development of novel CP exhibiting polymers. Therefore, model 2-D was used to predict the CP of polymers using monomer structures which were not present in the dataset used to build the model.

The CPs of monomers identified from the literature which were structurally similar to the monomers in the training set used to build the model were predicted. These monomers were successfully polymerised and characterised by ^{1}H NMR, FITR and GPC. Of these synthesised polymers, poly(N-methoxypropyl acrylamide) was the only one to exhibit a CP of 76.4 ± 0.3 °C for a 10 kDa polymer in 100 mg/mL aqueous solution. However, this was predicted to occur at 38.5 °C. The monomers which were used to test the model had average Tanimoto coefficients between 0.3 and 0.5 when compared to the training set used to build the model. The monomer which exhibited a CP had an average Tanimoto coefficient of 0.41. Thus, a threshold average Tanimoto coefficient of 0.4 may be used to screen monomers before the CP is predicted.

[3.7] References

1   G. Melagraki, A. Afantitis, H. Sarimveis, P. A. Koutentis, J. Markopoulos and O. Igglessi-Markopoulou, *J. Mol. Model.*, 2007, **13**, 55–64.

2   J. Xu, L. Liu, W. Xu, S. Zhao and D. Zuo, *J. Mol. Graph. Model.*, 2007, **26**, 352–359.

3   H. Cheng, D. J. Garrick and R. L. Fernando, *J. Anim. Sci. Biotechnol.*, 2017, **8**, 1–5.

4   A. Cherkasov, E. N. Muratov, D. Fourches, A. Varnek, I. I. Baskin, M. Cronin, J. Dearden, P. Gramatica, Y. C. Martin, R. Todeschini, V. Consonni, V. E. Kuz'min, R. Cramer, R. Benigni, C. Yang, J. Rathman, L. Terfloth, J. Gasteiger, A. Richard and A. Tropsha, *J. Med. Chem.*, 2014, **57**, 4977–5010.

5   S. H. Unger, *J. Pharm. Sci.*, 1987, **76**, 269–270.

6   J. B. Ghasemi, A. Abdolmaleki and N. Mandoumi, *J. Hazard. Mater.*, 2009, **161**, 74–80.

7   T. Wilson, A. Markey, K. V. Camarda and S. Kieweg, *Comput. Aided Chem. Eng.*, 2011, **29**, 1480–1484.

8   R. Chris Lacher, *Math/chem/comp 1987: Proceedings of an international course and conference on the interfaces between mathematics, chemistry and computer science.*, Elsevier, 1990, vol. 208.

9   FMX.Maps.TMapCircleDescriptor - RAD Studio API Documentation, http://docwiki.embarcadero.com/Libraries/Rio/en/FMX.Maps.TMapCircleDescriptor, (accessed 8 March 2020).

10   R. Todeschini and V. Consonni, *Molecular Descriptors for Chemoinformatics: Volume I: Alphabetical Listing*, 2009.

11   G. Hanrahan and F. A. Gomez, *Chemometric Methods in Capillary Electrophoresis*, 2009.

12   A. Bandyopadhyay, *Hands-On GPU Computing with Python : Explore the Capabilities of GPUs for Solving High Performance Computational Problems.*, 2019.

13   R. B. King and D. H. Rouvray, *Theor. Chim. Acta*, 1986, **69**, 1–10.

14   J. Fei, Q. Mao, L. Peng, T. Ye, Y. Yang and S. Luo, *Molecules*, 2018, **23**, 1–8.

15   F. Ding, J. Guo, W. Song, W. Hub and Z. Li, *Chem. Ecol.*, 2011, **27**, 359–368.

16   D. J. W. Blum, I. H. Suffet and J. P. Duguet, *Water Res.*, 1994, **28**, 687–699.

17   A. P. Freidig and J. L. M. Hermens, *Quant. Struct. Relationships*, 2001, **19**, 547–553.

18   A. Malik, H. Singh, M. Andrabi, S. A. Husain and S. Ahmad, *Cancer Inform.*, 2007, **2**, 99–111.

19   C. C. Group, Chemical Computing Group (CCG) | Computer-Aided Molecular Design, https://www.chemcomp.com/index.htm, (accessed 8 March 2020).

20   N. M. O'Boyle, M. Banck, C. A. James, C. Morley, T. Vandermeersch and G. R. Hutchison, *J. Cheminform.*, 2011, **3**, 33–40.

21   T. Puzyn, J. Leszczyński and M. Cronin, *Recent Advances in QSAR Studies: Methods and Applications*, 2010.

22   D. Bajusz, A. Rácz and K. Héberger, *J. Cheminform.*, 2015, **7**, 1–13.

23   J. Ali, P. Camilleri, M. B. Brown, A. J. Hutt and S. B. Kirton, *J. Chem. Inf. Model.*, 2012, **52**, 2950–2957.

24   T. M. Martin, P. Harten, D. M. Young, E. N. Muratov, A. Golbraikh, H. Zhu and A. Tropsha, *J. Chem. Inf. Model.*, 2012, **52**, 2570–2578.

25   J. T. Leonard and K. Roy, *QSAR Comb. Sci.*, 2006, **25**, 235–251.

26   S. S. Shapiro and M. B. Wilk, *Biometrika*, 1965, **52**, 591.

27   G. I. Webb, C. Sammut, C. Perlich, T. Horváth, S. Wrobel, K. B. Korb, W. S. Noble, C. Leslie, M. G. Lagoudakis, N. Quadrianto, W. L. Buntine, N. Quadrianto, W. L. Buntine, L. Getoor, G. Namata, L. Getoor, J. Han, Xin Jin, J.-A. Ting, S. Vijayakumar, S. Schaal and L. De Raedt, in *Encyclopedia of Machine Learning*, Springer US, 2011, pp. 600–601.

28   R. Veerasamy, H. Rajak, A. Jain, S. Sivadasan, C. P. Varghese and R. K. Agrawal, *Int. J. Drug Des. Disocovery*, 2011, **2**, 511–519.

29   V. Consonni, D. Ballabio and R. Todeschini, *J. Chem. Inf. Model.*, 2009, **49**, 1669–1678.

30   Z. Liu, Y. Guo and K. Inomata, *Polym. J.*, 2010, **42**, 901–904.

31   L. Zhao, W. Wang, A. Sedykh and H. Zhu, *ACS Omega*, 2017, **2**, 2805–2812.

32   F. S. Du, X. N. Huang, G. T. Chen, S. S. Lin, D. Liang and Z. C. Li, *Macromolecules*, 2010, **43**, 2474–2483.

33   R. Moerkerke, F. Meeussen, R. Koningsveld, H. Berghmans, W. Mondelaers, E. Schacht, K. Dusek and K. Solc, *Macromolecules*, 1998, **31**, 2223–2229.

34   L. H. Gan, Y. Y. Gan and G. R. Deen, *Macromolecules*, 2002, **33**, 7893–7897.

35   D. Popescu, R. Hoogenboom, H. Keul and M. Moeller, *Polym. Chem.*, 2010, **1**, 878–890.

36   Y. Maeda, J. Sakamoto, S. Y. Wang and Y. Mizuno, *J. Phys. Chem. B*, 2009, **113**, 12456–12461.

37   R. Gomes De Azevedo, L. P. N. Rebelo, A. M. Ramos, J. Szydlowski, H. C. De Sousa and J. Klein, *Fluid Phase Equilib.*, 2001, **185**, 189–198.

38   V. Aseyev, H. Tenhu and F. M. Winnik, *Adv. Polym. Sci.*, 2011, **242**, 18–56.

39   D. DeRossi, K. Kajiwara, Y. Osada and A. Yamauchi, *Polymer Gels: Fundamentals and Biomedical Applications*, Springer US, 1991, vol. 53.

40   F.-S. S. Du, X.-N. N. Huang, G.-T. T. Chen, S.-S. S. Lin, D. Liang and Z.-C. C. Li, *Macromolecules*, 2010, **43**, 2474–2483.

41   Y. Zou, D. E. Brooks and J. N. Kizhakkedathu, *Macromolecules*, 2008, **41**, 5393–5405.

42   E. Oyama, H.T. Sprycha, R. Partch, R.E. Matijevic, *J. Colloid Interface Sci.*, 1993, **160**, 298–303.

43   H. Ajiro, Y. Takahashi and M. Akashi, *Macromolecules*, 2012, **45**, 2668–2674.

44   T. Trellenkamp and H. Ritter, *Macromol. Rapid Commun.*, 2009, **30**, 1736–1740.

45   V. Bütün, S. . P. Armes and N. . C. Billingham, *Polymer (Guildf).*, 2001, **42**, 5993–6008.

46   Y. Maeda, H. Yamauchi and T. Kubota, *Langmuir*, 2009, **25**, 479–482.

47   D. G. Lessard, M. Ousalem, X. X. Zhu, A. Eisenberg and P. J. Carreau, *J. Polym. Sci. Part B Polym. Phys.*, 2003, **41**, 1627–1637.

48   Y. Zou, D. E. Brooks and J. N. Kizhakkedathu, *Macromolecules*, 2008, **41**, 5393–5405.

49   T. Aoki, *J. Colloid Interface Sci Macromol. N. React. Funct. Polym.*, 1968, **25**, 1441–1445.

50   D. Yu, C. Luo, W. Fu and Z. Li, *Polym. Chem.*, 2014, **5**, 4561–4568.

51   W. Tachaboonyakiat, H. Ajiro and M. Akashi, *Polym. J.*, 2013, **45**, 971–978.

52   W. S. Ng, L. A. Connal, E. Forbes, K. Mohanarangam and G. V Franks, *J. Colloid Interface Sci.*, 2017, **494**, 139–152.

53   F. Hua, X. Jiang, D. Li and B. Zhao, *J. Polym. Sci. Part A Polym. Chem.*, 2006, **44**, 2454–2467.

54   N. A. Cortez-Lemus and A. Licea-Claverie, *Prog. Polym. Sci.*, 2016, **53**, 1–51.

55   A. Gandhi, A. Paul, S. O. Sen, K. K. Sen, K. Sen Kumar and K. K. Sen, *Asian J. Pharm. Sci.*, 2015, **10**, 99–107.

56   W. Xue, M. B. Huglin and T. G. J. J. Jones, *Macromol. Chem. Phys.*, 2003, **204**, 1956–1965.

57   P. Dimitrov, N. Toncheva, P. Weda, S. Rangelov, B. Trzebicka, A. Dworak and C. B. Tsvetanov, *Macromol. Symp.*, 2009, **278**, 89–95.

58   A. Ghasemi and S. Zahediasl, *Int. J. Endocrinol. Metab.*, 2012, **10**, 486–489.

59   N. M. M. Bhatia, K. R. R. Mahadik and M. S. S. Bhatia, *Daru*, 2010, **18**, 230–6.

60   H. L. Yao, Y. C. Shi, S. L. Yuan and G. Z. Li, *J. Dispers. Sci. Technol.*, 2009, **30**, 1223–1230.

61   R. M. Kramer, V. R. Shende, N. Motl, C. N. Pace and J. M. Scholtz, *Biophys. J.*, 2012, **102**, 1907–1915.

62   D. L. J. Alexander, A. Tropsha and D. A. Winkler, *J. Chem. Inf. Model.*, 2015, **55**, 1316–1322.

63   S. Kausar and A. O. Falcao, *J. Cheminform.*, 2018, **10**, 1–5.

64   T. Hattori, R. Hallberg and P. L. Dubin, *Langmuir*, 2000, **16**, 9738–9743.

65   B. A. Miller-Chou and J. L. Koenig, *Prog. Polym. Sci.*, 2003, **28**, 1223–1270.

66   S. Lanzalaco, M. Fantin, O. Scialdone, A. Galia, A. A. Isse, A. Gennaro and K. Matyjaszewski, *Macromolecules*, 2016, **50**, 192–202.

67   P. A. Gurr, M. F. Mills, G. G. Qiao and D. H. Solomon, *Polymer (Guildf).*, 2005, **46**, 2097–2104.

68   W. Tang and K. Matyjaszewski, *Macromolecules*, 2007, **40**, 1858–1863.

69   A. Heise, C. Nguyen, R. Malek, J. L. Hedrick, C. W. Frank and R. D. Miller, *Macromolecules*, 2000, **33**, 2346–2354.

70   K. Bebis, M. W. Jones, D. M. Haddleton and M. I. Gibson, *Polym. Chem.*, 2011, **2**, 975–982.

71   N. S. Ieong, M. Hasan, D. J. Phillips, Y. Saaka, R. K. O'Reilly and M. I. Gibson, *Polym. Chem.*, 2012, **3**, 794–799.

72   K. Van Durme, G. Van Assche and B. Van Mele, *Macromolecules*, 2004, **37**, 9596–9605.

73   S. C. Moldoveanu and V. David, in *Essentials in Modern HPLC Separations*, Elsevier, 2013, pp. 53–83.

74   Q. Zhang, C. Weber, U. S. Schubert and R. Hoogenboom, *Mater. Horizons*, 2017, **4**, 109–116.

Chapter Four: Selection, Synthesis and Characterisation of Temperature Responsive Homopolymers and Tri-block Copolymers

[4.1] Introduction

This chapter describes the selection and synthesis of temperature-responsive homo and tri-block copolymers with the aim of developing thermogelling materials. The dataset used to develop the QSPR models from Chapter 3 was used to identify LCST-exhibiting polymers which may be used to synthesise thermogelling materials, where the models themselves were not sufficiently predictive to do so. Polymers were selected based upon the temperature at which the LCST occurs and their predicted and reported safety. Considering this, to achieve a physiologically relevant gelation temperature, homopolymers with LCSTs between 25 and 37 °C must be identified. In addition to this, these materials must be safe for use as pharmaceutical excipients. Safety may be evaluated in a number of ways including clinical trials, *in vivo* experimentation or by *in silico* prediction, however the strongest evidence is a history of use in human medicine. Clinical trials are considered the best test for confirming the safety of pharmaceutical products, but these are both costly and time consuming. Therefore, knowledge-based software such as Derek by Nexus and reported safety through *in vitro* cell culture may be used to mitigate the risk in the development of safe novel thermogelling material excipients.

Polymers may be synthesised by chain-reaction (addition) or step-reaction (condensation) polymerisation.[1] Linear block copolymers may be synthesised by controlled polymerisation techniques including; atom-transfer radical polymerisation (ATRP), reversible addition-fragmentation chain transfer radial polymerisation (RAFT), ionic polymerisation, nitroxide-mediated radical polymerisation and group transfer polymerisation (GTP).[2] ATRP and RAFT are preferable methods of polymerisation due to their ability to synthesise polymers with narrow polydispersities with relative ease.[3] Within this project, ATRP was selected as the preferred method of polymerisation over RAFT. Both are capable of forming block copolymers with low polydispersity for a similar range of monomer types. However, RAFT polymerisation utilises sulphur containing chain-transfer agents (CTAs) which are incorporated into the polymer structure.[4] The CTAs result in polymers which are unstable, highly coloured and often have a pungent odour due to decomposition.[5] As such, polymers synthesise by RAFT polymerisation may not be applicable as drug delivery excipients. In contrast, polymers synthesised by ATRP do not require chain-transfer agents and as such are more stable, non-coloured and do not exhibit pungent odours. This does not mean ATRP is without its flaws. ATRP requires small quantities of transition metal-based catalysts, with the most commonly used being copper. Copper is known to induce cytotoxicity and thus must be removed prior to human exposure, which may be problematic.[6] There are reports of copper removal from the literature which utilise both extraction via neutral alumina[7] and dialysis, which results complete removal.[8] In addition to this, the ATRP reagents required for polymerisation can

significantly vary between monomer types, making synthetic design a lengthy process.[9] This balances against the relatively simple synthesis of ATRP macroinitiators, with acid bromide initiators commercially available. Therefore, ATRP was selected as the preferred method of triblock copolymer synthesis.

ATRP can be used to successfully synthesise both homo and tri-block copolymers with very narrow polydispersities.[10] Also, ATRP may be performed at room temperature in solvents such as water.[11] A typical ATRP synthesis requires a metal catalyst with an available +1 oxidation state, a halogen-containing initiator, a ligand such as bipyridine and an unsaturated monomer such as an acrylate or acrylamide.[9] Initiation of ATRP takes place by a single-electron transfer process. In this process, the metal-ligand complex abstracts the halogen from the initiator via homolytic bond fission resulting the formation of a carbon radical (Figure 4.1).[12] The newly formed radical then reacts with an unsaturated hydrocarbon (i.e. double or triple bond) resulting in a propagating radical.
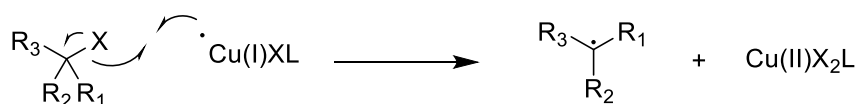
Figure 4. 1: The initiation step of ATRP where a copper catalyst (Cu(I)XL) forms a new bond with a halogen (X) via a single electron transfer process, resulting in the formation of a carbon radical.

ATRP is capable of controlled polymerisation due to the ratio of the activation (K_{act}) and deactivation (K_{deact}) rate constants (Figure 4.2).[13] Typically, the K_{deact} is greater than K_{act} which favours the formation of the original copper catalyst and carbon-halogen bond, also known as the dormant species.[14] This allows for a step-growth mechanism to polymerisation where a propagating radical is formed. This propagating radical reacts with an unsaturated monomer and then either terminates or reverts to the dormant species. If the ATRP is truly "living", termination doesn't occur because the K_{deact} is greater than the termination constant (K_t).[15] The process of activation and deactivation continues until no monomer remains. The polydispersity (PDI) of polymers synthesised by ATRP is typically low (< 1.2)[16] because all polymers grow at the same rate. Also, the chances of termination by recombination or disproportionation are reduced, aiding the synthesis of polymers with narrow PDIs.

Dormant   **Polymerisation**

$$R-X \quad + \quad Cu(I)XL \quad \underset{K_{deact}}{\overset{K_{act}}{\rightleftharpoons}} \quad X-Cu(II)XL \quad + \quad R^{\bullet} \enspace K_p \enspace +M$$

$$+R^{\bullet} \diagdown K_t$$

$$RR$$

Undesired Termination
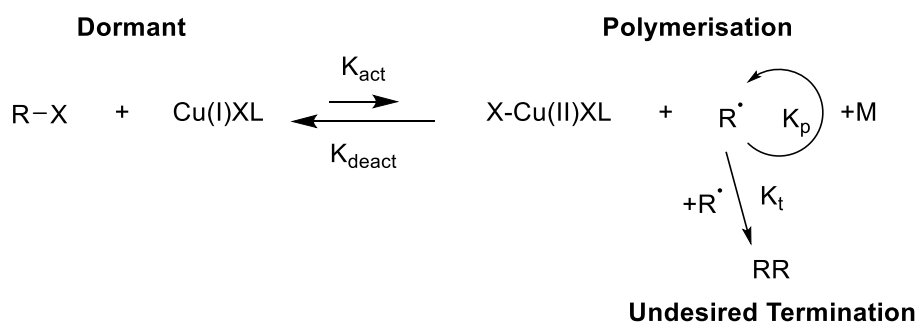
Figure 4. 2: The general reaction mechanism for ATRP where the polymerisation K_{act} is less than the K_{deact}. The process also shows the polymerisation rate constant (K_p) and the termination rate constant (K_t) which are less than K_{deact}.

The rate of polymerisation and the PDI of the resulting polymer may be tuned by altering the temperature[13], solvent[17], pressure[18] and catalyst and intiator[19] used in the reaction. As in many chemical reactions, increasing the temperature and pressure results in an increase in polymerisation rate. As the temperature and pressure are increased, the K_{act} increases, which results in polymers which are exhibit greater PDIs. The activity of the catalyst/ligand complex is an important factor in ATRP, and as such those which are bidentate in nature are typically less active than tetradentate ligands.[20] This is reported to be associated with a small entropic penalty in the ligand rearrangement upon catalyst activation.[20] The initiator is another important reagent in ATRP, where tertiary halides exhibit greater activation rate constant than primary halides, as a result of the inductive effect which may enhance the stability of the radical species.[14] Finally, the solvent in which the polymerisation is performed also has a profound impact upon the rate of polymerisation and the PDI of the resulting polymer.[21] Many studies have concluded that ATRP in polar solvents proceeds faster and forms very polydisperse polymers when compared to polymers synthesised in non-polar solvents. This is because protic solvents which are polar in nature can stabilise the metal-ligand complex after the propagating radical has been formed.[22] This results in a reduced deactivation equilibrium constant, preventing the stepwise growth of the polymer chain (Figure 4.3).

$$X\text{-}Cu(II)XL \quad + \quad 2H_2O \quad \rightleftharpoons \quad Cu(II)XL(H_2O) \quad + \quad X(H_2O)$$
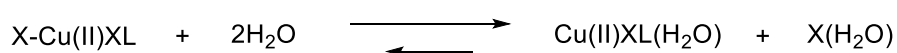
Figure 4. 3: The stabilisation of the X-Cu(II)XL complex formed after ATRP initiation in protic solvents.[23]

As discussed in chapter 2, the architecture of thermogelling materials has been found to directly impact the strength of the gel formed.[24] Thermogelling materials may have architectures including di-block, tri-block and star-shaped block and graft copolymers. Studies in the literature have found that the gels formed by thermogelling block copolymers of PEG and poly(N-isopropyl acrylamide) (PNIPAM) increased in strength when the number of temperature responsive arms is increased.[24] The polymer architecture selected for synthesis was ABA tri-block structure, where A is temperature-responsive and B is PEG, as these may form gels which are stronger than di-block copolymers and are cheaper and easier to synthesise when compared to star-shaped block copolymers, an important requirement for translation to pharmaceutical applications. Therefore, a variety of temperature-responsive polymer types were used to synthesise ABA tri-block copolymers using selected temperature-responsive A blocks. As the type of temperature responsive polymer is varied the molecular weight of both blocks may also be varied. The target PEG molecular weights were 4 and 10 kDa and the target temperature-responsive block molecular weights were 10 and 20 kDa.[25] These molecular weights were selected as previous studies have confirmed PNIPAM-PEG-PNIPAM tri-block copolymers with these molecular weights may form viscous thermogelling materials.[26]

To this end, this chapter focuses on the selection of temperature responsive materials from the literature guided by their LCST and predicted safety. These materials were synthesised using a range of ATRP methods. Those which achieved an appropriate degree of polymerisation and PDI were selected for the synthesis of block copolymers for evaluation as thermogelling materials in future chapters.

[4.2] Aims and Objectives

The aim of this phase of research was to synthesise thermoresponsive ABA tri-block copolymers consisting of PEG (B) and LCST-exhibiting polymers (A) which are predicted to be safe for pharmaceutical use and exhibited gelation between 25 and 37 °C. This aim was achieved by the following objectives:

- Polymers were identified from the literature which exhibit LCSTs between 25 and 37 °C which are expected to be safe for pharmaceutical use.
- These polymers were synthesised and fully characterised using ATRP methods compatible with PEG macroinitiators.
- PEG macroinitiators with molecular weights of 4 and 10 kDa were synthesised.
- ABA triblock copolymers with temperature responsive A blocks and PEG B blocks were synthesised using the macroinitiators at 10-4-10, 20-4-20, 10-10-10 and 20-10-20 and fully characterised using the methods found for homopolymer synthesis.

[4.3] Materials

N-isopropyl acrylamide (NIPAM) (97 %), 2-hydroxyethyl 2-bromoisobutyrate (95 %), copper (I) bromide (CuBr) (98 %), (2-N-dimethylamino)ethyl methacrylate (DMAEMA) (98 %), N,N-diethyl acrylamide (DEA) (99 %), tetrahydrofuran (THF) (99 %), N,N,N',N'',N''-pentamethyldiethylenetriamine (PMDETA) (99 %), anhydrous 1,4-dioxane (99.8 %), triethylamine (TEA) (99.5 %) and diethylene glycol methyl ether methacrylate (DEGMEMA) (95 %) were purchased from Sigma-Aldrich (U.K.). Tris[2-(dimethylamino)ethyl]amine (Me6TREN) (99 %), 2-Bromoisobutyryl bromide (BiBB) (97 %) and copper (I) chloride (CuCl) (99.9 %) were purchased from Alfa Aesar (U.K.). Isopropyl alcohol (iPA) (99 %), ethanol (EtOH) (99 %), methanol (MeOH) (99%), dichloromethane (99 %) and sodium chloride (99 %) were purchased from Fisher Scientific (U.K.). Bipyridine (99 %), dimethylamino pyridine (DMAP) (97 %) and polyethylene glycol (PEG) 10 kDa were purchased from Aldrich (U.K.). PEG 4 kDa was purchased from Fluka (U.K.). N-vinyl caprolactam (NVCL) (98 %) and N-vinyl pyrrolidone (NVP) (99 %) were purchased from Sigma-Aldrich (U.K.) and passed through neutral alumina to remove inhibitor before use. Aluminium oxide, neutral, Brockmann I was purchased from Acros Organics (U.K.). Dialysis tubing with a molecular weight cut off (MWCO) ~ 3500 Da was purchased from Medicell Membrane Ltd (U.K.) and soaked in deionised H_2O before use. GPC EasiVial poly(methyl methacrylate) (PMMA) mixed standards and a PMMA single standard (72 kDa) were purchased from Agilent (U.K.). Deionised H_2O was used in all experiments. All reagents were used as supplied, unless indicated otherwise.

[4.4] Methods

[4.4.1] Selection of LCST-exhibiting polymers from the literature

Using the database established in chapter 3, of polymers with LCSTs were identified as candidate polymers for use in this phase. Firstly, the database was refined to polymers with LCST between 25 – 37 °C i.e. between room and body surface temperature. From these polymers, the following criteria was then used to rank the likely safety of the materials:

1. The polymer was already used in pharmaceutical products.
2. The polymer has been reported as non-cytotoxic in the literature.
3. The toxicophore predictor Derek by Nexus (U.K.) identified no toxic components.

If the polymer was in used in pharmaceutical products it will be selected for synthesis, if not already in use then reported toxicity will decide if the polymer is chosen. If not used in commercial products and cytotoxicity is not reported, then Derek Nexus will be used to identify the polymer most likely to be safe. The results produced from Derek, however, must be taken with caution as Derek is known to be applicable to small molecules, not polymers.

[4.4.1.1] Toxicophore identification

Toxicophores were predicted for a pentamer *in silico* using Derek by Nexus (U.K.). Predictions were made for polymers with a degree of polymerisation greater of 5, as this accounted for any structural features between monomer units in the centre of the polymer, at the end of the polymer chains, and units adjacent to terminal groups. The identified toxicophores were then used to evaluate whether or not a polymer would be investigated further. If all polymers exhibited toxicophores, the polymers with fewer toxicophores were selected in attempt to minimise risk.

[4.4.2] Synthesis of LCST-exhibiting homopolymers identified from the literature

Homopolymers were synthesised by ATRP to target 100 kDa number average molecular weight (Mn). The same method was used for all polymerisations, but the catalyst, ligand and solvent system were varied (Table 4.1). Only solvents that can solubilise PEG (e.g. H_2O, methanol, ethanol and isopropyl alcohol above 40 °C) were used for homopolymer synthesis so that the methods could be used in later experiments for block copolymer synthesis. Firstly, the copper catalyst was sealed in a round bottom flask and degassed for 30 min by nitrogen purging. Following this, the ligand, monomer and initiator were dissolved in solvent (quantity in table 4.1) within a sealed round bottomed flask. The solution was then degassed by nitrogen bubbling for 30 min. The solution containing ligand, initiator and monomer was then transferred to the flask containing the catalyst via a degassed syringe. The reaction was allowed to proceed with stirring at the temperature stated in table 4.1. Samples were taken at regular intervals using a degassed syringe and analysed using GPC to monitor the

polymerisation. Once polymerisation ceased, the reaction mixture was dried in vacuo and dissolved in THF (10 mL). This solution was passed through a short length of neutral aluminium oxide (Brockmann I) to remove the catalyst-ligand complex. The crude product was then dissolved in H_2O (10 mL) and dialysed against water using a cellulose dialysis membrane (MWCO ~ 3500 Da) for 48 h. The resulting solution was then freeze-dried yielding pure polymer.

Table 4. 1: The reagents and conditions used to perform the polymerisations to produce homopolymers 1 to 18, and the quantities of each used. The percentage yield of each polymer is also included.

Code	Monomer (Quantity)	Catalyst (Quantity)	Ligand (Quantity)	Solvent (Quantity)	Temp (°C)	Yield (%)
1	NIPAM (12.5 g, 0.11 mol)	CuBr (18 mg, 125 µmol)	Me$_6$TREN (33.2 µL, 125 µmol)	DI water (10 mL)	RT	88.3
2	DMAEMA (5.25 mL, 31.1 mmol)	CuCl (5.0 mg, 49 µmol)	Bipyridine (15.6 mg, 98 µmol)	MeOH (5 mL)	RT	65.3
3	DMAEMA (5.25 mL, 31.1 mmol)	CuBr (7.0 mg, 49 µmol)	Bipyridine (15.6 mg, 98 µmol)	4:1 iPA: DI water (5 mL)	RT	73.5
4	DMAEMA (5.25 mL, 31.1 mmol)	CuBr (7.0 mg, 49 µmol)	Bipyridine (15.6 mg, 98 µmol)	2:1 MeOH: DI water (5 mL)	RT	82.7
5	NVCL (7.00 g, 50.3 mmol)	CuBr (10 mg, 70 µmol)	PMDETA (14.4 µL, 70 µmol)	2:1 iPA: DI water (10 mL)	80	N/A
6	NVCL (7.00 g, 50.3 mmol)	CuBr (10 mg, 70 µmol)	PMDETA (14.4 µL, 70 µmol)	2:1 EtOH: DI water (10 mL)	80	N/A
7	NVCL (7.00 g, 50.3 mmol)	CuBr (10 mg, 70 µmol)	PMDETA (14.4 µL, 70 µmol)	2:1 MeOH: DI water (10 mL)	80	N/A
8	NVCL (7.00 g, 50.3 mmol)	CuBr (10 mg, 70 µmol)	PMDETA (14.4 µL, 70 µmol)	1,4-Dioxane (10 mL)	80	N/A
9	NVP (6.73 mL, 63.0 mmol)	CuBr (10 mg, 70 µmol)	Bipyridine (22.0 mg, 140 µmol)	DI water (10 mL)	80	N/A
10	NVP (6.73 mL, 63.0 mmol)	CuBr (10 mg, 70 µmol)	Me$_6$TREN (18.6 µL, 70 µmol)	DI water (10 mL)	80	N/A

Code	Monomer (Quantity)	Catalyst (Quantity)	Ligand (Quantity)	Solvent (Quantity)	Temp (°C)	Yield (%)
11	NVP (6.73 mL, 63.0 mmol)	CuBr (10 mg, 70 µmol)	PMDETA (14.4 µL, 70 µmol)	DI water (10 mL)	80	56.8
12	DEA (7.58 mL, 55.0 mmol)	CuBr (10 mg, 70 µmol)	Me$_6$TREN (18.6 µL, 70 µmol)	DI water (10 mL)	RT	82.1
13	DEA (7.58 mL, 55.0 mmol)	CuBr (10 mg, 70 µmol)	Me$_6$TREN (18.6 µL, 70 µmol)	MeOH (10 mL)	RT	43.5
14	DEA (7.58 mL, 55.0 mmol)	CuBr (10 mg, 70 µmol)	Me$_6$TREN (18.6 µL, 70 µmol)	EtOH (10 mL)	RT	N/A
15	DEA (7.58 mL, 55.0 mmol)	CuBr (10 mg, 70 µmol)	Me$_6$TREN (18.6 µL, 70 µmol)	1:1 MeOH: Di water (10 mL)	RT	66.9
16	DEGMEMA (6.86 mL, 37.2 mmol)	CuBr (10 mg, 70 µmol)	Bipyridine (22.0 mg, 140 µmol)	MeOH (10 mL)	RT	N/A
17	DEGMEMA (6.86 mL, 37.2 mmol)	CuBr (10 mg, 70 µmol)	Bipyridine (22.0 mg, 140 µmol)	EtOH (10 mL)	RT	N/A
18	DEGMEMA (6.86 mL, 37.2 mmol)	CuBr (10 mg, 70 µmol)	Bipyridine (22.0 mg, 140 µmol)	iPA (10 mL)	RT	74.2

[4.4.3] Synthesis of 4 and 10 kDa PEG macroinitiators

PEG macroinitiators were synthesised of 4 and 10 kDa Mn using methods published in the literature.[27] DMAP (1.17 g, 9.6 mmol) in anhydrous dichloromethane (8 mL) was mixed with TEA (0.89 mL, 6.4 mmol) and cooled to 0 °C. BiBB (1.97 mL, 16.0 mmol) in anhydrous dichloromethane (8 mL) was added to the DMAP and TEA solution. A solution of PEG (10 kDa, 16.0 g; or 4 kDa, 6.4 g; 1.6 mmol) in dichloromethane (160 mL) was then added dropwise over 1 h. When the PEG addition finished, the reaction was allowed to rise to room temperature and stirred for 18 h. The solution was filtered, and half of the solvent removed in vacuo. The PEG initiator was precipitated in cold diethyl ether (480 mL) and filtered. The PEG macroinitiator was then recrystalised from absolute ethanol (300 mL) overnight. The PEG macroinitiator was then filtered and washed with cold diethyl ether, before drying in vacuo to yield pure product (4 kDa; 74.5 % and 10 kDa; 83.6 %).

[4.4.4] Synthesis of ABA tri-block copolymers of an LCST-exhibiting polymer (A) and PEG (B)

Methods were selected from the syntheses described in section [4.4.2] and were used in the synthesis of the tri-block copolymers. Tri-block copolymers were synthesised using di-functionalised PEG macroinitiators from section [4.4.3]. The reagents and quantities and experimental conditions used for the synthesis of tri-block copolymers is shown below in Table 4.2. The general procedure is as follows. The macro-initiator, ligand and monomer were placed into a flask and dissolved in the solvent. In a separate flask, the copper(I) bromide was added and both flasks were sealed and degassed with nitrogen bubbling for 30 min. After degassing, the monomer, macro-initiator, ligand and solvent mix was transferred to the copper(I) bromide via a degassed syringe. The flask was then stirred and heated were required until polymerisation ceased. To ensure polymerisation had finished, aliquots were removed and analysed by GPC. The polymerisation had finished when the Mn failed to increase. It has been reported that removal of copper by neutral alumina alone causes copper-related cytotoxicity, whereas using neutral alumina and dialysis shows negligible cytotoxicity.[28] Therefore, all tri-block copolymers were passed through alumina and dialysed for purification.

Table 4. 2: The reagents and conditions used to synthesise tri-block copolymers with designated codes 19 to 34, and the quantities used. The percentage yield of each polymer is also included.

Code	Tri-block Copolymer	Monomer (Quantity)	Initiator (Quantity)	Catalyst (Quantity)	Ligand (Quantity)	Solvent (Quantity)	Temp (°C)	Yield (%)
19	PNIPAM$_{10}$-PEG$_4$-PNIPAM$_{10}$	NIPAM (4.2 g, 37.1 mmol)	PEG$_{4kDa}$ (0.5 g, 125 µmol)	CuBr (35.9 mg, 250 µmol)	Me6TREN (66.8 µL, 250 µmol)	DI Water (10 mL)	RT	91.2
20	PNIPAM$_{20}$-PEG$_4$-PNIPAM$_{20}$	NIPAM (7.0 g, 61.9 mmol)	PEG$_{4kDa}$ (0.5 g, 125 µmol)	CuBr (35.9 mg, 250 µmol)	Me6TREN (66.8 µL, 250 µmol)	DI Water (10 mL)	RT	88.6
21	PNIPAM$_{10}$-PEG$_{10}$-PNIPAM$_{10}$	NIPAM (4.0 g, 35.3 mmol)	PEG$_{10kDa}$ (1.0 g, 100 µmol)	CuBr (28.7 mg, 200 µmol)	Me6TREN (53.5 µL, 200 µmol)	DI Water (10 mL)	RT	90.3
22	PNIPAM$_{20}$-PEG$_{10}$-PNIPAM$_{20}$	NIPAM (6.0 g, 53.0 mmol)	PEG$_{10kDa}$ (1.0 g, 100 µmol)	CuBr (28.7 mg, 200 µmol)	Me6TREN (53.5 µL, 200 µmol)	DI Water (10 mL)	RT	89.5
23	PDMAEMA$_{10}$-PEG$_4$-PDMAEMA$_{10}$	DMAEMA (5.4 mL, 31.8 mmol)	PEG$_{4kDa}$ (0.5 g, 125 µmol)	CuCl (24.7 mg, 250 µmol)	Bipyridine (78.0 mg, 500 µmol)	MeOH (20 mL)	RT	86.2
24	PDMAEMA$_{20}$-PEG$_4$-PDMAEMA$_{20}$	DMAEMA (8.0 mL, 47.7 mmol)	PEG$_{4kDa}$ (0.5 g, 125 µmol)	CuCl (24.7 mg, 250 µmol)	Bipyridine (78.0 mg, 500 µmol)	MeOH (20 mL)	RT	84.7
25	PDMAEMA$_{10}$-PEG$_{10}$-PDMAEMA$_{10}$	DMAEMA (4.3 mL, 25.4 mmol)	PEG$_{10kDa}$ (1.0 g, 100 µmol)	CuCl (19.8 mg, 200 µmol)	Bipyridine (62.5 mg, 400 µmol)	MeOH (20 mL)	RT	90.0
26	PDMAEMA$_{20}$-PEG$_{10}$-PDMAEMA$_{20}$	DMAEMA (6.4 mL, 38.2 mmol)	PEG$_{10kDa}$ (1.0 g, 100 µmol)	CuCl (19.8 mg, 200 µmol)	Bipyridine (62.5 mg, 400 µmol)	MeOH (20 mL)	RT	85.3

Code	Tri-block Copolymer	Monomer (Quantity)	Initiator (Quantity)	Catalyst (Quantity)	Ligand (Quantity)	Solvent (Quantity)	Temp (°C)	Yield (%)
27	$PDEA_{10}\text{-}PEG_4\text{-}PDEA_{10}$	DEA (5.4 mL, 39.3 mmol)	PEG_{4kDa} (0.5 g, 125 µmol)	CuBr (35.9 mg, 250 µmol)	Me6TREN (66.8 µL, 250 µmol)	MeOH: Water (1:1) (20 mL)	RT	92.3
28	$PDEA_{20}\text{-}PEG_4\text{-}PDEA_{20}$	DEA (8.1 mL, 59.0 mmol)	PEG_{4kDa} (0.5 g, 125 µmol)	CuBr (35.9 mg, 250 µmol)	Me6TREN (66.8 µL, 250 µmol)	MeOH: Water (1:1) (20 mL)	RT	91.6
29	$PDEA_{10}\text{-}PEG_{10}\text{-}PDEA_{10}$	DEA (4.3 mL, 31.5 mmol)	PEG_{10kDa} (1.0 g, 100 µmol)	CuBr (28.7 mg, 200 µmol)	Me6TREN (53.5 µL, 200 µmol)	MeOH: Water (1:1) (20 mL)	RT	88.2
30	$PDEA_{20}\text{-}PEG_{10}\text{-}PDEA_{20}$	DEA (6.5 mL, 47.3 mmol)	PEG_{10kDa} (1.0 g, 100 µmol)	CuBr (28.7 mg, 200 µmol)	Me6TREN (53.5 µL, 200 µmol)	MeOH: Water (1:1) (20 mL)	RT	86.0
31	$PDEGMEMA_{10}\text{-}PEG_4\text{-}PDEGMEMA_{10}$	DEGMEMA (4.9 mL, 26.6 mmol)	PEG_{4kDa} (0.5 g, 125 µmol)	CuBr (35.9 mg, 250 µmol)	Bipyridine (78.0 mg, 500 µmol)	iPA (20 mL)	40	84.1
32	$PDEGMEMA_{20}\text{-}PEG_4\text{-}PDEGMEMA_{20}$	DEGMEMA (7.4 mL, 39.9 mmol)	PEG_{4kDa} (0.5 g, 125 µmol)	CuBr (35.9 mg, 250 µmol)	Bipyridine (78.0 mg, 500 µmol)	iPA (20 mL)	40	86.2
33	$PDEGMEMA_{10}\text{-}PEG_{10}\text{-}PDEGMEMA_{10}$	DEGMEMA (3.9 mL, 21.3 mmol)	PEG_{10kDa} (1.0 g, 100 µmol)	CuBr (28.7 mg, 200 µmol)	Bipyridine (62.5 mg, 400 µmol)	iPA (20 mL)	40	88.9
34	$PDEGMEMA_{20}\text{-}PEG_{10}\text{-}PDEGMEMA_{20}$	DEGMEMA (5.9 mL, 32.0 mmol)	PEG_{10kDa} (1.0 g, 100 µmol)	CuBr (28.7 mg, 200 µmol)	Bipyridine (62.5 mg, 400 µmol)	iPA (20 mL)	40	87.6

[4.4.5] Polymer Characterisation

^{1}H NMR and ^{1}H diffusion ordered spectroscopy (DOSY) NMR were performed on an Oxford Instrument ECA600 600 MHz NMR spectrometer with Delta 4.3.6 software. All samples were measured in D_2O unless otherwise stated. All spectra were analysed using MNOVA by Mestrelab (Spain). NMR was used to confirm synthesis of homopolymers, block copolymers and macroinitiators. The Mn of the PEG macro-initiators and tri-block copolymers were calculated from ^{1}H NMR. In the case of PEG, the Mn was calculated by using the ratio of the integral for the two terminal CH_2 groups to the integral of the remaining CH_2 groups present in the polymer. For the tri-block copolymers, the ratio of the PEG peak integral to that of the peaks formed for the new polymer arms was used to predict the Mn.

IR spectroscopy was performed on homopolymers with a Perkin Elmer Fourier Transform Infra-red (FTIR) Spectrometer Frontier with a Perkin Elmer Universal attenuated total reflectance (ATR) Sample Accessory. A wavelength range of 650-4000 cm^{-1} was used with a resolution of 4 cm^{-1}. The instrument was cleaned with isopropyl alcohol before and after use.

An Agilent 12600 Infinity II GPC equipped with a refractive index (RI) detector was used to predict the Mn of the homopolymers and the PDI of both homo and tri-block copolymers. A Phenomenex Phenogel 10 μm 10E5 Å column was used with DMF with 0.1 % LiBr as an eluent, at a flow rate of 0.4 mL/min with the column and detector held at 30 °C. The GPC was calibrated with Agilent Easivial poly(methyl methacrylate) (PMMA) standards with Mn ranging from 370 to 364000 Da. The calibration had an r^2 of 0.9998 (Figure 4.4).
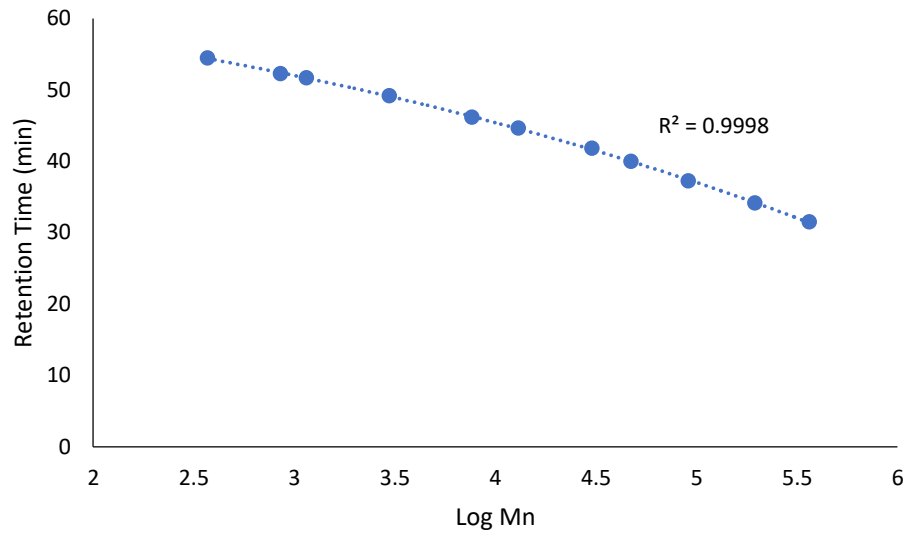
Figure 4. 4: The narrow calibration curve of the GPC using Agilent PMMA standards. The curve is a third-order polynomial with an r^2 of 0.9998.

[4.5] Results and Discussion

[4.5.1] Selection of LCST-exhibiting polymers from the literature

The database of polymers constructed for the QSPR model described in Chapter 3 was used to identify polymers reported to exhibit LCSTs in the range of 25 to 37 °C. 12 polymers were identified with LCSTs in the desired range, these are shown in Figure 4.5 with the LCST in aqueous solution noted.

N,N-diethyl acrylamide
LCST 28 °C

N-isopropyl acrylamide
LCST 32 °C

3-ethyl-1-vinyl-2-pyrrolidone
LCST 27 °C

N-(2-methoxy-1,3-dioxan-5-yl)methacrylamide
LCST 36 °C

N-vinyl caprolactam
LCST 32 °C

2-(2-(2-ethoxyethoxy)ethoxy)ethyl acrylate
LCST 34 °C

2-morpholinoethyl methacrylate
LCST 34 °C

N-vinyl pyrrolidone
LCST 30 °C (in 1.5 M KI)

diethylene glycol methyl ether methacrylate
LCST 28 °C

methyl methacryloyl-*L*-alaninate
LCST 35 °C

2-(dimethylamino)ethyl methacrylate
LCST 32 °C

(*S*)-*N*-(1-(isopropylamino)-1-oxopropan-2-yl)methacrylamide
LCST 30 °C

N-(L)-(1-hydroxymethyl)propylmethacrylamide
LCST 30 °C

Figure 4. 5: The monomer structure, name and LCST of the polymers found in the literature that exhibit an LCST between 25 and 37 °C.

The number of polymers was reduced using the method described in section [4.4.1]. Firstly, polymers present in the FDA's inactive ingredients database[29] were selected, as sufficient toxicity studies would have been performed previously to confirm their safety.[30] Three polymers, poly(N-vinyl caprolactam) (PNVCL), poly(N-vinyl pyrrolidone) (PNVP) and poly(2-N-(dimethylamino)ethyl methacrylate) (PDMAEMA), were identified as a component of Soluplus, Povidone and Eudragit E100 respectively. Due to their known use in pharmaceutical grade excipients, PNVCL, PNVP, and PDMAEMA polymers were selected for further study. The chemical structures of Eudragit E100, Soluplus and Povidone are shown below in Figures 4.6a, 4.6b and 4.6c respectively. A fourth

polymer, poly(N,N-diethyl acrylamide) (PDEA), was selected as this met the strict criteria of a physiologically relevant LCST (Ca. 28 °C)[31] and has been reported to be non-cytotoxic.[32] Given the LCST and reported non-cytotoxicity, PDEA could offer a replacement to the reportedly cytotoxic PNIPAM in thermogelling materials.[33]
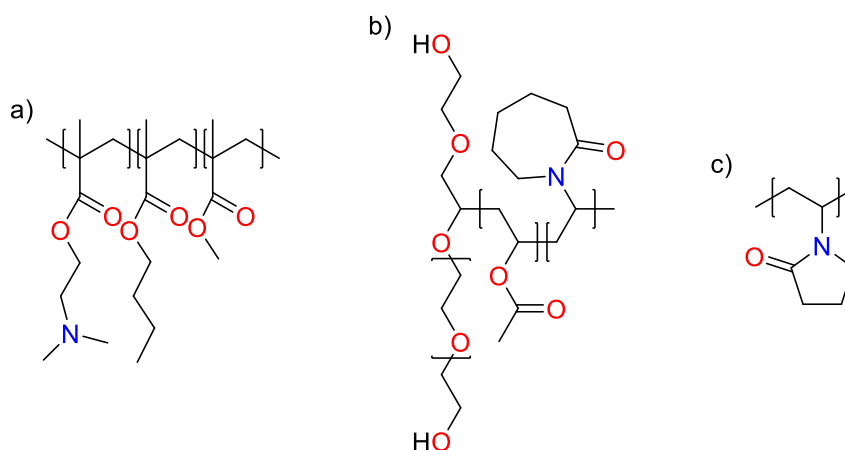
Figure 4. 6: The molecular structures of Eudragit E100 (a), Soluplus (b) and povidone (c).

Four monomers were initially selected for polymerisation; PNVP, PNVCL, PDMAEMA and PDEA. If polymerisation by ATRP was not achievable for any of the selected polymers, contingencies were identified. Polymers which were reported as non-cytotoxic in the literature were preferentially selected, which identified poly(diethylene glycol methyl ether methacrylate) (PDEGMEMA) and poly(2-(2-methoxyethoxy)ethyl methacrylate) for further study. The toxicophore predictor Derek was applied to a pentamer of the two polymers. Derek identified poly(2-(2-(2-ethoxyethoxy)ethoxy)ethyl acrylate) as a potential irritant to the gastrointestinal tract and a possible nephrotoxin, while PDEGMEMA was identified as potentially nephrotoxic. The two contingency polymers selected, in order of preference, were PDEGMEMA followed by poly(2-(2-methoxyethoxy)ethyl methacrylate). If polymerisation of PDEGMEMA failed, synthesis of poly(2-(2-methoxyethoxy)ethyl methacrylate) would be attempted.

[4.5.2] Synthesis of LCST-exhibiting homopolymers identified from the literature

[4.5.2.1] Synthesis and characterisation of PNIPAM homopolymers

NIPAM was polymerised by ATRP using a method published in the literature.[34] The method utilised a 1:1:1 ratio of copper (I) bromide, Me$_6$TREN and initiator in aqueous solution. The polymerisation was successful, as determined by ^{1}H NMR, ATR-FTIR and GPC.

The ^{1}H NMR of both N-isopropyl acrylamide and PNIPAM are given below in Figure 4.7. The monomer NMR exhibits four peaks, two associated with the vinyl protons and two for the isopropyl group. The two vinyl peaks are present as a multiplet and a doublet of doublets between 5.5 and 6.5 ppm. The isopropyl peaks are present at 3.6 and 1.1 as a septet and doublet respectively. In the polymer spectra, the vinyl peaks between 5.5 and 6.5 ppm are missing indicating that no monomer is present. Also, the two peaks at 3.6 and 1.1 ppm have broadened which is a sign of polymerisation, as there are many protons present in similar environments.[35] There are also two new broad peaks present at 1.4 and 1.8 ppm, which represent the alkyl polymer backbone. Both spectra show a peak at a chemical shift of 4.7 ppm, which is characteristic of residual water in the D$_2$O NMR solvent.[36] In all other spectra in this chapter a sharp peak at ca. 4.7 ppm has been attributed to residual water.
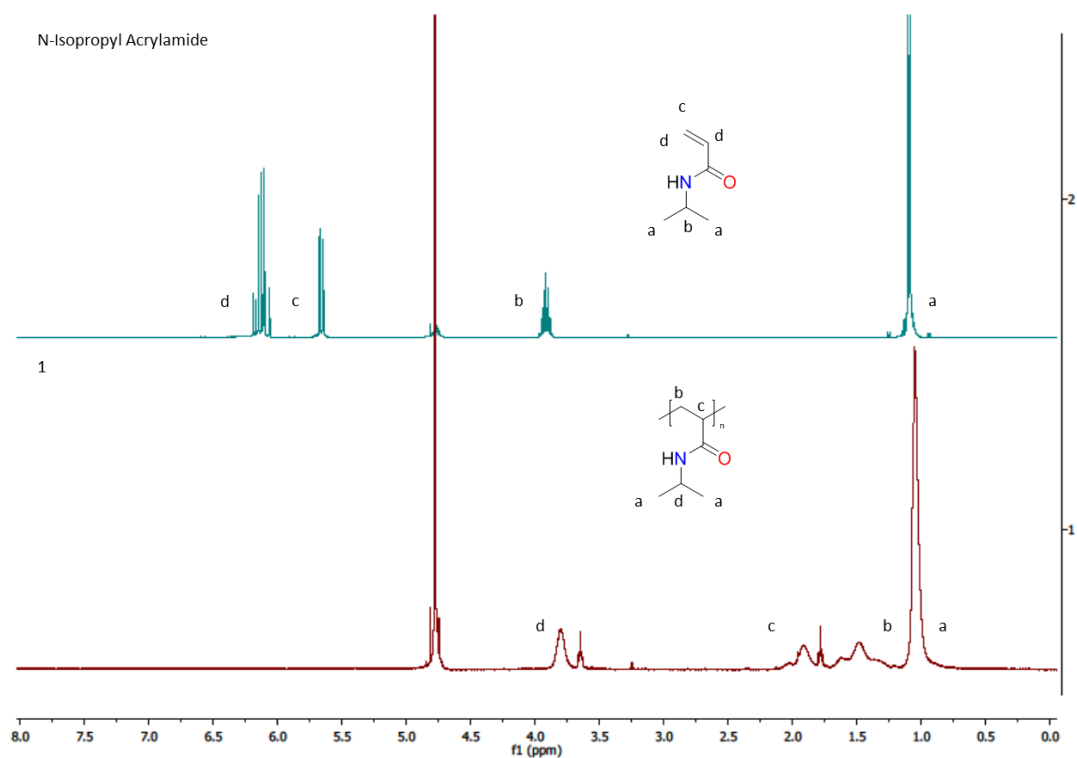
Figure 4. 7: The ^{1}H NMR spectra of NIPAM (blue) and polymer **1** (red) in D$_2$O at 600 MHz.

The IR spectra of NIPAM and PNIPAM are given below in Figure 4.8. IR spectrometry was used to confirm the absence of the vinyl peak, indicating monomer conversion to polymer. The IR spectrum of the monomer shows three peaks at 1547, 1620 and 1655 cm^{-1} for the N-H bending of the amide, the vinyl group stretching and the carbonyl stretching, respectively. In the polymer spectrum only two peaks remain at 1638 and 1528 cm^{-1}, these represent the remaining carbonyl stretch and N-H amide bending respectively, confirming the monomer has been polymerised.
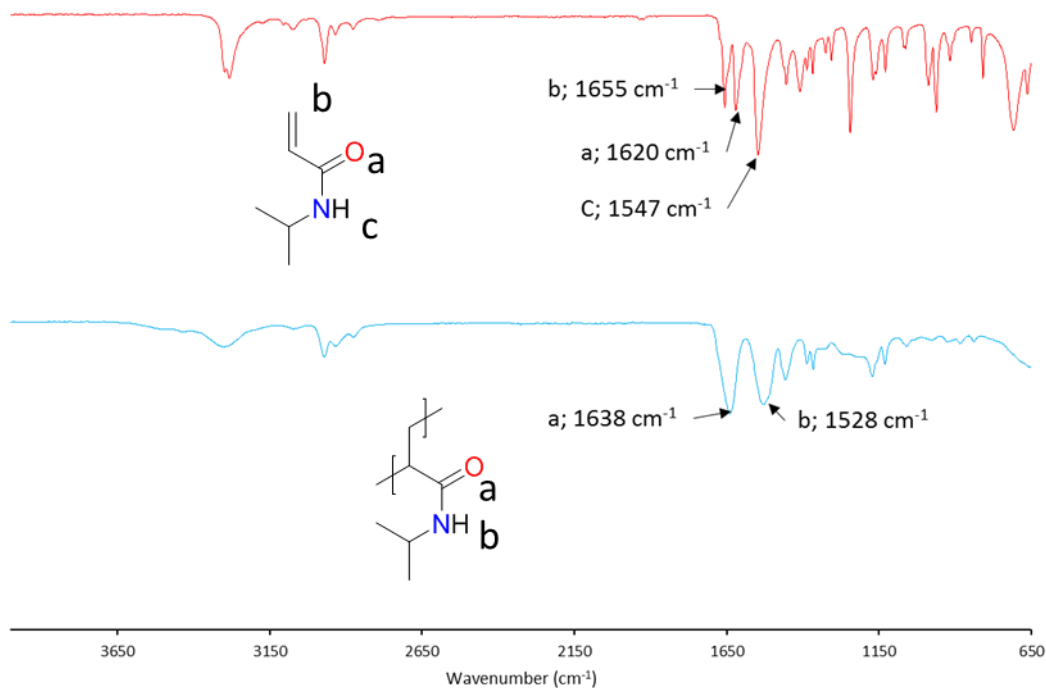
Figure 4. 8: The IR spectra of NIPAM (blue) and polymer **1** (red).

The GPC trace of polymer **1** is shown in Figure 4.9**.** The trace is monomodal indicating a single population of Mn. The Mn and PDI of polymer **1** as identified by GPC were 26 kDa and 2.05, respectively. The PDI is broad, indicating an uncontrolled polymerisation which is in agreement with previous literature reports.[37] However, the PDI of polymer **1** should not affect LCST, as PNIPAM exhibits type II demixing which is not dependent on polymer Mn.[38]
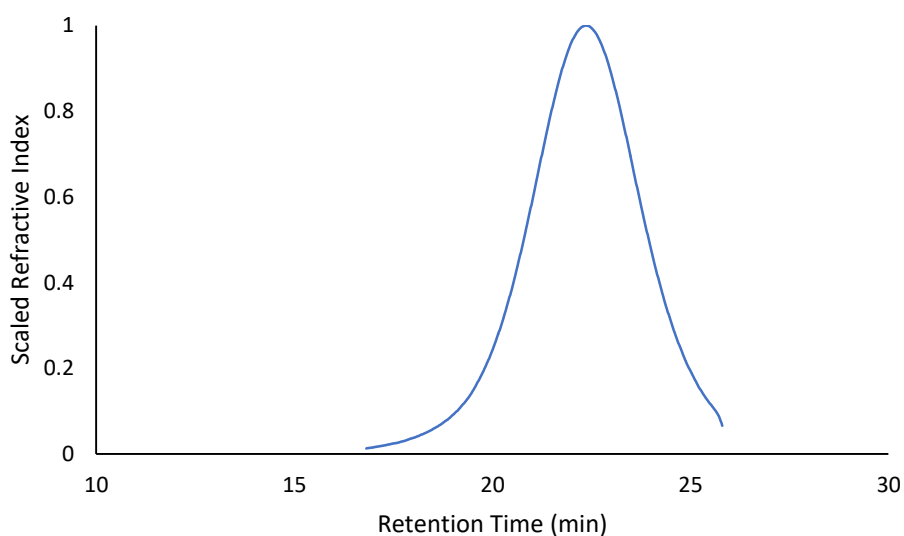
Figure 4. 9: The GPC trace of polymer **1** in DMF + 0.1 % LiBr at a flow rate of 0.4 mL/min.

The LCST of polymer **1** at 10, 20 and 30 % w/v in aqueous solution was investigated to identify the effect of concentration. The LCST of polymer **1** at 10, 20 and 30 % w/v were found to be 31.92 ± 0.11, 31.90 ± 0.17 and 31.92 ± 0.10 °C. The LCST was found to not significantly differ with concentration as identified by one-way ANOVA with Tukey post-hoc test (P < 0.05), in agreement with the literature.[39]

[4.5.2.2] Synthesis and characterisation of PDMAEMA homopolymers

The polymerisation of DMAEMA was carried out using a 1:2:1 ratio of copper catalyst: bipyridine: initiator as described in the literature.[40–42] One method in the literature reported the use of Cu(I)Cl as a catalyst in methanol[42], while others report the use of Cu(I)Br in 4:1 iPA:water[24] and 2:1 methanol:water.[25]

The ^{1}H NMR traces of DMAEMA and polymers **2**, **3** and **4** of PDMAEMA (Figure 4.10). The ^{1}H NMR spectrum of DMAEMA shows two doublets between 5.0 and 6.0 ppm, which represent the vinyl protons. The peaks at 4.0, 2.5, 2.0 and 1.7 represent the remaining proton environments and are presented as two triplets and two singlets respectively. The ^{1}H NMR spectra of polymers **2**, **3** and **4** do not show these vinyl protons, and the remaining signals have broadened. The chemical shift for methyl group bound to the vinyl has shifted from 1.7 to 0.7 ppm, indicating the double bond is no longer present. Also, there is a new peak present between 0.5 and 1.0 ppm, indicating the alkyl polymer backbone. Therefore, the ^{1}H NMR spectra of polymer **2**, **3** and **4** confirm successful polymerisation.
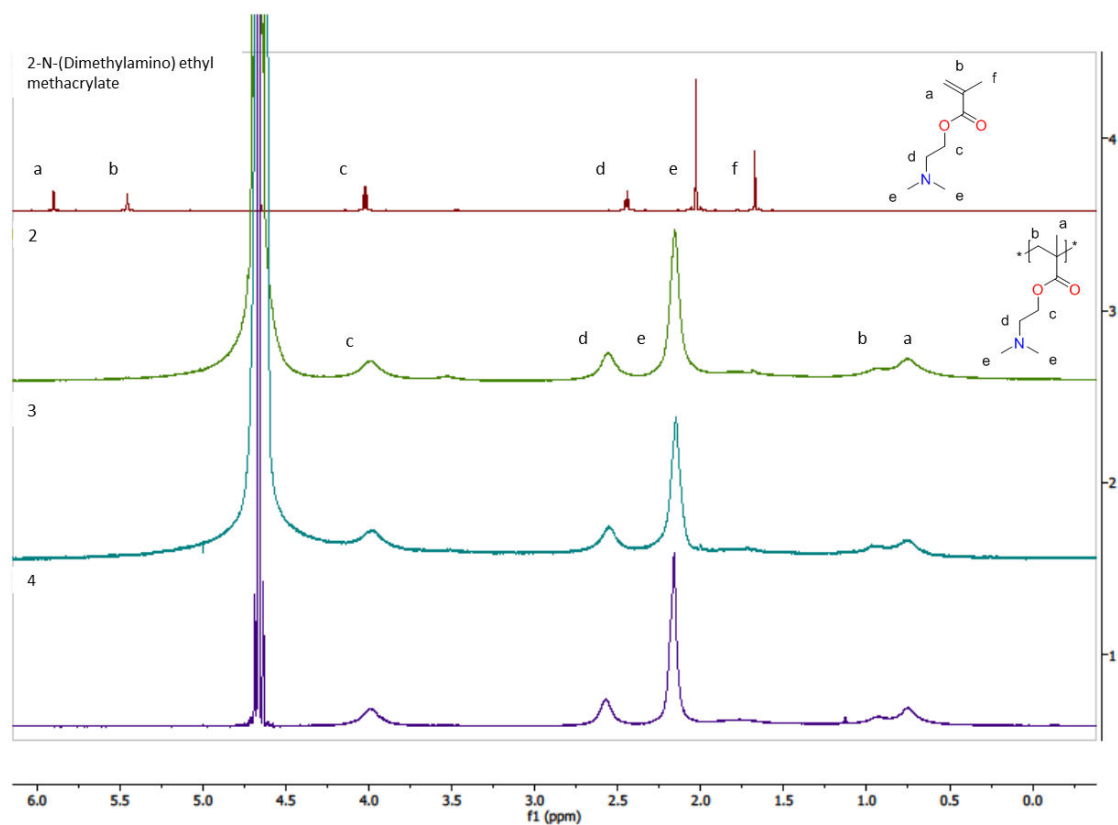
Figure 4. 10: The ^{1}H NMR spectra of DMAEMA (red) and polymers **2** (green), **3** (teal) and **4** (purple) in D$_2$O at 600 MHz.

The IR spectra for DMAEMA and polymers **2**, **3** and **4** are shown below in Figure 4.11. The monomer spectrum shows two peaks at 1717 and 1638 cm^{-1} which represent the carbonyl stretch of the ester and the stretch of the vinyl group respectively. In the spectra for polymers **3** and **4**, there is only one peak present at 1723 and 1725 cm^{-1} respectively. One peak present indicates that the vinyl group is no longer present, only the carbonyl remains. In the IR spectrum for polymer **2**, however, there is a broad peak next to the carbonyl peak at 1725 cm^{-1} which may indicate the presence of residual monomer.
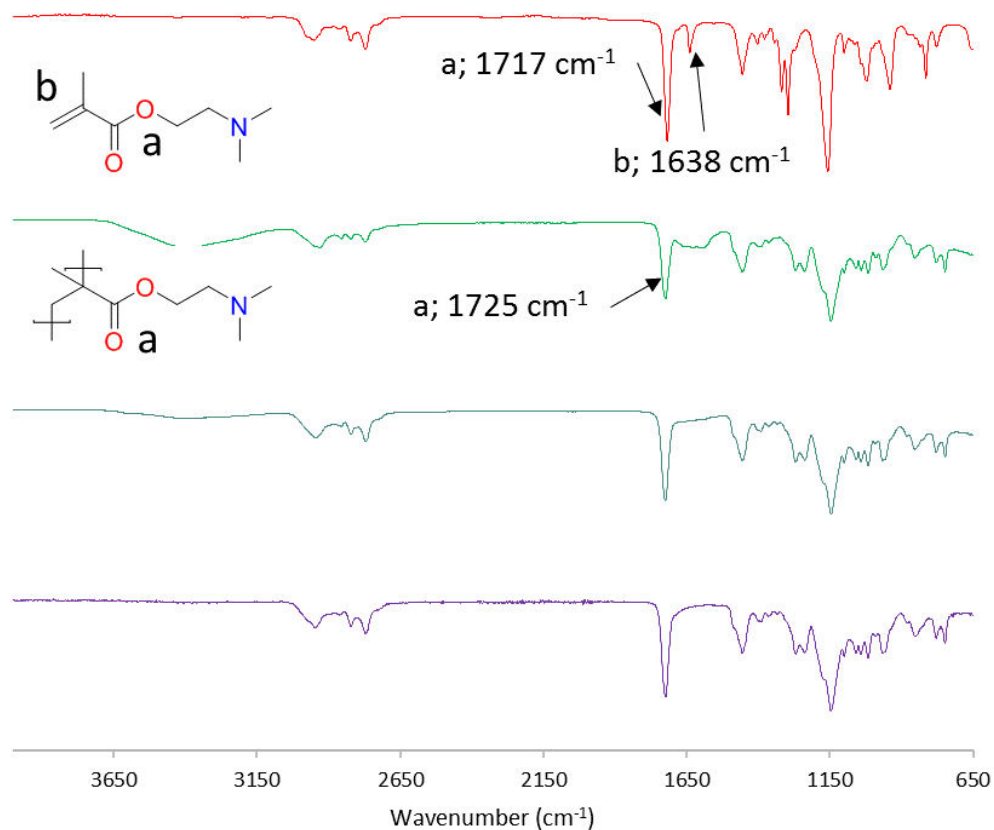
Figure 4. 11: The IR spectra of DMAEMA (red) and polymers **2** (green)**, 3** (teal) and **4** (purple).

The GPC traces shown in Figure 4.12 represent polymers **2**, **3** and **4**. All peaks are monomodal, indicating a single population of Mn. The Mn achieved were 27, 37 and 41 kDa for polymers **2**, **3** and **4** respectively. The Mn indicate that polymerisation **4** achieved greater conversion compared to **2** and **3**, which is due to the polarity of the solvent as previously discussed.[43] In addition to this, polymerisation 2 resulted in a polymer with a PDI of 1.77 while the PDI from polymerisations 3 and 4 were 1.88 and 1.92 respectively. This increase in Mn and PDI is attributed to the increasing polarity of the solvent. Polar solvents stabilise the activated copper (II) ligand complex which decreases the K_{deact}, solvents with increasing polarity exhibit a further reduction in K_{deact}.[44] The decreased K_{deact} prevents the reformation of the dormant species, preventing the stepwise growth of the polymer.
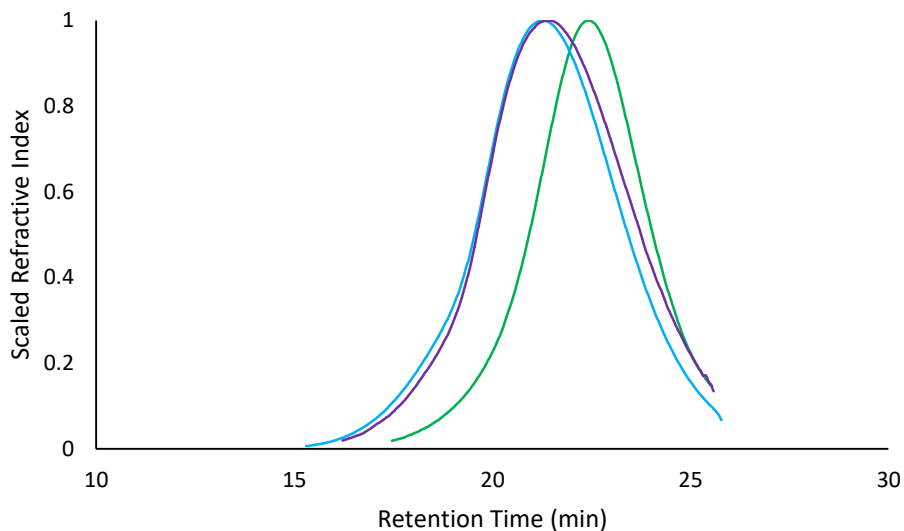
Figure 4. 12: The GPC trace of polymers **2** (green), **3** (teal) and **4** (purple) in DMF + 0.1 % LiBr at a flow rate of 0.4 mL/min.

The LCSTs of polymers **2**, **3** and **4** at 10, 20 and 30 % w/v concentration in water were investigated and are shown in Table 4.3. The LCST was found to decrease as the Mn increased. For example, for 30 % w/v solutions, the LCST decreased from 34.03 ± 0.15 to 37.63 ± 0.12 °C when the Mn increased from 27 to 41 kDa. When the concentration was increased from 10 to 30 % w/v aqueous solution for 41 kDa PDMAEMA, the LCST decreased from 38.54 ± 0.07 to 37.63 ± 0.12 °C. The dependency of the LCST on both Mn and concentration indicates a type II demixing behaviour, which is in agreement with the literature.[45] The degree of conversion to a 27 kDa polymer with a PDI of 1.77 and physiologically relevant LCST makes polymerisation method **2** ideal for use in the development of thermogelling topical drug delivery excipients. Thus, this method was taken forward for tri-block copolymer synthesis.

Table 4. 3: The LCSTs of polymers **2**, **3** and **4** in aqueous solution at 10, 20 and 30 % w/v. All LCSTs were statistically different to one another ($P < 0.05$). Data is presented as mean ± standard deviation (n=3).

Polymer (Mn (kDa))	LCST (°C)		
	10 % (w/v)	20 % (w/v)	30 % (w/v)
2 (27)	34.97 ± 0.15	34.47 ± 0.12	34.03 ± 0.15
3 (37)	37.23 ± 0.06	36.73 ± 0.15	36.07 ± 0.31
4 (41)	38.54 ± 0.07	38.01 ± 0.25	37.63 ± 0.12

[4.5.2.3] Synthesis and characterisation of PNVCl homopolymers

ATRP of NVCL has been reported in the literature using a 1:1 ratio of Cu(I)Br and PMDETA in anhydrous 1,4-dioxane.[46] In this study the ligand and catalyst were remained constant, but the solvent was varied. Since the K_{act} of ATRP is greater in polar solvents but N-vinyl caprolactam has limited solubility in water, mixtures of methanol, ethanol and isopropyl alcohol with water were explored as well as 1,4-dioxane. Although the conditions reported by Singh et al. (2012), which included degassing by freeze-pump-thaw cycles, were followed the polymerisations were not successful as identified by ^{1}H NMR, ATR-FTIR and GPC.[46] The failure of this polymerisation is likely due to the structure of N-vinyl caprolactam. In a radical polymerisation, the vinyl moiety of NVCL would react to produce a propagating radical. However, the propagating radical is not stable enough to continue the polymerisation as the radical cannot be stabilised by conjugation, and the radical is then quickly terminated.[47] Thus, NVCL is thought of as a "less-activated monomer".[48] As the polymerisation by ATRP cannot be carried out in solvents in which PEG is soluble in, the monomer was not taken forward for tri-block copolymer synthesis.

[4.5.2.4] Synthesis and Characterisation of PNVP homopolymers

Polymerisation of NVP by ATRP has not been reported in the literature prior to this study. NVP is structurally similar to NVCL, so can be classed as a "less-activated monomer" and was expected to be difficult to polymerise by ATRP. However, NVP is soluble in water whereas the solubility of NVCL is minimal. Therefore, all polymerisations were performed in water with Cu(I)Br as a catalyst, but the ligand was varied. The three ligands used were bipyridine, in a ratio of 2:1 with Cu(I)Br, and Me$_6$TREN and PMDETA, both in a 1:1 ratio with Cu(I)Br.

^{1}H NMR was used to confirm the production of polymer, and in the case of NVP, only method **11** was successful. The ^{1}H NMR spectra of NVP and polymer **11** confirm polymerisation (Figure 4.13). The ^{1}H NMR spectrum of NVP shows two peaks at 6.6 and 4.4 ppm, a doublet of doublets and a multiplet respectively, which represent the vinyl protons. There are three remaining proton signals in the ^{1}H NMR spectrum of N-vinyl pyrrolidone at 3.4, 2.2 and 1.8 ppm which represent the protons present on the ring. In the spectrum for polymer **11**, the vinyl peaks at 4.4 and 6.6 ppm are missing, and the peaks from the protons on the ring have broadened. Also, two new peaks are present at 3.6 and 1.5 ppm, which represent the newly formed alkyl polymer backbone.
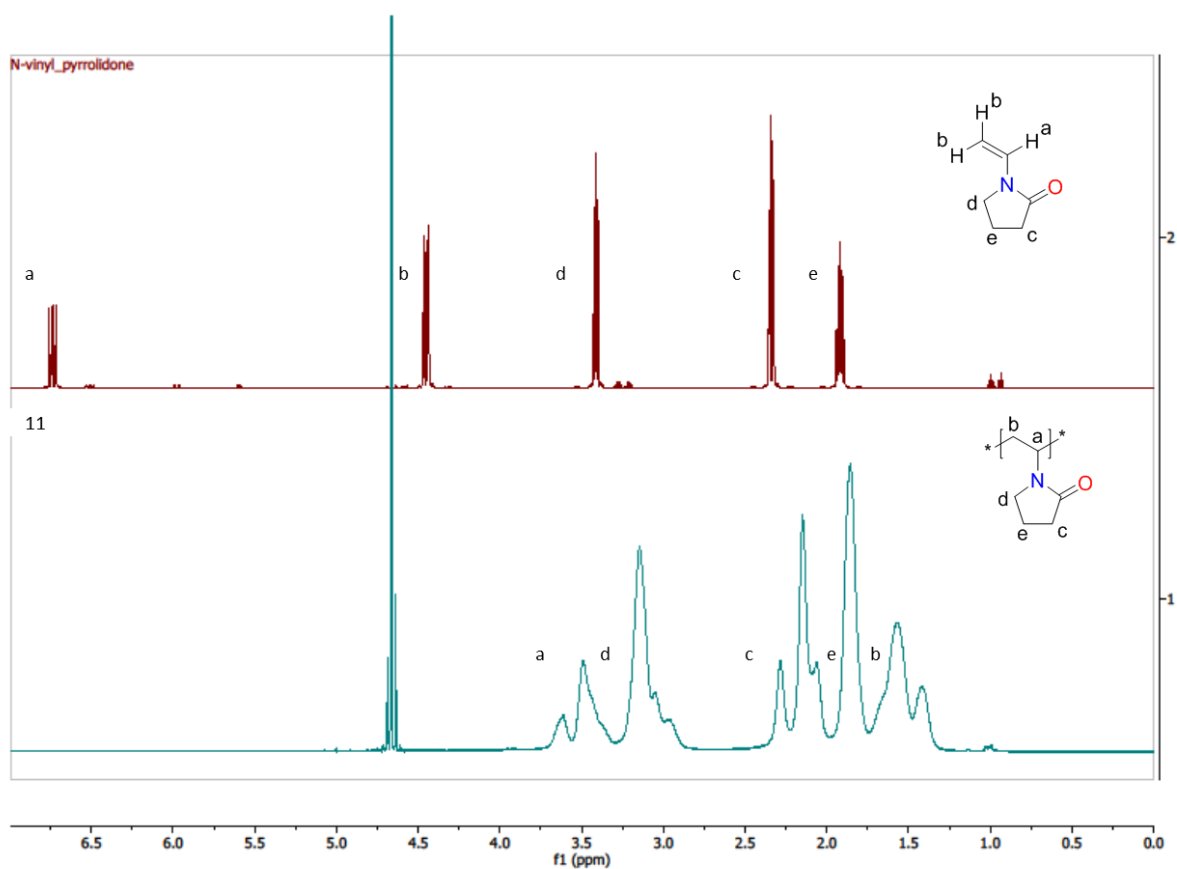
Figure 4. 13: The ^{1}H NMR spectra of NVP (red) in CDCl$_3$ and polymer **15** (teal) in D$_2$O at 600 MHz.

The IR spectra of NVP and polymer **11** are shown in Figure 4.14. The spectrum of N-vinyl pyrrolidone shows two peaks at 1696 and 1624 cm^{-1} which represent the carbonyl stretch and vinyl stretching respectively. The IR spectrum of polymer **15** shows a single peak between 1700 and 1600 cm^{-1} at 1668 cm^{-1} which represents the carbonyl stretch. The absence of the vinyl peak confirms polymerisation was successful, and that no monomer remains in the sample.
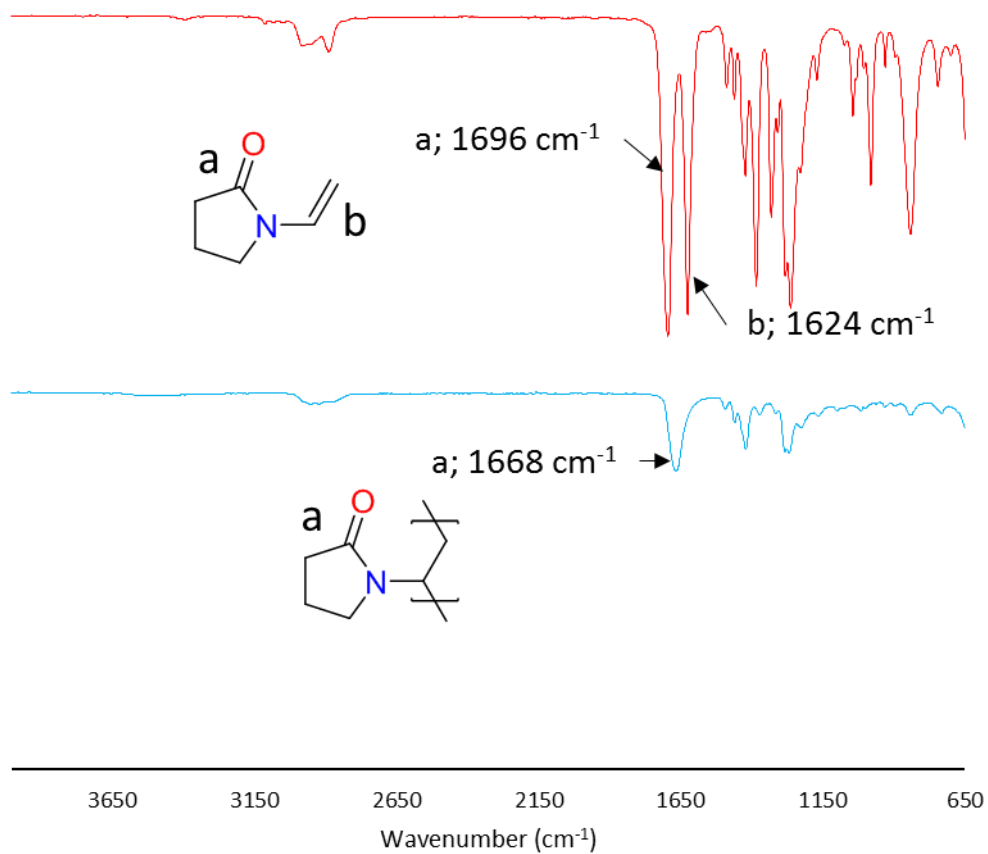
Figure 4. 14: The IR spectra of N-vinyl pyrrolidone (red) and polymer **11** (teal).

The GPC trace of polymer **11** is shown below in Figure 4.15. The peak is monomodal indicating that one population of polymer was synthesised. The polymer was found to have a Mn of 27 kDa with a PDI of 1.67.
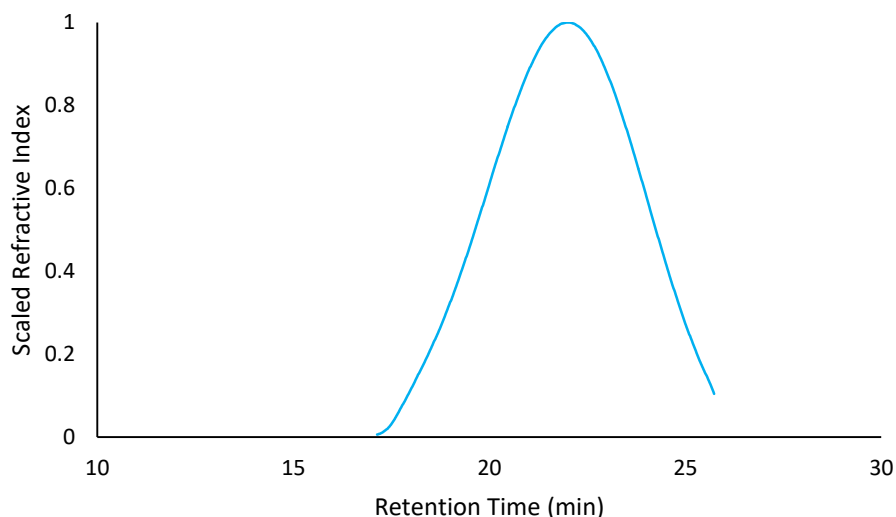
Figure 4. 15: The GPC trace of polymer **11** in DMF + 0.1 % LiBr at a flow rate of 0.4 mL/min.

PNVP does not exhibit an LCST in pure water, but reports in the literature found poly(N-vinyl pyrrolidone) to exhibit an LCST at 30 °C at a concentration of 5 % in 1.5 M KF.[49] KF is cytotoxic,[50] and therefore cannot be used in topical drug delivery. NaCl is another salting out agent which is non-cytotoxic. Therefore, NaCl solution was used at concentrations ranging from 1.5 to 6.0 M with polymer **11** concentrations at 10, 20 and 30 % w/v. PNVP did not exhibit an LCST in 1.5 M NaCl solution at 10, 20 and 30 % concentration but was found to exhibit LCSTs in 3.0 and 6.0 M NaCl (Table 4.5). Increasing the concentration of polymer **11** from 10 to 30 % w/v in 3.0 M NaCl decreased the LCST from 90.56 ± 0.10 to 88.36 ± 0.18 °C. Also increasing the concentration of NaCl from 3.0 to 6.0 M for a 30 % w/v solution of polymer **11** saw the LCST decrease from 88.36 ± 0.18 to 54.08 ± 0.16 °C. When compared to KF, NaCl was unable to induce a physiologically relevant LCST because, chloride is a weaker chaotrope when compared to fluoride, as indicated in the Hofmeister series.[51] As a result of this, this polymer was not selected for further study in the generation of thermogelling materials.

Table 4. 4: The LCSTs of polymer **11** in 3 and 6 M NaCl solution at 10, 20 and 30 % w/v. All LCSTs were found to be statistically significantly different (P < 0.05). The LCSTs are presented as a mean ± standard deviation (n=3).

Polymer	LCST		
	10 % (w/v)	20 % (w/v)	30 % (w/v)
11 in 3.0 M NaCl	90.56 ± 0.10	89.43 ± 0.07	88.36 ± 0.18
11 in 6.0 M NaCl	55.89 ± 0.09	54.92 ± 0.13	54.08 ± 0.16

[4.5.2.5] Synthesis and characterisation of PDEA homopolymers

The ATRP of DEA has not yet been reported in the literature. The method described in section [4.5.2.1] for the polymerisation of NIPAM was adopted, due to the structural similarity of NIPAM to DEA. The reactions used a 1:1 ratio Cu(I)Br and Me_6TREN, and were performed in water, methanol, absolute ethanol or 1:1 volume of methanol to water. The ^{1}H NMR confirmed the synthesis of polymers **12**, **14** and **15**. The ^{1}H NMR of DEA and polymers **12**, **14** and **15** are shown in Figure 4.16. The ^{1}H NMR spectrum of DEA shows two doublet of doublets and a multiplet between 5.5 and 6.5 ppm, which represent the protons present on the vinyl group. The peaks in the monomer spectrum at 3.3 and 1.0 ppm represent the ethyl groups present. The three polymer spectra do not show peaks above 5.5 ppm, indicating the monomer is no longer present. Also, two new broad peaks are present at 1.5 and 2.5 ppm, which represent the polymer backbone. Finally, the two peaks at 3.3 and 1.0 ppm have broadened, which is characteristic of polymer ^{1}H NMR spectra. Therefore, polymerisation methods **12**, **14** and **15** were successful.
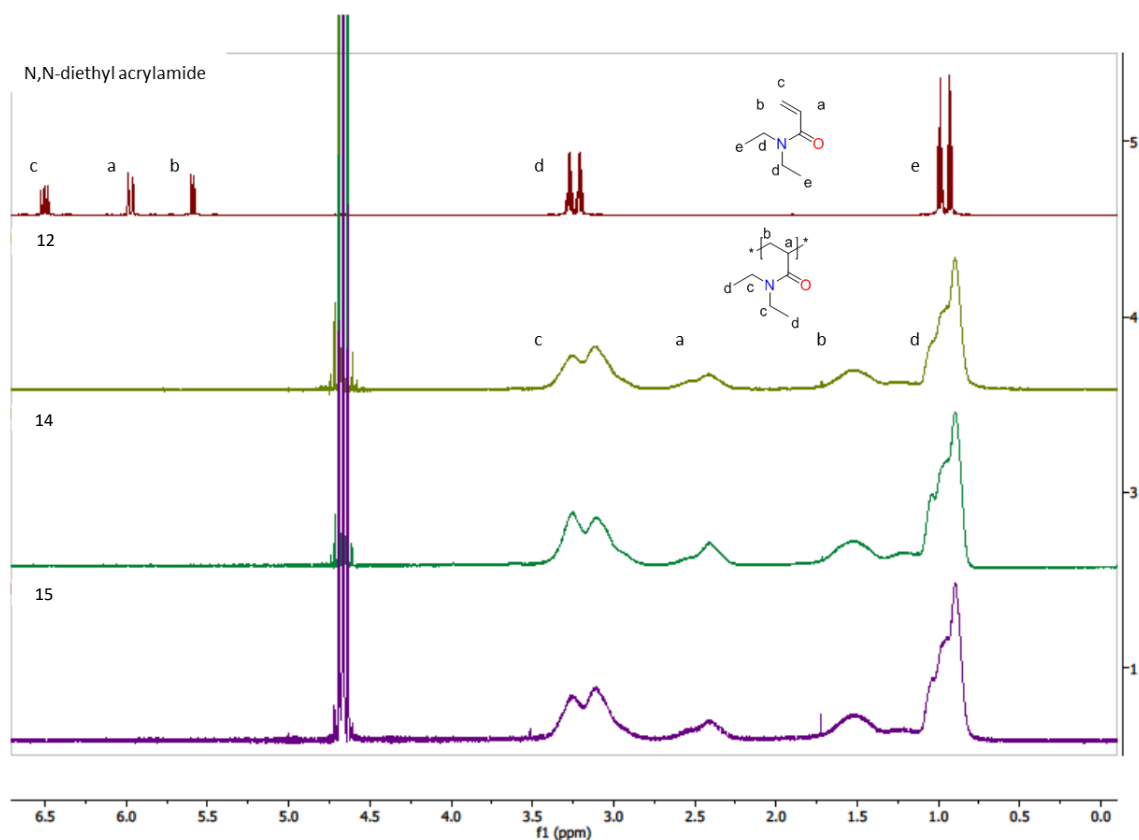
Figure 4. 16: The ^{1}H NMR spectra of DEA (red) and polymers **12** (light green), **14** (dark green) and **15** (purple) in D$_2$O at 600 MHz.

The FTIR spectra of DEA and polymers **12**, **14** and **15** are shown in Figure 4.17. DEA shows two peaks in the IR spectrum at 1607 and 1648 cm^{-1} which represent the stretching of the vinyl and carbonyl of the amide respectively. The IR spectra for polymers **12**, **14** and **15** only show one peak between 1500 and 1600 cm^{-1}, at 1618, 1626 and 1624 cm^{-1} respectively. The single peak present identifies that the double bond is no longer present, supporting successful polymer synthesis.
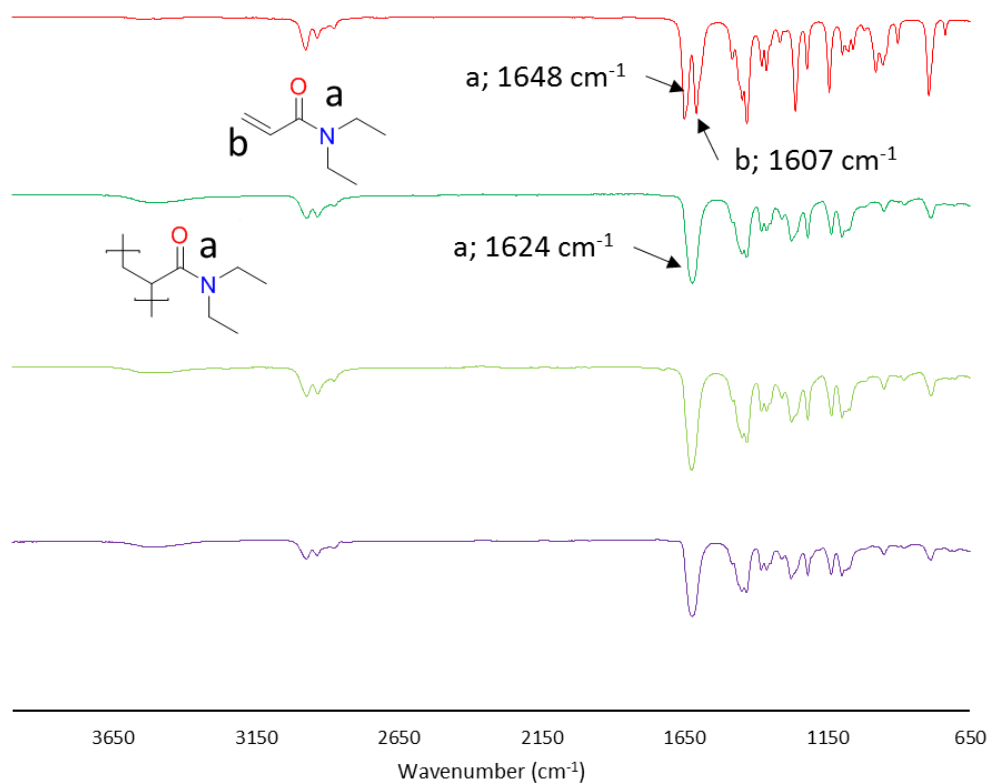
Figure 4. 17: The IR spectra of DEA (red) and polymers **12** (dark green)**, 14** (light green) and **15** (purple).

The GPC traces for polymers **12**, **14** and **15** are shown below in Figure 4.18. Each trace shows the formation of a single population of Mn. Polymers **12**, **14** and **15** showed conversion up to 43, 7 and 21 kDa with polydispersities of 2.42, 1.54 and 1.56 respectively. The Mn show that increasing the polarity of the solvent increases the conversion of monomer to polymer and decreases polymerisation control, as reported in the literature for general ATRP processes.[52]
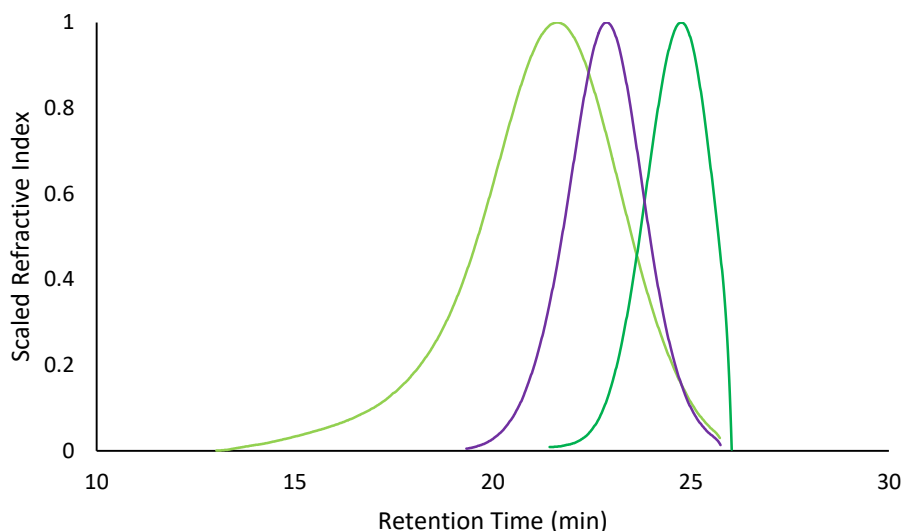
Figure 4. 18: The GPC trace of polymers **12** (light green), **14** (dark green) and **15** (purple) in DMF + 0.1 % LiBr at a flow rate of 0.4 mL/min.

The LCSTs of polymers **12**, **14** and **15** were investigated at 10, 20 and 30 % w/v aqueous solution (Table 4.4). Increasing the Mn from 7 to 43 kDa significantly decreased the LCST from 35.23 ± 0.10 to 29.40 ± 0.10 °C when in 30 % aqueous solution (P<0.001). Also decreasing the concentration from 20 to 10 % w/v for a 43 kDa Mn polymer significantly decreased the LCST from 29.23 ± 0.06 to 28.87 ± 0.21 °C (P<0.01). Therefore, increasing Mn decreases the LCST and increasing the concentration increases the LCST, in agreement with previous literature.[31]

Table 4. 5: The LCSTs of polymers **12**, **14** and **15** in aqueous solution at 10, 20 and 30 % w/v.

Polymer (Mn (kDa))	LCST (°C)		
	10 % (w/v)	**20 % (w/v)**	**30 % (w/v)**
12 (43)	28.87 ± 0.21	29.23 ± 0.06	29.40 ± 0.10
14 (7)	34.03 ± 0.15	34.77 ± 0.06	35.23 ± 0.25
15 (21)	29.20 ± 0.10	29.90 ± 0.10	30.47 ± 0.15

The polymerisation method selected for tri-block copolymer synthesis was that for polymer **15**. Method **15** showed the greatest conversion to a 21 kDa polymer with the lowest PDI of 1.56. Also, the LCST of polymer **15** is between room and body surface temperature, making it ideal for topical drug delivery.

[4.5.2.6] Synthesis and characterisation of PDEGMEMA homopolymers

The ATRP of DEGMEMA has previously been performed using a 2:1 ratio of bipyridine to Cu(I)Br.[53] The solvent was varied for the ATRP of DEGMEMA, as this is directly known to impact the control over ATRP. The three solvents used were; methanol, ethanol and isopropyl alcohol as PEG is soluble in these. DEGMEMA has limited solubility in water, methanol and ethanol but is completely soluble in isopropyl alcohol. As a result of this, ATRP polymerisation was only successful using isopropyl alcohol as a solvent.

The ^{1}H NMR of DEGMEMA and polymer **18** confirm the production of polymer (Figure 4.19). The monomer spectrum shows two doublets of doublets between 5.5 and 6.0 ppm, which represent the two vinyl protons. The remaining peaks at 4.1, 3.6, 3.5, 3.4 and 3.2 ppm represent the pendant group of the monomer. The ^{1}H NMR spectrum of polymer **18** the two vinyl peaks are missing, and the remaining peaks have broadened which is characteristic of polymer spectra. Also, two new broad peaks are present at in the ^{1}H spectrum of polymer **18** at 0.7 and 0.9 ppm, these represent the polymer backbone which is newly formed. Therefore, there is evidence in the ^{1}H NMR for successful polymer synthesis.
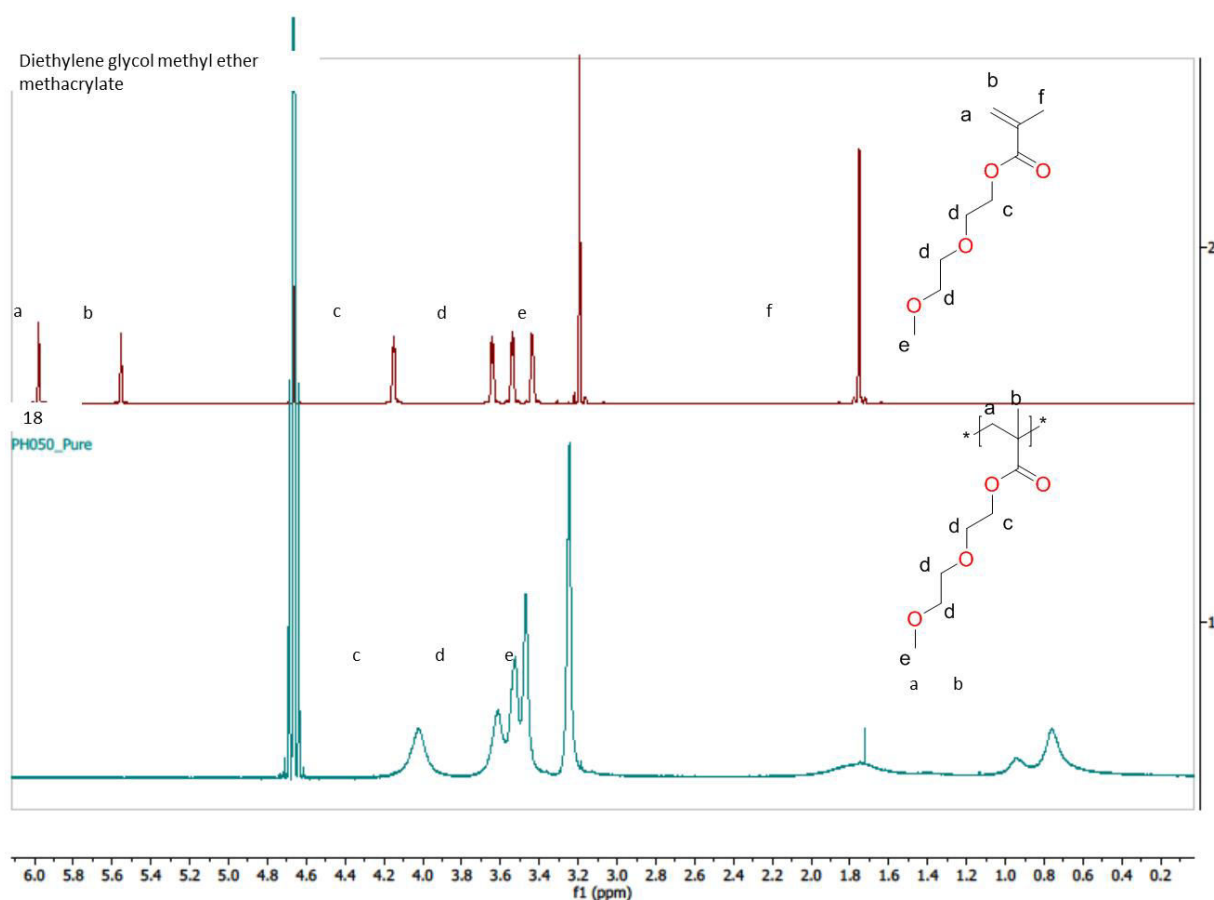
Figure 4. 19: The ^{1}H NMR spectra of DEGMEMA (red) and polymer **18** (teal) in D_2O at 600 MHz.

The IR spectra of DEGMEMA and polymer **18** are shown below in Figure 4.20. The IR spectrum of DEGMEMA shows two peaks at 1717 and 1640 cm^{-1}, which represent the stretch of the ester carbonyl and the stretch of the alkene. The spectrum of polymer **18** shows a single peak between at 1721 cm^{-1}, which indicates that the vinyl double bond is no longer present, and the polymerisation was a success.
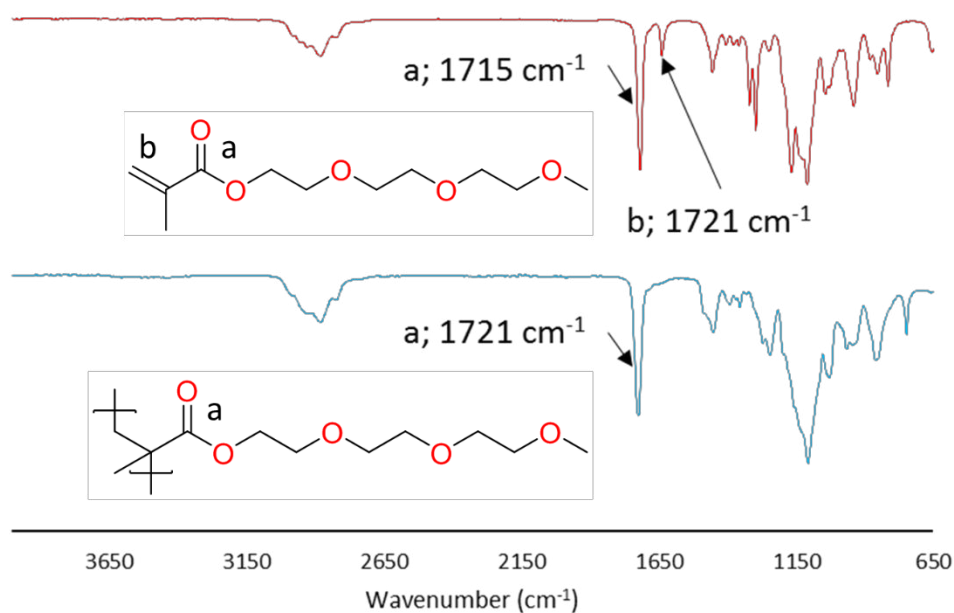
Figure 4. 20: The IR spectra of DEGMEMA (red) and polymer **18** (teal).

The GPC trace of polymer **18** was bimodal, suggesting two populations of polymer Mn (Figure 4.21). The two peaks present for polymer **18** were found to have Mn of 100 and 53 kDa. The peak which eluted first is approximately double the size of the second peak, indicating that partial polymerisation could have been terminated by recombination of two chains [54]. The recombination was found to occur after 24 h of reaction time. When analysing the peaks together the Mn was found to be 44 kDa with a PDI of 1.33.
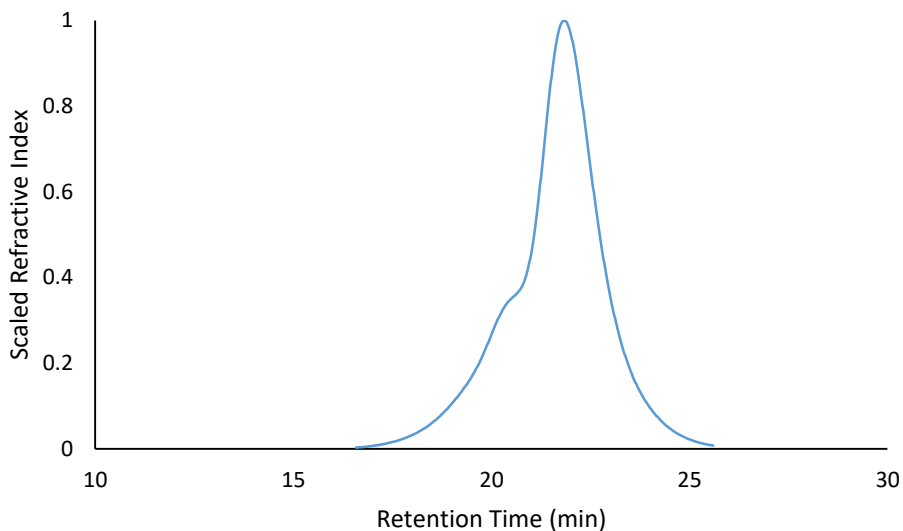
Figure 4. 21: The GPC trace of polymer **18** in DMF + 0.1 % LiBr at a flow rate of 0.4 mL/min.

The LCSTs of polymer **18** in 10, 20 and 30 % aqueous solution were 24.47 ± 0.06, 24.60 ± 0.10 and 24.67 ± 0.06 °C respectively. There were no statistically significant changes in LCST with change in concentration as identified using 1-way ANOVA with Tukey post-hoc analysis (P>0.05). This is in agreement with observations within the literature.[53]

Homopolymers of poly(diethylene glycol methyl ether methacrylate) have successfully been polymerised by ATRP to reach Mn of 44 kDa with a PDI of 1.33. The LCST exhibited is at a physiologically relevant temperature. Thus, the polymer was selected for the development of ABA triblock copolymers.

[4.5.3] Synthesis of 4 and 10 kDa PEG macroinitiators

PEG macroinitiators were synthesised using PEG (4 and 10 kDa), BiBB, DMAP and TEA in dichloromethane (Figure 4.22).[27] DMAP behaves as an activator by reacting with the BiBB, making the carbonyl more susceptible to S_N2 attack from the lone pair of electrons available on the oxygen of the primary alcohol present in PEG.
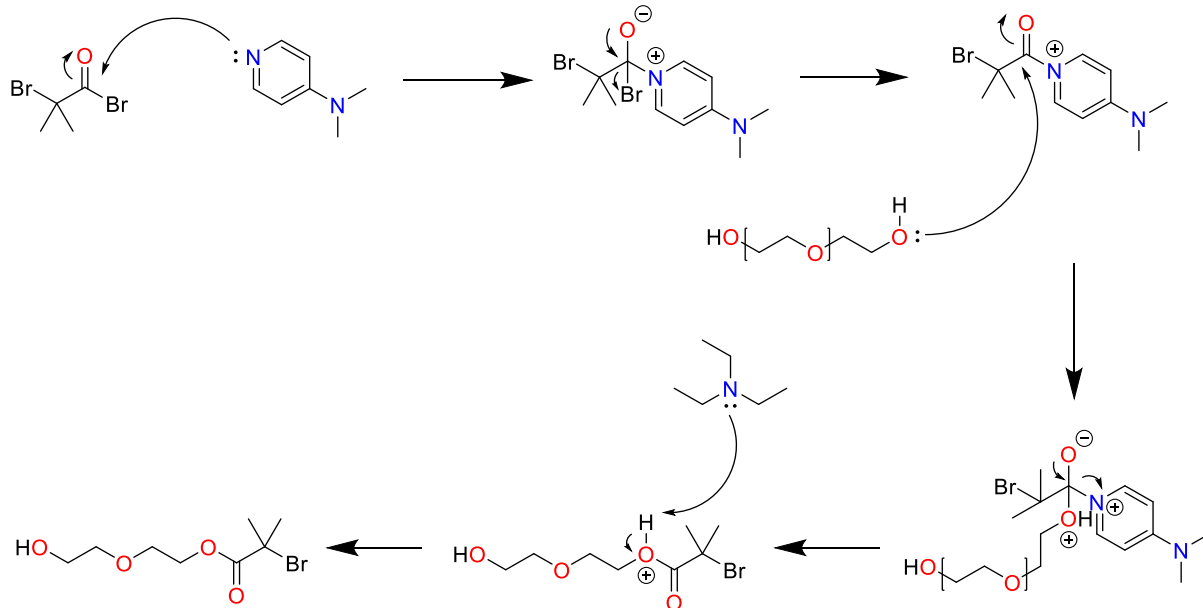
Figure 4. 22: The general reaction mechanism for the synthesis of the 4 and 10 kDa PEG macroinitiators using DMAP, TEA and BiBB.

Two types of ^{1}H NMR experiment were used in the analysis of the PEG and synthesised PEG macroinitiators; ^{1}H NMR (Figure 4.23) and ^{1}H DOSY NMR (Figure 4.24). The ^{1}H NMR was used to calculate the Mn of PEG and to confirm both termini were functionalised. DOSY was used to unambiguously confirm the groups were bound to the end groups of the PEG. The Mn were calculated using the ratio of the integrals of the proton signals from environment "a" to those in environment "b". The Mn of the 4 and 10 kDa PEG were found to be 5 and 11 kDa respectively. To ensure both ends were successfully functionalised, the ratio of the integrals of the BiBB groups (a) to the PEG backbone (b) were investigated. Both 4 and 10 kDa PEG showed complete functionalisation at both ends of the molecule.
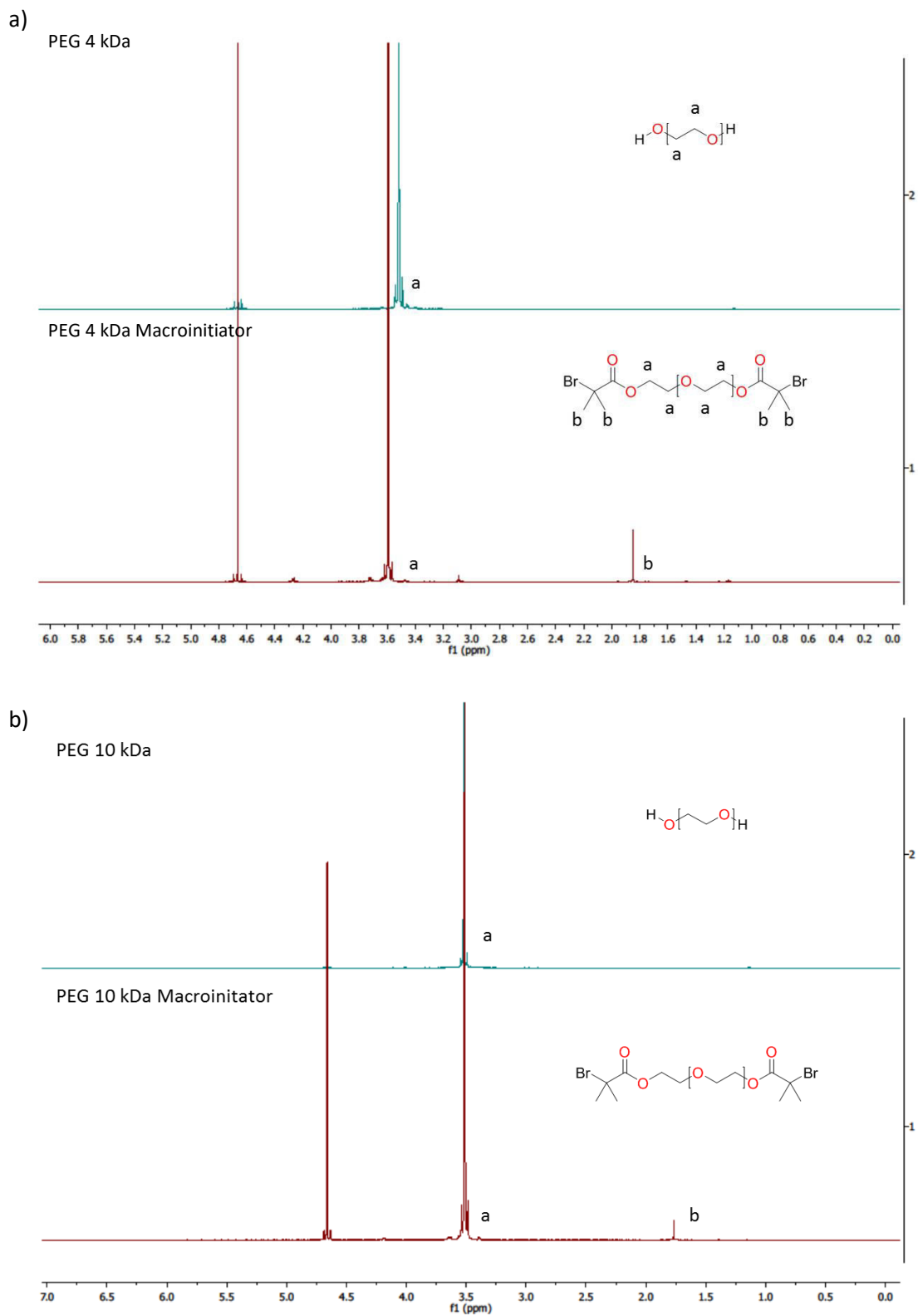
Figure 4. 23: The ^{1}H NMR spectra of a) PEG 4 kDa and the 4 kDa PEG macroinitiator and b) PEG 10 kDa and the 10 kDa PEG macroinitiator in D$_2$O at 600 MHz.

The ^{1}H DOSY NMR further demonstrated that the BiBB functionality was bound to the PEG macromolecule (Figure 4.24). DOSY relates the ^{1}H NMR signals to their diffusion coefficients, and if the signals diffuse through solution at the same rate, they must be found on the same molecule.[55] The DOSY spectra in Figure 4.31a and Figure 4.31b confirm the BiBB functionality and the PEG backbone are diffusing through solution at the same speed – therefore the functionalisation was successful.

a)

b)
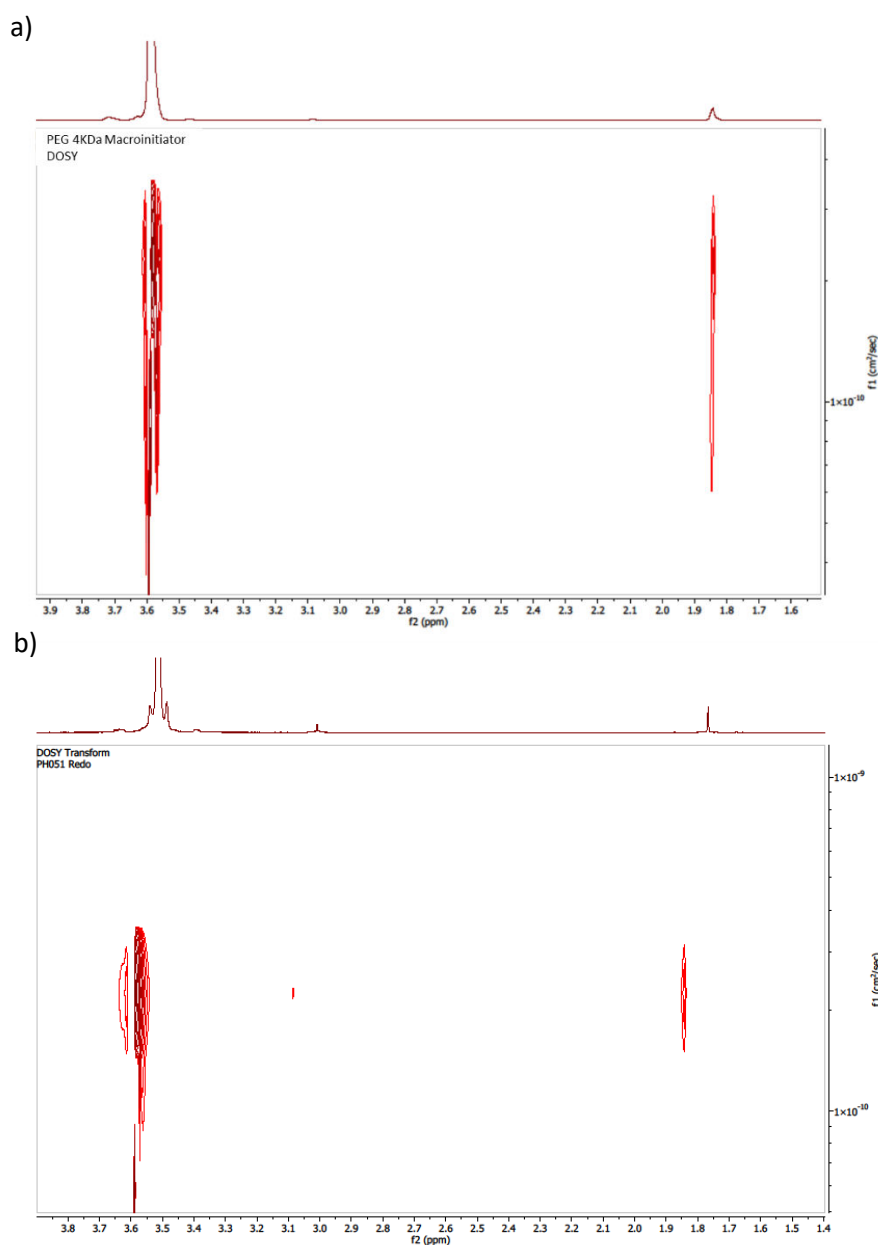
Figure 4. 24: The ^{1}H DOSY NMR spectra of a) the PEG 4 kDa macroinitiator and b) the PEG 10 kDa macroinitiator in CDCl$_3$ at 600 MHz.

The two synthesised PEG macroinitiators were analysed using GPC (Figure 4.25). The GPC identified a single population of Mn for both 4 and 10 kDa PEG macroinitiators which were 7 and 17 kDa, with PDIs of 1.12 and 1.13 respectively.
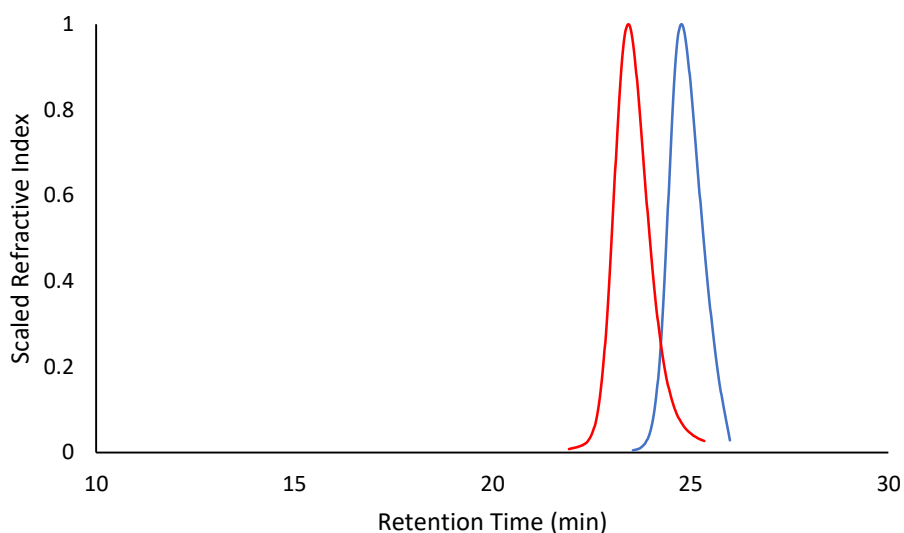
Figure 4. 25: The GPC traces of the 4 kDa macroinitiator (blue) and the 10 kDa macroinitiator (red).

[4.5.4] Synthesis of ABA tri-block copolymers of an LCST-exhibiting component (A) and PEG (B)

[4.5.4.1] Synthesis and characterisation of PNIPAM-*b*-PEG-*b*-PNIPAM tri-block copolymers

PNIPAM-PEG-PNIPAM tri-block copolymers were synthesised using method **1,** as for PNIPAM homopolymers. Four PEG and PNIPAM tri-block copolymers were synthesised as shown in Table 2 and characterised using ^{1}H NMR and DOSY NMR. The ^{1}H NMR of NIPAM, PEG 4 kDa macroinitiator and tri-block copolymer **19** are given in Figure 4.26a. The peaks were assigned in the same manner as homopolymer **1** in Figure 4.7. The ^{1}H DOSY NMR of tri-block copolymer **19** is shown in Figure 4.26b and confirms successful polymerisation from the macroinitiator, as all peaks are diffusing through the solvent at the same velocity. The ^{1}H and ^{1}H DOSY NMR for the remaining PNIPAM tri-block copolymers are given in the appendix (Figures A.6 and A.7).

The GPC trace for tri-block copolymer **19** is shown in Figure 4.26c, while the remaining are shown in appendix (Figure A.8). The Mn, as given by GPC, of copolymers **19** to **22** were 31, 46, 33 and 55 kDa respectively. The polydispersities of block copolymers **19** to **22** were 2.62, 2.51, 1.88 and 1.84 respectively. The broad polydispersities were expected as the reaction was performed in water, which is known to cause uncontrolled polymerisation.[56] The LCST of PNIPAM has been reported as

32 °C and does not vary with Mn, therefore this should not affect the gelation temperature and should result in a sharp sol-gel transition.
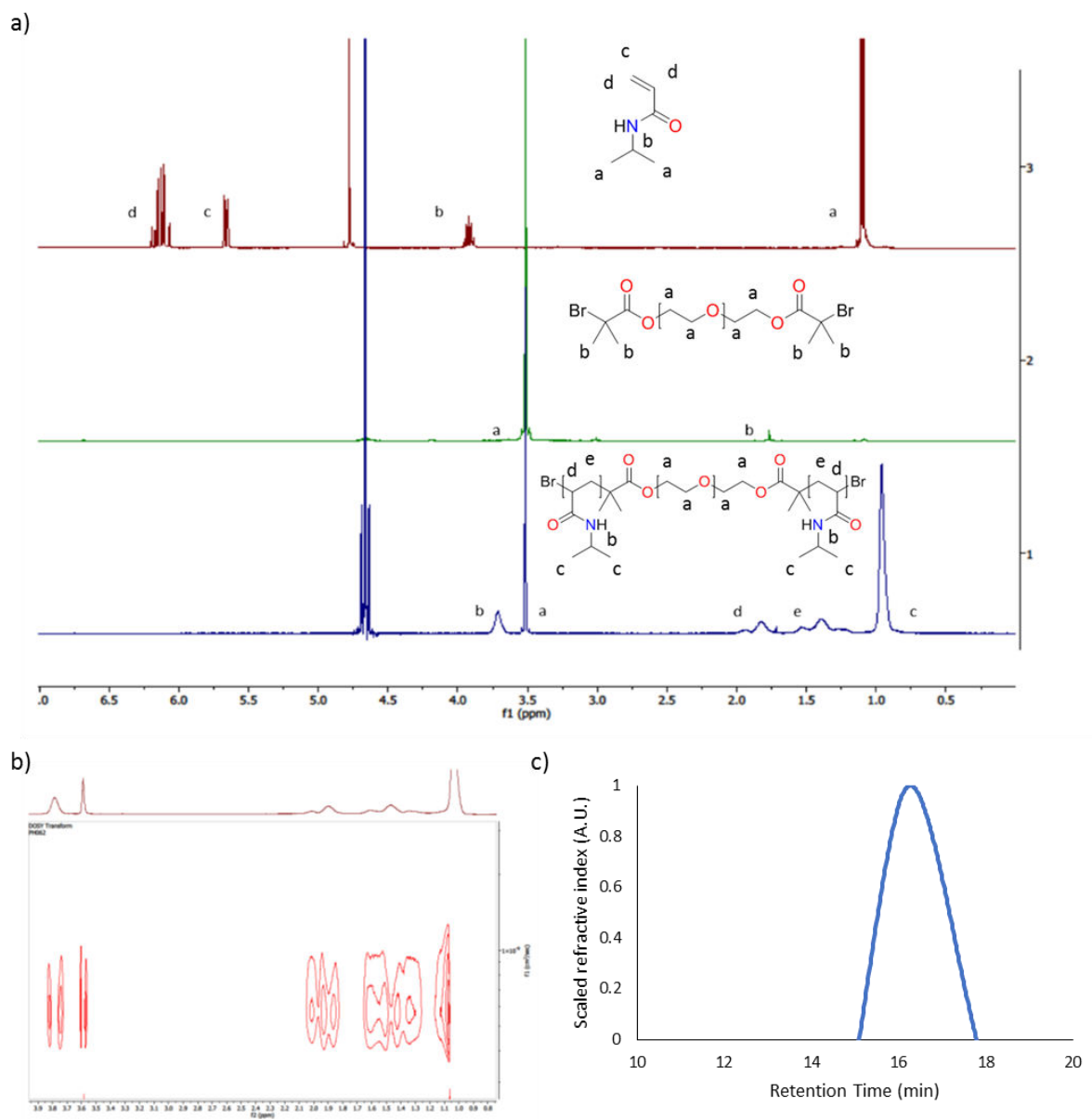
Figure 4. 26: The a) ^{1}H NMR spectra of NIPAM (red), 4 kDa PEG macroinitiator (Green) and tri-block copolymer 18 (Blue), b) the ^{1}H DOSY spectra of tri-block copolymer 18 and the c) the GPC trace of tri-block copolymer 18.

As mentioned above, the GPC was calibrated using PMMA standards which generated a narrow calibration. Since the GPC was calibrated with homopolymers of PMMA, it is not possible to

accurately predict the Mn of block copolymers, and all molecular weights would be relative to PMMA.[57] Therefore, the Mn were predicted using ^{1}H NMR, by relating the integral of the central PEG block to the integrals of the newly formed carbon backbone.[58] The Mn of the PNIPAM arms of copolymers **19** to **22** as predicted by ^{1}H NMR were 13, 20, 11 and 22 kDa respectively. The Mn by ^{1}H NMR and polydispersities for copolymers **19** to **22** are summarised in Table 4.6.

[4.5.4.2] Synthesis and characterisation of PDMAEMA-*b*-PEG-*b*-PDMAEMA tri-block copolymers

Tri-block copolymers of PEG and PDMAEMA were synthesised using the same method as for the synthesis of polymer **2**. The ^{1}H NMR spectrum of DMAEMA, PEG 10 kDa macroinitiator and block copolymer **23** are shown in Figure 4.27a. The peak assignment was performed in the same way as homopolymer **2**. The ^{1}H DOSY NMR confirms the polymerisation from the PEG macroinitiator, as all peaks are diffusing at the same rate (Figure 4.27b). The ^{1}H and ^{1}H DOSY NMR of tri-block copolymers **24** to **26** are given in appendix (Figures A.9 and A.10). The GPC traces of tri-block copolymer **23** is shown in Figure 4.27c. The polydispersities of copolymers **23** to **26** were found to be 1.24, 1.31, 1.14 and 1.32 respectively, indicating a controlled polymerisation. ^{1}H NMR was used to predict the Mn of the PDMAEMA, and these were found to be 11, 19, 13 and 18 kDa for copolymers **23** to **26** respectively. The GPC traces for tri-block copolymers **24** to **26** are given in appendix (Figure A.11). The Mn by ^{1}H NMR and polydispersities for copolymers **23** to **26** are summarised in Table 4.6.
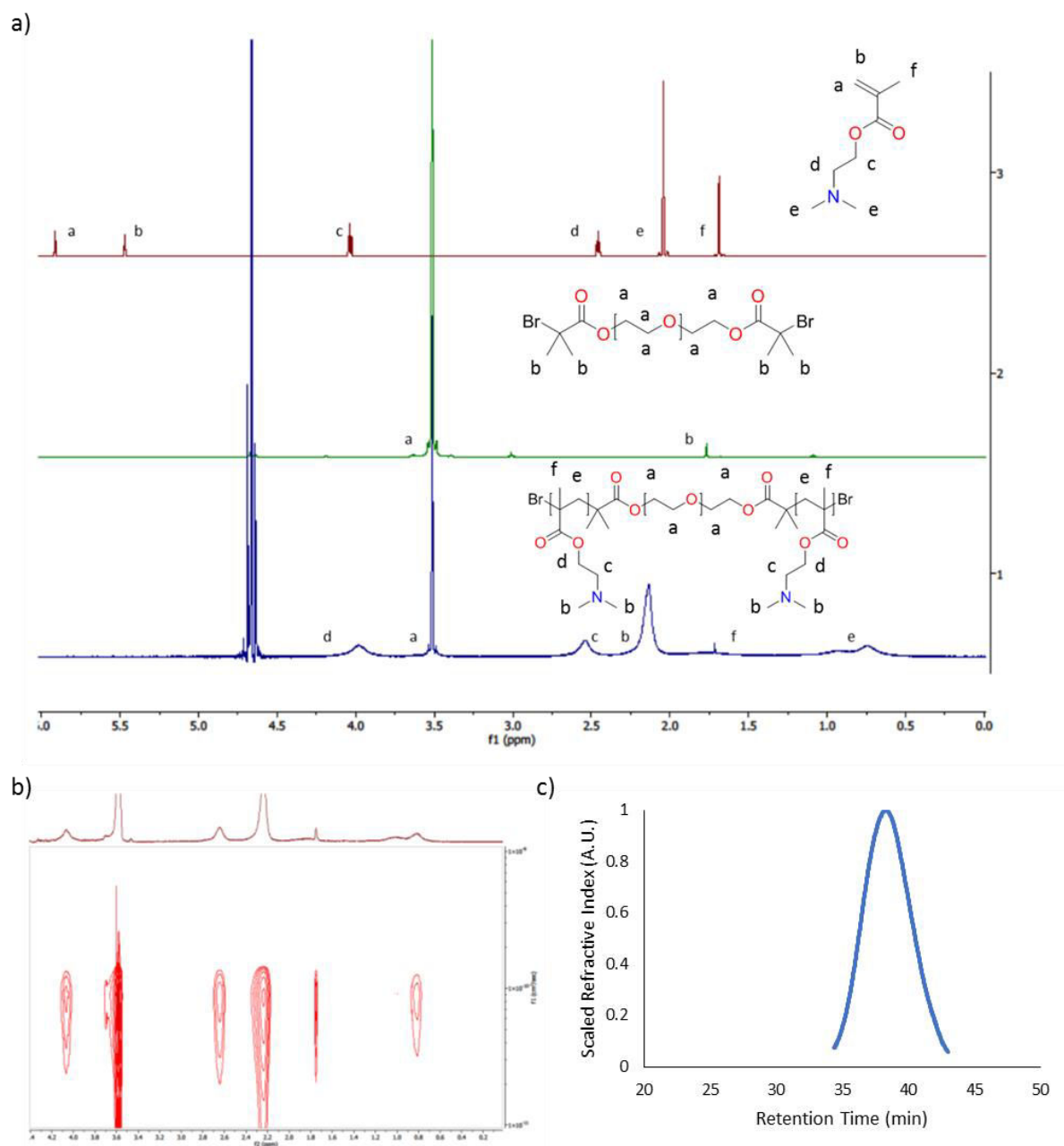
Figure 4. 27: The a) ^{1}H NMR spectra of DMAEMA (red), 4 kDa PEG macroinitiator (Green) and tri-block copolymer 23 (Blue), b) the ^{1}H DOSY spectra of tri-block copolymer 23 and the c) the GPC trace of tri-block copolymer 23.

[4.5.4.3] Synthesis and characterisation of PDEA-*b*-PEG-*b*-PDEA tri-block copolymers

PDEA and PEG tri-block copolymers were synthesised using the method for homopolymer **15** synthesis. The ^{1}H NMR spectrum of DEA, the PEG 10 kDa macroinitiator and tri-block copolymer **27** are given in Figure 4.28a**.** The peak assignment for homopolymer **15** was used to identify the polymer ^{1}H NMR peaks. The ^{1}H DOSY NMR of block copolymer **27** confirms the polymerisation occurred from the PEG macroinitiator, as all peaks are diffusing at the same rate (Figure 4.28b). The ^{1}H and ^{1}H DOSY NMR spectra for PDEA-*b*-PEG-*b*-PDEA tri-block copolymers **28** to **30** are given in appendix (Figures A.12 and A.13). The GPC trace of tri-block copolymers **27** confirms the formation of a polymer (Figure 4.28c). The polydispersities of tri-block copolymers **27** to **30** were found to be 1.40, 1.35, 1.18 and 1.32, indicating controlled polymerisation. The Mn of the PDEA blocks were calculated using ^{1}H NMR. The LCST arms were found to have Mn of 13, 21, 13 and 21 kDa for copolymers **27** to **30** respectively. The GPC traces of the PDEGMEMA tri-block copolymers **28** to **30** are given in appendix (Figure A.14). The Mn by ^{1}H NMR and polydispersities for copolymers **27** to **30** are summarised in Table 4.6.
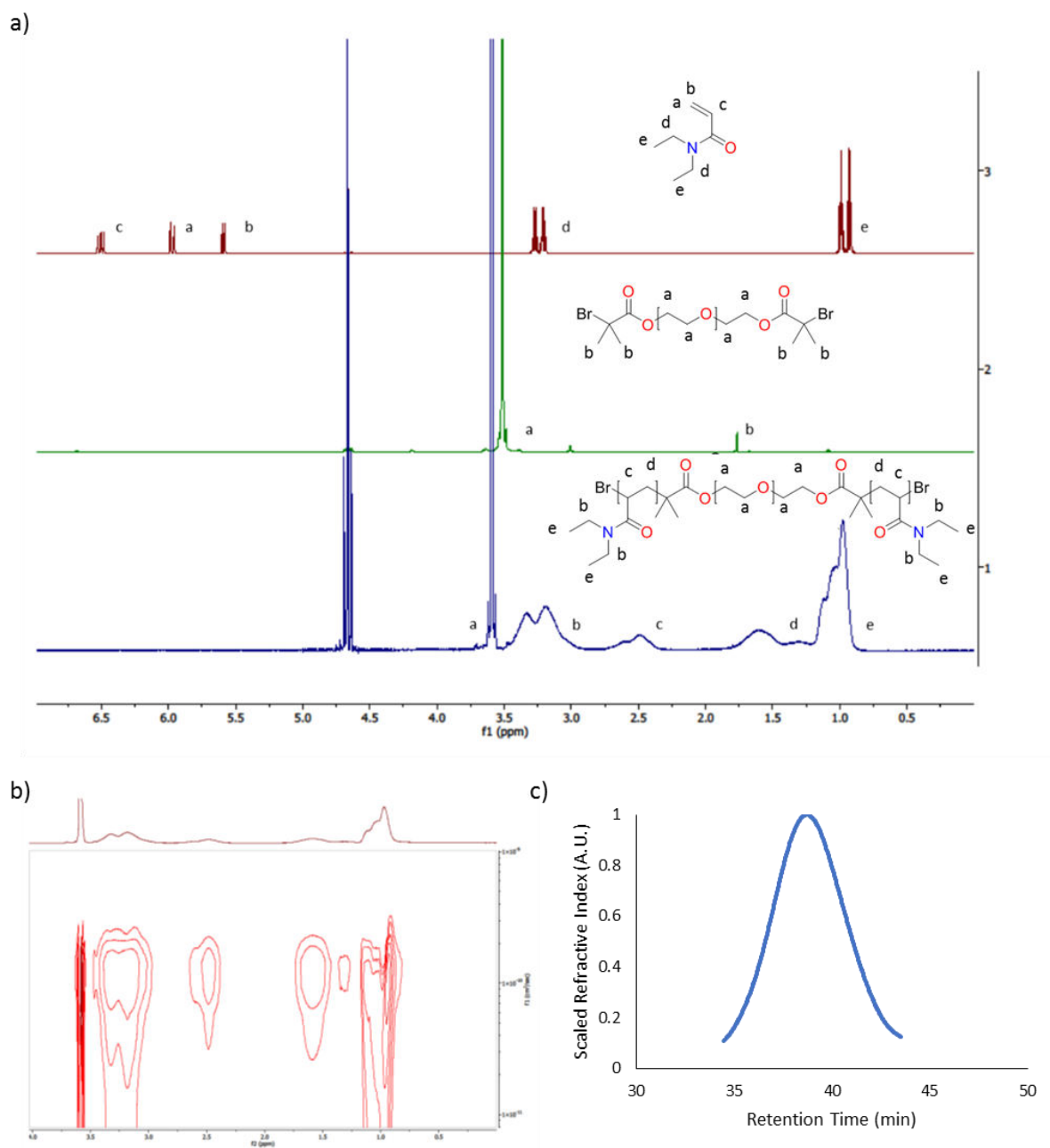
Figure 4. 28: The a) ^{1}H NMR spectra of DEA (red), 4 kDa PEG macroinitiator (Green) and tri-block copolymer 27 (Blue), b) the ^{1}H DOSY spectra of tri-block copolymer 27 and the c) the GPC trace of tri-block copolymer 27.

[4.5.4.4] Synthesis and characterisation of PDEGMEMA-*b*-PEG-*b*-PDEGMEMA tri-block copolymers

Tri-block copolymers of PDEGMEMA and PEG were synthesised using the same method as was used to synthesise polymer **18**. The ^{1}H NMR spectrum of DEGMEMA, PEG 10 kDa macroinitiator and copolymer **30** are shown in Figure 4.29a. The peak assignment used for homopolymer **18** was used to assign the peaks of copolymers **30** to **34**. The ^{1}H DOSY NMR confirmed the polymerisation from the functionalised PEG macroinitiator, as all peaks are diffusing through solution at the same rate (Figure 4.29b). The ^{1}H NMR and ^{1}H DOSY NMR for the remaining PDEGMEMA triblock copolymers are shown in appendix (Figures A.15 and A.16). The GPC traces of copolymer **31** is shown below in Figure 4.29c and copolymer 32, 33 and 34 are shown in appendix (Figures A.17). The GPC traces of copolymers 31 to 34 identified monomodal peaks with polydispersities of 1.18, 1.19, 1.13 and 1.09 respectively, indicating highly controlled polymerisation. The Mn by ^{1}H NMR of the PDEGMEMA blocks for copolymers **31** to **34** were found to be 10, 22, 10 and 20 kDa respectively. The Mn by ^{1}H NMR and polydispersities for copolymers **31** to **34** are summarised in Table 4.6.
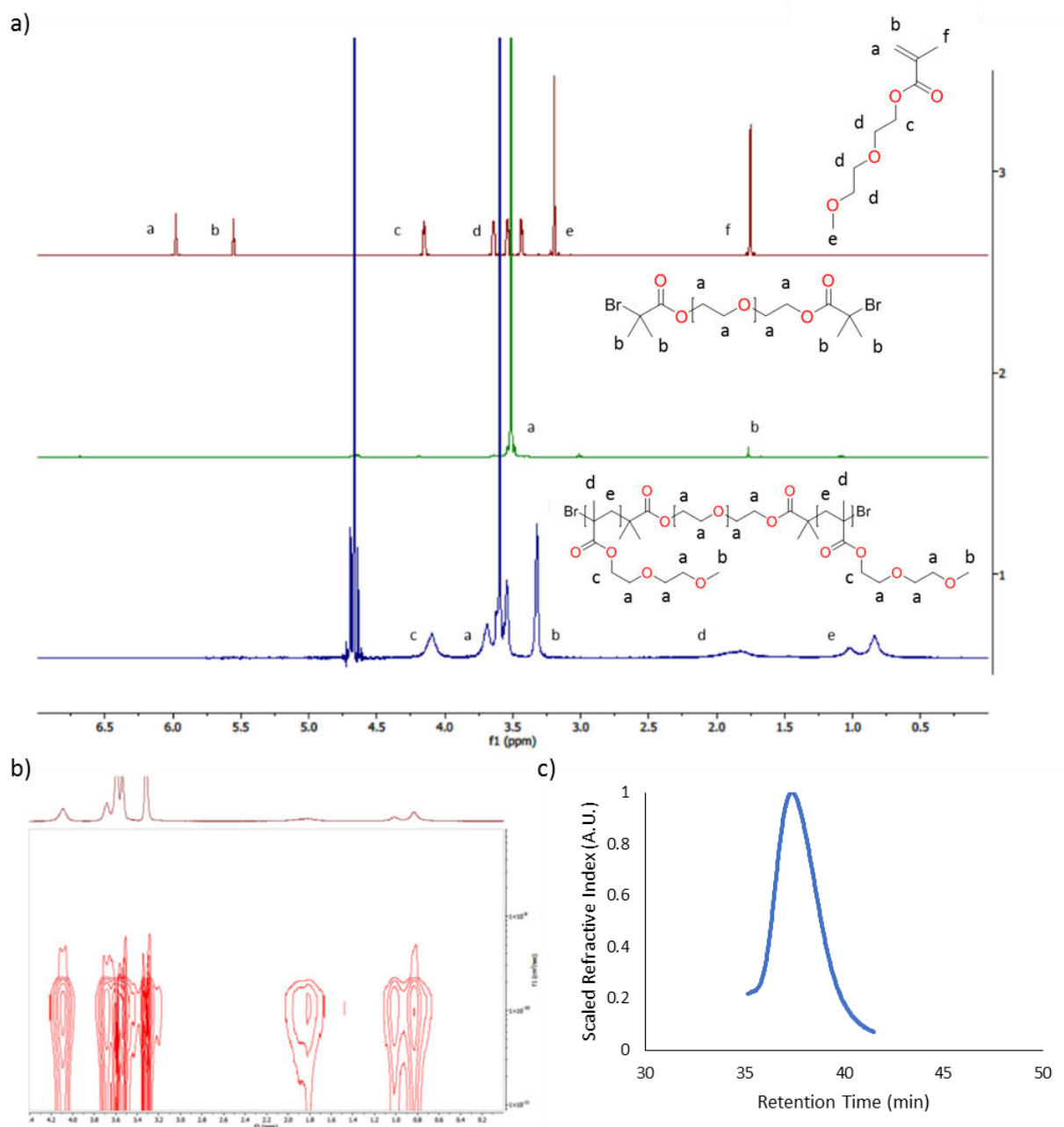
Figure 4. 29: The a) ^{1}H NMR spectra of DEGMEMA (red), 4 kDa PEG macroinitiator (Green) and tri-block copolymer 31 (Blue), b) the ^{1}H DOSY spectra of tri-block copolymer 31 and the c) the GPC trace of tri-block copolymer 31.

The syntheses described in the chapter aimed to prepare ABA triblock copolymers consisting of a temperature responsive component (A) and PEG (B) with molecular weights of 10-4-10, 20-4-20, 10-10-10 and 20-10-20. For each type of temperature responsive polymer, these ABA copolymers have been successfully synthesised and the desired molecular weights have largely been achieved (Table

4.6). Whilst 100 % conversion was not achieved in all cases, the library contains clear low and high levels at the targeted 10 and 20 kDa LCST blocks. Thus, this library is suitable to investigate the effect of molecular weight on the temperature responsive properties of the ABA copolymers.

Table 4. 6: Summary of the Mn of the tri-block copolymers synthesised. Shown below are the Mn and PDI by GPC, and the Mn of the copolymer and the LCST arms by ^{1}H NMR.

Copolymer	Target Polymer	GPC PDI	Mn by NMR (kDa)	Mn of LCST Arm by NMR (kDa)
19	$PNIPAM_{10}$-PEG_4-$PNIPAM_{10}$	2.62	31	13
20	$PNIPAM_{20}$-PEG_4-$PNIPAM_{20}$	2.51	46	20
21	$PNIPAM_{10}$-PEG_{10}-$PNIPAM_{10}$	1.88	33	11
22	$PNIPAM_{20}$-PEG_{10}-$PNIPAM_{20}$	1.84	55	22
23	$PDMAEMA_{10}$-PEG_4-$PDMAEMA_{10}$	1.24	28	11
24	$PDMAEMA_{20}$-PEG_4-$PDMAEMA_{20}$	1.31	44	19
25	$PDMAEMA_{10}$-PEG_{10}-$PDMAEMA_{10}$	1.14	36	13
26	$PDMAEMA_{20}$-PEG_{10}-$PDMAEMA_{20}$	1.32	47	18
27	$PDEA_{10}$-PEG_4-$PDEA_{10}$	1.40	31	13
28	$PDEA_{20}$-PEG_4-$PDEA_{20}$	1.35	47	21
29	$PDEA_{10}$-PEG_{10}-$PDEA_{10}$	1.18	36	13
30	$PDEA_{20}$-PEG_{10}-$PDEA_{20}$	1.32	53	21
31	$PDEGMEMA_{10}$-PEG_4-$PDEGMEMA_{10}$	1.18	26	10
32	$PDEGMEMA_{20}$-PEG_4-$PDEGMEMA_{20}$	1.19	50	22
33	$PDEGMEMA_{10}$-PEG_{10}-$PDEGMEMA_{10}$	1.13	31	10
34	$PDEGMEMA_{20}$-PEG_{10}-$PDEGMEMA_{20}$	1.09	51	20

[4.6] Conclusions

Six polymers were identified from the literature with LCSTs between 25 − 37 °C, namely: PNIPAM, PDMAEMA, PNVCl, PVP, PDEA and PDEGMEMA. All polymers aside from PNVCl were successfully synthesised by ATRP. The ATRP of PNVCl failed as a result of the poor radical stability present during propagation. It was observed that the polymer M_n and PDI typically increased when the polymerisation was performed in increasingly polar media. Of the 5 successfully synthesised polymers, PNIPAM, PDMAEMA, PDEA and PDEGMEMA were selected for the synthesis of tri-block copolymers. These were selected due to their physiologically relevant LCSTs of 31.92 ± 0.10, 34.47 ± 0.12, 29.90 ± 0.10 and 24.60 ± 0.10 °C, respectively, in 20 % w/v aqueous solutions. PVP, however, was rejected as the polymer failed to show an LCST in water alone and in the presence of NaCl did exhibit an LCST lower than 54.08 ± 0.16 °C. Two PEG macroinitiators at 4 and 10 kDa were successfully synthesised and characterised by ^{1}H NMR, ^{1}H DOSY NMR and GPC. A series of 4 ABA tri-block copolymers were then successfully synthesised with M_n of 10-4-10, 20-4-20, 10-10-10 and 20-4-20 where A was either PNIPAM, PDMAEMA, PDEA or PDEGMEMA and B was PEG, generating a library of 16 copolymers. Of these 16 copolymers, those with PNIPAM and PDMAEMA have been reported at different degrees of polymerisation whereas those containing PDEA and PDEGMEMA are novel. These 16 block copolymers are predicted to exhibit a temperature induced transition at physiologically relevant temperatures, with the risk of toxicity mitigated by a strict selection procedure.

[4.7] References

1 J. R. Ebdon, in *New Methods of Polymer Synthesis*, Springer Netherlands, 1991, pp. 1–21.

2 N. Hadjichristidis, M. Pitsikalis and H. Iatrou, *Adv. Polym. Sci.*, 2005, **189**, 1–124.

3 Y. Kwak, R. Nicolaÿ and K. Matyjaszewski, *Aust. J. Chem.*, 2009, **62**, 1384–1401.

4 G. Moad, E. Rizzardo and S. H. Thang, *Aust. J. Chem.*, 2009, **62**, 1402–1472.

5 G. Sun, C. Cheng and K. L. Wooley, *Macromolecules*, 2007, **40**, 793–795.

6 F. Canturk, B. Karagoz and N. Bicak, *J. Polym. Sci. Part A Polym. Chem.*, 2011, **49**, 3536–3542.

7 N. H. Yarkandi, *Int.J.Curr.Microbiol.App.Sci*, 2014, **3**, 415–431.

8 A. Herberg, X. Yu and D. Kuckling, *Polymers (Basel).*, 2019, **11**, 10–16.

9 K. Matyjaszewski, Atom Transfer Radical Polymerization - Matyjaszewski Polymer Group - Carnegie Mellon University, https://www.cmu.edu/maty/chem/fundamentals-atrp/atrp.html, (accessed 27 April 2020).

10 E. Mastan and S. Zhu, *Macromolecules*, 2015, **48**, 6440–6449.

11 R. Krishnan and K. S. V. Srinivasan, *Macromolecules*, 2004, **37**, 3614–3622.

12 B. M. Rosen and V. Percec, *Chem. Rev.*, 2009, **109**, 5069–5119.

13 F. Seeliger and K. Matyjaszewski, *Macromolecules*, 2009, **42**, 6050–6055.

14 W. Tang and K. Matyjaszewski, *Macromolecules*, 2007, **40**, 1858–1863.

15 N. Rattanathamwat, J. Wootthikanokkhan, N. Nimitsiriwat, C. Thanachayanont and U. Asawapirom, *Adv. Mater. Sci. Eng.*, 2015, **2015**, 19–26.

16 V. Yadav, N. Hashmi, W. Ding, T. H. Li, M. K. Mahanthappa, J. C. Conrad and M. L. Robertson, *Polym. Chem.*, 2018, **9**, 4332–4342.

17 W. A. Braunecker, N. V. Tsarevsky, A. Gennaro and K. Matyjaszewski, *Macromolecules*, 2009, **42**, 6348–6360.

18 J. Morick, M. Buback and K. Matyjaszewski, *Macromol. Chem. Phys.*, 2011, **212**, 2423–2428.

19 W. Tang, Y. Kwak, W. Braunecker, N. V. Tsarevsky, M. L. Coote and K. Matyjaszewski, *J. Am. Chem. Soc.*, 2008, **130**, 10702–10713.

20 W. Tang and K. Matyjaszewski, *Macromolecules*, 2006, **39**, 4953–4959.

21 M. Horn and K. Matyjaszewski, *Macromolecules*, 2013, **46**, 3350–3357.

22 K. Matyjaszewski, Solvent Effects and Selection of a Catalyst for Aqueous Media - Matyjaszewski Polymer Group - Carnegie Mellon University, https://www.cmu.edu/maty/chem/catalyst-development/solvent-effects-and-selection-of-a-catalyst-for-aqueous-media.html, (accessed 27 April 2020).

23 N. V. Tsarevsky, T. Pintauer and K. Matyjaszewski, *Macromolecules*, 2004, **37**, 9768–9778.

24 H. H. Lin and Y. L. Cheng, *Macromolecules*, 2001, **34**, 3710–3715.

25 A. P. Constantinou and T. K. Georgiou, *Eur. Polym. J.*, 2016, **78**, 366–375.

26 M. Teodorescu, I. Negru, P. O. Stanescu, C. Drghici, A. Lungu and A. Sârbu, *React. Funct.*

Polym., 2010, **70**, 790–797.

27 M. Garcia, M. P. Beecham, K. Kempe, D. M. Haddleton, A. Khan and A. Marsh, *Eur. Polym. J.*, 2015, **66**, 444–451.

28 C. W. Chang, E. Bays, L. Tao, S. N. S. Alconcel and H. D. Maynard, *Chem. Commun.*, 2009, **10**, 3580–3582.

29 FDA, Inactive Ingredients Database Download File, https://www.fda.gov/drugs/drug-approvals-and-databases/inactive-ingredients-database-download, (accessed 26 January 2020).

30 R. Duncan, *Nat. Rev. Drug Discov.*, 2003, **2**, 347–360.

31 D. G. Lessard, M. Ousalem and X. X. Zhu, *Can. J. Chem.*, 2001, **79**, 1870–1874.

32 M. Panayiotou, C. Pöhner, C. Vandevyver, C. Wandrey, F. Hilbrig and R. Freitag, *React. Funct. Polym.*, 2007, **67**, 807–819.

33 M. A. Cooperstein and H. E. Canavan, *Biointerphases*, 2013, **8**, 19–25.

34 M. T. Cook, S. K. Filippov and V. V. Khutoryanskiy, *Colloid Polym. Sci.*, 2017, **295**, 1351–1358.

35 J. U. Izunobi and C. L. Higginbotham, *J. Chem. Educ.*, 2011, **88**, 1098–1104.

36 G. R. Fulmer, A. J. M. Miller, N. H. Sherden, H. E. Gottlieb, A. Nudelman, B. M. Stoltz, J. E. Bercaw and K. I. Goldberg, *Organometallics*, 2010, **29**, 2176–2179.

37 J. Ye and R. Narain, *J. Phys. Chem. B*, 2009, **113**, 676–681.

38 D. Christova, R. Velichkova, W. Loos, E. J. Goethals and F. Du Prez, *Polymer (Guildf).*, 2003, **44**, 2255–2261.

39 H. G. Schild, M. Muthukumar and D. A. Tirrell, *Macromolecules*, 1991, **24**, 948–952.

40 F. Zeng, Y. Shen and S. Zhu, *Macromol. Rapid Commun.*, 2002, **23**, 1113–1117.

41 X. Liu, P. Ni, J. He and M. Zhang, *Macromolecules*, 2010, **43**, 4771–4781.

42 X. Jin, Y. Shen and S. Zhu, *Macromol. Mater. Eng.*, 2003, **288**, 925–935.

43 G. Chambard, B. Klumperman and A. L. German, *Macromolecules*, 2000, **33**, 4417–4421.

44 J. Zhang, K. Pan, L. Jiang, Z. Yi and Y. Dan, *J. Appl. Polym. Sci.*, 2007, **104**, 2751–2754.

45 J. Y. Zheng, M. J. Tan, P. Thoniyot and X. J. Loh, *RSC Adv.*, 2015, **5**, 62314–62318.

46 P. Singh, A. Srivastava and R. Kumar, *J. Polym. Sci. Part A Polym. Chem.*, 2012, **50**, 1503–1514.

47 P. Krys, Y. Wang, K. Matyjaszewski and S. Harrisson, *Macromolecules*, 2016, **49**, 2977–2984.

48 K. Nakabayashi and H. Mori, *Eur. Polym. J.*, 2013, **49**, 2808–2838.

49 C. Jumeaux, R. Chapman, R. Chandrawati and M. M. Stevens, *Polym. Chem.*, 2015, **6**, 4116–4122.

50 A. M. Khalil and A. A. Da'dara, *Arch. Environ. Contam. Toxicol.*, 1994, **26**, 60–3.

51 W. Kunz, J. Henle and B. W. Ninham, in *Current Opinion in Colloid and Interface Science*, Elsevier, 2004, vol. 9, pp. 19–37.

52 V. A. Pereira, P. V. Mendonçą, J. F. J. Coelho and A. C. Serra, *Polym. Chem.*, 2019, **10**, 4904–

4913.

53   J. F. Lutz, *J. Polym. Sci. Part A Polym. Chem.*, 2008, **46**, 3459–3470.

54   T. G. Ribelli, K. F. Augustine, M. Fantin, P. Krys, R. Poli and K. Matyjaszewski, *Macromolecules*, 2017, **50**, 7920–7929.

55   C. S. Johnson, *Prog. Nucl. Magn. Reson. Spectrosc.*, 1999, **34**, 203–256.

56   P. Millard, N. Mougin, A. Boker and A. Muller, *Phys. Chemie*, 2008, **1**, 2–3.

57   F. S. C. Chang, in *Polymer Molecular Weight Methods*, 1973, vol. 125, pp. 14–154.

58   S. C. Shit and S. Maiti, *Eur. Polym. J.*, 1986, **22**, 1001–1008.

Chapter Five: Investigating the Aqueous Solution Properties and Cytotoxicity of Temperature Responsive Triblock Copolymers

[5.1] Introduction

This chapter focuses on investigating the aqueous solution properties of the triblock copolymers synthesised in chapter 4. In that chapter LCST-exhibiting polymers were selected from the literature in a manner which may mitigate potential safety risks when developing thermogelling materials for drug delivery applications. ABA triblock copolymers were then synthesised using these LCST-exhibiting polymers (A) and PEG (B). In aqueous solution, these ABA triblock copolymers are predicted to be responsive to temperature, which will be the focus of the experiments conducted within this chapter. Rheometry will be coupled to nanoscale characterisation techniques to identify thermogelling materials in the library and to probe the mechanisms behind gelation processes.

Thermoresponsive ABA copolymers may self-assemble in aqueous solution to form larger structures constituted by a number of macromolecules. The formation of both ordered and disordered aggregates of temperature responsive triblock copolymers may occur above a critical micellization temperature (CMT).[1–4] The aggregates of such polymers may be investigated by transition and scanning electron microscopy[5,6] or in dilute solutions using techniques such as ultraviolet-visible spectroscopy (UV-VIS)[7] and dynamic light scattering (DLS).[8] The formation of aggregates above the CMT may be detected using techniques including UV-VIS spectroscopy and DLS as a result of an increase in the degree of light scattered by the polymer solutions. In addition to this, DLS may be used to determine the hydrodynamic diameter and polydispersity of such aggregates. The CMT is reported to be related to the gelation temperature of thermogelling materials,[9] as these aggregates are believed to drive gel formation when above a critical phase volume.

For poloxamer 407, the cause of gelation is the formation of spherical core-shell micelles with an increase in temperature.[10] When the volume fraction of micelles surpass a critical point, they pack into a cubic close packed lattice which results in the formation of a gel (Figure 5.1a).[10] However, for thermogelling ABA triblock copolymers with lower critical solution temperature (LCST) components, the mechanism of gelation is less well-studied, and may not be universal. Semenov proposed that ABA triblock with hydrophobic A blocks form flower-like micelles which may be bridged by the hydrophilic B blocks (Figure 5.1b).[11] There are reports of PNIPAM-PEG-PNIPAM triblock copolymers forming aggregates with small domains of partially phase-separated PNIPAM blocks interconnected by PEG chains,[12] which may support the Semenov mechanism of gelation, however this study was of nanoparticles at concentrations where a gel phase was not formed. Furthermore, this type of has not been extended to ABA triblock copolymers containing alternative temperature responsive A blocks. Throughout the literature the link between nanoparticle formation and thermogel formation is often disregarded. Thus, there is a need to investigate the solutions properties of ABA triblock

copolymers in both dilute and concentrated solution, in order to understand the mechanisms by which gelation may occur.
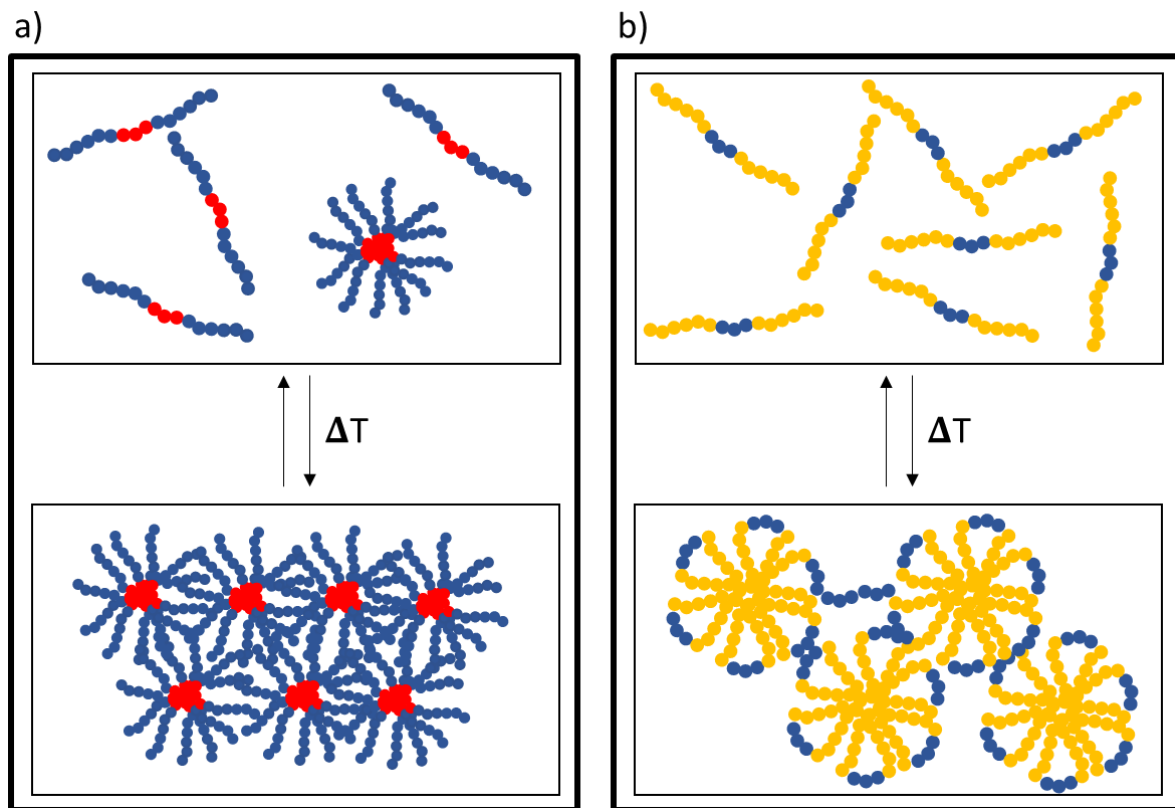
Figure 5. 1: a) The proposed gelation mechanism for poloxamer 407 triblock copolymers in aqueous solution showing the formation of core-shell micelles with poly(propylene glycol) (red) cores and PEG (blue) coronas which pack above a critical concentration, forming a gel. b) The proposed gelation mechanism for ABA temperature responsive polymers with temperature responsive A blocks (yellow) and PEG B blocks (blue), showing the formation of aggregates which may pack and be bridged by polymer chains.

The physical properties of thermogelling materials are crucially important for their performance, requiring low viscosity at room temperature, transition to a gel between room temperature and body temperature, and a high viscosity in the gel state. The increase in viscosity exhibited by thermogelling polymers has been investigated using methods such as tube inversion,[13] viscometry[14] and rheology.[15] The identification of the gelation temperature by tube inversion is conducted by simply warming a vial containing the polymer solution then inverting and observing whether it flows under gravitational forces.[16] This technique may be biased and inaccurate, as gelation is determined by eye at a single force and heat transfer across the sample will depend on several factors such as

thickness and size of the vial. Classical viscometry can track any increase in sample viscosity, but the technique cannot distinguish between viscous and elastic behaviour. Temperature ramp rheology is the most common and preferred thermogel characterisation method reported within the literature.[17–19] Rheology enables measurement of both the storage modulus (G') and loss modulus (G'').[20] G' and G'' represent the solid-like (elastic) behaviour and fluid-like (viscous) behaviour of the sample, respectively. The temperature at which G' exceeds G'' is generally taken as the gelation temperature, as the sample has become more solid-like than fluid-like.[16] Thus, measurement of these two parameters reveal whether the sample is a viscous fluid, where G'' exceeds G', or a gel, where G' exceeds G''. The viscosity of a sample, i.e. its resistance to flow, is then related to the overall magnitude of the two moduli via the complex modulus (G*). Thus, rheology is the preferred method for thermogel characterisation, giving accurate measurement of gelation temperatures, viscoelasticity and overall resistance to flow.

There are several studies reporting the effect of polymer architecture or block molecular weights on thermogelling behaviour.[21–23] However, there is a paucity of studies which investigate the effect of temperature responsive polymer type on the aqueous solution properties of block copolymers. This chapter addresses that gap in the literature by investigating the link between the dilute and concentrated solution properties of temperature responsive ABA triblock copolymers. As well as investigating the effect of temperature responsive polymer type and block molecular weights on the rheology of such solutions, as a function of temperature.

[5.2] Aims and Objectives

The aim of this phase of research was to study the phase behaviour of the triblock copolymers synthesised in Chapter 4 in aqueous solution and explore the rheological properties of any thermogelling materials identified. To streamline selection of the optimal thermogelling materials for drug delivery, cytotoxicity was also determined. The aim was achieved by the following objectives:

- Phase diagrams were prepared for each copolymer in 1, 5, 10, 15 and 20 % aqueous solution from 20 to 70 °C at each 5 °C increment. The phase diagrams described the physical appearance of the sample with concentration and temperature.

- The self-assembly behaviour of dilute triblock copolymer aqueous solutions (1 mgmL^{-1}) with an increase in temperature from 20 to 70 °C was investigated using DLS.

- The rheological properties of concentrated triblock aqueous solutions (20 % (w/v)) with an increase in temperature from 20 to 70 °C was investigated.

- The cytotoxicity of the tri-block copolymers to human immortalised keratinocytes (HaCat) was evaluated.

[5.3] Materials

The ABA triblock copolymers of poly(N-isopropyl acrylamide) (PNIPAM), poly(2-(N-dimethylamino)ethyl methacrylate) (PDMAEMA), poly(N,N-diethyl acrylamide) (PDEA) or poly(diethylene glycol methyl ether methacrylate) (PDEGMEMA) (A) and poly(ethylene glycol) (B) with molecular weights of 10-4-10, 20-4-20, 10-10-10 and 20-10-20, synthesised in chapter 4, were used without further purification. Sterile phosphate buffered saline (PBS), penicillin-streptomycin (PenStrep), L-glutamine (200 mM), foetal bovine serum (FBS) and Triton X-100 (Triton X) were purchased from Sigma-Aldrich (U.K.) and were used as purchased. Dulbecco's modified eagles medium – high glucose with 4500 mg/L glucose, L-glutamine, sodium pyruvate and sodium bicarbonate (DMEM) was purchased from Sigma-Aldrich (U.K.) was used for cell culture, but 50 mL of the media was replaced with FBS and 10 mL of both PenStrep and L-glutamine were added. The final DMEM solution was 10 % FBS, 1 % PenStrep and 1% L-glutamine. Adherent human keratinocytes (HaCat) cells were purchased from ThermoFisher Scientific (U.K.) and were washed with sterile PBS and grown in DMEM. CytoTox 96 non-radioactive cytotoxicity assay and CelTiter 96 aqueous one solution cell proliferation assay were purchased from Promega (U.K.) and used as purchased.

[5.4] Methods

[5.4.1] Phase diagram preparation

Each polymer was dissolved in deionised water at 20 % (w/v). The sample was held in a water bath at 20 °C for 1 min, then removed and inverted. The physical appearance of the solution was evaluated. Materials were considered to be gels if they did not flow under gravitational force. The temperature was then increased in 5 °C increments and the physical appearance evaluated, until the water bath reached 70 °C. This was then performed for 20, 15, 10, 5, and 1 % (w/v) aqueous solutions of block copolymers.

[5.4.2] Rheology

All rheology experiments were performed on a TA AR 1500 ex rheometer with a Julabo AWC 100 cooling unit using rheology advantage software and a 40 mm parallel plate geometry. The gap between the Peltier plate and geometry was 650 μm and a frequency of 1 Hz was used for all experiments. All samples were prepared at 20 % (w/v) aqueous solution and left overnight in the fridge before performing rheology experiments.

[5.4.2.1] Oscillatory stress sweep experiments

The oscillatory stress sweep (OSS) experiments were performed at 20 °C and the oscillatory stress was increased from 1 to 100 Pa. The linear viscoelastic region (LVR) was identified as the region before the increase in oscillatory stress caused both storage modulus (G') and loss modulus (G'') to decrease, which was determined to be the yield stress. The sample was replaced, and the experiment was repeated 3 times.

[5.4.2.2] Temperature ramp experiments

The temperature ramps were performed at 1 Pa of oscillatory stress and a frequency of 1 Hz, with an increase in temperature from 20 to 70 °C at a rate of 2 °C per minute. The gelation temperature (Tgel) was taken as the point where the sample transitioned from G'' > G' to G' > G'' and the gel strength was taken as the maximum value of G' reached. The sample was replaced, and the experiment repeated 3 times.

[5.4.3] Dynamic light scattering experiments

All dynamic light scattering (DLS) experiments were performed on a Malvern Zetasizer Nano ZS, using 1 mg/mL aqueous polymer solutions and a scattering angle of 173 °. Polymer solutions were stored in the fridge overnight before use. Size measurements were taken at 25, 30, 35, 40, 45, 50, 55, 60, 65 and 70 °C in triplicate. A 5-minute equilibration period was used before each measurement, which was conducted in triplicate. The process was repeated until 70 °C was reached. The derived count rate and polydispersity were plotted as a function of temperature. The micellization temperature was taken as the temperature at which the derived count rate increased.

[5.4.3.2] Zeta potential experiments

Zeta potential measurements were performed on a Malvern Nano ZS with a 1mg/mL aqueous polymer solution, using DTS1070 folded capillary cells. The sample was loaded into the capillary cells and held at 50 °C for triblock copolymers containing PNIPAM, PDEA and PDEGMEMA and 70 °C for those with PDMAEMA. After 5 minutes of equilibration the zeta potential was measured in triplicate.

[5.4.4] Cytotoxicity testing

HaCat cells were seeded at 10,000 cells per well and grown for 4 days in an incubator at 37 °C with 5 % CO_2. Assays were conducted on each polymer at 10 mg/mL four times. A blank of culture media without cells and polymer was used for each polymer test, and a positive control and a negative control was used for the LDH and MTS assays, respectively. The positive control was cells treated with Triton-X to lyse their membranes and the negative control was healthy cells which were not treated with either Triton-X or polymer solution. Cytotoxicity was investigated by adding 50 µL of 20 mg/mL polymer solution to the cells in 50 µL of culture media to yield a triblock copolymer concentration of 10 mg/mL. The dosed cells were stored in the incubator at 37 °C in 5 % CO_2 for 2 h before running the cytotoxicity assays. Preliminary studies following the assay protocols on both culture media and 10 mg/mL polymer solutions in culture media were performed. This was to ensure that changes in the fluorescence and absorbance during the LDH and MTS were solely due to the cells.

[5.4.4.1] LDH assay

For the LDH assay, 50 µL of cell supernatant was removed from each well and transferred to the wells on a black 96-well plate and 50 µL of assay solution was added to each well. The assay was covered by foil and left for 10 minutes the fluorescence examined using a Promega Glomax Multi Detection System fluorescence plate reader at an excitation wavelength of 560 nm and an emission wavelength of 590 nm. The data was then expressed as a percent cytotoxicity which was calculated from the fluorescence intensity of the dosed cells (dosed cells), the media background (Background) and the positive control (Triton X control) (Equation 5.1).

$$\text{Equation 5.1: Percent Cytotoxicity} = \frac{(\text{Dosed Cells} - \text{Background})}{(\text{Triton X Control} - \text{Background})} \text{ X } 100$$

[5.4.4.2] MTS assay

After the LDH assay, the remaining HaCat cells in 50 µL of polymer in cell culture media (10 mg/mL) were then used for the MTS assay. The MTS assay solution (10 µL) was added to the polymer dosed HaCat cells and incubated at 37 °C with 5 % CO_2 for 2 h. The absorbance of the assay solution was then investigated at a wavelength of 490 nm, using the same instrument as the LDH assay. The data was expressed as percent metabolic activity which was calculated from the absorbance of the dosed cells, the media background and the negative control (healthy cells) (Equation 5.2).

$$\text{Equation 5.2: Percent Metabolic Activity} = \frac{(\text{Dosed Cells} - \text{Background})}{(\text{Healthy Cells} - \text{Background})} \text{ X } 100$$

[5.5] Results and discussion

[5.5.1] Phase diagrams

The effect of temperature on the solution behaviour of the triblock copolymers in aqueous solution at concentrations of 1, 5, 10, 15 and 20 mg/mL was investigated (Figure 5.2). The phase diagrams show any observable changes in viscosity and the onset of turbidity (T_c). The increase in viscosity was identified by the tube inversion method, which is commonly used as a screening tool to identify potential gelation, but confirmation is required by a complimentary technique, e.g. rheology.[16]

All triblock copolymers exhibited a physical transition with an increase in temperature, which varied between polymer type, concentration and molecular weight. The T_c significantly varied between polymer type, concentration and molecular weight, with the exception of PNIPAM where molecular weight did not alter this transition temperature. The PNIPAM block copolymers consistently became turbid above ca. 35 °C, which is in agreement with previous studies.[24] Triblock copolymers containing PDEA and PDEGMEMA exhibited a transition from clear to turbid at ca. 40 and 30 °C, respectively, while the homopolymers exhibit LCSTs at ca. 28 and 25 °C. This is thought to be as a result of an increase in the overall polymer hydrophilicity, due to polymerisation from a PEG macroinitiator.[25] In addition to this, the T_c observed for PDEA and PDEGMEMA triblock copolymers was decreased upon increasing the molecular weight of the temperature responsive component. For example, in 20 % (w/v) solution PDEA10-PEG4-PDEA10 became turbid above 40 °C, while PDEA10-PEG10-PDEA10 became turbid above 25 °C. This phenomenon has been shown before and is reportedly as result of an increase in relative hydrophobicity of the copolymer above the LCST.[26] For PDMAEMA, the 10-4-10 polymer was the only one to transition from clear to turbid, while 20-4-20, 10-10-10 and 20-10-20 were turbid at all temperatures. This is thought to be as a result of the formation of aggregates below the LCST of PDMAEMA, which is in agreement with previous studies which report the formation of aggregates from PEG-PDMAEMA diblock copolymers below the LCST of PDMAEMA.[27] These aggregates may be in equilibrium with the free chains, much like poloxamer 407, and upon an increase in temperature this equilibrium shifts to drive formation of aggregates which results in an increase in viscosity.[10] Generally, all triblock copolymers required a concentration above or equal to 15 % (w/v) to exhibit gel formation, with PDMAEMA 20-4-20 and PDEGMEMA 20-10-20 requiring a minimum concentration ca. 10 % (w/v).

Figure 5. 2: The phase diagrams of the 10-4-10, 20-4-20, 10-10-10 and 20-10-20 ABA triblock copolymers of PNIPAM, PDMAEMA, PDEA or PDEGMEMA (A) and PEG (B). The colours blue, green, red and black represent a solution, a viscous solution, a gel and a sediment respectively, while the shape represents a clear solution (triangle) or a turbid one (square). The dashed lines represent increases in viscosity to a viscous fluid (green) or a gel (red) or the formation of a sediment (black).

[5.5.2] Rheology

Rheology experiments were used to study temperature-induce changed in viscoelasticity of 20 % (w/v) polymer solutions. When performing temperature rheology experiments, the oscillatory stress used must be carefully selected from within the LVR. If the oscillatory stress applied is outside of this region, the internal structure of the sample may be changed by shear forces, and this may impact the identification of a gel, for instance by forcing it to yield. To ensure this did not occur, OSS experiments were first performed on the polymers in solution at 20 °C. Viscous samples can generally withstand a greater oscillatory stress before yielding than less viscous samples.[28] As such, when the thermogels increase in viscosity with temperature their resistance to oscillatory stress is expected to be greater. Thus, any force applied within the LVR of the sample at low temperature (i.e. a fluid state) is not expected to affect the internal structure of the sample at elevated temperature.[29] The low values of oscillatory stress selected enable the rheology of the native state to be evaluated, representative of a low shear scenario such as remaining untouched upon the application site. The OSS experiments for all triblock copolymers in 20 % aqueous solution identified that for all samples an oscillatory stress of 1 Pa was within the LVR (Figure 5.3). The selected stress for temperature ramp experiments was 1 Pa in order to minimise any risk of destroying the internal structure of the sample as temperature increases.

Figure 5. 3: The OSS experimental data for the 10-4-10, 20-4-20, 10-10-10 and 20-10-20 ABA triblock copolymers of PNIPAM, PDMAEMA, PDEA or PDEGMEMA (A) and PEG (B). G' (blue) and G'' (orange) are given across 1-100 Pa of oscillatory stress. Data presented as mean ± standard deviation (n=3).

The temperature ramp rheograms of triblock copolymers in 20 % (w/v) aqueous solution indicate that all solutions exhibit a degree of thermothickening (Figure 5.4). This thermothickening was identified by increases in both G' and G'' which varied between temperature responsive polymer type and their molecular weights. In addition to this, not all triblock copolymers resulted in the formation of a gel, where G' exceeded G''. All 10-4-10 triblock copolymers resulted in the formation of a viscous fluid, where G'' remained dominant at all temperatures. This has been previously observed by Teodorescu et al (2010), where PNIPAM-PEG-PNIPAM triblock copolymers with PEG and PNIPAM molecular weights of 4 and 10 kDa, respectively, did not gel.[30] This study found that triblock polymers with PEG and PNIPAM molecular weights require a minimum of 4 and 20 kDa, respectively, to form a gel. This is thought to be as a result of fewer entanglements[26] and micellar bridges as described by Semenov (1995)[11] formed by polymers of lower molecular weight. Generally, all triblock copolymers with the architectures 10-10-10 and 20-10-20 formed rheological gels (G' > G''), with the exception of PDMAEMA triblock copolymers. In addition to this, the PNIPAM, PDEA and PDEGMEMA triblock copolymers exhibited a sharp transition from fluid to viscous solution or gel over the course of ca. 5-10 °C, while the PDMAEMA triblock copolymers gradually increased in viscosity as the temperature increased from 20 to 70 °C. The temperature at which this broad transition began to occur was at ca. 30 and ca. 35 °C for PDMAEMA10-PEG10-PDMAEMA10 and PDMAEMA20-PEG10-PDMAEMA20, respectively. This decrease is in agreement with what is observed with the PDMAEMA homopolymer, where the LCST may be tuned to a lower temperature by increasing the molecular weight.[31] The formation of viscous fluids and slow sol-gel transition of the PDMAEMA triblock copolymers may be as a result of protonation of the tertiary amine present in the polymer backbone. PDMAEMA homopolymers exhibit pKas of approximately 7.5, depending on polymer molecular weight.[32] Copolymers of PDMAEMA, however, have been shown to exhibit pKas as low as 6.1 depending on both copolymer and molecular weight.[33] As such, both homopolymers and block copolymers of PDMAEMA become increasingly protonated in acidic media, which has been shown to hinder the desolvation process above the LCST as a result of charge repulsion and an increase in solubility.[34] This is theorised to also negatively impact the aggregation behaviour of block copolymers, which may prevent the formation of a gel as a result of a relatively reduced number of micellar bridges. To overcome this, buffered solutions may be used to maintain the pH above the pKa and prevent this protonation.
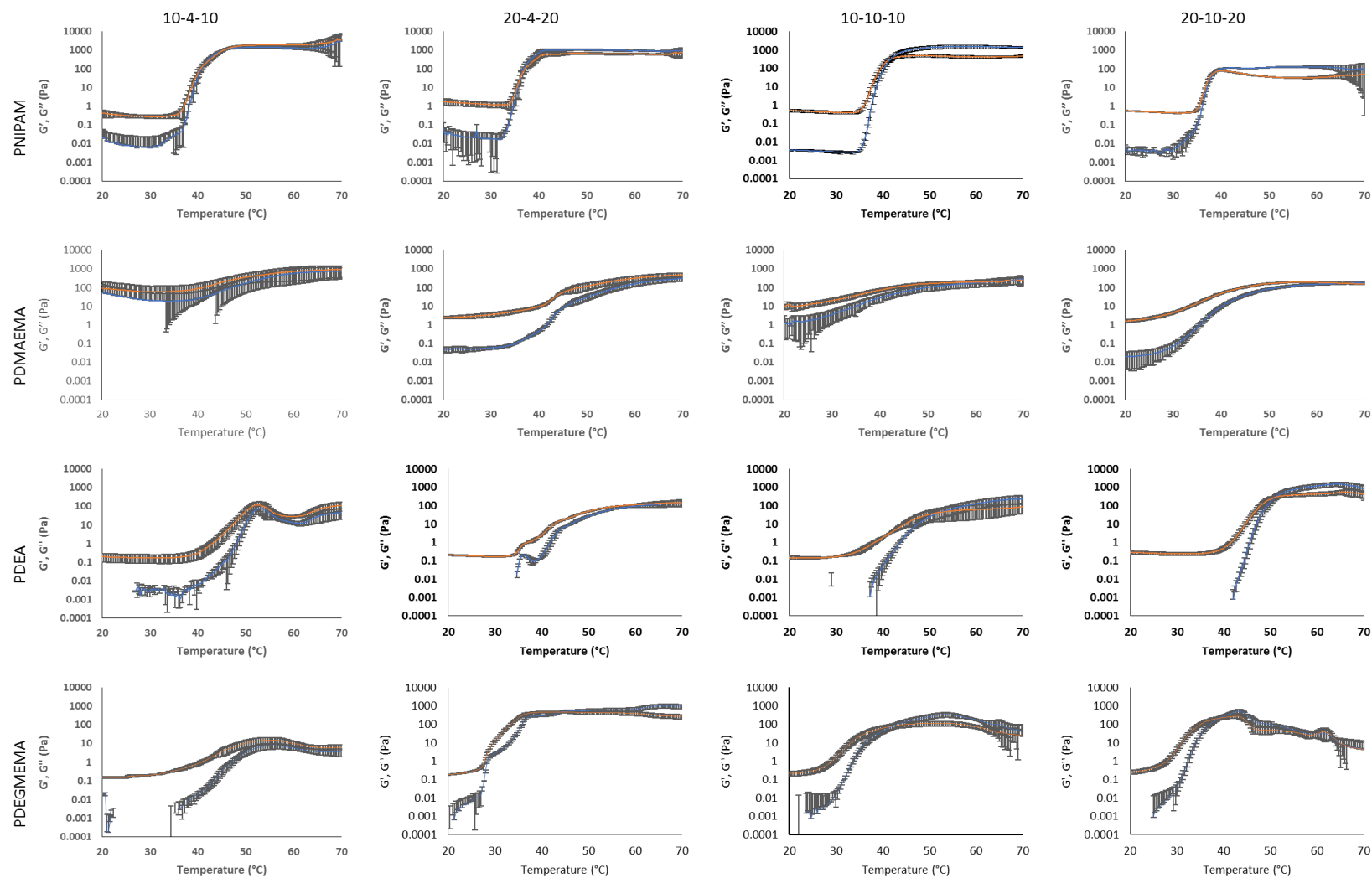
Figure 5. 4: The temperature sweep rheograms for the 10-4-10, 20-4-20, 10-10-10 and 20-10-20 ABA triblock copolymers of PNIPAM, PDMAEMA, PDEA or PDEGMEMA (A) and PEG (B). G' (blue) and G'' (orange) are given across a range of temperatures from 20 to 70 °C. Data presented as mean ± standard deviation (n=3)

A single temperature ramp of the PDMAEMA triblock copolymers at 20 % w/v in pH 8.0 phosphate buffered solution was performed (Figure 5.5). This was in order to maintain the pH above the pKa in an effort to improve the thermogellation properties. Phosphate buffer at pH 8.0 was selected as pHs greater than 8.0 may not be suitable for topical drug delivery applications due to the potential for irritation.[35] In pH 8.0 the PDMAEMA triblock copolymers showed the same trends as in deionised water. These solutions exhibited a broad transition from solution to either viscous fluid or gel. With the exception of the PDMAEMA10-PEG4-PDMAEMA10 triblock copolymer which was a gel at all temperatures. The breadth of this transition is thought to arise from the LCST molecular weight dependence. The LCST of homopolymers of PDMAEMA may be tuned to lower temperatures by increasing the molecular weight, where this transition may be altered by up to 40 °C in pH 7.0 media. The PDI of these polymers ranged from 1.14 to 1.32 (Chapter 4). Therefore, these solutions may exhibit broad transitions as a result of the variation in polymer molecular weight. When compared to deionised water, the 10-10-10 and 20-10-20 PDMAEMA triblock copolymers formed viscous fluids in pH 8.0 media, but gels in deionised water. This is thought to be as a result of the formation of larger disorganised aggregates in pH 8.0 media when compared to deionised water, which may negatively impact the ability of micelles to pack in an ordered structure. A study by Manga et al (2018) found that increasing the pH from 3.0 to 10.0 of a poly(methyl methacrylate)—block—poly (2-dimethylaminoethyl methacrylate) diblock copolymer solution lead to the increase in aggregate size.[36] This is thought to be as a result of particle aggregation which is driven by favoured interactions between the DMAEMA chains, over the DMAEMA-water interactions, as the pH is increased over the apparent pKa (ca 6-7). The increased salt content of the pH 8 buffer will also screen any charge, and therefore interparticle interactions and potentially affect LCST.
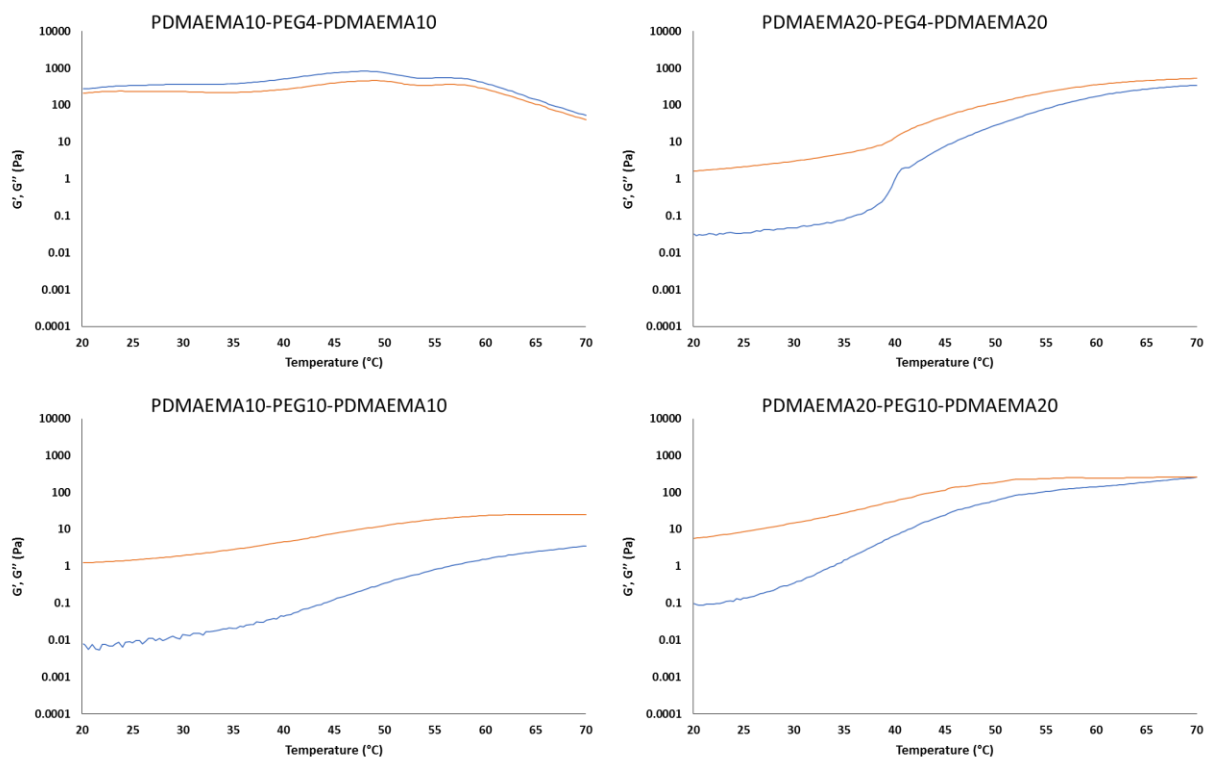
Figure 5. 5: The rheograms of PDMAEMA10-PEG4-PDMAEMA10, PDMAEMA20-PEG4-PDMAEMA20, PDMAEMA10-PEG10-PDMAEMA10 and PDMAEMA20-PEG10-PDMAEMA20 in phosphate buffers solution at pH 8. The rheograms show the change in G' (Blue) and G'' (Orange) as the temperature is increased from 20 to 70 ºC.

Key parameters to characterise thermogelling materials may be extracted from the temperature ramp rheograms including the Tgel and the maximum strength of the gel formed (G'max) at elevated temperature (Table 5.1). The Tgel is taken as the temperature at which G' exceeds G'', and the sample gains a greater solid-like behaviour than fluid-like. Generally, for all triblock copolymers, increasing the molecular weight of the temperature responsive component resulted in a decrease in the gelation temperature. For example, the Tgel of the PNIPAM triblock copolymers with 10 kDa PEG significantly decreased from 41.7 ± 0.4 to 38.9 ± 0.2 °C with an increase in PNIPAM molecular weight from 10 to 20 kDa (P<0.05). This decrease has been documented within the literature and is reported to be as a result of an increase in the relative hydrophobicity of the polymer.[37] Comparatively, for all triblock copolymers, except those containing PDEGMEMA, increasing the PEG molecular weight resulted in an increase in gelation temperature. For example, Tgel increased from 36.1 ± 0.5 to 38.9 ± 0.2 °C for the 20 kDa PNIPAM triblock copolymers when the PEG length was increased from 4 to 10 kDa. As mentioned above, this is reported to be as a result of an increase in

hydrophilicity of the polymer.[30] The decrease observed in Tgel from 44.0 ± 0.0 to 39.1 ± 0.2 °C when the PEG molecular weight was increased for PDEGMEMA triblock copolymers may be as a result of increased favour for the gelation process. Shorter PEG chains are likely to be less flexible than longer PEG chains, and as such may restrict aggregate formation upon desolvation of the PDEGMEMA blocks, while longer chains may not.[38] In addition to this, the PDEGMEMA monomer is the largest of the 4 and as a result steric hinderance may prevent aggregate formation in the those with 4 kDa PEG. When the PEG molecular weight is longer, the PDEGMEMA blocks are separated further from one another, reducing this steric hinderance.[39] As a result, these triblock copolymers may require less energy to drive aggregate formation and subsequently a gel. With regards to gel strength, there were no common trends observed between the block molecular weights and the G' max. Within the literature, it has been observed that increasing the molecular weight of the PNIPAM block increases the strength of the gel formed, as identified by rheology.[40] However, differences in ramp rate, frequency and applied oscillatory stress may structurally deform the molecular structure, resulting in the formation of a weaker gel.[41] One such study by Teodorescu et al found the gel strength increased from ca. 1 to ca. 100 MPa when the PNIPAM molecular weight was increased from 10 to 20 kDa with a central 4 kDa PEG block.[30] This rheology was performed at a gap of 500 μm, at a frequency of 0.16 Hz, at a controlled undefined stress and a ramp rate of 0.5 °C/min, while the rheology presented in this chapter was performed at 650 μm, 1 Hz, 1 Pa and 2 °C/min. The difference observed between the literature and this study may be due to frequency dependence of the rheology, which was not studied. Finally, the results of Teodorescu and co-workers are based on single rheological measurements and the reproducibility of their result is unknown.

Table 5. 1: The Tgel and gel strength (G' maximum) extracted from the temperature ramp rheology experiments of the 10-4-10, 20-4-20, 10-10-10 and 20-10-20 ABA triblock copolymers of PNIPAM, PDMAEMA, PDEA and PDEGMEMA (A) and PEG (B) in 20 % (w/v) aqueous solution. The data are presented as mean ± standard deviation (n=3).

Polymer	Tgel (°C)	G' Maximum (Pa)
PNIPAM10-PEG4-PNIPAM10	N/A	1296 ± 166
PNIPAM20-PEG4-PNIPAM20	36.1 ± 0.5	957 ± 56
PNIPAM10-PEG10-PNIPAM10	41.7 ± 0.4	1579 ± 303
PNIPAM20-PEG10-PNIPAM20	38.9 ± 0.2	146 ± 37
PDMAEMA10-PEG4-PDMAEMA10	N/A	329 ± 90
PDMAEMA20-PEG4-PDMAEMA20	N/A	159 ± 47
PDMAEMA10-PEG10-PDMAEMA10	66.9 ± 3.0	135 ± 26
PDMAEMA20-PEG10-PDMAEMA20	65.8 ± 0.7	149 ± 17
PDEA10-PEG4-PDEA10	N/A	90 ± 28
PDEA20-PEG4-PDEA20	N/A	135 ± 52
PDEA10-PEG10-PDEA10	51.2 ± 1.8	235 ± 114
PDEA20-PEG10-PDEA20	45.9 ± 0.5	1518 ± 399
PDEGMEMA10-PEG4-PDEGMEMA10	N/A	7.5 ± 2.6
PDEGMEMA20-PEG4-PDEGMEMA20	44.0 ± 0.0	982 ± 250
PDEGMEMA10-PEG10-PDEGMEMA10	42.2 ± 0.4	341 ± 95
PDEGMEMA20-PEG10-PDEGMEMA20	39.1 ± 0.2	514 ± 140

Of the materials presented in this study, the PDEA-PEG-PDEA and PDEGMEMA-PEG-PDEGMEMA materials have not be reported previously. In addition to this, the investigation of the thermogelling behaviour of these two types of polymer and the PDMAEMA-PEG-PDMAEMA triblock copolymers has not previously been investigated. Overall, the poorest performing materials were those which contained PDMAEMA, as these exhibited broad transitions from solution to gel at temperatures above 50 $^{\circ}$C and resulted in the formation of weak gels with G' maxima below 400 Pa. The best performing triblock copolymers were PNIPAM-PEG-PNIPAM (10-10-10), PDEA-PEG-PDEA (20-10-20) and PDEGMEMA-PEG-PDEGMEMA (20-4-20). All sharply transitioned at 41.7 ± 0.4, 45.9 ± 0.5 and 44.0 ± 0.0 $^{\circ}$C from solution to gels with strengths of 1579 ± 303, 1518 ± 399 and 982 ± 250 Pa, respectively. In addition to this, the molecular aggregation may also impact the gelation of temperature responsive triblock copolymers. The gelation mechanism proposed by Semenov (1995) describes the formation of close packed bridged flower-like micelles in concentrated solution, resulting in the formation of a macroscopic gel.[11] The size of these aggregates and their relative packing motifs may drastically impact the strengths of the gels formed.[42] As aggregates which associate in a denser manner with more bridging are expected to form stronger gels, for example. Thus, nanostructural information is required in addition to macromolecular descriptors to build a holistic view of the relationship between polymer and rheology. This process was investigated initially by DLS.

[5.5.3] Dynamic Light Scattering

To understand the changes in Tgel and gel strength associated with the changes in block molecular weight the dilute solution properties of the triblock copolymers was investigated using DLS (Figure 5.6). The derived count rate and polydispersity of the samples was investigated as the temperature was increased by 5 °C increments from 25 to 70 °C. All triblock copolymers in 1 mg/mL aqueous solution formed aggregates with an increase in temperature, as given by the increase in the derived count rate. The temperature at which this occurred was denoted the CMT. The CMT of the PNIPAM and PDEGMEMA triblock copolymers remained constant at ca. 35 and ca. 30 °C, respectively, regardless of polymer molecular weight. The lack of change is expected to be as a result of the LCSTs of the homopolymers of PNIPAM and PDEGMEMA 32[43] and 25 °C,[44] respectively, which are independent of molecular weight. The slight increase in CMT seen in the block copolymers compared to the homopolymers is thought to be as a result of the PEG block, which increases the overall hydrophilicity of the polymers.[37] It has also been demonstrated that PEG blocks may interfere with phase separation processes.[12] The CMT observed here for PNIPAM is in agreement with previous literature studies,[24] while the CMT of PDEGMEMA-containing block copolymers has not previously been investigated. The CMT of PDEA containing triblock copolymers remained consistent at ca. 30 and ca. 40 °C for the copolymers with 4 and 10 kDa PEG blocks, respectively. The increase from 30 to 40 °C is as a result of increased hydrophilicity due to the longer PEG block.[45] The CMT of PDMAEMA triblock copolymers significantly varied depending on both block molecular weights, where 10-4-10, 20-4-20, 10-10-10 and 20-10-20 exhibited CMTs at ca. 50, 35, 40 and 60 °C, respectively. The LCST of PDMAEMA is significantly affected by molecular weight, where the LCST can decrease from 85 to 50 °C with an increase in molecular weight from 5.5 to 85.7 kDa.[34] The formation of these PDMAEMA aggregates occurred gradually as the temperature increases, in a similar manner to the viscosity in the rheology experiments. Conversely, the PNIPAM, PDEA and PDEGMEMA triblock copolymers formed both aggregates in dilute solution over a narrow range, consistent with the sol-gel transition observed by rheometry.
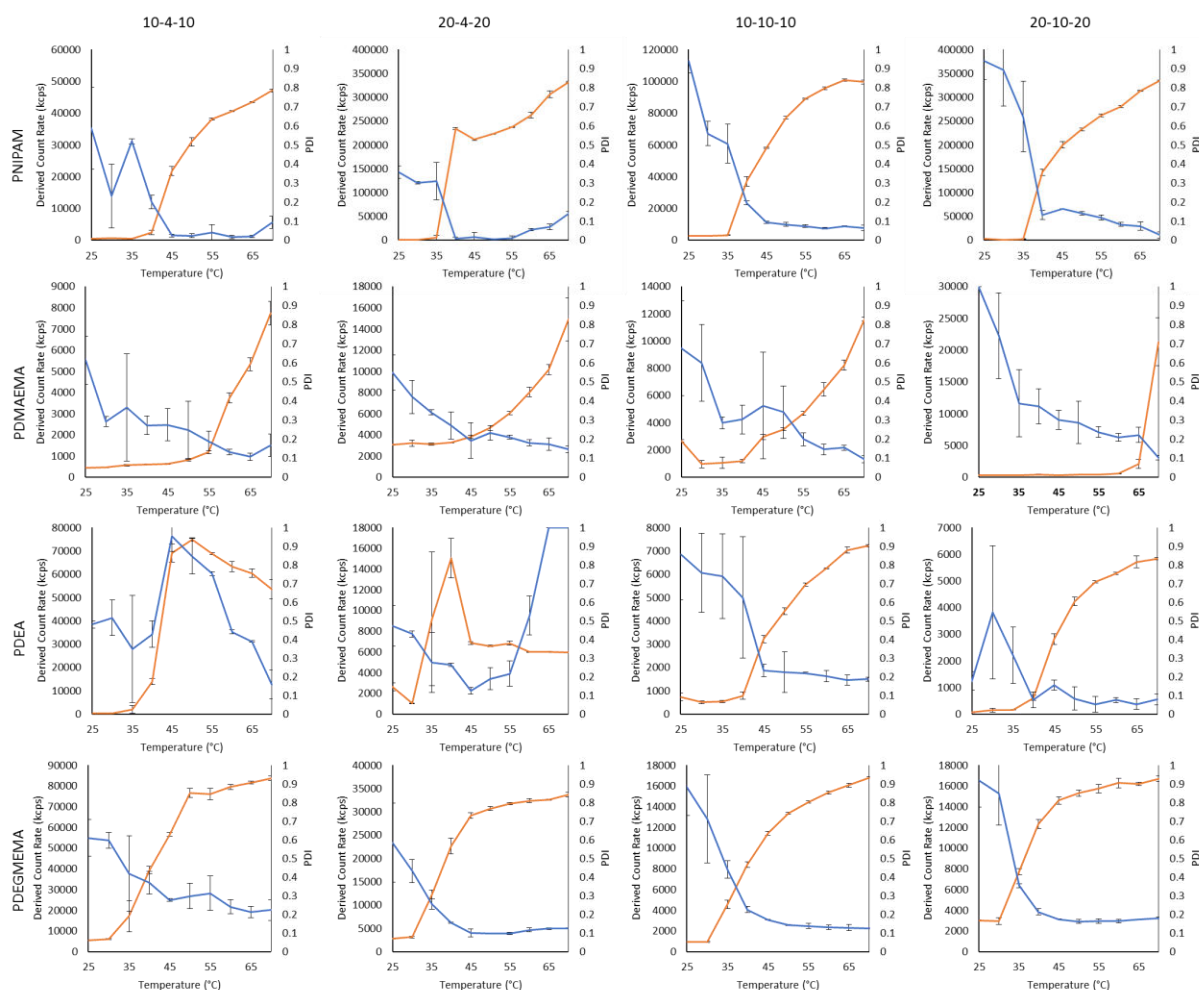
Figure 5. 6: The DLS data showing the change in derived count rate (orange) and PDI (blue) as the temperature of 1 mg/mL aqueous solution of 10-4-10, 20-4-20, 10-10-10 and 20-10-20 ABA triblock copolymers using PNIPAM, PDMAEMA, PDEA or PDEGMEMA (A) and PEG (B) was increased from 25 to 70 °C. Data presented as mean ± standard deviation (n=3).

In addition to the increase in derived count rate, nearly all triblock copolymers exhibited in a reduction in polydispersity (PDI) to less than 0.3, with the exception of PDEA 10-4-10 and 20-4-20. This indicates that most of these polymers formed organised, well-defined, aggregates upon an increase in temperature. PNIPAM, PDEA and PDEGMEMA copolymers formed a single population of particle sizes at 50 °C, while PDMAEMA formed aggregates of a single population of particle size above 70 °C (Figure 5.7). These temperatures were selected based on the relative CMTs observed by these polymers.
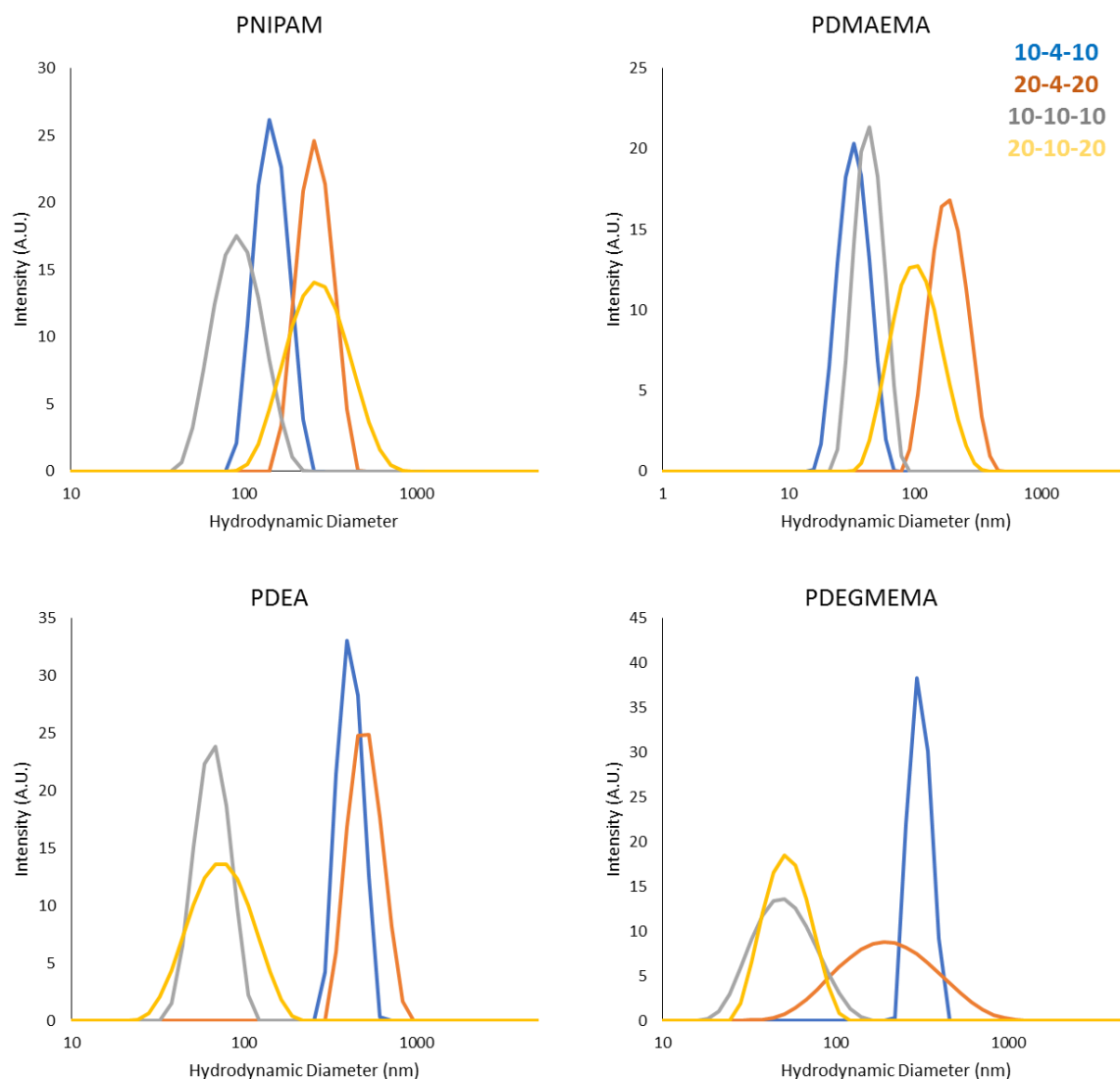
Figure 5. 7: The size histograms obtained from DLS of the PNIPAM, PDMAEMA, PDEA and PDEGMEMA triblock copolymers with architectures of 10-4-10 (blue), 20-4-20 (orange), 10-10-10 (grey) and 20-10-20 (yellow) in 1 mg/mL aqueous solution. The particle sizes for PNIPAM, PDEA and PDEGMEMA triblock copolymers were taken at 50 °C, while PDMAEMA were taken at 70 °C.

The average hydrodynamic diameter, PDI and zeta-potential of the aggregates formed by PNIPAM, PDEA and PDEGMEMA triblock copolymers in 1 mg/mL solution at 50 °C, and those formed by PDMAEMA at 70 °C are shown below in Table 5.2. For PNIPAM and PDMAEMA triblock copolymers, increasing the molecular weight of both the LCST-exhibiting and PEG blocks led to an increase in aggregate diameter. While for PDEA and PDEGMEMA, increasing the molecular weight of these blocks led to a decrease in aggregate size. The differences in size as a result of changes in molecular weight may be as a result of changes in aggregate morphology or aggregation number.[46] The

morphology of these aggregates is unknown, as DLS cannot differentiate between aggregate shape and approximates to a sphere with the same diffusion coefficient. The aggregates are believed to form flower-like core-shell micelles as this has previously been proven to occur for PNIPAM-PEG-PNIPAM triblock copolymers.[24] This study found PNIPAM-PEG-PNIPAM triblock copolymers formed aggregates with hydrodynamic radii of ca. 75 nm, which is comparable to the diameters found for the PNIPAM polymers in this work (Table 5.2). The size the micelle is dependent on both the size of the chain forming the corona (i.e. PEG) and the volume of the thermoresponsive arm which makes the micelle core. These polymers, however, may alternatively form rod-like or worm-like micelles instead of core-shell micelles.[47] This micellar shape can be predicted by the packing parameter, which is calculated from the area per unimer at the aggregate-solution interface (i.e. PEG) and the volume and length of the hydrophobic chain (i.e. thermoresponsive chain).[48] Thus, above the respective LCSTs of PNIPAM, PDMAEMA, PDEA and PDEGMEMA, their volume may determine the aggregate shape and in turn hydrodynamic diameter. Considering this, an aggregate with a small head area and a long tail may be expected to form rod-like aggregates with a packing parameter between 0.3 − 0.5. Monomers such as PDEGMEMA and PDMAEMA are significantly larger in molecular weight than PNIPAM and PDEA, and as such may form aggregates with are significantly different in both size and shape. In the case of the aggregates formed by PNIPAM, PDEA and PDEGMEMA, the 10-4-10 triblock copolymers had hydrodynamic diameters of 171.2 ± 1.5, 479.2 ± 29.9 and 187.9 ± 23.4 nm, respectively. These were some of the largest aggregates formed and given the small PEG molecular weight relative to the temperature responsive chain, these aggregates may form rod-like or worm-like micelles rather than those which are spherical. Figure 5.8 shows the correlations between aggregate hydrodynamic diameter and G', G'' and tan delta. Correlations were generally weak, with polymer class having a great effect on behaviour, as previously discussed. A weak negative correlation was observed between aggregate hydrodynamic diameter and both G' and G'' within each class. G' and G'' represent the elastic and plastic character of the sample, respectively. This indicates that for 20 % (w/v) aqueous solutions of the triblock copolymers discussed in this work, there is a tendency for a greater viscosity in samples which form smaller aggregates. Tan delta, however, is a measure of the sample viscoelasticity and is calculated from the ratio of G'' and G'. Typically, when tan delta is greater than 1, the sample is more viscous than elastic, and the opposite when less than 1. In terms of the samples presented in this work, Figure 5.8c shows the correlation between the aggregate hydrodynamic diameter and tan delta. For PNIPAM and PDMAEMA samples, a negative correlation was observed, while a positive correlation was observed for PDEA and PDEGMEMA samples. This suggests that PNIPAM and PDMAEMA triblock copolymers become more elastic-like as the aggregate size falls, while PDEA and PDEGMEMA

triblock copolymers exhibit a more liquid-like rheology. Therefore, particle size is not be the only important factor that may determine the strength of gels formed by temperature responsive triblock copolymers. A contributing factor may be the morphology of the micelles, which may determine the packing density and the degree of intermicellar interaction.
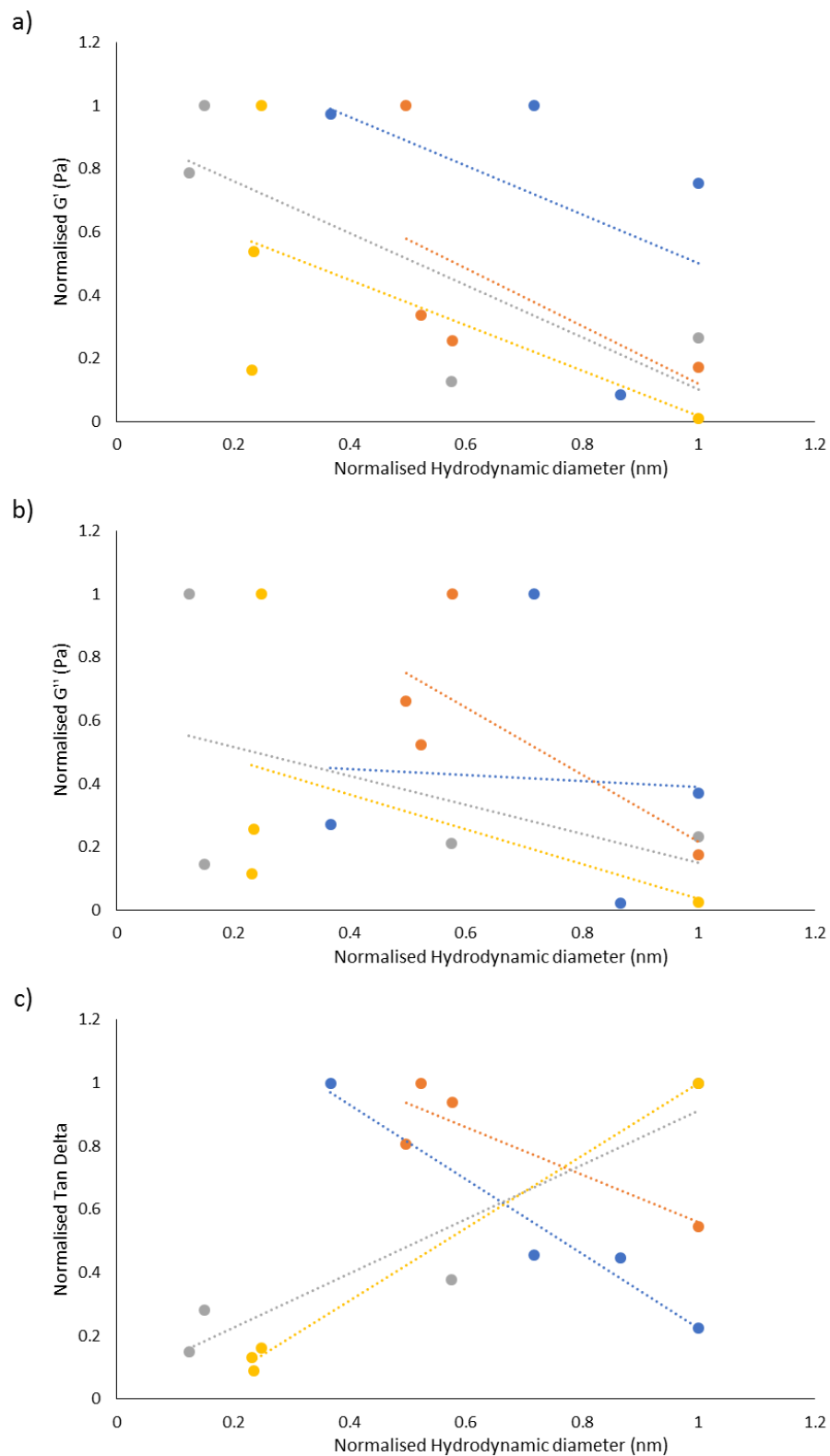
Figure 5. *8*: The correlation between the normalised hydrodynamic diameters of the aggregates formed at 50 °C by the PNIPAM (Blue), PDEA (Grey) and PDEGMEMA (Yellow) and at 70 °C by the PDMAEMA (Orange), triblock copolymers and the normalised G' (a), normalised G'' (b) and tan delta (c) at the specified temperature, of the in 20 % (w/v) aqueous solution.

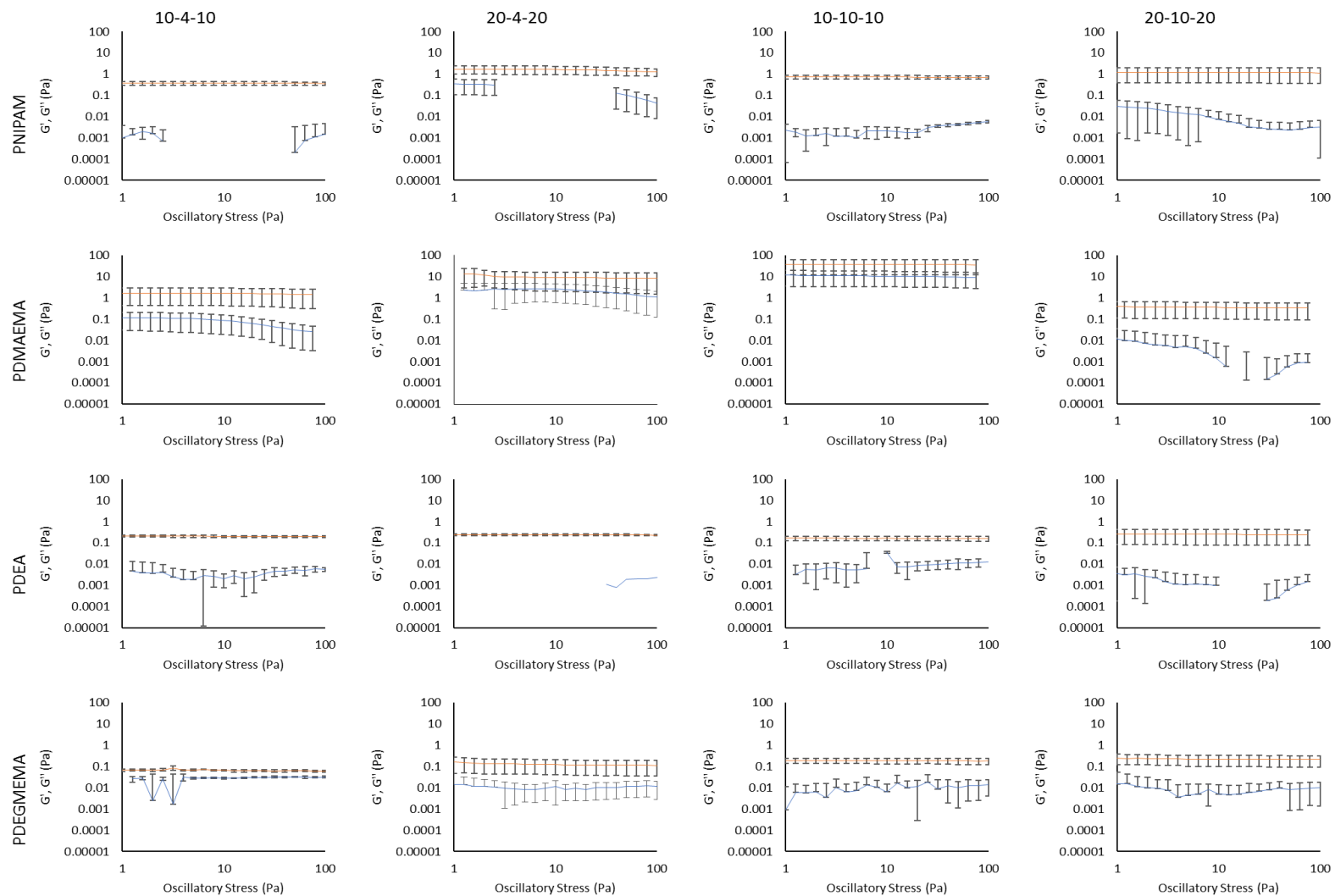Table 5. 2: The hydrodynamic diameter (nm), PDI and zeta potential (mV) of the 10-4-10, 20-4-20, 10-10-10 and 20-10-20 ABA triblock copolymers of PNIPAM, PDMAEMA, PDEA or PDEGMEMA (A) and PEG (B) in 1 mg/mL aqueous solution. Triblock copolymers containing PNIPAM, PDEA and PDEGMEMA were investigated at 50 °C, while PDMAEMA was investigated at 70 °C. Data presented as mean ± standard deviation (n=3).

Polymer	Diameter (nm)	PDI	Zeta Potential (mV)
PNIPAM10-PEG4-PNIPAM10	171.2 ± 1.5	0.02 ± 0.01	-26.67 ± 0.86
PNIPAM20-PEG4-PNIPAM20	238.8 ± 2.2	0.01 ± 0.00	-17.97 ± 1.22
PNIPAM10-PEG10-PNIPAM10	87.7 ± 1.0	0.08 ± 0.01	-12.43 ± 0.32
PNIPAM20-PEG10-PNIPAM20	206.9 ± 0.5	0.14 ± 0.01	-31.67 ± 0.38
PDMAEMA10-PEG4-PDMAEMA10	37.9 ± 2.0	0.14 ± 0.04	12.03 ± 0.42
PDMAEMA20-PEG4-PDMAEMA20	39.8 ± 0.4	0.15 ± 0.02	12.33 ± 0.59
PDMAEMA10-PEG10-PDMAEMA10	43.9 ± 0.4	0.09 ± 0.02	8.60 ± 0.54
PDMAEMA20-PEG10-PDMAEMA20	76.2 ± 0.4	0.10 ± 0.01	7.49 ± 0.39
PDEA10-PEG4-PDEA10	479.2 ± 29.9	0.85 ± 0.09	0.40 ± 0.29
PDEA20-PEG4-PDEA20	275.6 ± 12.8	0.30 ± 0.24	0.34 ± 1.42
PDEA10-PEG10-PDEA10	72.2 ± 3.7	0.23 ± 0.11	-13.10 ± 0.61
PDEA20-PEG10-PDEA20	59.2 ± 1.2	0.08 ± 0.06	1.09 ± 0.26
PDEGMEMA10-PEG4-PDEGMEMA10	187.9 ± 23.4	0.30 ± 0.07	-23.63 ± 0.60
PDEGMEMA20-PEG4-PDEGMEMA20	46.7 ± 0.7	0.10 ± 0.00	-20.73 ± 2.16
PDEGMEMA10-PEG10-PDEGMEMA10	44.2 ± 0.7	0.14 ± 0.00	-19.33 ± 1.42
PDEGMEMA20-PEG10-PDEGMEMA20	43.5 ± 0.9	0.16 ± 0.01	-14.30 ± 0.44

With regards to particles in a suspension, factors such as particle shape and size distribution and presence of electrical charges may influence the observed rheological properties. Einstein proposed that for a suspension of non-interacting spherical particles in dilute solution, the effective viscosity (μ^*) arises from the viscosity of the suspending fluid (μ_0) and the phase volume fraction of particles (φ) in suspension (Equation 5.3).[49] Given this, the lower the particle size the greater the volume fraction of particles as a result of an increase in surface area and subsequent solvation. Thus, it may be assumed that reducing the particle sizes may increase the suspension viscosity. In addition to this, if these hard spheres particles were repelling one another, a correlation between the solution viscosity and zeta potential may also be observed.

$$\text{Equation 5.3: } \mu^* = \mu_0 \left(1 + \frac{5}{2}\phi \right)$$

The Einstein approximation, however, is only applicable to dilute solutions, while concentrated solutions are described by the Krieger and Dougherty equation, which also describes the μ^* dependency upon φ. The Krieger and Dougherty equation relates the μ^* to the φ but also includes a term which described the maximum packing fraction or volume fraction (φ_{max}) (Equation 5.4).[50]

$$\text{Equation 5.4: } \mu^* = \left(1 - \frac{\phi}{\phi_{max}} \right)^{-2.5\phi_{max}}$$

As previously mentioned, a correlation was observed between the aggregate hydrodynamic diameter and the maximum strength of the gel formed (Figure 5.8). Triblock copolymers which formed aggregates with smaller hydrodynamic diameter, resulted in stronger gels (Figure 5.8). For example, PNIPAM10-PEG10-PNIPAM10 formed aggregates with an average hydrodynamic diameter of 87.7 ± 1.0 nm and a gel with a strength of 1579 ± 303 Pa, while PNIPAM20-PEG10-PNIPAM20 formed aggregates with 206.9 ± 0.5 nm hydrodynamic diameter and a gel with a strength of 146 ± 37 Pa. Considering the Krieger and Dougherty equation, the smaller aggregates are expected to result in a greater volume fraction and in turn a greater viscosity. These two models, however, assume the particulates are spherical and the shape of the aggregates formed by these triblock copolymers was neglected in these experiments. Furthermore, these equations are designed for hard spheres, whereas the polymer micelles are expected to be relatively soft. Also, the viscosity of such

aggregates in solution is not solely dependent upon the size and shape of the aggregates formed. At the low shear rate used in the rheology presented in this study, the interaction between the particles must also be considered. Strongly aggregated particles are known to be more viscous when compared to those which are weakly aggregated. A smaller particle will have a greater surface area to volume ratio, and a such will exhibit a greater number of contact points available for particle-particle interactions. This will enhance interparticulate forces including bridging which may contribute to the formation of a strong gel.

The zeta-potential is the measure of the charge at the slipping plane of a particle, where ions are no longer sufficiently strongly bound to the particles' surface to remain associated with it during Brownian motion. This charge may can be used to evaluate the probability of two particles aggregating in solution. Typically, particles with zeta potentials greater than an absolute value of 30 mV are considered to exhibit sufficient repulsive force. Therefore, these particles are less likely to aggregate in solution. In terms of the formation of a gel, it could be assumed that particles with a zeta-potential greater than an absolute value of 30 mV may be less likely to form a gel, due to particle-particle repulsion. For the samples presented in this work, all particles formed aggregates with zeta-potentials less than an absolute value of 30 mV with the exception of PNIPAM20-10-20. Also, there was no common observable trend between the zeta-potential and the G', G'' or tan delta (Figure 5.9). Therefore, it may be assumed that zeta-potential is not a contributing factor to the strength of the gel formed. Whilst low values of zeta potential may favour intermicelle association, this is weighed against the strength of attractive interactions, as described by classical DLVO theory.
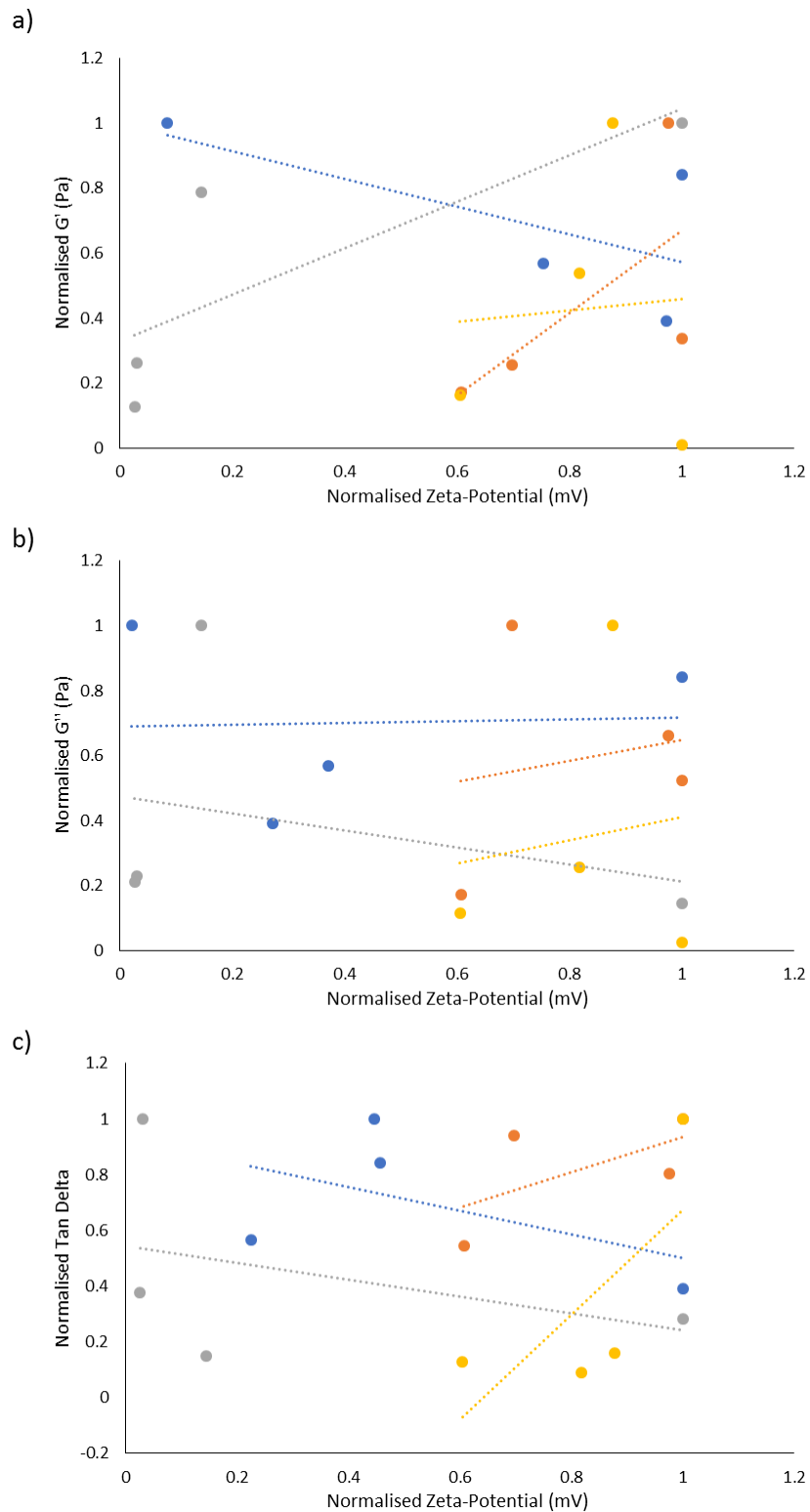
Figure 5. 9: The correlation between the normalised zeta-potentials of the aggregates formed at 50 °C by the PNIPAM (Blue), PDEA (Grey) and PDEGMEMA (Yellow) and at 70 °C by the PDMAEMA (Orange), triblock copolymers and the normalised G' (a), normalised G'' (b) and tan delta (c) at the specified temperature, of the in 20 % (w/v) aqueous solution.

Generally, it was noted that all 10-4-10 triblock copolymers did not result in the formation of a 'rheological gel' where G' > G'' with an increase in temperature, while the 10-10-10 triblock copolymers did. In addition to this, the G' maxima of the PNIPAM, PDEA and PDEGMEMA 10-10-10 triblock copolymers were greater than the 10-4-10. For example, PDEGMEMA 10-4-10 formed a viscous fluid with a G' maxima of 7.5 ± 2.6 Pa and the 10-10-10 copolymer formed a gel with a G' maxima of 341 ± 95 Pa (P < 0.005). The investigation of the dilute solution properties identified that the hydrodynamic diameter of the PNIPAM, PDEA and PDEGMEMA triblock copolymers significantly reduced between the 10-4-10 and 10-10-10 architectures. For example, the same PNIPAM 10-4-10 triblock copolymers formed aggregates with average hydrodynamic diameters of 171.2 ± 1.5 nm while the 10-10-10 aggregates had hydrodynamic diameters of 87.7 ± 1.0 nm. Contrary to this, the PDMAEMA triblock copolymers 10-4-10 and 10-10-10 exhibited G' maxima from 329 ± 90 to 135 ± 26 Pa, respectively and an increase in hydrodynamic diameter from 37.9 ± 2.0 to 43.9 ± 0.4 nm. In terms of varying the triblock copolymer architecture from 10-4-10 to 20-4-20, the PNIPAM and PDMAEMA triblock copolymers experienced an increase in aggregate size and a subsequent decrease in gel strength. For example, the PNIPAM gel strength decreased from 1296 ± 166 to 957 ± 56 Pa as the aggregate hydrodynamic diameter increased from 171.2 ± 1.5 to 238.8 ± 2.2 nm for the 10-4-10 and 20-4-20 architectures, respectively. While the gel strengths of the PDEA and PDEGMEMA triblock copolymers fell upon changing architecture from 10-4-10 to 20-4-20 and the aggregate hydrodynamic diameters increased. For example, the PDEA 10-4-10 and 20-4-20 formed viscous fluids with a G' maxima of 90 ± 28 and 135 ± 52 Pa, and aggregates with hydrodynamic diameters of 479.2 ± 29.9 and 275.6 ± 12.8 nm, respectively.

If the aggregates form worm-like or rod-like micelles, these will exhibit a reduced surface area to volume ratio, when compared to spherical micelles, and considering the Einstein and Krieger and Dougherty approximations, the volume fraction of aggregates will be reduced. As a result of this, a less viscous gel may form due to fewer interparticulate contact points. This may reduce the aggregate packing density in concentrated solution and fewer aggregate bridges.[51] Small angle neutron scattering (SANS) experiments have been conducted to understand the morphology of these aggregates in solution, but data analysis is ongoing. Preliminary results have confirmed that 5 % solutions of triblock copolymers with 4 kDa and 10 kDa PEG blocks fit a core-shell cylinder and a core-shell sphere model, respectively (Figures 5.10 a and b). At 20 %, the 10 kDa PEG samples include a sticky hard sphere interaction parameter (Figure 5.10 c). Such a trend has been observed in the synthesis of diblock copolymers of poly(glycerol monomethacrylate)–poly(2-hydroxypropyl methacrylate), which can form spheres, worms or vesicles depending on block molecular weight.[52] When the hydrophilic poly(glycerol monomethacrylate) component is longer, the aggregates are

more likely to form spheres, while shorter chains form worms or vesicles. Thus, in all cases the 10-4-10 triblock copolymers presented in this work are thought to form rod-like or worm-like aggregates which are unable to form gels. The 10-10-10 and 20-10-20 samples are believed to be core-shell sphere which interact attractively at a short distance, consistent with Semenov theory.[11]
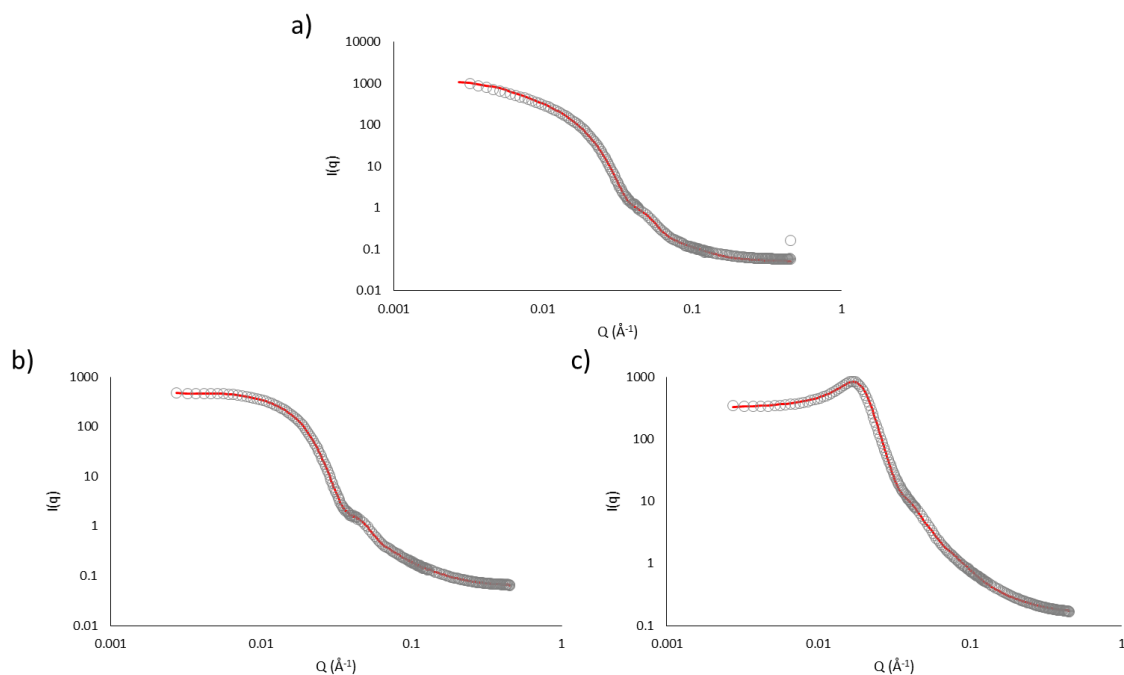
Figure 5. 10: The SANS data (grey circles) and fits (red line) for the a) PDMAEMA 10-4-10 triblock copolymer to the core-shell cylinder model, b) PDMAEMA 10-10-10 triblock copolymer to the core-shell sphere model and c) PDMAEMA 10-10-10 triblock copolymer to the core-shell sphere model with a sticky hard sphere interaction parameter in 5, 5 and 20 % (w/v) aqueous solution, respectively.

[5.5.4] Cytotoxicity testing

[5.5.4.1] HaCat cell batch growth curve

The batch growth of the HaCat cells was investigated prior to conducting any cytotoxicity testing. This was performed to identify the exponential growth phase of the cells after seeding. If the cytotoxicity testing is performed too soon after seeding, the cells will be still adapting to their new environment and will not be ready for testing.[53] On the other hand, if the cytotoxicity testing is performed too late, the cells will begin to die from overcrowding and a lack of nutrients, resulting in false positive results.[54] Thus, the point at which the cells are rapidly growing, known as the log phase, was selected for cytotoxicity testing as outlined in the ISO's "Biological evaluation of medical devices" (ISO 10993-5).[55]

The cells were seeded at a density of 10,000 cells per well to ensure the cells were in close enough proximity to promote growth, following existing protocols.[56] The cell growth was investigated using trypan blue cell counting over the course of a week (Figure 5.11). Trypan blue is an azo dye which can selectively stain dead cells or tissues, which in turn highlights living cells.[57] The number of cells in 20 µL were then counted using a haemocytometer. Using this method, the exponential growth phase was identified as between 2 and 6 days. Thus, the cytotoxicity testing was performed after 4 days of seeding the cells.
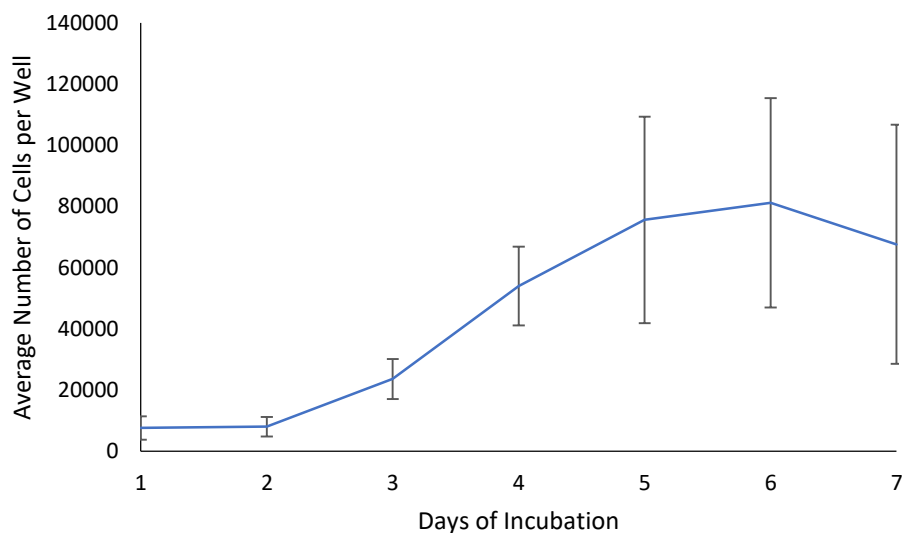
Figure 5. 11: The HaCat cell growth over the course of a week after being seeded at a density of 10,000 cells per well. The number of cells in each well was counted using trypan blue cell counting. The data is presented as mean ± standard deviation (n=6).

[5.5.6.1] Polymer cytotoxicity

The LDH assay is a measure of membrane integrity. LDH is present within many different types of cell and when the membrane becomes compromised, this is leached into the surrounding culture media.[58] The amount of LDH release can be quantified by a reaction between the conversion of lactate to pyruvate via the reduction of nicotinamide adenine dinucleotide, which is catalysed by LDH.[59] Thus, the degree of conversion may be related to the concentration of LDH present, and this is compared to a control of cells in which their membrane is completely lysed. In this assay, polymer were considered cytotoxic if the decrease in relative percent cytotoxicity's was significantly decreased as identified aby a 2-way ANOVA.[60,61] The MTS assay is a measure of cell metabolic activity. In this assay, a tetrazolium salt is reduced by the activity of the mitochondria within the cells, which indicates metabolic activity. Both assays are used to assess cytotoxicity, as cells may become metabolically inactive by the material in question without lysing the membrane, thus both assays are required.[62]

The cytotoxicity testing revealed PNIPAM, PDEA and PDEGMEMA containing triblock copolymers were non-cytotoxic to HaCat cells at 10 mg/mL concentrations after a 2 h dosage time (Figure 5.12). The LDH and MTS assays confirmed that PNIPAM, PDEA and PDEGMEMA containing triblock copolymers did not destroy the cell membrane or induce a reduction in metabolic activity. In the literature, PNIPAM has been reported as both cytotoxic[63] and non-cytotoxic.[64] These studies of PNIPAM suggest the cytotoxicity is strongly dependent on the cell line used and thus, should be evaluated on a cell line relevant to the proposed application. The cytotoxicity of the homopolymer of PDEGMEMA has not been reported in the literature, however cytotoxicity testing of a random copolymer of PDEGMEMA and poly(oligoethylene glycol methyl ether methacrylate) was performed and found the polymer to be non-cytotoxic.[65] This is in line with the LDH results seen in this experiment, whereas, the MTS assay found the metabolic activity increased above that shown by the healthy cells. This increase has been shown before and is thought to be as a result of detachment of the cells from the well plate, as a result of the polymer. The detachment of these cells results in an increased cell metabolic activity in order to attempt to counteract this cleavage from the well plate. Conversely, PDMAEMA containing triblock copolymers were found to be relatively cytotoxic to HaCat cells as both cell membrane integrity and cell metabolic activity were reduced. The cytotoxicity of PDMAEMA has been reported in the literature to be dependent on the pH of the solution and polymer molecular weight.[66–68] PDMAEMA has been reported to induce cytotoxicity due to the formation of complexes between the tertiary amine of the PDMAEMA and the negatively charged proteins bound to the cell membrane, which is expected to disrupt cellular pathways and result in cell death.[67] As previously stated, pharmaceutical excipients need to be non-hazardous to

human health to be used as drug delivery excipients. Therefore, the relative cytotoxicity of the triblock copolymers was used to rule out polymers from further study.
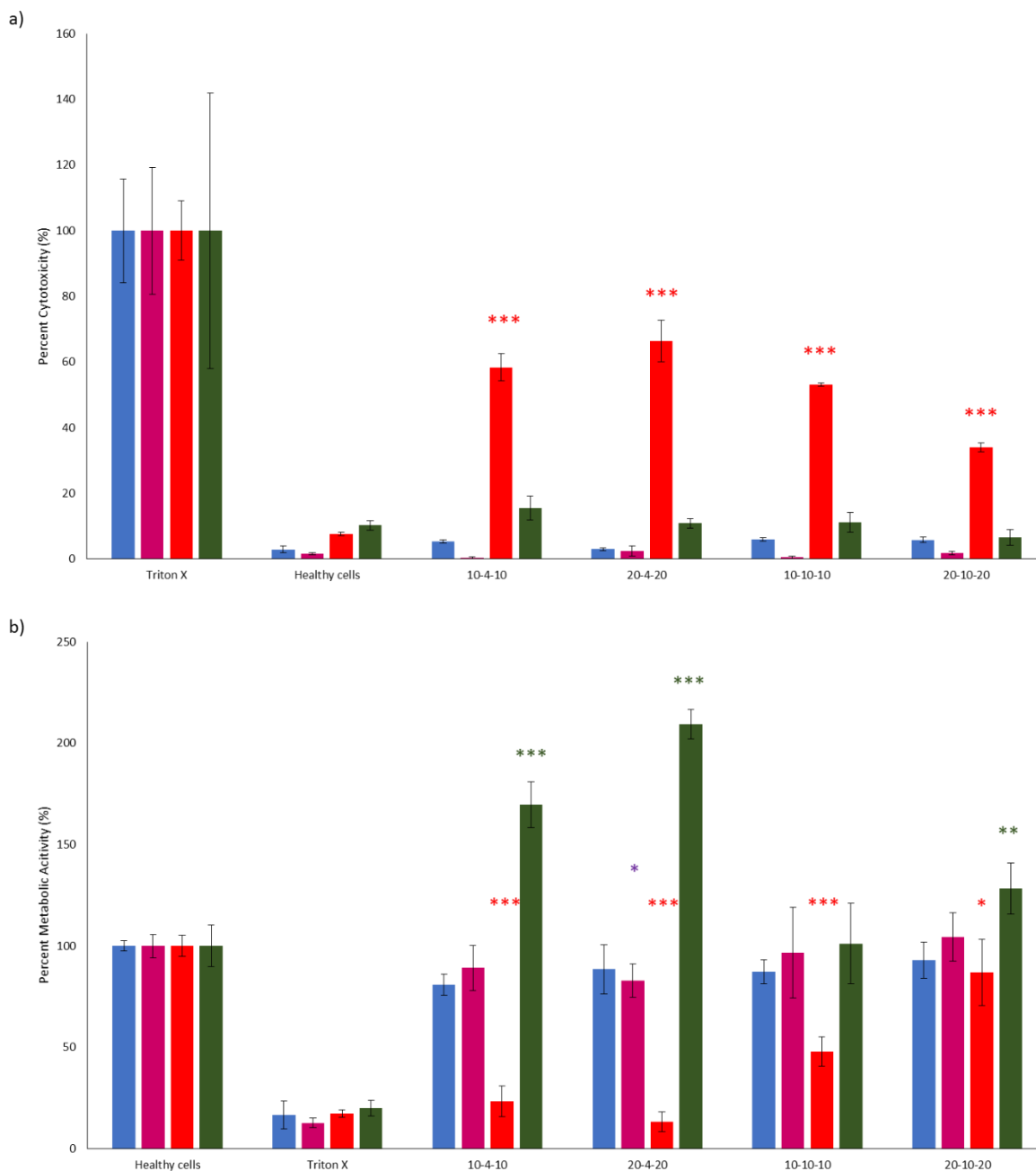
Figure 5. 12 The a) relative percent cytotoxicity and b) relative percent metabolic activity of HaCat cells dosed with PNIPAM (blue), PDEA (pink), PDMAEMA (red) and PDEGMEMA (green) containing triblock copolymers at 10 mg/mL as identified by LDH and MTS assays, respectively. Results which are statistically different to healthy cells are denoted by *, **, *** where P values were greater than 0.05, 0.01 and 0.001 respectively. Data is presented as mean ± SD (n=4).

[5.5.7] Selection of triblock copolymers for further study

The relative cytotoxicity and gel strength of the triblock copolymers were used in tandem to select two triblock copolymers to take forward for further study. The PDMAEMA triblock copolymers formed the weakest gels (G' maxima ca. 130-300 Pa) and exhibited significant cytotoxicity to HaCat cells. In addition to this, the PDEGMEMA triblock copolymers induced a significant increase in metabolic activity and formed weaker gels in comparison to some of the PNIPAM and PDEA triblock copolymers. Therefore, these two classes of polymer, PDMAEMA and PDEGMEMA, were rejected from further study. The remaining two classes, PDEA and PNIPAM were not cytotoxic to HaCat cells, so the two polymers which resulted in the strongest gels were selected for further study. These were PNIPAM 10-10-10 and PDEA 20-10-20, which had G' maxima of 1579 ± 303 and 1518 ± 399 Pa, respectively. These two polymers gelled at 41.7 ± 0.4 and 45.9 ± 0.5 ^{o}C, respectively, which were outside of the physiological range (25 – 37 ^{o}C). Tgel was not used as a metric for selection of polymers for further study as this may be reduced by either increasing the polymer concentration or by the inclusion of 'salting out' agents, or a combination of the two, which will be explored in future chapters.[69]

[5.6] Conclusions

All triblock copolymers synthesised in chapter 4 were found to exhibit thermothickening. PNIPAM, DEGMEMA and DEA copolymers typically exhibited thermogelling behaviour, forming rheological gels with G'>G'', whilst DMAEMA copolymers typically formed "thermothickening" materials with a balance of viscous and elastic behaviour. The sharpest sol-gel transitions were observed in PNIPAM copolymers, but transitions observed DEGMEMA and DEA copolymers were relatively sharp compared to DMAEMA copolymers which exhibited thickening over a broad range. For NIPAM, DEGMEMA and DEA materials, the 10-10-10, 20-10-20, and 20-4-20 molecular weight systems exhibited thermogelling behaviour, but all 10-4-10 triblock copolymers resulted in the formation of a viscous fluid (G''>G'). This is thought to be as a result of the lower PEG molecular weight which causes the formation of worm-like or cylindrical micelles which have fewer contact points when compared to spheres, possibly reducing both the degree of micellar bridging and aggregate volume fraction. Simple trends were not observed between molecular weight and either gelation temperature or gel strength, however the class of material was crucial in determining the behaviour as a thermogelling material. For PNIPAM, PDMAEMA and PDEA triblock copolymers, generally the gelation temperature increased with a decrease in temperature responsive molecular weight and an increase in PEG molecular weight. In dilute solution, all triblock copolymers exhibited the formation of aggregates above a CMT. Generally, as the aggregates were formed the PDI of the sample fell indicating that the system was becoming more ordered. In addition to this, the polymers which exhibited a reduction in PDI formed a single population of nanoparticles. A correlation was identified between the size of the aggregates and G' and G'', where smaller aggregates resulted in greater G' and G'', however this correlation was weak and further information is required to fully understand the systems. Preliminary SANS experiments suggest that polymers with a 10 kDa PEG block form core-shell spherical micelles which interact to form a gel. Furthermore, the SANS study supports the theory that the 10-4-10 triblock copolymers form of cylindrical micelles, which may contain fewer contact points for the interparticulate interaction than spheres. This in turn may prevent micellar bridging and the formation of a gel. The cytotoxicity testing found all PDMAEMA triblock copolymers were cytotoxic to HaCat cells as identified by the LDH and MTS assays. Whereas, the remaining three types of temperature responsive triblock copolymer were found to not be cytotoxic when compared to healthy cells. The cytotoxicity of the PDMAEMA triblock copolymers was attributed to the pH responsive tertiary amine present in the pendant group of the polymer.

The gel strength, as dictated by the G' maximum, and relative cytotoxicity's of the triblock copolymers were used to select triblock copolymers for further study. The selected polymers were PNIPAM 10-10-10 and PDEA 20-10-20 due to their low relative cytotoxicity's and G' maxima of 1579

± 303 and 1518 ± 399 Pa, respectively, making them the strongest gels identified. The PNIPAM 10-10-10 and PDEA 20-10-20 triblock copolymers' Tgels were higher than body temperature (37 °C). Therefore, in future work attempts will be made to adjust the gelation temperature to a physiologically relevant point. If a physiologically relevant temperature can be achieved, properties such as resistance to shear, gelation time, recoverability and mucoadhesion must be evaluated to understand how these formulations may behave as drug delivery excipients.

[5.7] References

1   W. Agut, A. Brûlet, C. Schatz, D. Taton and S. Lecommandoux, *Langmuir*, 2010, **26**, 10546–10554.

2   J. P. O'Shea, G. G. Qiao and G. V. Franks, *J. Colloid Interface Sci.*, 2010, **348**, 9–23.

3   Z. Zhang, S. Maji, A. B. da F. Antunes, R. De Rycke, Q. Zhang, R. Hoogenboom and B. G. De Geest, *Chem. Mater.*, 2013, **25**, 4297–4303.

4   Y. J. Chen, L. W. Huang, H. C. Chiu and S. C. Lin, *Enzyme Microb. Technol.*, 2003, **32**, 120–130.

5   I. S. Oliveira, M. Lo, M. J. Araújo and E. F. Marques, *Soft Matter*, 2019, **15**, 3700–3711.

6   S. Il Yun, G. E. Gadd, V. Lo, M. Gauthier and A. Munam, *Macromolecules*, 2008, **41**, 7166–7172.

7   L. Ahmadkhani, M. Abbasian and A. Akbarzadeh, *Des. Monomers Polym.*, 2017, **20**, 406–418.

8   Y. C. Chen, L. C. Liao, P. L. Lu, C. L. Lo, H. C. Tsai, C. Y. Huang, K. C. Wei, T. C. Yen and G. H. Hsiue, *Biomaterials*, 2012, **33**, 4576–4588.

9   M. Taylor, P. Tomlins and T. Sahota, *Gels*, 2017, **3**, 4–20.

10   A. M. Bodratti and P. Alexandridis, *J. Funct. Biomater.*, 2018, **9**, 1–8.

11   A. N. Semenov, J. F. Joanny and A. R. Khokhlov, *Macromolecules*, 1995, **28**, 1066–1075.

12   M. T. Cook, S. K. Filippov and V. V. Khutoryanskiy, *Colloid Polym. Sci.*, 2017, **295**, 1351–1358.

13   J. Lou, W. Hu, R. Tian, H. Zhang, Y. Jia, J. Zhang and L. Zhang, *Int. J. Nanomedicine*, 2014, **9**, 2517–2525.

14   C. C. Chen, C. L. Fang, S. A. Al-Suwayeh, Y. L. Leu and J. Y. Fang, *Int. J. Pharm.*, 2011, **415**, 119–128.

15   S. M. Hashemnejad, A. Z. M. Badruddoza, B. Zarket, C. Ricardo Castaneda and P. S. Doyle, *Nat. Commun.*, 2019, **10**, 541–555.

16   K. Shi, Y.-L. L. Wang, Y. Qu, J.-F. F. Liao, B.-Y. Y. Chu, H.-P. P. Zhang, F. Luo and Z.-Y. Y. Qian, *Sci. Rep.*, 2016, **6**, 2–36.

17   I. C. Tung, *Int. J. Pharm.*, 1994, **107**, 85–90.

18   L. Yu, Z. Zhang and J. Ding, *Biomacromolecules*, 2011, **12**, 1290–1297.

19   M. A. Ward and T. K. Georgiou, *Polym. Chem.*, 2013, **4**, 1893–1902.

20   K. D. Weiss, J. D. Carlson and D. A. Nixon, *J. Intell. Mater. Syst. Struct.*, 1994, **5**, 772–775.

21   H. H. Lin and Y. L. Cheng, *Macromolecules*, 2001, **34**, 3710–3715.

22   Y. Hao, M. Zhang, J. Xu, C. Liu and P. Ni, *J. Macromol. Sci. Part A Pure Appl. Chem.*, 2010, **47**, 941–951.

23   A. Alexander, Ajazuddin, J. Khan, S. S. S. Saraf and S. S. S. Saraf, *Eur. J. Pharm. Biopharm.*, 2014, **88**, 575–585.

24   S. K. Filippov, A. Bogomolova, L. Kaberov, N. Velychkivska, L. Starovoytova, Z. Cernochova, S. E. Rogers, W. M. Lau, V. V. Khutoryanskiy and M. T. Cook, *Langmuir*, 2016, **32**, 5314–5323.

25   A. Maleki, K. Zhu, R. Pamies, R. R. Schmidt, A. L. Kjøniksen, G. Karlsson, J. G. Hernández Cifre, J. García De La Torre and B. Nyström, *Soft Matter*, 2011, **7**, 8111–8119.

26   M. Teodorescu, I. Negru, P. O. Stanescu, C. Drghici, A. Lungu and A. Sârbu, *React. Funct. Polym.*, 2010, **70**, 790–797.

27   S. Välimäki, A. Khakalo, A. Ora, L. S. Johansson, O. J. Rojas and M. A. Kostiainen, *Biomacromolecules*, 2016, **17**, 2891–2900.

28   J. C. Chang, F. F. Lange and D. S. Pearson, *J. Am. Ceram. Soc.*, 1994, **77**, 19–26.

29   Y. Huang, P. P. Singh, J. Tang and B. G. Swanson, *Carbohydr. Polym.*, 2004, **56**, 27–33.

30   M. Teodorescu, I. Negru, P. O. Stanescu, C. Drăghici, A. Lungu and A. Sârbu, *React. Funct. Polym.*, 2010, **70**, 790–797.

31   J. Y. Zheng, M. J. Tan, P. Thoniyot and X. J. Loh, *RSC Adv.*, 2015, **5**, 62314–62318.

32   O. Samsonova, C. Pfeiffer, M. Hellmund, O. M. Merkel and T. Kissel, *Polymers (Basel).*, 2011, **3**, 693–718.

33   A. P. Constantinou, H. Zhao, C. M. McGilvery, A. E. Porter and T. K. Georgiou, *Polymers (Basel).*, 2017, **9**, 31.

34   M. Mohammadi, M. Salami-Kalajahi, H. Roghani-Mamaqani and M. Golshan, *Int. J. Polym. Mater. Polym. Biomater.*, 2017, **66**, 455–461.

35   C. Schaude and G. J. Mohr, *Fash. Text.*, 2017, **4**, 1–7.

36   M. S. Manga, O. J. Cayre, S. Biggs and T. N. Hunter, *Front. Chem.*, 2018, **6**, 301–310.

37   I. Negru, M. Teodorescu, P. O. Stănescu, C. Drăghici, A. Lungu and A. Sârbu, *Soft Mater.*, 2013, **11**, 149–156.

38   J. Tan, Z. He, Y. Miao and D. Zhou, *J. Solution Chem.*, 2019, **48**, 891–904.

39   M. Nguyen-Misra and W. L. Mattice, *Macromolecules*, 1995, **28**, 1444–1457.

40   M. Teodorescu, I. Negru, P. O. Stanescu, C. Drăghici, A. Lungu and A. Sârbu, *J. Macromol. Sci. Part A Pure Appl. Chem.*, 2011, **48**, 177–185.

41   M. M. Zgoda and J. Kołodziejska, *Polim. Med.*, 2006, **36**, 11–25.

42   P. Malo de Molina and M. Gradzielski, *Gels*, 2017, **3**, 30–39.

43   L. Hou and P. Wu, *Soft Matter*, 2014, **10**, 3578–3586.

44   J.-F. F. Lutz, *J. Polym. Sci. Part A Polym. Chem.*, 2008, **46**, 3459–3470.

45   D. G. Lessard, M. Ousalem, X. X. Zhu, A. Eisenberg, P. J. Carreau, A. Eisenberg, X. X. Zhu, D. G. Lessard, M. Ousalem, X. X. Zhu, A. Eisenberg, P. J. Carreau, A. Eisenberg, X. X. Zhu and D. G. Lessard, *J. Polym. Sci. Part B Polym. Phys.*, 2003, **41**, 1627–1637.

46   S. Jain and F. S. Bates, *On the origins of morphological complexity in block copolymer surfactants*, American Association for the Advancement of Science, 2003, vol. 300.

47   J. Schmelz, A. E. Schedl, C. Steinlein, I. Manners and H. Schmalz, *J. Am. Chem. Soc.*, 2012, **134**, 14217–14225.

48   J. N. Israelachvili, in *Intermolecular and Surface Forces*, Elsevier, 2011, pp. 535–576.

49   D. J. Jeffrey and A. Acrivos, *AIChE J.*, 1976, **22**, 417–432.

50   N. Willenbacher and K. Georgieva, in *Product Design and Engineering: Formulation of Gels and Pastes*, 2013, pp. 7–49.

51   D. S. Lee and C. He, *Biomedical Applications of Hydrogels Handbook*, 2010.

52   N. J. Warren, M. J. Derry, O. O. Mykhaylyk, J. R. Lovett, L. P. D. Ratcliffe, V. Ladmiral, A. Blanazs, L. A. Fielding and S. P. Armes, *Macromolecules*, 2018, **51**, 8357–8371.

53   A. F. L. Specian, J. M. Serpeloni, K. Tuttis, D. L. Ribeiro, H. L. Cilião, E. A. Varanda, M. Sannomiya, W. Martinez-Lopez, W. Vilegas and I. M. S. Cólus, *Cytotechnology*, 2016, **68**, 2729–2744.

54   Ö. S. Aslantürk, in *Genotoxicity - A Predictable Risk to Our Actual World*, InTech, 2018.

55   ISO, Biological evaluation of medical devices — Part 5: Tests for in vitro cytotoxicity, http://nhiso.com/wp-content/uploads/2018/05/ISO-10993-5-2009.pdf, (accessed 23 June 2020).

56   CASTEP. The official website, https://www.celprogen.com/cms.php?page_alias=cell-culture-faq, (accessed 23 June 2020).

57   B. G. T. I-Ju Fang, Trypan blue - an overview | ScienceDirect Topics, https://www.sciencedirect.com/topics/medicine-and-dentistry/trypan-blue, (accessed 23 June 2020).

58   J. Sepulveda, Lactate Dehydrogenase - an overview | ScienceDirect Topics, https://www.sciencedirect.com/topics/pharmacology-toxicology-and-pharmaceutical-science/lactate-dehydrogenase, (accessed 23 June 2020).

59   N. V. Bhagavan, C.-E. Ha, N. V. Bhagavan and C.-E. Ha, *Essentials Med. Biochem.*, 2015, **1**, 165–185.

60   H. Li, P. Z. Toh, J. Y. Tan, M. T. Zin, C. Y. Lee, B. Li, M. Leolukman, H. Bao and L. Kang, *Sci. Rep.*, 2016, **6**, 37664.

61   S. Sawan, T. Yaacoub, S. Hraoui-Bloquet, R. Sadek, W. Hleihel, Z. Fajloun and M. Karam, *Exp. Toxicol. Pathol.*, 2017, **69**, 173–178.

62   K. L. Rock and H. Kono, *Annu. Rev. Pathol. Mech. Dis.*, 2008, **3**, 99–126.

63   H. Vihola, A. Laukkanen, L. Valtola, H. Tenhu and J. Hirvonen, *Biomaterials*, 2005, **26**, 3055–3064.

64   M. A. Cooperstein and H. E. Canavan, *Biointerphases*, 2013, **8**, 19–25.

65   J. F. Lutz, *J. Polym. Sci. Part A Polym. Chem.*, 2008, **46**, 3459–3470.

66   Y. Li, M. Leng, M. Cai, L. Huang, Y. Chen and X. Luo, *Colloids Surfaces B Biointerfaces*, 2017, **154**, 397–407.

67   J. Cai, Y. Yue, D. Rui, Y. Zhang, S. Liu and C. Wu, *Macromolecules*, 2011, **44**, 2050–2057.

68   L. A. B. Rawlinson, P. J. O'Brien and D. J. Brayden, *J. Control. Release*, 2010, **146**, 84–92.

69   A. P. Constantinou and T. K. Georgiou, *Eur. Polym. J.*, 2016, **78**, 366–375.

Chapter Six: Optimising and Characterising the Thermogellation Properties of Poloxamer 407 and Two Novel Thermogelling Materials

[6.1] Introduction

This chapter focuses on the optimisation and characterisation of the gelation properties exhibited by Poloxamer 407, PNIPAM10-PEG10-PNIPAM10 and PDEA20-PEG10-PDEA20. PNIPAM10-PEG10-PNIPAM10 and PDEA20-PEG10-PDEA20 were selected from initial testing in chapter five, where these two thermogelling materials were found to be relatively non-cytotoxic to HaCat cells and formed the strongest gels out of the sixteen triblock copolymers synthesised. However, the gelation temperature (Tgel) of PNIPAM10-PEG10-PNIPAM10 and PDEA20-PEG10-PDEA20 were above 37 °C and thus may not be used for topical drug delivery, where internal temperatures in healthy humans is 37 °C. It is known that Tgel of Poloxamer 407 may be tuned to a physiologically relevant point by varying the polymer concentration and including salting out agents. Nie et al. (2011) found increasing the concentration of Poloxamer 407 in aqueous solution results in both a reduced gelation temperature and increased gel strength.[1] Alternatively, Jiang et al. (2008) found the inclusion of the salting out agent sodium chloride and calcium chloride reduce the Tgel of Poloxamer 407 but at a cost to the gel strength.[2] These approaches can be explored for modifying Tgel of PNIPAM10-PEG10-PNIPAM10 and PDEA20-PEG10-PDEA20. Upon reaching a physiologically relevant gelation temperature, the potential applications of the thermogelling materials may be explored. If the gelation temperature falls below the skin surface temperature (ca. 33.2 °C)[3], the thermogelling materials may be used in transdermal or ocular drug delivery. However, if the gelation temperature is between skin surface temperature and internal body temperature (ca. 37 °C)[4], the thermogelling materials may have applications in rectal, vaginal or buccal drug delivery.

Rheological studies such as time sweeps, oscillatory stress sweeps (OSS) and oscillatory frequency sweeps (OFS) may be used to further characterise the performance of the gels *in situ*. Time sweeps characterise the length of time required for the sol-gel transition to occur when at the temperature of the target site. This must be fast enough to prevent leakage from the target site, but long enough to ensure efficient spreading. OSS experiments apply increasing amounts of oscillatory stress to the sample, until the internal structure yields.[5] This evaluates the maximum degree of shear force the sample can withstand before altering structure which may influence formulation residence time.[6] OFS, however, applies the same oscillatory stress to the sample but at increasing frequencies. OFS may be used to determine if a sample is a 'true gel', whereby G'>G'' at all frequencies.[7] The temperature sweeps aim to investigate the recoverability of the gel when the temperature is fluctuated below and above the gelation temperature. The recoverability of the gel is important for formulation storage, rather than the application itself.

The rheology of such formulations may be used to determine an appropriate target site. For example, formulations which are not resistant to shear stress may not be appropriate for ocular formulations, where blinking may remove the formulation from this site. Upon identifying a target site, the effect of environment must be investigated to understand how the gel will behave as a drug delivery vehicle. The rheology has previously been characterised in aqueous solution, but the fluids at target sites such as the eye, rectum, vagina and buccal mucosa vary significantly. Factors such as salt content[8], pH[9] and protein concentration[10] are known to impact the properties of semi-solid formulations. Work by Edsman, Carlfors and Petersson investigated the rheology of poloxamer 407 gels in varying ratios of simulated tear fluid for an ocular thermogelling formulation.[11] Mixing the formulation with tear fluid resulted in a decrease in gelation temperature, as a result of a decreased poloxamer 407 concentration. In addition to this, the ionic strength of the simulated fluid reduced the gelation temperature. Chang et al. performed similar studies on poloxamer 407, but in the presence of a vaginal fluid simulant.[12] The vaginal fluid simulant was found to not impact the gelation temperature, but significantly reduced both G' and G'' of the gel. Therefore, fluids simulants from the literature may be used to replicate the gel properties once at the target site and ensure the formulation is appropriate. There are a number of fluids designed to replicate those found in the mouth, eye, rectum and vagina, for example, which can be used to probe these effects.[13,14]

Additional factors which must also be considered for a novel drug delivery excipient such as, residence time, adhesion and stability. Residence time is known to be directly impacted by both sample viscosity[15,16,17] and adherence to the target site.[18,19,20] Adhesion is the attractive forces between two materials, while mucoadhesion is the attractive force between a material and mucosa membranes. Edsman, Carlfors and Harju found a direct link between sample viscosity and residence time of ophthalmic formulations, where samples with increased viscosity were retained on their site for longer.[15] While Baloglu et al. published a review which found supporting evidence from many sources that increased mucoadhesion results in a prolonged residence time.[19] Ultimately, it is accepted that mucoadhesion arises as a result of the interaction between mucins present in the mucus and the polymeric chains present in the adhesive material.[21]There are a number of theories which can be used to explain mucoadhesion mechanistically. These mechanisms include; transfer of electrons resulting in an attractive electrostatic double layer,[22] adsorption between the mucus and material as a result of hydrogen bonds and van der Waals forces,[23] the wettability of the mucoadhesive material on the mucosa layer as a result of their surface tensions (where lower surface tensions promote wetting),[24] interpenetration of the mucins and polymers within formulations as a result of diffusion[25] and the effect of surface topology favouring interaction.[26,27] Mucoadhesion may be determined in a number of ways, including force-detachment, rotating discs,

flow-through methods and rheology.[27] The most widely used method is force-detachment, which involves bringing the mucosa membrane and material into contact, and measuring the force required to separate the two surfaces.[28] This generates force/distance curve also known as a detachment profile. From this profile the force of adhesion and work of adhesion may be identified as the maximum force and area under the curve respectively. The force of adhesion is a measure of the attraction between the two surfaces while the work of adhesion is the reversible thermodynamic work required to separate the two phases to an infinite distance.[29] A sample which is relatively mucoadhesive will have a greater force and work of adhesion than a comparator. Increased formulation residence time as a result of adhesion can reduce frequency of dosing, which in turn directly improves patient compliance.[30]

Novel excipients must also be stable to ensure patient safety and allow for potentially long shelf lives and *in vivo* residence times. The ICH guidelines recommend the length and storage conditions of a stability test should be sufficient enough to cover storage, shipment and subsequent use.[31] Typically the study should last 6-12 months long term testing at 25 ± 2 °C at 60 ± 5 % relative humidity and accelerated testing at 40 ± 2 °C at 75 ± 5 % relative humidity. However, these conditions may be varied depending on the nature of the material in question. The stability of poloxamer 407 at 25 and 40 °C has previously been investigated by Erlandsson, and was found to be stable over a 6 month period.[32] For LCST-type temperature responsive polymers it is unknown whether stability is enhanced or reduced above the transition temperature and to date no such studies have been performed for PNIPAM-PEG-PNIPAM or PDEA-PEG-PDEA block copolymers. These polymers contain ester linkages between the LCST group and the PEG chain and amide functionalities in the LCST blocks. It may be possible that these two groups undergo hydrolysis reactions in solution separating the LCST block from the PEG and/or releasing the amine from the LCST blocks.[33] These reactions may result in the formation of degradation products which cause irritation and other adverse side effects and are therefore important to investigate prior to use as thermogelling excipients.

[6.2] Aims and Objectives

This phase of work aimed to develop PNIPAM10-PEG10-PNIPAM10 and PDEA20-PEG10-PDEA20 thermogelling formulations with gelation temperatures between 25 and 37 °C. In addition to this, the gels formed by PNIPAM10-PEG10-PNIPAM10 and PDEA20-PEG10-PDEA20 were evaluated for use as thermogelling excipients and their properties were compared to Poloxamer 407. These aims were achieved by:

- Determining the effect of polymer concentration and salt content on the thermogelling materials to achieve Tgel between 25 and 37 °C.
- Investigating the effect of simulated vaginal fluid on the thermoreversible gelators, to ensure gelation could still be achieved between 25 and 37 °C.
- Rheological evaluation of the thermoreversible gelators determining gelation time, resistance to oscillatory stress, resistance to oscillatory frequency, and reversibility of gelation.
- Determining gel dissolution time, adhesion, mucoadhesion and stability of poloxamer 407, PNIPAM10-PEG10-PNIPAM10 and PDEA20-PEG10-PDEA20 formulations.

[6.3] Materials

Sodium chloride (NaCl) (97 %), potassium hydroxide (KOH) (90 %), calcium hydroxide (Ca(OH)$_2$) (95 %), bovine serum albumin (98 %), lactic acid (85 %), acetic acid (99 %), glycerol (99 %), urea (99.5 %), glucose (99.5 %) and Poloxamer 407 (100 %) were all purchased from Sigma-Aldrich (U.K) and used as purchased.

Vaginal fluid simulant (VFS) was prepared by dissolution of NaCl (3.510 g, 0.060 mol), KOH (1.400 g, 0.025 mol), Ca(OH)$_2$ (0.222 g, 0.003 mol), bovine serum albumin (0.018 g), lactic acid (2.000 g, 0.022 mol), acetic acid (1.000 g, 0.011 mol), glycerol (0.160 g, 0.002 mol), urea (0.400 g, 0.007 mol) and glucose (5.000 g, 0.028 mol) in 1 L of deionised water. The solution was then adjusted to pH 4 with 1 M hydrochloric acid. This formula follows that recommended by Owen and Katz.[34]

Porcine vaginal tissue was purchased from WetLab (U.K.) and supplied frozen. The porcine vaginal mucosa was removed by incision with a scalpel. Once the tissue was removed it was cut into 1 cm^2 squares which were attached to the texture analyse probe using adhesive pads.

[6.4] Methods

[6.4.1] Rheological evaluation of polymer solutions

All samples for rheometry were prepared to the required concentration in deionised water or VFS and refrigerated overnight before measurements were taken. Rheology was performed on an AR 1500ex rheometer by TA instruments (U.S.A.) with a Julabo AWC100 cooling unit and a 40 mm plate geometry with a gap of 650 μm. Rheological measurements were taken in triplicate.

Oscillatory stress sweeps were performed at 1 Hz between 1 and 1000 Pa at 37 °C. Frequency sweeps were measured at 37 °C between 0.1 and 10 Hz at a shear stress of 1 Pa. Temperature ramps were performed at a frequency of 1 Hz and a shear stress of 1 Pa. The temperature was increased at a rate of 2 °C per minute, from 15 to 50 °C.

Reversibility of the phase transition was assessed by rheological measurement at 25 °C for 1 min, followed by 37 °C for 1 min, which was repeated once more. A 2 min equilibration period was included between temperature changes and the measurements were recorded at 1 Pa and 1 Hz.

To determine the gelation time, the temperature of the peltier plate was held at 25 °C for 1 min, then increased to 37 °C and held for a further 4 min. All measurements were made at a constant shear stress of 1 Pa and a frequency of 1 Hz. The time taken for G' to exceed G'' at 37 °C was taken as the gelation time.

[6.4.2] Dissolution of polymer gels in VFS

The thermoreversible gelator (20, 30, 50 % (w/v) poloxamer 407, 30 % (w/v) PDEA20-PEG10-PDEA20 or 50 % (w/v) PNIPAM10-PEG10-PNIPAM10) dissolution rate was identified using a Copley USP II dissolution apparatus held at 37 °C with 400 mL VFS using an immersion cell developed in house consisting of a plastic cylinder with a closed weighted base, where the cylinder had a depth of 8.5 mm and a surface area of 306 mm^2. The immersion cell was weighed and 2 mL sample was placed within. The cell was then placed in an oven for 5 minutes at 37 °C prior to starting the experiment to induce gel formation. The immersion cell was then weighed and placed into the AVF. The paddle was set to 50 rpm and the weight of the immersion cell was measured every 5 minutes to track the mass change as a combination of both swelling and erosion.[35] The mass change was by expressed relative to the starting mass (Equation 6.1). Where Tx is the weight of the immersion at each time point, To is the weight of the immersion cell with gel at time = 0 and IC is the weight of the immersion cell.

$$\text{Equation 6.1: Mass change (\%)} = \frac{\text{Tx} - \text{IC}}{\text{To} - \text{IC}} \text{ X } 100$$

[6.4.3] Assessment of Gel Adhesion and Mucoadhesion

The adhesion and mucoadhesion of 20, 30 and 50 % (w/v) poloxamer 407, 30 % (w/v) PDEA20-PEG10-PDEA20 and 50 % (w/v) PNIPAM10-PEG10-PNIPAM10) was assessed using a TA.XT Plus Texture Analyser (Stable Micro Systems, UK) with a poly(propylene) probe with a surface area of 1.25 cm^2. This probe was used to determine adhesion values, whereas mucoadhesion was evaluated using porcine vaginal mucosa tissue (WetLab, UK). The thermoreversible gelator was placed into a water bath at 25 °C, the probe was lowered until contact between the probe or vaginal mucosa tissue was made (Figure 6.1). The temperature of the water bath was then increased to 37 °C and held at this temperature for 2 min to ensure gel formation, and mimic *in situ* gelation. Once a gel had formed, the probe was withdrawn at a rate of 10.0 mms^{-1} until complete detachment was observed, as recommended in prior studies.[28] The maximum force of detachment and the area under the force-displacement curve were determined using Texture Exponent 32 software (Stable Micro Systems, UK) and designated the "force of adhesion" and "work of adhesion", respectively. All adhesion testing was performed 6 times. The mucoadhesion testing was performed using three different porcine vaginal tissues where three samples of vaginal tissue were taken from each vagina. Data was expressed as a mean of triplicate experiments (N=3), where N was the mean value of the three measurements taken from a single vagina.
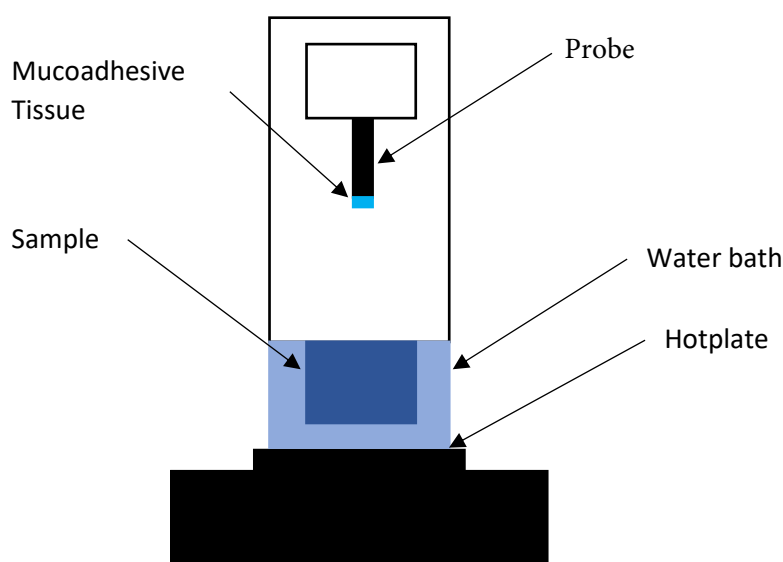
Figure 6. 1: Experimental set up for the measurement of mucoadhesion to porcine vaginal tissue using a texture analyser.

[6.4.4] Polymer Stability Study

The stability of thermoreversible gelators (20 % (w/v) poloxamer 407, 30 % (w/v) PDEA20-PEG10-PDEA20 or 50 % (w/v) PNIPAM10-PEG10-PNIPAM10) was assessed over 12 weeks. The polymer solutions were prepared in HPLC vials sealed with parafilm and placed in the refrigerator (4°C) or in ovens set at 25 and 40 °C representing room temperature and accelerated storage conditions, respectively. At weekly intervals, the samples were lyophilised, and the molecular weight determined by GPC, as described previously in chapter 4. Sufficient samples were prepared so that each weekly measurement was taken on a separate sample. The experiment was performed in triplicate.

[6.5] Results and Discussion

[6.5.1] Modulation of the thermogelling properties

The thermoresponsive gelation process exhibited by both PNIPAM10-PEG10-PNIPAM10 and PDEA20-PEG10-PDEA20 were studied by rheometry with variation of polymer concentration between 20-50 % (w/v) (Figure 6.2). The PNIPAM10-PEG10-PNIPAM10 copolymer exhibited dramatic increases in G' and G'' above a critical temperature (Tthick), at ca. 30-35 °C while the Tthick of PDEA10-PEG10-PDEA20 occurred between 30-40 °C. This increase in both G' and G'' is believed to be associated with the desolvation of the temperature responsive PNIPAM and PDEA chains which promotes physical association of copolymers.[36] All rheograms exhibited a gelation temperature (Tgel) above ca. 35 °C, at which point the absolute value of G' surpassed that of G'', indicative of a transition from a viscous fluid to an elastic gel state. Poloxamer 407 exhibited a markedly different thermoresponsive gelation to both PNIPAM10-PEG10-PNIPAM10 and PDEA20-PEG10-PDEA20. Low viscosity gels (G' ca 100 Pa) were formed at 15 % (w/v), with Tgel at 45 °C. Viscous gels (G' ca. 10kPa) were formed at 20 and 25 % (w/v) with Tgel < 25 °C. At 30 % (w/v) the materials were gels over the whole temperature range studied.
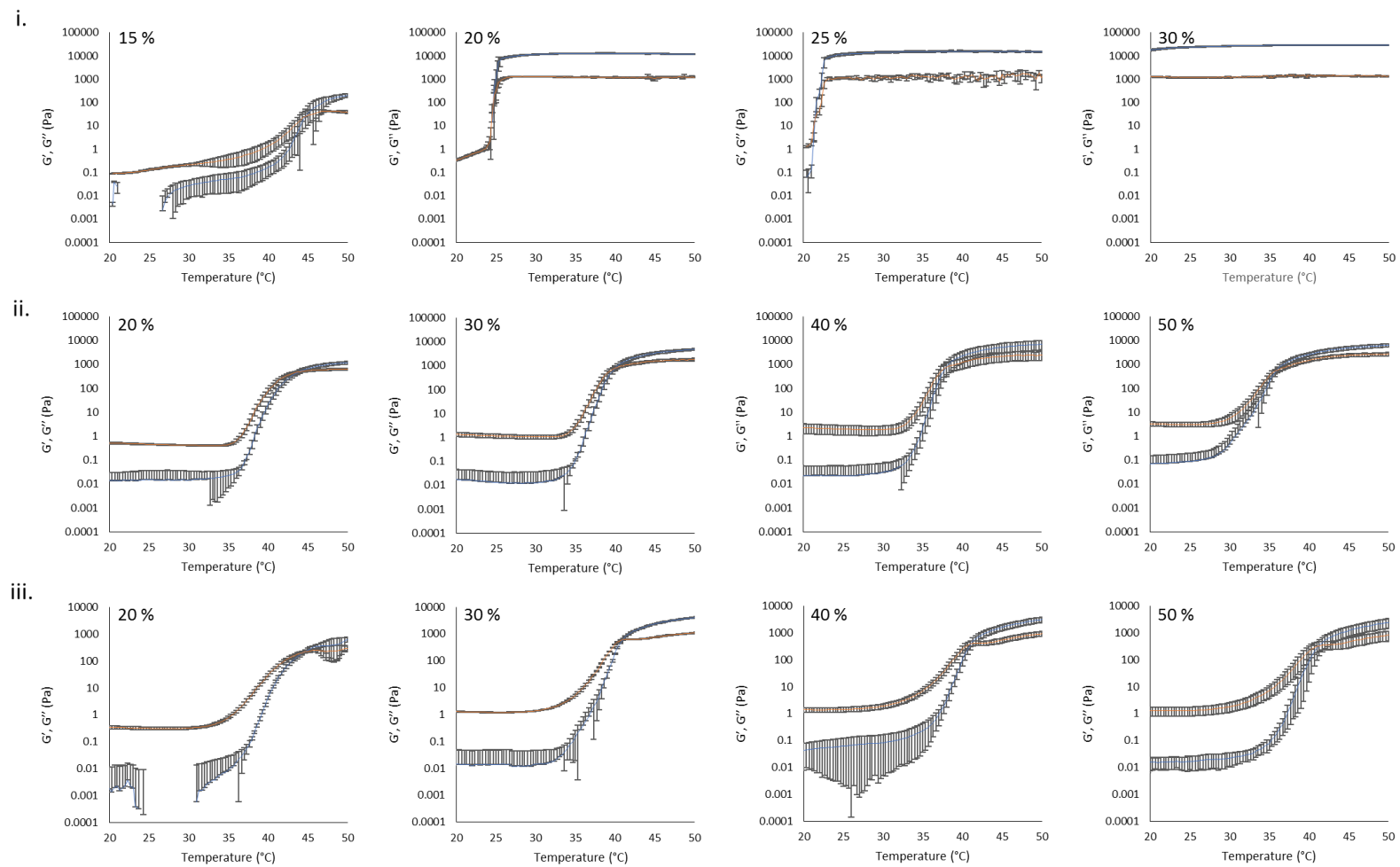
Figure 6. 2: Temperature ramp rheograms of poloxamer 407 (i), PNIPAM10-PEG10-PNIPAM10 (ii) and PDEA20-PEG10-PDEA20 (iii) with variation of concentration (% w/v) at a fixed shear stress (1 Pa) and frequency (1 Hz). G' is presented as blue, whilst orange corresponds to G''. Data presented as mean ± standard deviation, n = 3.

Tgel, Tthick and the maximum absolute value of G' reached (G'max) were extracted from the rheograms shown in Figure 6.2 and Appendix Figure A.18 and are presented in Figure 6.3. PNIPAM10-PEG10-PNIPAM10 (Figure 6.3 (b)) exhibited a monotonic, near-linear, decrease in Tgel from 44 to 36 °C across the concentration range studied. A linear fit (R^2 = 0.96) indicates that the rate of Tgel depression is -0.25 °C.g^{-1}.dL, allowing tight control of Tgel over this range. Tthick decreased from 36 to 29 °C between 20 and 50 % (w/v) concentration, allowing thickening to occur upon warming by the body. PDEA20-PEG10-PDEA20, however, also showed a decrease in Tgel from 44 to 41 °C but this only occurred between 20 and 30 % (w/v) concentration and remained constant above this concentration range. This was matched by Tthick which decreased from 35 to 33 °C over the same concentration range. An inverse proportionality between Tgel and concentration has previously been observed in PNIPAM-poly(N,N-dimethylacrylamide)-PNIPAM solutions, and was attributed to the depressed LCST observed in PNIPAM solutions at high concentrations.[37] G'max of PNIPAM10-PEG10-PNIPAM10 increased with concentration from 1.5 kPa at 20 % (w/v) to a maximum of 12.7 kPa at 45 % (w/v), while the G' max of PDEA20-PEG10-PDEA20 increased from 1.2 kPa at 20 % (w/v) to 5.5 kPa at 30 % (w/v). An increase in gel strength with concentration was also observed by Kirkland et al[37] when studying PNIPAM-poly(N,N-dimethylacrylamide)-PNIPAM. The authors rationalise this phenomenon using the theory of Semenov et al,[38] that telechelic polymers with associating end-groups form flower-like micelles bridged by polymer chains resulting in elasticity. Kirkland et al suggest that a greater number of polymer chains results in additional bridges formed between micellar domains, increasing viscosity.[37] However, this number of additional bridges may become saturated above a critical concentration which is individual to the polymer type. For example, the G' max of PNIPAM10-PEG10-PNIPAM10 and PDEA20-PEG10-PDEA20 failed to increase past 45 and 30 % (w/v), respectively. This could, in future, be confirmed by small angle neutron scattering experiments, where the intensity of the interaction parameter present in the core-shell sphere model discussed in Chapter 5 may be tracked as polymer concentration is increased. Values of Tgel for PNIPAM10-PEG10-PNIPAM10 and PDEA20-PEG10-PDEA20 were typically ca. 5 °C greater than Tthick, whereas poloxamer 407 gave a sharper transition at 20 and 25 % (w/v) with Tgel within 1 °C of Tthick.

Poloxamer 407 exhibited a far greater dependence of Tgel on concentration than PNIPAM10-PEG10-PNIPAM10 and PDEA20-PEG10-PDEA20 (Figure 6.3 (a)), with Tgel decreasing from 45 to 21 °C as the concentration was increased from 15 to 25 % (w/v). At 30 % (w/v) no Tgel was determined, with the rheograms exhibiting G'>G'' at all temperatures. These findings are in line with established phase behaviour of pluronics.[39] Of the concentrations studied, only 17.5 and 20 % (w/v) poloxamer 407 samples (Tgel of 30 and 25 °C, respectively) exhibited Tthick/Tgel at a temperature suitable for *in*

situ thickening upon contact with the body (i.e. 25°C < Tthick < 37 °C), albeit with a Tgel which may be reached at real room temperatures in warmer climates, e.g. WHO climatic zones III and IV (30 °C).[40] The Tthick of 15 % poloxamer 407 was at body temperature (37 °C). Poloxamer 407's G'max was proportional to concentration and had a value of 6.5 kPa at 17.5 % (w/v) poloxamer 407 and 12.7 kPa at 20 % (w/v). Due to the larger gel strength of the 20 % (w/v) formulation and its prevalence in the literature,[41] this concentration was selected for comparison with PNIPAM10-PEG10-PNIPAM10 in future experiments. It is known that poloxamer 407 forms a gel via the packing of micelles into a cubic structure and increasing concentration leads to an increased volume fraction of micelles, and thus a greater degree of overlap between the micelles.[42] The increase in G'max with concentration observed for the poloxamer samples is attributed to this greater degree of overlap causing increased internal friction. The gels formed by PNIPAM10-PEG10-PNIPAM10 and PDEA20-PEG10-PDEA20 were translucent, whilst the 20 % (w/v) poloxamer 407 gels were clear. This indicates that the poloxamer micelles are sufficiently small to avoid scattering of visible light, but that the PNIPAM10-PEG10-PNIPAM10 and PDEA20-PEG10-PDEA20 aggregates are larger and the Tyndall effect is observed. This is confirmed by dynamic light scattering, where poloxamer 407 micelles have hydrodynamic diameters of ca. 20 nm, whereas PNIPAM10-PEG10-PNIPAM10 and PDEA20-PEG10-PDEA20 formed aggregates with hydrodynamic diameters of ca. 88 and 59 nm, respectively (discussed in Chapter 5 section [5.5.3]). The turbidity of the PNIPAM10-PEG10-PNIPAM10 and PDEA20-PEG10-PDEA20 gels may limit their possible applications. For example, a turbid gel is not ideal for ocular drug delivery as this may impair the patients sight.
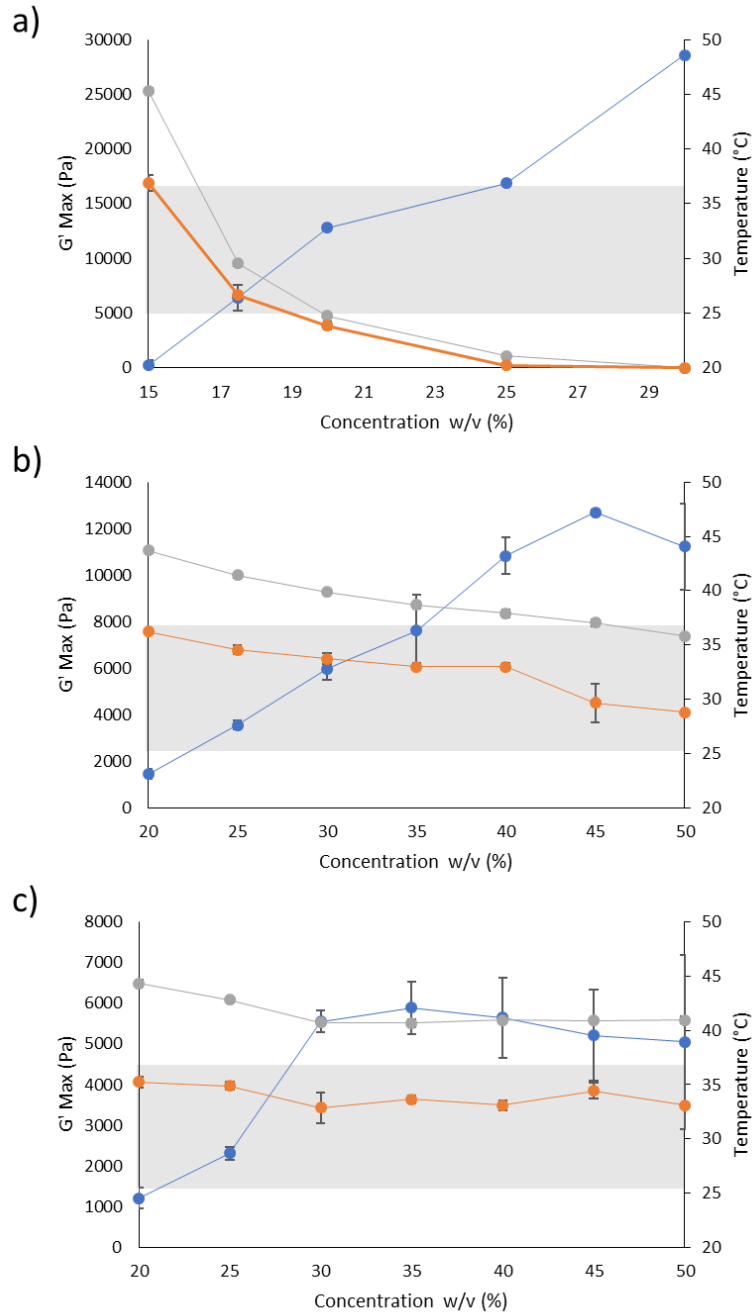
Figure 6. 3: Tthick (Orange), Tgel (Grey), and G'max (Blue) as a function of concentration for Poloxamer 407 (a), PNIPAM10-PEG10-PNIPAM10 (b) and PDEA20-PEG10-PDEA20 (c). The temperature range which would allow for in situ thickening of polymer solutions is overlaid in grey.

Regardless of concentration, the gelation temperature of PDEA20-PEG10-PDEA20 remained > 37 °C, which does not allow *in situ* gelation upon contact with the body's heat. Salting out agents or chaotropes from the Hofmeister series have previously been reported to suppress the LCST of temperature responsive polymers through an increased surface tension between PNIPAM hydrophobic domains (i.e. isopropyl groups and the carbon backbone) and their hydration layer.

[43,44,45] NaCl is both a common ingredient in drug delivery formulations and a member of the Hofmeister series. Therefore, the effect of NaCl on the thermogelling properties of 30 % (w/v) PDEA20-PEG10-PDEA20 solution was selected for further study, as this exhibited the lowest Tgel of 41 °C and greatest G' max of 5.5 kPa in aqueous solution. On the inactive ingredients database, NaCl may be used up to 10 % (w/w) in solution but this is dependent upon the target site.[46] For example, for ocular formulations a maximum concentration of 0.9 % (w/v) cannot be exceeded as a result of potential irritation,[47] vaginal formulations have contained up to 10 % (w/w) (1.7 M). Concentrations of 0.1, 0.3 and 0.5 M NaCl were selected for investigation, as this would not exceed the 10 % (w/w) and may allow for the development of a thermogelling formulation with gelation below 37 °C. Figure 6.4 shows the Tthick, Tgel and G' max dependence upon NaCl concentration. As the NaCl concentration increased from 0 to 0.5 M, the Tthick, Tgel and G' max significantly decreased from 33 to 27 °C, 41 to 34 °C and 5.5 kPa to 3.8 kPa, respectively (p<0.001 by one-way ANOVA). This has previously been observed by Kinekawa et al for whey protein gels, where salts screen the attractive forces between protein chains resulting in a weaker gel.[48] In terms of the gels presented in this work, which are thought to form due to bridging of micelles above a critical concentration, the NaCl present in the extra-micellar fluid may limit the proximity of PDEA20-PEG10-PDEA20 micelles. This limited proximity may prevent micelle-micelle overlap and increasing the NaCl concentration may further enhance this distancing. Therefore, the reduction in gel strength observed for PDEA20-PEG10-PDEA20 is thought to be as a result of NaCl present in the extra-micellar fluid at elevated temperature.
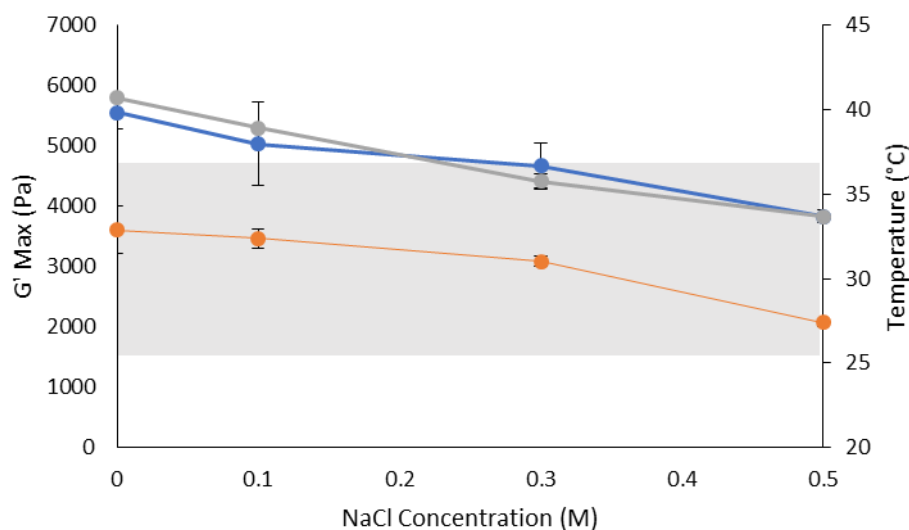
Figure 6. 4: Tthick (Orange), Tgel (Grey), and G'max (Blue) as a function of NaCl concentration for PDEA20-PEG10-PDEA20. The temperature range which would allow for in situ thickening of polymer solutions is overlaid in grey.

Overall, the rheological behaviour of PNIPAM10-PEG10-PNIPAM10, PDEA20-PEG10-PDEA20 and poloxamer 407 with temperature are distinct. Where 20-50 % (w/v) PNIPAM10-PEG10-PNIPAM10 and PDEA20-PEG10-PDEA20 solutions would increase in viscosity when warmed from room to body temperature, this was observed only in 17.5 and 20 % (w/v) poloxamer 407 solutions. The lower concentration dependence of Tgel seen for both PNIPAM10-PEG10-PNIPAM10 and PDEA20-PEG10-PDEA20 is attractive where dilution effects have been observed to affect poloxamer 407's gelation *in vivo* – mild dilution was seen to elevate Tgel above physiological temperature.[11] Achieving *in situ* thickening at high polymer concentrations also allows for viscous gels to be formed with >40 % (w/v) PNIPAM10-PEG10-PNIPAM10 and 30 % (w/v) in 0.3 M NaCl PDEA20-PEG10-PDEA20, achieving G' Max values of 11-13 and 4.6-5.0 kPa, respectively, whilst retaining a Tthick/Tgel close to body temperature.

[6.5.2] Rheological Evaluation

PNIPAM10-PEG10-PNIPAM10 (50 % (w/v)) and PDEA20-PEG10-PDEA20 (30 % (w/v) in 0.3 M NaCl) were further explored as smart materials for drug delivery by rheometry. Their Tgels of 36 °C are highly attractive for administration onto or into the body at sites where the temperature is 37 °C. In particular, the materials may have application in vaginal drug delivery where the local temperature is expected to be 37 °C. Rheology was used to simulate the topical application process of poloxamer 407 (20 % (w/v)), PNIPAM10-PEG10-PNIPAM10 (50 % (w/v)) and PDEA20-PEG10-PDEA20 (30 % (w/v) in 0.3 M NaCl) and determine the time required for the gel phase to form (Figure 6.5 (i)). PNIPAM10-PEG10-PNIPAM10 (50 % (w/v)) and PDEA20-PEG10-PDEA20 (30 % (w/v) in 0.3 M NaCl) were oscillated at 1 Pa shear stress and a frequency of 1 Hz while temperature was varied. The sample was set constant to room temperature (25 °C) for 60 s before holding at body temperature (37 °C) for 240 s. The transition from 25 to 37 °C lead to immediate thickening of the PNIPAM10-PEG10-PNIPAM10 (50 % (w/v)) and PDEA20-PEG10-PDEA20 (30 % (w/v) in 0.3 M NaCl) samples, which formed a gels after 87 ± 5 and 67 ± 6 s and plateaued at a G' of ca. 700 and 1400 Pa, respectively. These relatively long gelation times may have clinical implications, where a patient may be asked to remain still until gel formation has occurred. The same experimental procedure for poloxamer 407 (20 % (w/v) gave a time for gel of 27 ± 5 s, with a plateau at ca. 5.5 kPa indicating a more rapid and rigid gel formation for this sample. The PNIPAM10-PEG10-PNIPAM10 gel formed at 37 °C was subjected to an oscillatory stress sweep which demonstrated thinning above ca. 200 Pa with a gel yield observed at 247 ± 72 Pa, which was not significantly different (p > 0.05 by T-test) than poloxamer 407 (20 % (w/v) which exhibited a yield at 256 ± 58 pa (Figure 6.5 (ii)). PDEA20-PEG10-PDEA20 (30 % (w/v) in 0.3 M NaCl), however, was found to yield at 863 ± 119 pa, which was

significantly greater than both PNIPAM10-PEG10-PNIPAM10 (50 % (w/v)) and poloxamer 407 (20 % (w/v)) ($p > 0.05$ by one-way ANOVA). The yield strength is an indicator of the force required to make the sample undergo viscous flow, and may be taken as the point where G' becomes lower than G'' during an oscillatory stress sweep in the gel phase.[49] Thus, the PDEA-PEG-PDEA material will resist a greater degree of shear before flowing. The greater yield stress observed by PDEA20-PEG10-PDEA20 (30 % (w/v) in 0.3 M NaCl) is thought to be as a result of the molecular weight of the polymer. Previous work by Rochas, Rinaudo and Landry found the yield stresses of kappa carrageenan gels increased linearly with polymer molecular weight.[50] This was as a result of a greater number of polymer entanglements present in the samples with a greater molecular weight. Therefore, it is assumed that the PDEA20-PEG10-PDEA20 triblock copolymers form a greater number of entanglements, which increases the resistance to shear at elevated stresses. Oscillatory frequency sweeps of PNIPAM10-PEG10-PNIPAM10 (50 % (w/v)) and PDEA20-PEG10-PDEA20 (30 % (w/v) in 0.3 M NaCl) at 37 °C confirm that the structures are rheological gels, with G'>G'' at all frequencies measured (Figure 6.5 (iii)). The low dependence of G' and G'' in these experiments indicates that the samples do not exhibit relaxation behaviour, i.e. the internal structures remain unchanged by these shear forces. Finally, the PNIPAM10-PEG10-PNIPAM10 (50 % (w/v)) and PDEA20-PEG10-PDEA20 (30 % (w/v) in 0.3 M NaCl) were cycled between 25 and 37 °C at 1 Pa and 1 Hz (Figure 6.5 (iv)), which indicated that the thermoresponsive gelation process was reversible and repeatable.
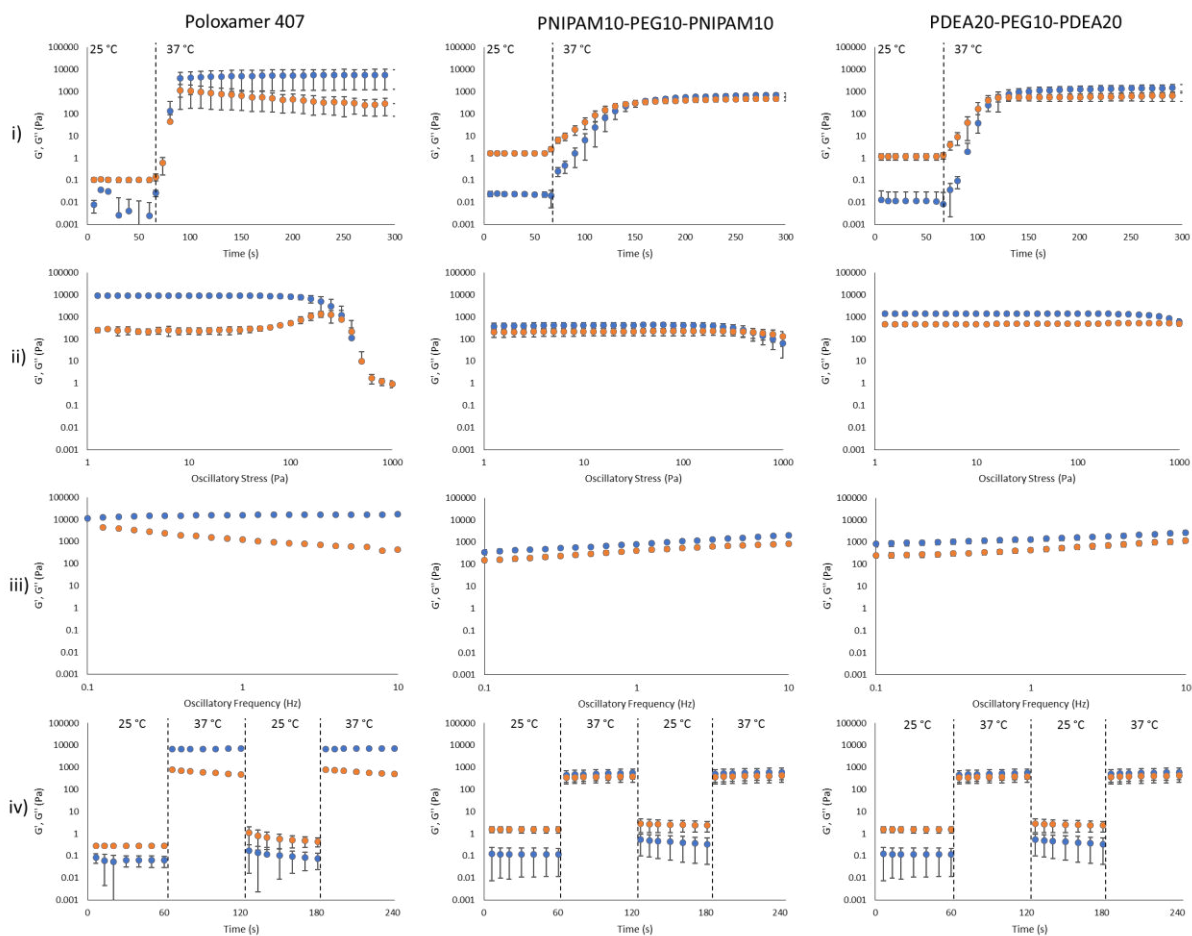
Figure 6. 5: (i) The determination of gelation time, (ii) oscillatory stress sweep, (iii) oscillatory frequency sweep and (iv) thermal cycling of Poloxamer 407 (20 % (w/v)), PNIPAM10-PEG10-PNIPAM10 (50 % (w/v)) and PDEA20-PEG10-PDEA20 (30 % (w/v) in 0.3 M NaCl). G' and G'' are shown as blue and orange markers, respectively. Data presented as mean ± standard deviation, n = 3.

The effect of physiological fluids on the phase transition of poloxamer 407, PNIPAM10-PEG10-PNIPAM10 and PDEA20-PEG10-PDEA20 was then evaluated by preparing polymer solutions in VFS (Figure 6.6).[34] The rheological temperature ramp for PNIPAM10-PEG10-PNIPAM10 (50 % (w/v)) and PDEA20-PEG10-PDEA20 (30 % (w/v)) were altered considerably in VFS relative to deionised water. The Tgels of PNIPAM10-PEG10-PNIPAM10 (50 % (w/v)) and PDEA20-PEG10-PDEA20 (30 % (w/v)) were significantly reduced to 32.9 ± 0.2 and 37.5 ± 0.4 °C in VFS relative to 35.8 ± 0.2 and 40.7 ± 0.0 °C in deionised water. This depression of Tgel was also seen in poloxamer 407 which formed a gel at 22.3 ± 0.4 °C in VFS compared to 24.7 ± 0.2 °C in deionised water (p > 0.05 by t-test). The depression of Tgel seen in both PNIPAM10-PEG10-PNIPAM10 (50 % (w/v)) and PDEA20-PEG10-PDEA20 (30 % (w/v)) is attributed to salting-out of the temperature responsive PNIPAM and PDEA blocks, as

previously seen for PDEA20-PEG10-PDEA20 in NaCl solutions. Tgel depression in poloxamer 407 is also attributed to salting-out. Zhang et al. found the LCST of PNIPAM can be reduced by salts as these increase the strength between water molecules and the overall polarity of the solvent. This results in increased surface tension between the hydrophobic moieties in the polymer (i.e. the carbon backbone and isopropyl group). This depresses the LCST, as the increased surface tension results in fewer polymer-water interactions.[43] A similar effect is expected to occur for the PDEA20-PEG10-PDEA20 triblock copolymer, where surface tension between he PDEA blocks and water is increase in the presence of salts, which promotes the micellization process, and presents as a lower transition temperature.[51] VFS did not affect G'max of PNIPAM10-PEG10-PNIPAM10 (50 % (w/v)) or PDEA20-PEG10-PDEA20 (30 % (w/v)), which were 11.7 ± 1.5 and 5.6 ± 0.8 kPa in VFS and 11.2 ± 1.8 and 5.5 ± 0.2 kPa in deionised water, respectively ($p < 0.05$ by one-way ANOVA). However, the depression in Tgel did result in a greater value of G' at 37 °C for PNIPAM10-PEG10-PNIPAM10 (50 % (w/v)) and PDEA20-PEG10-PDEA20 (30 % (w/v)) in VFS of 4.8 ± 0.3 and 0.3 ± 0.2 kPa compared to 1.1 ± 0.8 and 0.001 ± 0.001 kPa in deionised water, respectively. The low G' of the PDEA20-PEG10-PDEA20 (30 % (w/v)) in deionised water and VFS occurred because the gelation temperature was > 37 °C. This may be problematic, as upon administration the mixing of the formulation with vaginal fluid may increase gelation temperature above the physiological range, preventing gel formation and subsequent retention of the formulations. G' of poloxamer 407 (20 % (w/v)) at 37 °C was unaffected by the presence of VFS, with both VFS and deionised water leading to values of G' of ca 13 kPa at this temperature.
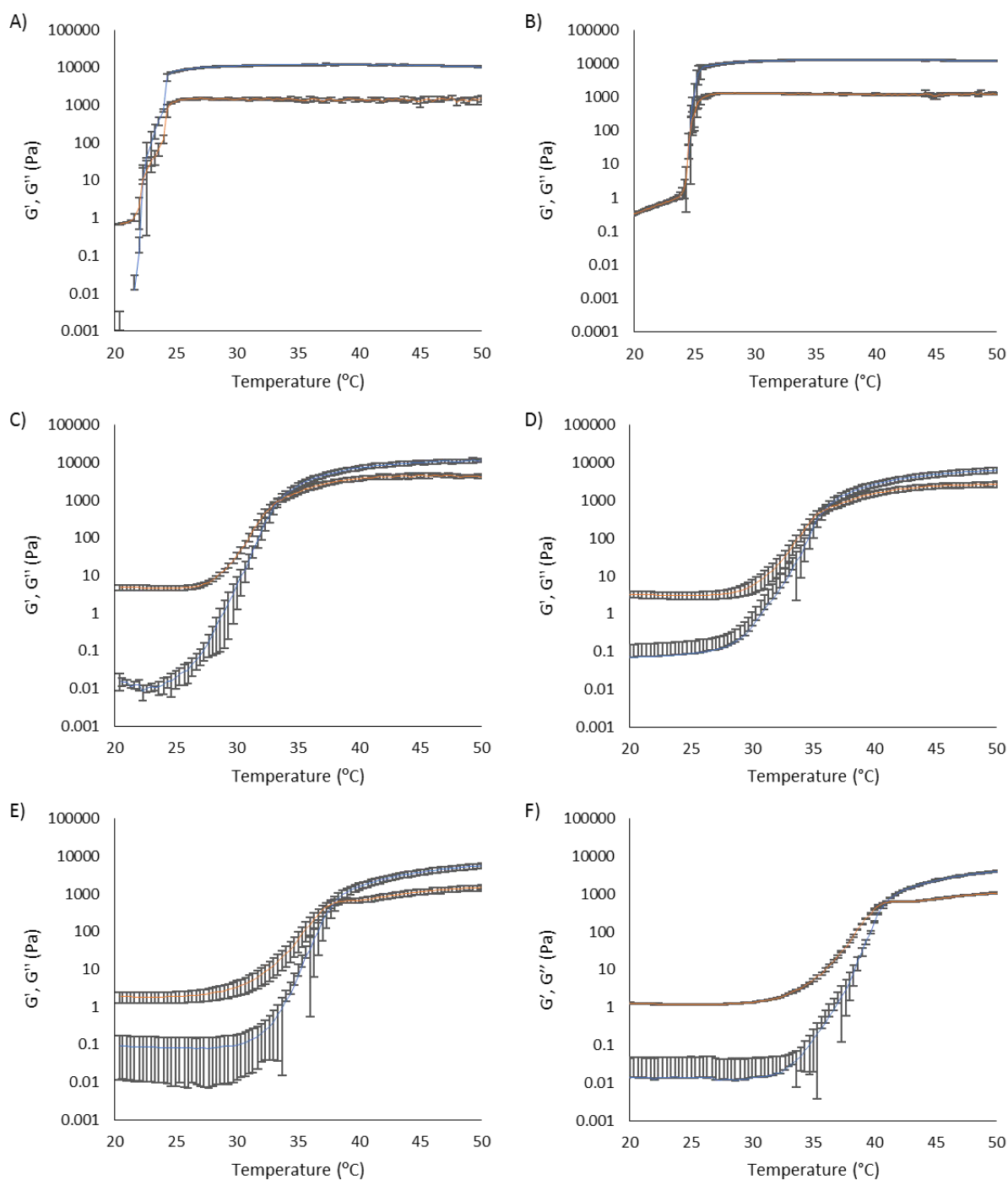
Figure 6. 6: Temperature ramp rheology of 20 % w/v Poloxamer 407 in A) VSF and B) aqueous solution, C) 50 % w/v PNIPAM10-PEG10-PNIPAM10 in VSF and D) aqueous solution and E) 30 % w/v PDEA20-PEG10-PDEA20 in VSF and F) aqueous solution. The graphs show G' (blue) and G'' (orange) as a function of temperature. Data presented as mean ± SD (n=3).

[6.5.3] The Dissolution Rate of the Gels in VSF

A significant limitation of poloxamer 407 as a thermoresponsive gelator is its rapid dissolution in physiological fluids.[41] 20 % (w/v) solutions of poloxamer 407 dissolved in VFS within 60 min (Figure 6.7). Both PNIPAM10-PEG10-PNIPAM10 (50 % (w/v)) or PDEA20-PEG10-PDEA20 (30 % (w/v) in 0.3 M NaCl), had significantly (p<0.05) greater resistance to dissolution, requiring 230 min for dissolution to occur. Controls of 30 and 50 % (w/v) poloxamer 407 dissolved after 140 and 190 min, respectively, which indicated that this difference is not solely explained by concentration. It is hypothesised that where poloxamer 407 gels are composed of non-interacting polymeric micelles, the liberation of micelles into the dissolution medium occurs rapidly. PNIPAM10-PEG10-PNIPAM10 and PDEA20-PEG10-PDEA20 micelles, however, are thought to be bridged by polymeric unimers which reduce the favourability of micelle liberation into the dissolution medium.[38,52] These experiments were conducted in a large excess of dissolution media, and the dissolution process in the real, smaller, volumes of physiological fluid present *in vivo* is likely to occur over a longer period of time.
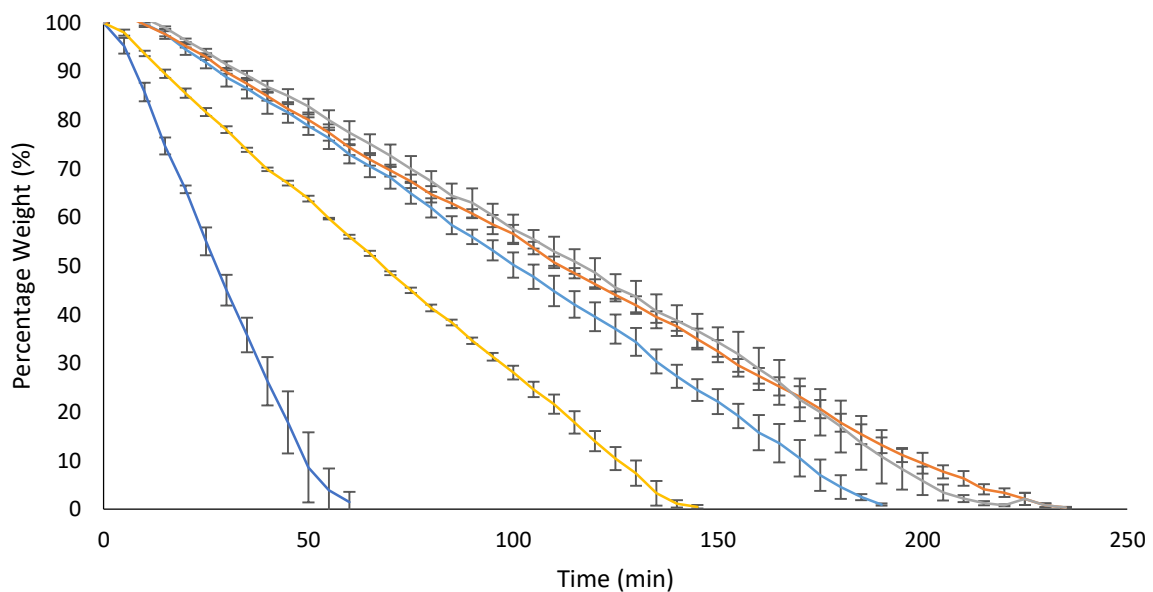
Figure 6. 7: The dissolution rate of PNIPAM10-PEG10-PNIPAM10 (50 % w/v) (orange), PDEA20-PEG10-PDEA20 (30 % in 0.3 M NaCl) (grey) and Poloxamer 407 at 20 (dark blue), 30 (yellow) and 50 % w/v (light blue) into 400 mL VSF at 37 °C. Data is presented as mean ± standard deviation (n=3).

[6.5.4] The Adhesion and Mucoadhesion of the Gels

The mucoadhesion of poloxamer 407 is weak,[53] which limits its residence time on mucosal membranes. Mucoadhesion is mediated by several different factors, which are not mutually exclusive. Briefly, entanglements may occur between macromolecules in the dosage form and mucin glycoproteins coating the mucosa, which are supported by non-covalent interactions, enhancing adhesion.[54] The viscosity of a gel will enhance retention, whilst the movement of moisture from the mucosa to the dosage form will either improve or decrease mucoadhesion depending on levels of hydration.[55] Several other theories exist.[56] The most common method to determine mucoadhesion is by measuring the force-displacement curve during removal of the dosage form from a membrane, where the peak force is termed the "force of adhesion" and the total area under the curve is the "work of adhesion".[27] However, this method is not without its limitations. Tensile detachments aim to reproduce processes occurring in vivo, but these are relatively rare when compared to shear forces.[27] Also, the experimental conditions for these tests, such as detachment speed, have a profound effect upon the results, limiting comparison to literature results.[57] These tests may be complimented using the flow-through method which will also take in account the flow of biological fluids in vivo.[58] Tensile detachment adhesion experiments were studied for 50 % (w/v) solutions of PNIPAM10-PEG10-PNIPAM, 30 % (w/v) PDEA20-PEG10-PDEA20 in 0.3 M NaCl as well as 20, 30, and 50 % (w/v) poloxamer 407. Only 20% (w/v) solutions of poloxamer 407 exhibit Tgel at a relevant temperature (25 °C), but 30 and 50 % (w/v) solutions were explored to account for differences in concentration between the three thermoreversible gelators and understand whether adhesion processes are affected by chemical structure or concentration. Firstly, the adhesion of PNIPAM10-PEG10-PNIPAM10, PDEA20-PEG10-PDEA20 and poloxamer 407 to a poly(propylene) probe was assessed (Figure 6.8a). In this control experiment, van der Waals forces are believed to be the major contributor to adhesion. The data demonstrates that the adhesion of poloxamer 407 increases with concentration, and that 50 % (w/v) solutions of PNIPAM10-PEG10-PNIPAM10 and poloxamer 407 had equivalent ($p > 0.05$) adhesion to the probe. The adhesion of PDEA20-PEG10-PDEA20, however, was not statistically different to the 20 % (w/v) poloxamer sample. This is may be a result of the NaCl present which may form a barrier between the sample and poly(propylene) probe and reduce the Waals forces between them. The mucoadhesion of 20, 30 and 50 % (w/v) poloxamer 407, 50 % (w/v) PNIPAM10-PEG10-PNIPAM10 and 30 % (w/v) PDEA20-PEG10-PDEA20 in 0.3 M NaCl is shown in figure 6.8b. PNIPAM10-PEG10-PNIPAM10 (50 % (w/v)) had greater force and work of adhesion than 20 % (w/v) poloxamer 407 ($p < 0.01$) which is desirable for mucosal drug delivery. A control of 50 % (w/v) poloxamer 407 was equivalent to the PNIPAM10-PEG10-PNIPAM10 (50 % (w/v) which demonstrates that this enhanced adhesion is likely to be related to concentration, rather than

enhanced specific intermolecular interactions between polymer and mucosa. However, concentrations of poloxamer 407 above 20 % (w/v) did not exhibit a Tgel in the range required and thus are not appropriate for in situ gelation with topical administration. Conversely, both the force and work of adhesion of 30 % (w/v) PDEA20-PEG10-PDEA20 in 0.3 M NaCl and 20 % (w/v) poloxamer 407 were not significantly different. This is thought to be as a result of fewer entanglements between the mucins and PDEA20-PEG10-PDEA20. Vaginal mucins are typically negatively charged as a result of their sulphate and sialic acid groups.[59] The positively charged sodium ions may diffuse independently of the PDEA20-PEG10-PDEA20 chains, from the formulation into the mucosa before the polymer chains as a result of their smaller size. This may create a localised effect, whereby the concentration of sodium present in the formulation at the interface between the mucosa and formulation is reduced. As previously mentioned in section [6.5.1], NaCl is required to induce gelation below 37 °C. Therefore, it is possible that the gelation temperature is increased above 37 °C due to this diffusion, and in turn the gel structure is broken down at the formulation-mucin interface. This is thought to result in a less viscous formulation and as a result, a reduced mucoadhesion. Additionally, the NaCl may increase the surface tension of the PDEA20-PEG10-PDEA20 formulations, which may disfavour wetting on the surface mucosa.[60] Conversely, poloxamer 407 without the presence of NaCl exhibited gelation well below 37 °C and as such is free to diffuse into the mucin matrix while remaining sufficiently viscous to enhance mucoadhesion. Overall, PNIPAM10-PEG10-PNIPAM10 allows the formation of *in situ* gelators (25 < Tgel < 37 °C) at 50 % (w/v), which imparts a greater level of mucoadhesion than seen for 20 % (w/v) poloxamer 407 or 30 % (w/v) PDEA20-PEG10-PDEA20 in 0.3 M NaCl. 50 % (w/v) poloxamer 407 had equivalent mucoadhesion to 50 % (w/v) PNIPAM10-PEG10-PNIPAM10 but it is not a thermoreversible gelator, existing in a gel phase at all temperatures studied.
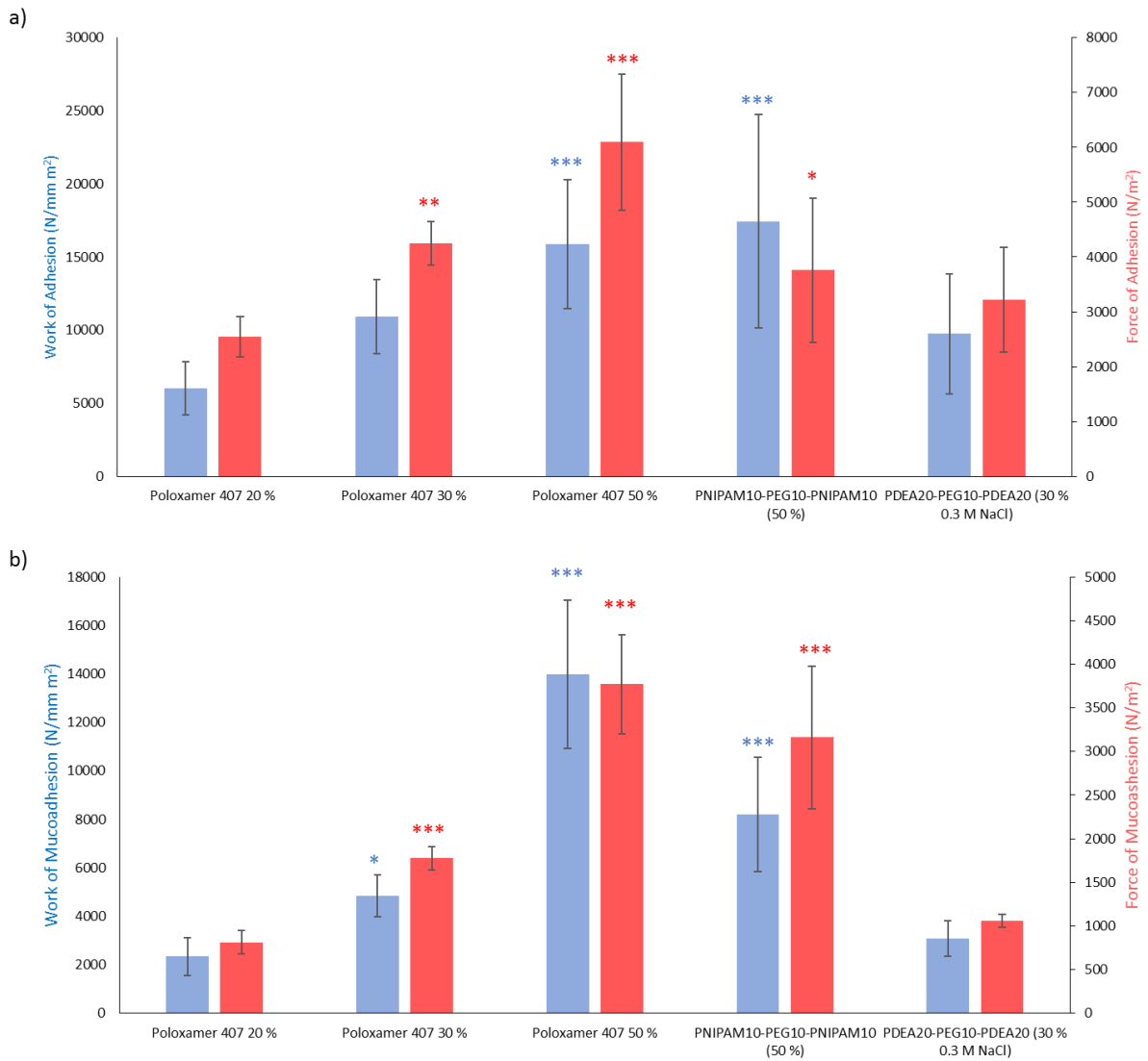
Figure 6.8: a) The work of adhesion (blue) and force of adhesion (red) of the gels to the poly(propylene) probe and b) the work of mucoadhesion (blue) and force of mucoadhesion (red) of the gels to porcine vaginal tissue. Results which are statistically significantly different to Poloxamer 407 (20 %) are identified by * ($P < 0.05$), ** ($P < 0.01$) and *** ($P < 0.001$). All data is presented as mean ± standard deviation (n=9).

[6.5.5] Long-term Thermogel Stability

The stability of poloxamer 407, PNIPAM10-PEG10-PNIPAM10 and PDEA20-PEG10-PDEA20 was assessed in aqueous solution at 4, 25, or 40 °C, reflecting refrigerated storage, storage at room temperature, and an accelerated storage condition, respectively (Figure 6.8). Accelerated storage at 40 °C aimed to predict longer-term storage at room temperature. GPC analysis demonstrated that all three polymers exhibit small reductions in molecular weight over 12 weeks, with losses accelerated in the PNIPAM10-PEG10-PNIPAM10 and PDEA20-PEG10-PDEA20 samples at elevated temperatures. However, at 4 and 25 °C the reduction in number-average molecular weight of PNIPAM10-PEG10-PNIPAM10 and PDEA20-PEG10-PDEA20 was not statistically significant, while at 40 °C there was a significant decrease ($p < 0.05$ by one-way ANOVA). GPC traces (Figure 6.9) of poloxamer at weeks 0 and 12 are near-identical, with the accelerated storage condition (yellow) exhibiting a small increase in a shoulder at low molecular weight. PNIPAM10-PEG10-PNIPAM10 traces exhibit a clear shift to a lower molecular weight under accelerated storage conditions, while PDEA20-PEG10-PDEA20 did not (Figure 6.8). Under all conditions the trace for PNIPAM10-PEG10-PNIPAM10 and PDEA20-PEG10-PDEA20 traces remained monomodal with no shoulder. Thus, hydrolysis was not observed at the ester linkages present between individual polymer blocks, but amide hydrolysis is possible. Poloxamer 407 does not possess hydrolytically unstable ester or amide linkages, and its molecular weight remained constant throughout the study. This is the first report on the long-term stability of either a PNIPAM or PDEA copolymer in water. Future studies on the stability of these materials should expand this experiment in-line with ICH standards.[61] Additionally, it is not known whether the degradation exhibited in the accelerated storage condition will be seen at 25 °C where typically only small extrapolations should be made from this data when the degradation routes have been established.[61]
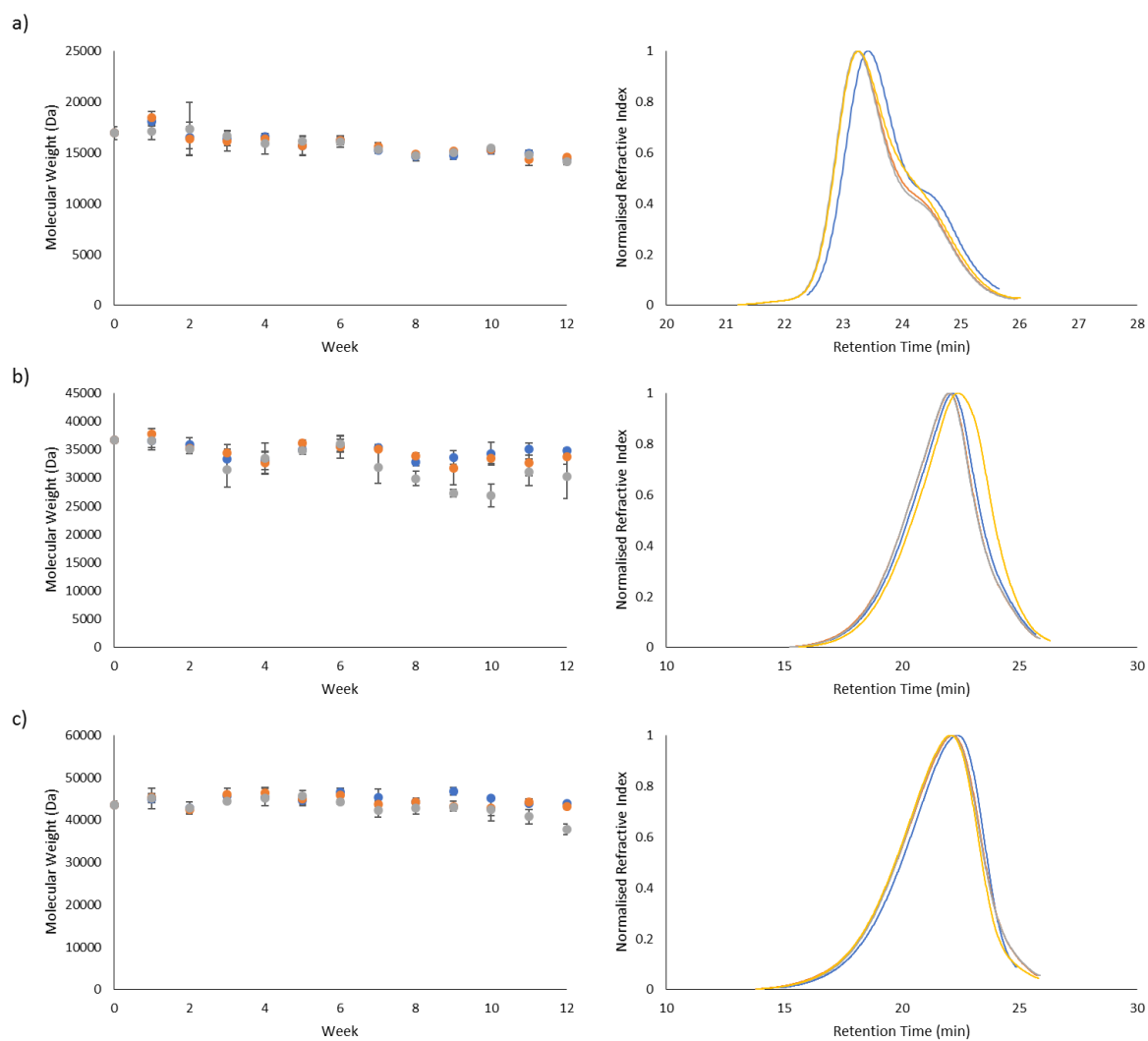
Figure 6. 9: The stability of Poloxamer 407 (20 %) (a), PNIPAM10-PEG10-PNIPAM10 (50 %) (b) and PDEA20-PEG10-PDEA20 (30 % in 0.3 M NaCl) (c) at 4 (blue), 15 (orange) and 40 ° C (grey). The variation in number-average molecular weight is shown on the left and the GPC traces at week 0 (blue) and week 12 at 4 (red), 25 (grey) and 40 °C (yellow). Variation in number average molecular weight is shown as mean ± SD (n=3) and while GPC traces are a single run.

[6.6] Conclusions

This study investigates the use of thermoreversible PNIPAM10-PEG10-PNIPAM10 and PDEA20-PEG10-PDEA20 gelators as smart materials for topical administration for the first time, with a critical comparison to poloxamer 407. The low dependence of Tgel on concentration allows PNIPAM10-PEG10-PNIPAM10 to exhibit *in situ* gelation at concentrations up to 50 % (w/v), where Tgel may be finely tuned to temperatures just below 37 °C. Tgel of PDEA20-PEG10-PDEA20, however, may be reduced by increasing the concentration up to 30 % (w/v), above this point Tgel plateaued at ca. 41 °C. For PDEA20-PEG10-PDEA20 to gel below 37 °C, a minimum concentration of 30 % w/v in 0.3 M NaCl was required. Thickening of both 50 % (w/v) PNIPAM10-PEG10-PNIPAM10 and 30 % (w/v) PDEA20-PEG10-PDEA20 in 0.3 M NaCl occurred only at temperatures above 28 °C, reducing the potential for increases in viscosity to occur at room temperature. This gives the system advantages over poloxamer 407 where values of Tgel typically occurred near or below room temperature (25 °C), making the materials unattractive in warmer climates (e.g. WHO climatic zones II (25 °C), III (30 °C) and IV (30 °C)).[40] PNIPAM10-PEG10-PNIPAM 50 % (w/v) gels exhibit enhanced mucoadhesion when compared to poloxamer 407, while 30 % (w/v) PDEA20-PEG10-PDEA20 in 0.3 M NaCl did not. Both 50 % (w/v) PNIPAM10-PEG10-PNIPAM and 30 % (w/v) PDEA20-PEG10-PDEA20 in 0.3 M NaCl exhibited prolonged dissolution times when compared to poloxamer 407. Therefore, PNIPAM10-PEG10-PNIPAM10 (50 % (w/v)) and PDEA20-PEG10-PDEA20 (30 % (w/v) in 0.3 M NaCl) offer significant advantages for mucosal drug delivery, when compared to poloxamer 407, where these two attributes are linked to retention at the site of administration. PNIPAM10-PEG10-PNIPAM10 and PDEA20-PEG10-PDEA20 was also found to be stable in solution at room temperature over 12 weeks.

The next phase of work is to investigate poloxamer 407, PNIPAM10-PEG10-PNIPAM10 and PDEA20-PEG10-PDEA20 in drug delivery. The dissolution of progesterone and tenofovir disoproxil fumarate in all three formulations will be investigated. In addition to this, their release kinetics will be evaluated using Franz Cell experiments, in order to understand if gelation enhances or retards drug release. The effect of the two therapeutics agents on the sample rheology will also be evaluated. This information may then be taken as a whole to provide a critical overview of the three materials for topical drug delivery, as well as generate knowledge concerning the behaviour of these thermoreversible gelators loaded with active pharmaceutical ingredients.

[6.7] References

1   S. Nie, W. L. W. Hsiao, W. Pan and Z. Yang, *Int. J. Nanomedicine*, 2011, **6**, 151–166.

2   J. Jiang, C. Li, J. Lombardi, R. H. Colby, B. Rigas, M. H. Rafailovich and J. C. Sokolov, *Polymer (Guildf).*, 2008, **49**, 3561–3567.

3   A. Karlsbad and S. Kopp, *Acta Odontol. Scand.*, 1991, **49**, 225–231.

4   J. Rodrigues, J. Caldeira and B. Vaidya, *Sensors*, 2009, **9**, 2797–2808.

5   T. Chen, *Rheological Techniques for Yield Stress Analysis*, 2000.

6   H. A. Barnes and K. Walters, *Rheol. Acta*, 1985, **24**, 323–326.

7   D. Khyati, *City Univ. New York*.

8   N. Badi and J.-F. F. Lutz, *J. Control. Release*, 2009, **140**, 224–229.

9   J. Hadgraft and C. Valenta, *Int. J. Pharm.*, 2000, **200**, 243–247.

10   V. K. Garripelli and S. Jo, *J. Bioact. Compat. Polym.*, 2012, **27**, 198–209.

11   K. Edsman, J. Carlfors and R. Petersson, *Eur. J. Pharm. Sci.*, 1998, **6**, 105–112.

12   J. Y. Chang, Y. K. Oh, H. gon Choi, Y. B. Kim and C. K. Kim, *Int. J. Pharm.*, 2002, **241**, 155–163.

13   K. Tietz and S. Klein, *Dissolution Technol.*, 2018, **25**, 40–51.

14   M. R. C. Marques, R. Loebenberg and M. Almukainzi, *Dissolution Technol.*, 2011, **18**, 15–28.

15   K. Edsman, J. Carlfors and K. Harju, *Int. J. Pharm.*, 1996, **137**, 233–241.

16   M. Zignani, C. Tabatabay and R. Gurny, *Adv. Drug Deliv. Rev.*, 1995, **16**, 51–60.

17   J. R. Paugh, R. C. Chatelier and J. W. Huff, in *Advances in Experimental Medicine and Biology*, Springer New York LLC, 1998, vol. 438, pp. 761–767.

18   Y. Bin Choy, J. H. Park, B. E. McCarey, H. F. Edelhauser and M. R. Prausnitz, *Investig. Ophthalmol. Vis. Sci.*, 2008, **49**, 4808–4815.

19   E. Baloglu, Z. A. Senyigit, S. Y. Karavana and A. Bernkop-Schnürch, *J. Pharm. Pharm. Sci.*, 2009, **12**, 312–336.

20   R. Shaikh, T. Raj Singh, M. Garland, A. Woolfson and R. Donnelly, *J. Pharm. Bioallied Sci.*, 2011, **3**, 89–100.

21   B. M. Boddupalli, Z. N. K. Mohammed, R. Nath A. and D. Banji, *Mucoadhesive drug delivery system: An overview*, Wolters Kluwer -- Medknow Publications, 2010, vol. 1.

22   H. C. Wang and W. John, *J. Aerosol Sci.*, 1988, **19**, 399–411.

23   A. J. Kinloch, *The science of adhesion - Part 1 Surface and interfacial aspects*, Kluwer Academic Publishers, 1980, vol. 15.

24   N. A. Peppas and P. A. Buri, *J. Control. Release*, 1985, **2**, 257–275.

25   N. A. Peppas and J. J. Sahlin, *Biomaterials*, 1996, **17**, 1553–1561.

26   N. Garti, *Delivery and controlled release of bioactives in foods and nutraceuticals*, 2008.

27   V. V. Khutoryanskiy, *Macromol. Biosci.*, 2011, **11**, 748–764.

28   J. B. da Silva, S. B. de S. Ferreira, A. V. Reis, M. T. Cook and M. L. Bruschi, *Polymers (Basel).*, 2018, **10**, 1–19.

29   N. W. Moore and J. E. Houston, *J. Adhes. Sci. Technol.*, 2010, **24**, 2531–2544.

30   P. KJER, *Nord. Med.*, 1961, **66**, 1321–1324.

31   ICH, Q 1 A Stability Testing Guidelines: Stability Testing of New Drug Substances and Products, http://www.eudra.org/emea.htmlCPMP/ICH/380/95, (accessed 1 September 2020).

32   B. Erlandsson, *Polym. Degrad. Stab.*, 2002, **78**, 571–575.

33   J. D. Debord and L. A. Lyon, *Bioconjug. Chem.*, 2007, **18**, 601–604.

34   D. H. Owen and D. F. Katz, *Contraception*, 1999, **59**, 91–95.

35   M. T. Cook, G. Tzortzis, D. Charalampopoulos and V. V. Khutoryanskiy, *Biomacromolecules*, 2011, **12**, 2834–2840.

36   B. Jeong, S. W. Kim and Y. H. Bae, *Adv. Drug Deliv. Rev.*, 2012, **64**, 154–162.

37   S. E. Kirkland, R. M. Hensarling, S. D. McConaughy, Y. Guo, W. L. Jarrett and C. L. McCormick, *Biomacromolecules*, 2008, **9**, 481–486.

38   A. N. Semenov, J. F. Joanny and A. R. Khokhlov, *Macromolecules*, 1995, **28**, 1066–1075.

39   M. Malmsten and B. Lindman, *Macromolecules*, 1992, **25**, 5440–5445.

40   W. Grimm, *Drug Dev. Ind. Pharm.*, 1993, **19**, 2795–2830.

41   M. A. Abou-Shamat, J. Calvo-Castro, J. L. Stair and M. T. Cook, *Macromol. Chem. Phys.*, 2019, **220**, 18–25.

42   R. K. Prud'homme, G. Wu and D. K. Schneider, *Langmuir*, 1996, **12**, 4651–4659.

43   Y. Zhang, S. Furyk, L. B. Sagle, Y. Cho, D. E. Bergbreiter and P. S. Cremer, *J. Phys. Chem. C*, 2007, **111**, 8916–8924.

44   H. Du, R. Wickramasinghe and X. Qian, *J. Phys. Chem. B*, 2010, **114**, 16594–16604.

45   I. Salah, M. A. Shamat and M. T. Cook, *J. Appl. Polym. Sci.*, 2019, **136**, 46915–46922.

46   FDA, Inactive Ingredient Search for Approved Drug Products, https://www.accessdata.fda.gov/scripts/cder/iig/index.cfm, (accessed 26 January 2020).

47   R. Rylander, K. Victorin and S. Sörensen, *J. Hyg. (Lond).*, 1973, **71**, 587–592.

48   Y. I. Kinekawa, T. Fuyuki and N. Kitabatake, *J. Dairy Sci.*, 1998, **81**, 1532–1544.

49   M. Castro, D. W. Giles, C. W. Macosko and T. Moaddel, *J. Rheol. (N. Y. N. Y).*, 2010, **54**, 81–94.

50   C. Rochas, M. Rinaudo and S. Landry, *Carbohydr. Polym.*, 1990, **12**, 255–266.

51   D. R. Perinelli, M. Cespi, S. Pucciarelli, L. Casettari, G. F. Palmieri and G. Bonacucina, *Colloids Surfaces A Physicochem. Eng. Asp.*, 2013, **436**, 123–129.

52   H. H. Lin and Y. L. Cheng, *Macromolecules*, 2001, **34**, 3710–3715.

53   G. Niu, F. Du, L. Song, H. Zhang, J. Yang, H. Cao, Y. Zheng, Z. Yang, G. Wang, H. Yang and S. Zhu, *J. Control. Release*, 2009, **138**, 49–56.

54   N. A. Peppas and Y. Huang, *Adv. Drug Deliv. Rev.*, 2004, **56**, 1675–87.

55   M. T. Cook and V. V. Khutoryanskiy, *Int. J. Pharm.*, 2015, **495**, 991–998.

56   J. D. Smart, *Adv. Drug Deliv. Rev.*, 2005, **57**, 1556–1568.

57   M. J. Tobyn, J. R. Johnson and P. W. Dettmar, *Eur. J. Pharm. Biopharm.*, 1997, **43**, 65–71.

58   M. T. Cook, S. L. Smith and V. V. Khutoryanskiy, *Chem. Commun.*, 2015, **51**, 14447–14450.

59   J. Leal, H. D. C. Smyth and D. Ghosh, *Int. J. Pharm.*, 2017, **532**, 555–572.

60   C. M. Lehr, J. A. Bouwstra, H. E. Boddé and H. E. Junginger, *Pharm. Res. An Off. J. Am. Assoc. Pharm. Sci.*, 1992, **9**, 70–75.

61   ICH, Q1A(R2) Stability Testing of New Drug Substances and Products,

https://www.ema.europa.eu/en/documents/scientific-guideline/ich-q-1-r2-stability-testing-new-drug-substances-products-step-5_en.pdf, (accessed 15 October 2020).

Chapter Seven: Evaluation of thermogelling materials for topical drug delivery

[7.1] Introduction

This chapter describes the preparation of topical vaginal formulations using thermogelling materials based on PNIPAM10-PEG10-PNIPAM10 (50 % w/v), PDEA20-PEG10-PDEA20 (30 % in 0.3 M NaCl) and poloxamer 407 (20 %). Two vaginally administered drugs with large differences in their aqueous solubilities were selected for this study. The first was progesterone (logP = 3.87),[1] which is considered to be hydrophobic, while the second drug to be investigated, tenofovir disoproxil fumarate (logP =1.25),[2] is more hydrophilic (Figure 7.1). In aqueous solution progesterone is not reported to exhibit a pKa, and as such remains unionised whereas, the free base of tenofovir disoproxil fumarate, tenofovir disoproxil, is reported to exhibit a pKa of 3.75.[3] This pKa centre is basic in nature and as such becomes protonated and increasingly soluble in acidic media. Tenofovir disoproxil fumarate has been reported to have a solubility of 13.4 mg/mL in distilled water, while progesterone has a reported solubility in aqueous solution of 8.81 µg/mL and as such is considered sparingly soluble.[2,4]
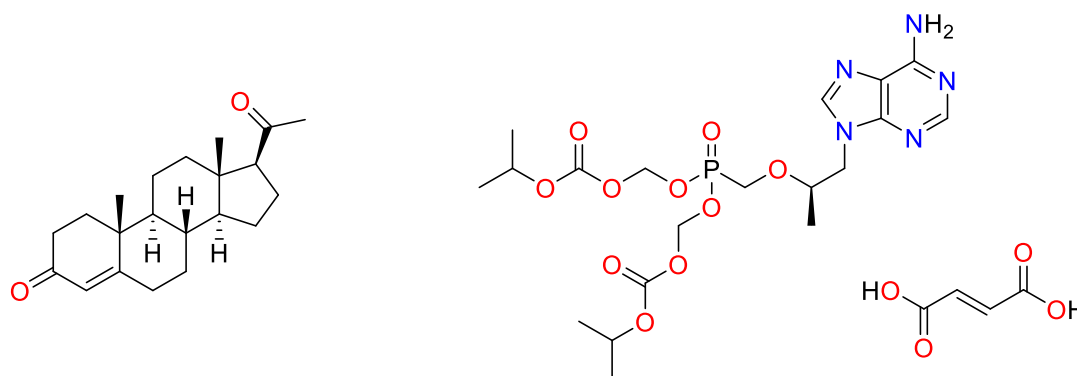
Figure 7. 1: The chemical structures of progesterone (left) and tenofovir disoproxil fumarate (right).

It is reported that thermogelling materials such as poloxamer 407 may be able to enhance the solubility of poorly water-soluble drugs, e.g. progesterone.[5–7] This chapter aims to explore if the novel materials developed in chapter 6 will also exhibit this property, and their efficacy compared to poloxamer 407. There is a paucity of studies which investigate the effect of thermogelling polymer solutions on the solubility and release of therapeutics which are soluble in water, such as tenofovir disoproxil fumarate.[8] Furthermore, the majority of studies reporting drug release from thermogelling materials focus on injectable formulations, rather than topical delivery, and rarely explore the effect of temperature on release.[9–11] In order to gain fundamental understanding of the effect of the sol-gel transition upon the rate of drug release, this was investigated at both 25 and 37 °C.

The first drug to be investigated was progesterone, which is commonly administered intravaginally. Progesterone is a hormone released by the female reproductive system which plays an important role in both the menstrual cycle and maintaining the early stages of pregnancy.[12] Progesterone is used in the treatment of low fertility, premenstrual syndrome and postnatal depression, as well as in vivo fertilisation and reducing the risk of pre-term delivery in pregnancy.[13–15] Progesterone is sparingly soluble in water[16] which poses a formulation challenge. Tenofovir disoproxil fumarate, the second drug to be studied, is a water soluble anti-retroviral medicine. When applied topically to the vagina, tenofovir disoproxil fumarate may prevent the transmission of human immunodeficiency virus (HIV) during sexual intercourse, and as such has been identified as a potential pre-exposure prophylaxis agent, as demonstrated in macaques.[17] Tenofovir disoproxil fumarate is typically taken as oral tablets under the trade names of Atripla, Delstrigo, Eviplera, Lamivudine and Stribild.[18–22] These oral dosage forms undergo first pass metabolism, where the tenofovir disoproxil fumarate is metabolised by the liver prior to achieving a therapeutic response.[23] This results in a higher dose requirement which may lead to an increased risk of adverse side-effects in the system.[24] Furthermore, local application to the vagina ensures a high concentration of drug at the site where transmission may occur. Thus, incorporation of tenofovir disoproxil fumarate into a topical formulation could reduce the required daily dose. This would be more cost-effective and there would be a lower risk of systemic side effects. Tenofovir disoproxil fumarate vaginal rings have been prepared and these are expected to improve on patient compliance as a result of a single monthly dose, due to sustained release, rather than an daily oral dose.[25] This vaginal ring has finished phase I clinical trials, where minor adverse side-effects were noted for all 6 patients. This ring scored an average of 3.5 on a Likert scale (1 – 5) where 5 was complete willingness to use the ring, while 1 was unwilling.[26] Topical preparations applied through an applicator, such as a thermogelling formulations, may improve upon this willingness and therefore patient adherence.

Thermogelling materials have been found to improve the solubility of poorly water-soluble therapeutics. For example domperidone,[27] emodin[28] and irinotecan[29] solubilities have been enhanced in poloxamer 407 formulations when compared to water alone. This solubility enhancement occurs due to the formation of hydrophobic domains as a result of micellization above a critical micellization temperature (CMT).[30] Not only has the solubility of poorly water soluble therapeutics been found to be enhanced in thermogelling materials, sustained release may also be achieved.[31] One study found the release of liraglutide from thermogelling poly(lactic-co-glycolic acid)-PEG-poly(lactic-co-glycol acid) (PLGA-PEG-PLGA) tri-block copolymers was sustained over a course of 8 days.[11] There are few studies which investigate the incorporation of hydrophilic drugs into thermogelling formulations. In one such study the total release of insulin, a water-soluble

peptide, from an injected PLGA-PEG-PLGA thermogelling drug delivery depot was achieved after 4 days.[32] The insulin was not absorbed into the core of the micelles formed with an increase in temperature, but the aqueous fluid which surrounded them. The slowed release was a result of the increased viscosity and the circuitous route the insulin must take to be liberated from the gel.

Several factors contribute to drug liberation from thermogels, including diffusion and gel erosion.[33] Therapeutics diffuse out of the gels due to the concentration gradient between the gel and the surrounding media, as described by Fick's laws of diffusion.[34] Fick's first law of diffusion relates flux, which is the amount of solute released per unit of area per unit of time, to the diffusion coefficient, concentration and diffusion path length.[35] The diffusion coefficient is dependent on the viscosity of the continuous medium and the size of the diffusing molecule/particle, where viscous fluids and large molecules/particles slow drug diffusion rates.[36] In addition to this, the relative lipophilicity of therapeutics also impacts their liberation from gel matrices.[37] Hydrophobic therapeutics experience a slow release from thermogelling poloxamer 407 formulations because of their greater affinity to the hydrophobic core of the micelles, rather than the extra-micellar aqueous media.[38] Hydrophilic therapeutics, however, will preferentially reside in the extra-micellar water of the thermogel over the hydrophobic cores.[39] As a result of this, the release of hydrophilic therapeutics from thermogelling formulations occurs relatively quickly when compared to hydrophobic drugs.[8] There are two factors which impact the diffusion rate of hydrophilic drugs from gelled systems; the sample viscosity at elevated temperature and the tortuosity of the route the therapeutic must take.[40] In addition to diffusion, gel erosion is also responsible for the release of therapeutics. Gels erode due to a relative reduction in the local micelle concentration at the interface with surrounding media, when compared to the bulk.[41] The low concentration of unimer in the bulk solution results in a drive for micelle to unimer transition at the interface, and a subsequent drug release.[42] It has also been demonstrated that some thermogelling materials shed micelles from their interface where the CMC may be exceeded in the bulk,[43] giving differential release from the gel and micelle phases. In this chapter, the release of hydrophilic and hydrophobic therapeutics from poloxamer 407, PNIPAM10-PEG10-PNIPAM10 and PDEA20-PEG10-PDEA20 thermogelling solutions will be investigated and modelled to understand release behaviour. This, in turn, will demonstrate the potential of these novel thermogelling materials in topical drug delivery.

[7.2] Aims and Objectives

The aim of this phase of research was to investigate PNIPAM10-PEG10-PNIPAM10 (50 % w/v) and PDEA20-PEG10-PDEA20 (30 % w/v in 0.3 M NaCl) for topical drug delivery compared to poloxamer 407 (20 % w/v), using tenofovir disoproxil fumarate and progesterone as model hydrophilic and hydrophobic active pharmaceutical ingredients (APIs), respectively. This investigation was achieved by:

- Calculation of solubilising power of the tri-block copolymers in aqueous solution at two temperatures, 25 and 37 $^{\circ}$C.
- Investigation of the saturation solubility of progesterone and tenofovir disoproxil fumarate in the thermogelling materials at 25 and 37 $^{\circ}$C.
- Studying the release of progesterone and tenofovir disoproxil fumarate from the thermogelling materials at 25 and 37 $^{\circ}$C using Franz diffusion cells.

[7.3] Materials

Potassium phosphate monobasic monohydrate (99 %) and tenofovir disoproxil fumarate (98 %) were purchased from Acros Organics (U.K) and were used as purchased. HPLC grade acetonitrile, sodium chloride (NaCl) (99.5 %), potassium hydroxide (KOH) (99%) and absolute ethanol (99 %) were purchased from Fisher Scientific (U.K) and were used as provided. Poloxamer 407 and progesterone (99 %) were purchased from Sigma (U.K) and were used as provided. PNIPAM10-PEG10-PNIPAM10 and PDEA20-PEG10-PDEA20 were synthesised as described in chapter 5. In the case of PDEA20-PEG10-PDEA20, PDEA20-PEG10-PDEA20 (30 %) denotes 30 % w/v in 0.3 M NaCl, while poloxamer 407 (20 %) and PNIPAM10-PEG10-PNIPAM10 (50 %) denote 20 and 50 % w/v in aqueous solution.

[7.4] Methods

[7.4.1] HPLC Methods

[7.4.1.1] Progesterone HPLC Method

The detection and quantification of progesterone using HPLC was performed on an Agilent 1260 Infinity system with a UV-Vis detector using a method from the literature.[44] The method used reverse-phase chromatography with an Agilent ZORBAX Rapid Resolution High Definition C18 1.8 μm column (150 x 4.6 mm). The mobile phase was acetonitrile and 0.03 M potassium phosphate monobasic monohydrate buffer adjusted to pH 6.4 at a flow rate of 1 mL/min. The buffer solution was prepared by dissolving potassium phosphate monobasic monohydrate (4.08 g) in HPLC grade water (950 mL) and adjusted to pH 6.4 using 1 M KOH. The mobile phase was then made up to 1 L volume in volumetric glassware. The composition of the mobile phase was varied during the run as shown in Table 7.1. An injection volume of 10 μL was used for all calibration samples and detection was carried out at 225 nm. A series of ten progesterone calibration samples between 2 and 20 mg/mL were prepared using a diluent of acetonitrile and water (70:30 v/v).

Table 7. 1: The gradient programme used for the HPLC analysis of progesterone.

Time	% A Buffer (v/v)	% B Acetonitrile (v/v)	Solvent mode
0.00	75	25	Isocratic
2.00	75	25	Isocratic
12.00	10	90	Gradient
12.01	75	25	Isocratic

[7.4.1.2] Tenofovir Disoproxil Fumarate HPLC Method

The detection and quantification of progesterone using HPLC was performed on an Agilent 1260 Infinity system with a UV-Vis detector using methods from the literature.[45] The method used reverse-phase chromatography with an Agilent ZORBAX Rapid Resolution High Definition C18 1.8 μm column (150 x 4.6 mm) and an acetonitrile and water (75:25 v/v) at a flow rate of 1 mL/min. An injection volume of 10 μL was used for all calibration samples, the run time was 5 min and the tenofovir disoproxil fumarate detection was carried out at 259 nm. A series of tenofovir disoproxil fumarate calibration samples were prepared between 2 and 20 mg/mL using the same mixture of acetonitrile and water as was used for the mobile phase.

[7.4.2] HPLC Method Validation

The progesterone and tenofovir disoproxil fumarate HPLC calibrations were performed in triplicate and the average response for each concentration was used to build the calibration. The calibrations were accepted if the correlation coefficient (R^2) was greater than 0.9995. The precision and percent accuracy of the HPLC methods were evaluated using three concentrations of analyte at low, medium and high concentration (5, 9 and 17 mg/mL). The three concentrations were prepared freshly on three consecutive days and injected 6 times each. The method was deemed precise if the relative standard deviation (RSD) of the 6 injections was less than or equal to 2 %. The percent accuracy of the HPLC calibrations were calculated by dividing the known concentration of the standard by the calculated concentration using the HPLC calibration and multiplying by 100 (Equation 7.1). The method was deemed accurate if the mean percent accuracy was between 98 and 102 % with an RSD equal or less than 2 %.

$$\text{Equation 7.1: Percent Accuracy} = \left(\frac{\text{Measured Concentration}}{\text{Theorectical Concentration}} \right) \text{x } 100$$

The limit of detection (LOD) and limit of quantification (LOQ) were calculated using Equations 7.2 and 7.3 respectively. Both the LOD and LOQ are calculated by dividing the standard error of the Y intercept by the slope of the linear calibration graph and multiplying these by 3.3 and 10 respectively.

$$\text{Equation 7.2: LOD} = \left(\frac{\text{Standard Error of the Y intercept}}{\text{Slope}} \right) \text{x } 3.3$$

$$\text{Equation 7.3: LOQ} = \left(\frac{\text{Standard Error of the Y intercept}}{\text{Slope}} \right) \text{x } 10$$

[7.4.3] Investigation of the Influence of Tri-block Copolymer on the Solubility of Progesterone and Tenofovir Disoproxil Fumarate

The effect of polymer concentration on drug solubility was investigated at both 25 and 37 °C. Polymer solutions (1 mL) ranging from 0.005 to 10 mg/mL were transferred to sample vials and either progesterone or tenofovir disoproxil fumarate (ca 5 mg) were added. The vials were then placed in a water bath at either 25 or 37 °C and were stirred for 24 h. If the polymer solution was

clear after 24 h, more drug was added and the vials were left again for 24 h under constant stirring, this process was repeated until the solutions remained turbid for 24 h. The turbid solutions were then centrifuged at 13,400 rpm for 10 min, and the supernatant was then analysed by HPLC. If the polymer resulted in an increase in drug solubility, the critical micelle concentration (CMC) was calculated as the concentration where drug solubility increased (Equation 7.4). The X intercept was calculated using the Y intercept and gradient of two linear lines of best fit to the data, one where the drug solubility was independent of polymer concentration ("Flat Line") and one where drug solubility increased with polymer concentration ("Increased Solubility"). The CMC, drug concentration in water (DW) and drug concentration at the greatest concentration of polymer in solution (DPS) was used to calculate the solubilising power (SP) of the polymer using Equation 7.5. Each of these polymer concentrations were investigated in triplicate and data is presented as mean ± standard deviation.

$$\text{Equation 7.4: CMC} = \left(\frac{\text{Intercept of Increased Solubility} - \text{Intercept of the Flat Line}}{\text{Gradient of Increased Solubility} - \text{Gradient of the Flat Line}} \right)$$

$$\text{Equation 7.5: SP} = \left(\frac{\text{DPS} - \text{DW}}{\text{Polymer Concentration} - \text{CMC}} \right)$$

[7.4.3.1] Dynamic Light Scattering of the Tri-block Copolymers in the Presence of Progesterone

Dynamic light scattering (DLS) was performed on a Malvern Zetasizer Nano ZS. Polymer solutions (5 mg/mL) were saturated with progesterone (10 mg) and stirred at 37 °C for 24 h. After 24 h the solution was still turbid and then passed through a syringe filter (0.45 μm). Size was measured in triplicate at 20, 22, 24, 26, 28, 30, 32, 34, 36, 38 and 40 °C. The hydrodynamic diameter and PDI were then averaged and plotted as a function of temperature.

[7.4.4] Investigation of the Saturation Solubilities of Progesterone and Tenofovir Disoproxil Fumarate in the Tri-block Copolymers and Water

The thermogelling materials (20 % w/v poloxamer 407, 50 % w/v PNIPAM10-PEG10-PNIPAM10 or 30 % PDEA20-PEG10-PDEA20 in 0.3 M NaCl) were prepared and stored in the fridge overnight. On the following day, 1 mL of thermogelling material solution or water was transferred to a sample vial and progesterone or tenofovir disoproxil fumarate (ca 5 mg) added. The solutions were then stored in a water bath at either 25 or 37 °C with constant stirring. If after 24 h the solution was clear, more drug was added and again left for 24 h in the water bath with constant stirring. This process was repeated until the solution remained turbid for 24 h. Excess drug was then removed by centrifugation (10 min at 14500 rpm) and the clear supernatant was analysed by HPLC. Each experiment was performed in triplicate.

[7.4.5] Release studies of Progesterone and Tenofovir Disoproxil Fumarate from the Tri-block Copolymer Formulations

The release of progesterone and tenofovir disoproxil fumarate from the thermogelling materials (20 % w/v poloxamer 407 , 50 % w/v PNIPAM10-PEG10-PNIPAM10 or 30 % PDEA20-PEG10-PDEA20 in 0.3 M NaCl) was investigated using Franz diffusion cells equipped with a cellulose membrane (MWCO 3.5 kDa) at both 25 and 37 °C. The experiments used Franz cells with an average phosphate buffer saline (PBS) receiver fluid volume of 10 mL and an average bore area of 174 mm^2. The release of 50 µg/mL progesterone or tenofovir disoproxil fumarate was investigated, where this concentration did not violate sink conditions. A 20 % w/v ethanol solution in PBS containing 50 µg/mL progesterone and a 50 µg/mL tenofovir disoproxil fumarate solution in PBS were used as controls. The Franz cells were then placed into a water bath for 30 min to allow the receiver fluid to reach the temperature of the surrounding water (25 or 37 °C). All Franz cells were dosed with 200 µL of sample and the release of drug measured at regular intervals by sampling receiver fluid (1000 or 200 µL for the progesterone and tenofovir disoproxil fumarate respectively). Receiver fluid was replaced with an equal volume of pre-warmed PBS. The samples were analysed by HPLC. The experiment was repeated 4 times.

[7.4.6] Rheology of the Tri-block Copolymer Solutions Containing Either Progesterone or Tenofovir Disoproxil Fumarate

Rheology was conducted using a TA AR 1500 ex rheometer with a Julabo AWC 100 cooling unit equipped with a 40 mm parallel plate geometry. The gap between the Peltier plate and geometry

was 650 μm, and a frequency of 1 Hz and oscillatory stress of 1 Pa was used for all experiments. The rheology of the thermogelling solutions (20 % poloxamer 407, 50 % PNIPAM10-PEG10-PNIPAM10 or 30 % PDEA20-PEG10-PDEA20 in 0.3 M NaCl) with progesterone or tenofovir disoproxil fumarate (50 μg/mL) was investigated. The tri-block copolymer solutions (~ 1 mL) were placed upon the peltier plate and the geometry was lowered to the gap distance. The temperature of the sample was then raised from 20 to 50 °C at a ramp rate of 2 °C per minute. The gelation temperature was taken as the point at which G' exceeded G'' and the gel strength was taken as the G' maximum. The rheology experiments were performed once.

[7.5] Results and Discussion

[7.5.1] HPLC Calibration and Validation

A progesterone HPLC method was identified from the literature, designed for the separation of structurally similar estrone, estradiol, estriol and progesterone.[44] The reported run time was 23 min and progesterone eluted after 16.2 min. In this study, the total run time was reduced to 16 min, with the HPLC sequence adjusted proportionally, and the progesterone elution time was reduced to 12.3 min. The progesterone peak was symmetrical in shape and exhibited no tailing, indicating the column was separating effectively and was not overloaded[46] (Figure 7.2a). In addition to the detection of progesterone, another peak was observed at ca. 14.5 min which is due to absorbance of the potassium phosphate buffer component which absorbs light at 225 nm.[47] This peak was confirmed to not be progesterone as the peak was independent of progesterone concentration. This peak is detected as a result of a drastic change in mobile phase composition, where the percent of buffer increases from 10 to 75 % after 12 min.

The HPLC column was calibrated over a concentration range of 2 – 20 μg/mL. The calibration was linear across this range with an r^2 of 0.9997 and was deemed acceptable for quantification analysis (Figure 7.2b). The LOD and LOQ were calculated to be 0.35 and 1.05 μg/mL using equations 7.2 and 7.3 respectively, and any values obtained beneath the LOQ in future experiments were reported as not quantifiable. The progesterone HPLC method was deemed both precise and accurate as the RSD of the replicate injections was less than 2 % and the percent accuracies of the 5, 9 and 17 μg/mL standards were 98.8, 98.2 and 98.0 % respectively.

a)

b)

y = 41.38x + 10.091
R² = 0.9997
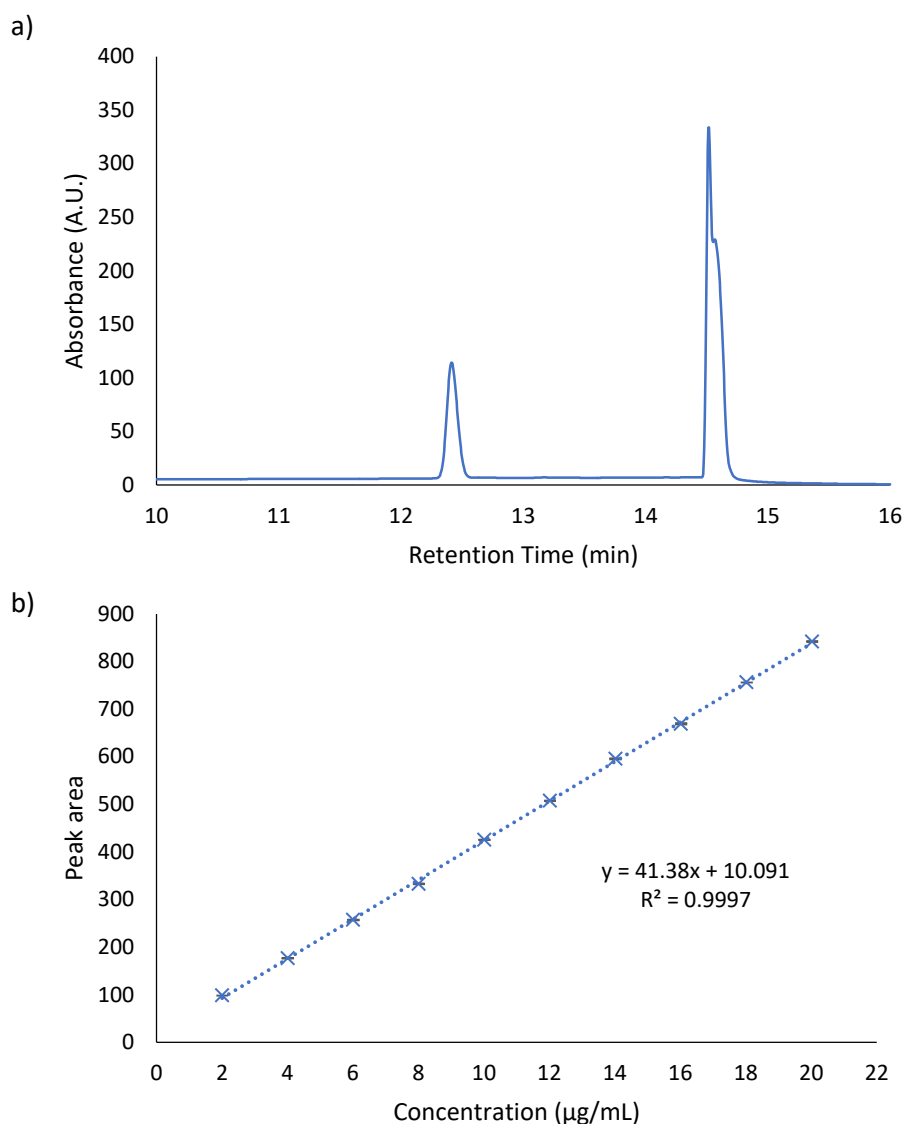
Figure 7. 2: A HPLC chromatogram for the analysis of progesterone (retention time: 12.41 min) (a) and the linear calibration (b) using progesterone standards with concentrations ranging from 2 – 20 µg/mL in 70:30 acetonitrile: water. The calibration data is presented as mean ± standard deviation (n=3), with an R^2 of 0.9997.

The tenofovir disoproxil fumarate HPLC method had a run time of 5 min and eluted from the HPLC column after 1.91 min. The peak was symmetrical and exhibited no tailing, indicating the column was not degraded or overloaded (Figure 7.3a)[46] The HPLC was calibrated over 2-20 µg/mL concentrations of tenofovir disoproxil fumarate. The calibration was linear across this concentration range with an r^2 of 0.9997 (Figure 7.3b). The LOD and LOQ of this calibration were found to be 0.37 and 1.13 µg/mL respectively. The average area of the tenofovir disoproxil fumarate peaks were

found to have an RSD less than 2 %. The percentage accuracy of the 5, 9 and 17 µg/mL standards were found to be 98.9, 98.1 and 98.5 % respectively with RSD less than 2 % and as such was deemed appropriate for quantification analysis.

a)

b)
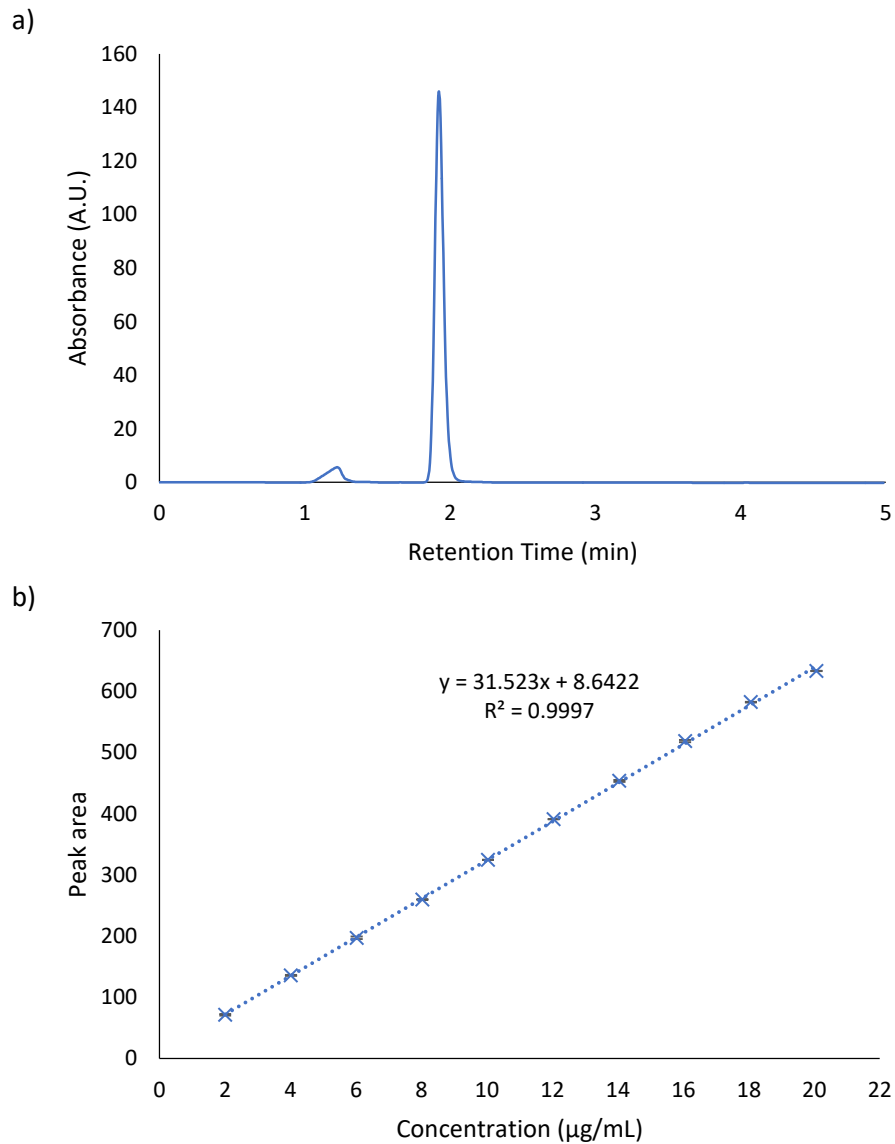
Figure 7. 3: A HPLC chromatogram for the analysis of tenofovir disoproxil fumarate (retention time: 1.92 min) (a) and the linear calibration (b) using tenofovir disoproxil fumarate standards ranging in concentration from 2 – 20 µg/mL in 75:25 acetonitrile: water. The calibration data is presented as mean ± standard deviation (n=3), with an r^2 of 0.9997.

[7.5.2] The Solubility of Progesterone and Tenofovir Disoproxil Fumarate in Dilute Tri-block Copolymer Aqueous Solutions

The thermoresponsive polymers were evaluated for their ability to solubilise two drugs relevant to intravaginal drug delivery: progesterone and tenofovir disoproxil fumarate. Progesterone and tenofovir disoproxil fumarate were selected as they have large differences in their water solubilities. Progesterone was determined to have a water solubility of 9.8 ± 0.1 μg/mL at 25 °C, whilst tenofovir disoproxil fumarate's solubility was approximately 1000-fold greater at 9.5 ± 1.0 mg/mL. Both values of solubility were in agreement with the reported values of 8.81 μg/mL[4] and 13.4 mg/mL (in distilled water of unreported pH),[48] respectively. The solubilities of the two drugs in the presence of the polymers at a range of concentrations between 5 μg/mL and 10 mg/mL were determined at 25 and 37 °C.

For progesterone, it was found that for all three tri-block copolymers, the solubility of progesterone was greatly increased above a critical concentration, believed to be the critical micelle concentration (CMC) (Figure 7.4). The CMC could then be extracted from the data, giving values of 1.88, 0.26 and 2.45 mg/mL at 25 °C for and poloxamer 407, PNIPAM10-PEG10-PNIPAM10 and PDEA20-PEG10-PDEA20 respectively, which rose to 1.95, 0.68 and 4.13 mg/mL at 37 °C. The CMC of poloxamer 407 is on the same order of magnitude as that reported previously (ca 3 mg/mL) for the pure polymer,[49] and the deviation is attributed to the presence of progesterone, as reported for other drugs.[50] Above this concentration which is believed to be the CMC, the solubility of progesterone in all tri-block copolymers increases at both 25 and 37 °C. This is thought to be due to solubilisation of the hydrophobic progesterone into the hydrophobic micelle cores. Micelles are well known to improve the solubility of hydrophobic therapeutics.[51,52]
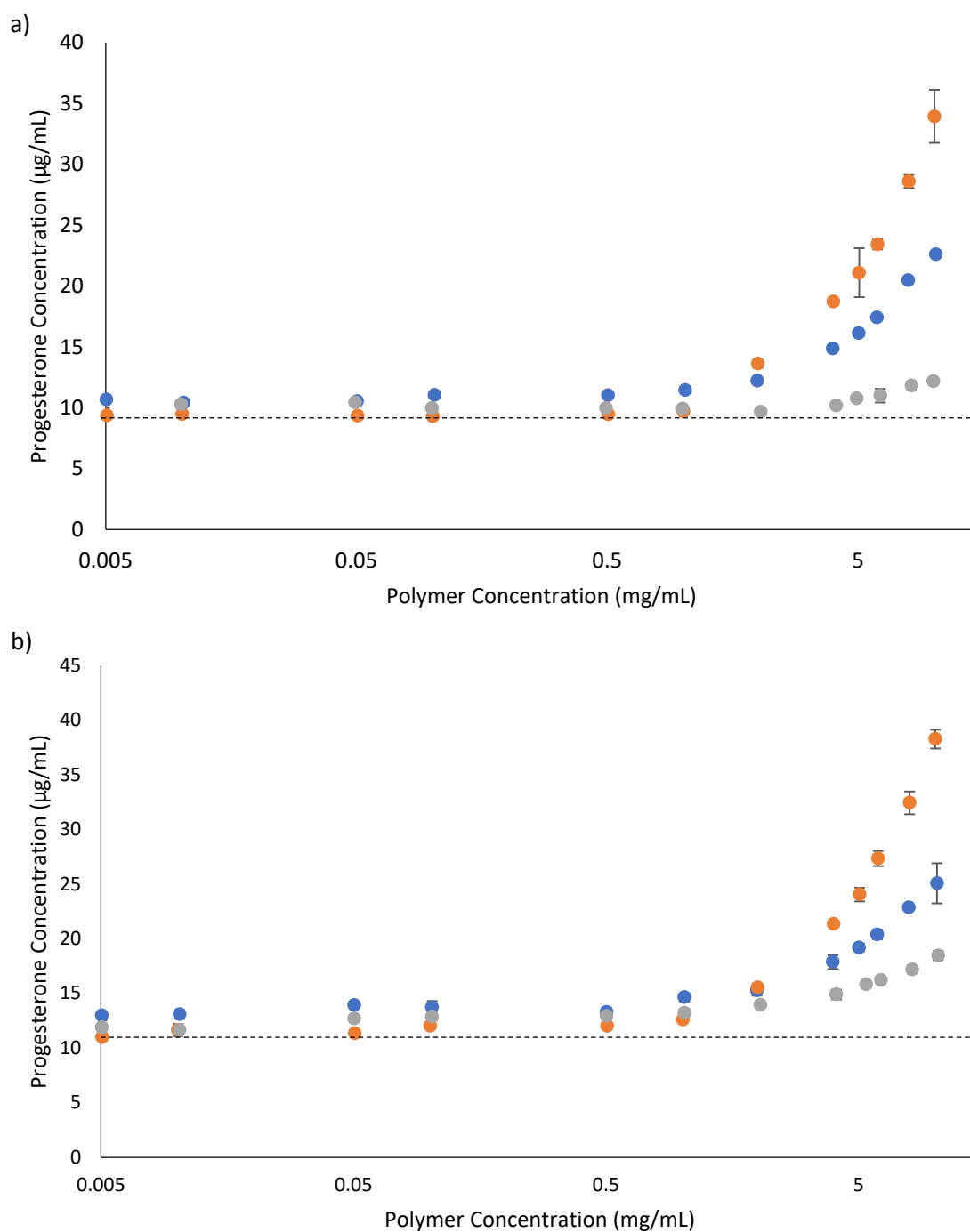
Figure 7. 4: The solubility of progesterone at 25 (a) and 37 °C (b) in aqueous solutions of poloxamer 407 (blue), PNIPAM10-PEG10-PNIPAM10 (orange) and PDEA20-PEG10-PDEA20 (grey) at concentrations ranging from 5 μg/mL to 10 mg/mL. The black dashed line represents the solubility of progesterone in aqueous solution without polymer present. Data presented as mean ± standard deviation (n=3).

Dynamic light scattering revealed a pronounced influence of progesterone on the micellization of both tri-block copolymers PNIPAM10-PEG10-PNIPAM10 and PDEA20-PEG10-PDEA20 (Figure 7.5). Solutions of PNIPAM10-PEG10-PNIPAM10 and PDEA20-PEG10-PDEA20 at 10 mg/mL exhibited no detectable particulates at 25 °C but when warmed to 40 °C transitioned to produce nanoparticles. In the presence of progesterone, PNIPAM10-PEG10-PNIPAM10 (Figure 7.5a) and PDEA20-PEG10-PDEA20 (Figure 7.5c) nanoparticle aggregates were detected at 25 °C with average hydrodynamic diameters of 15.1 ± 0.4 and 21.5 ± 0.2 nm, respectively. These PNIPAM10-PEG10-PNIPAM10 and PDEA20-PEG10-PDEA20 nanoparticles remained a constant size until a transition at 37 and 32 °C, respectively. Above these temperatures a pronounced increase in aggregate size was observed for both tri-block copolymers, where the hydrodynamic diameter rose to 69.0 ± 6.5 and 52.7 ± 0.7 nm for PNIPAM10-PEG10-PNIPAM10 and PDEA20-PEG10-PDEA20, respectively. The aggregates formed by PNIPAM10-PEG10-PNIPAM10 and PDEA20-PEG10-PDEA20 without progesterone had hydrodynamic diameters of 63.6 ± 10.4 and 54.5 ± 0.7 nm, respectively. These were not statistically different to the size of the aggregates observed in the presence of progesterone ($p < 0.05$). Thus, it is hypothesised that the presence of progesterone drives the formation of micellar nanoparticles for both PNIPAM10-PEG10-PNIPAM10 and PDEA20-PEG10-PDEA20. These aggregates form below the LCST-type transition of PNIPAM and PDEA, which, when triggered by a rise in temperature, leads to the aggregation or rearrangement of these micelles.
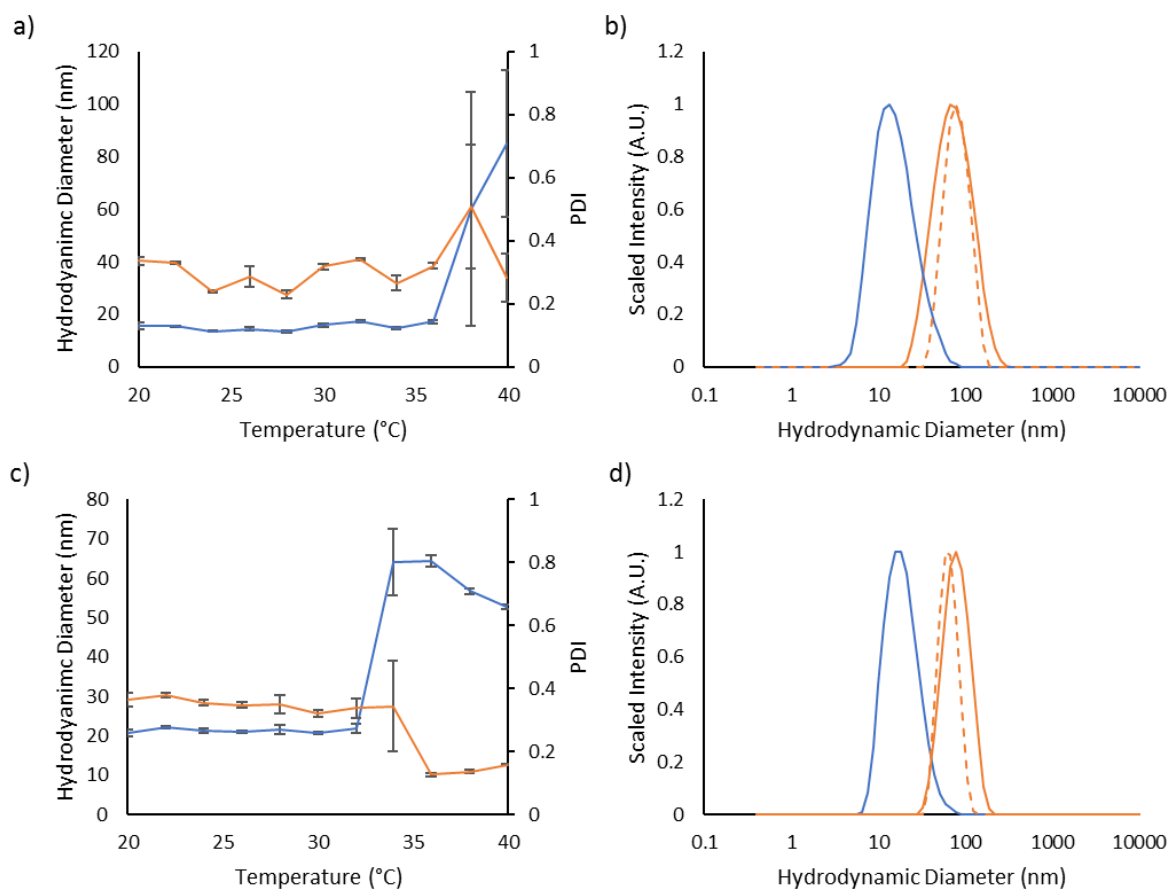
Figure 7. 5: The change in hydrodynamic diameter (blue) and PDI (orange) for PNIPAM10-PEG10-PNIPAM10 (a) and PDEA20-PEG10-PDEA20 (c) at 10 mg/mL saturated with progesterone presented as mean ± standard deviation (n=3). The particle size distribution graphs for PNIPAM10-PEG10-PNIPAM10 (b) and PDEA20-PEG10-PDEA20 (d) showing the size distribution of saturated progesterone samples at 25 (blue) and 40 °C (solid orange) and without progesterone at 40 °C (dashed orange).

The solubilising power of the polymer/drug mixtures were calculated from the progesterone solubilisation data in Figure 7.4 and are included in Table 7.2.[53] Briefly, the solubilising power reflects the unit mass increase in progesterone solubilised per unit mass of polymer. PNIPAM10-PEG10-PNIPAM10 had a solubilising power approximately 1.5-fold greater than poloxamer 407 at both temperatures. This difference was demonstrated to be statistically significant by two-way ANOVA with Bonferroni post-hoc testing (p<0.0001). PDEA20-PEG10-PDEA20 however, exhibited a solubilising power at 25 °C less than poloxamer 407 but at 37 °C the solubilising power was significantly greater. It is known that the greater the molecular weight of the relatively hydrophobic poly(propylene oxide) domains, the greater the solubilising power of poloxamers.[50] The microphase

separated domains in PNIPAM10-PEG10-PNIPAM10 and PDEA20-PEG10-PDEA20 are 20 and 40 kDa respectively, which are greater than the poly(propylene oxide) in poloxamer 407 (3.7 kDa) which may lead to a greater solubilising power. These considerations are balanced against the free energy of the solubilisation process, which will differ between the three polymers.[50]

A statistically significant ($p < 0.05$) increase in the mean value of solubilising power was only observed for PNIPAM10-PEG10-PNIPAM10 and PDEA20-PEG10-PDEA20. As no structural transition was observed between 25 and 37 °C for PNIPAM10-PEG10-PNIPAM10 by dynamic light scattering, it is hypothesised that this small increase is the result of entropic effects favouring polymer-progesterone interactions at the elevated temperature. This is suspected to be as a result of reorganisation of the aggregates formed around the progesterone, as previously seen in the literature for drugs including ibuprofen, aspirin and erythromycin.[30] This reorganisation did not increase the total volume available to solubilise the progesterone, and as such the solubilising power did not change. Whereas the increase in solubilising power from $0.70 \pm 0.10 \times 10^{-3}$ to $1.45 \pm 0.07 \times 10^{-3}$ observed for PDEA20-PEG10-PDEA20 is likely due to the formation of larger aggregates above 32 °C. This LCST type transition is hypothesized to result in the formation of hydrophobic domains which enhance the solubility of the progesterone.

Table 7. 2: The solubilising power at both 25 and 37 °C for progesterone in poloxamer 407, PNIPAM10-PEG10-PNIPAM10 and PDEA20-PEG10-PDEA20. Data presented at mean ± standard deviation (n=3).

Polymer	Solubilising Power (x10^{-3})	
	25 °C	37 °C
Poloxamer 407	1.53 ± 0.07	1.65 ± 0.22
PNIPAM10-PEG10-PNIPAM10	2.73 ± 0.24	3.04 ± 0.11
PDEA20-PEG10-PDEA20	0.70 ± 0.10	1.45 ± 0.07

The solubility of tenofovir disoproxil fumarate was decreased by the addition of polymer, even above the CMCs (Figure 7.6). Statistical analysis using 2-way ANOVA determined the solubility of tenofovir disoproxil fumarate was significantly reduced at both 25 and 37 °C upon surpassing 0.1 mg/mL poloxamer 407 ($p < 0.05$) and PDEA20-PEG10-PDEA20 ($p < 0.05$) solution, when compared to the pure aqueous solution. While, for PNIPAM10-PEG10-PNIPAM10 statistical analysis concluded that the concentration of tenofovir disoproxil fumarate did not significantly decrease at 37 °C with

increasing polymer concentration but did above a polymer concentration of 0.1 mg/mL at 25 °C (p<0.05). The solubility for tenofovir disoproxil fumarate in water increased 1.6-fold, while for 10 mg/mL solutions of poloxamer 407, PNIPAM10-PEG10-PNIPAM10 and PDEA20-PEG10-PDEA20 the increase was 2.0-fold. This 2-fold increase is thought to be as a result of an increase in the number of water molecules free to solvate the tenofovir disoproxil fumarate. Below the CMT, water molecules are solvating the temperature responsive polymer chains and as such are not available to solvate the API, but upon surpassing the CMT, this water is released and therefore, free to solvate more tenofovir disoproxil fumarate. Conversely, without polymer present, the number of free water molecules does not change and the increase in solubility at 37 ° is as a result of increased kinetic energy within the system alone.

Taken as a whole, the solubilising power data indicates that the formation of micelles occurs for all polymers above their CMC at 25 and 37 °C, at which point the micelles provide a locus for solubilisation for the relatively hydrophobic progesterone. Tenofovir disoproxil fumarate, however, is suspected to be largely excluded from the micelle as the solubility was not enhanced by the increase in polymer concentration. The solubilities of both drugs are increased at 37 °C, above and below the critical micelle concentration, with a more pronounced effect seen in tenofovir disoproxil fumarate where the solubility in water increased from 9.5 ± 1.0 to 15.6 ± 0.9 mg/mL. This is attributed to its enhanced water solubility at this temperature.

a)

b)

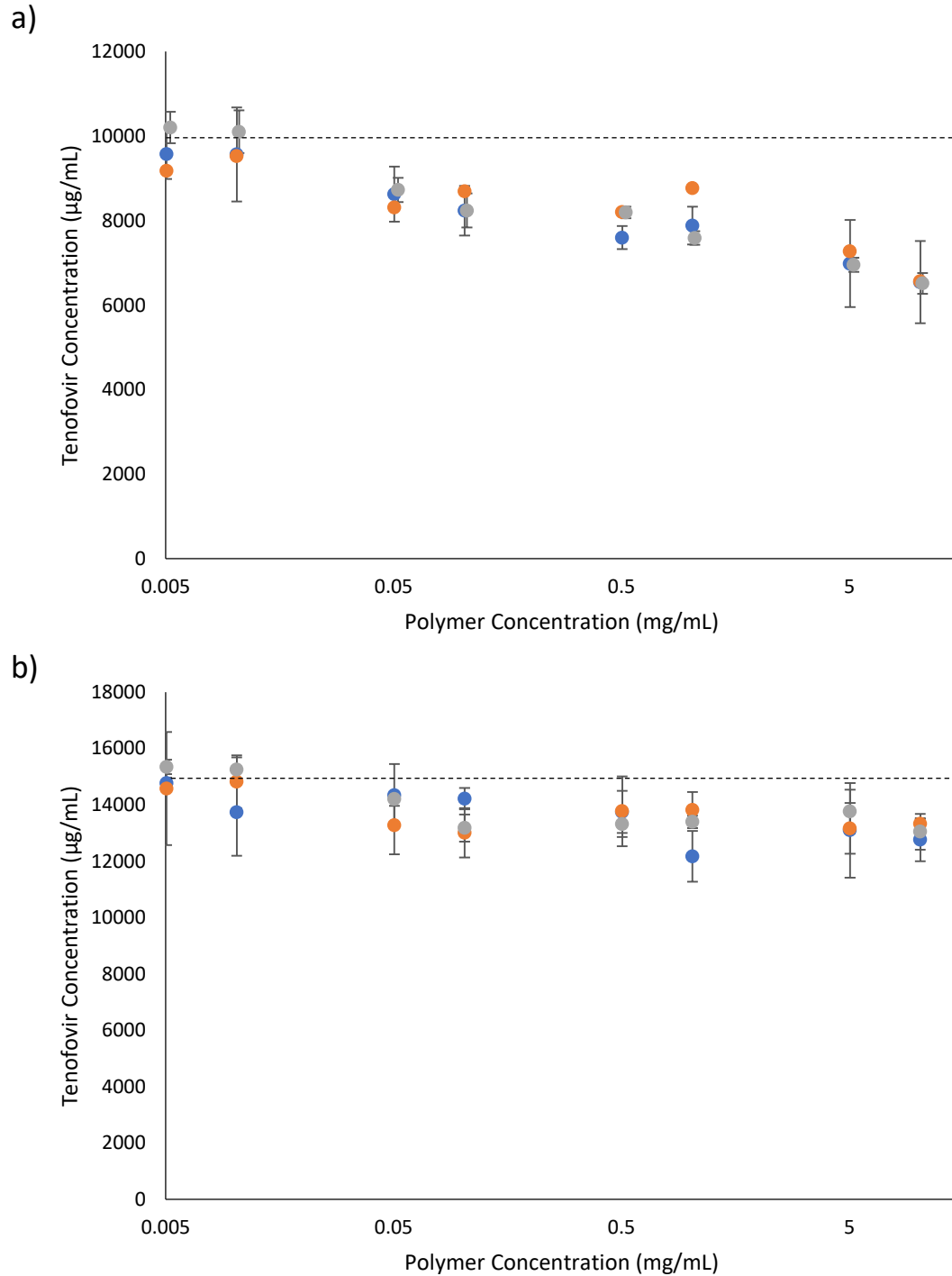Figure 7. 6: The solubility of tenofovir disoproxil fumarate at 25 (a) and 37 °C (b) in aqueous solutions of poloxamer 407 (blue), PNIPAM10-PEG10-PNIPAM10 (orange) and PDEA20-PEG10-PDEA20 (grey) at concentrations ranging from 5 µg/mL to 10 mg/mL. The black dashed line represents the solubility of tenofovir disoproxil fumarate in aqueous solution without polymer present. Data presented at mean ± standard deviation (n=3).

[7.5.3] The Saturated Solubility of Progesterone and Tenofovir Disoproxil Fumarate in Concentrated Tri-block Copolymer Aqueous Solutions

The saturation solubilities of progesterone and tenofovir disoproxil fumarate were then evaluated in the thermogelling materials at the high concentrations required for gelation (Figure 7.7a). Saturation solubility has important implications for drug delivery across a membrane, where liberation of drug from a dosage form is dictated by its thermodynamic activity within that base.[54] The greater the degree of saturation, the greater the driving force for liberation. If progesterone is loaded into the solutions at room temperature then applied to the body and warmed then the thermodynamic activity is expected to decrease, thus liberation from the dosage form is expected to be slowed at this higher temperature, which may allow for controlled release applications. The saturation solubility of progesterone in PBS showed a relatively minor in increase from 8.9 ± 0.7 to 11.3 ± 0.2 μg/mL with an increase in temperature from 25 to 37 °C. While progesterone solubility in the poloxamer 407 (20 % w/v), PNIPAM10-PEG10-PNIPAM10 (50 % w/v) and PDEA20-PEG10-PDEA20 (30 %) polymer solutions was dramatically enhanced at 37 °C, relative to 25 °C. The saturation solubility of progesterone at 37 °C in poloxamer 407 (20 %), PNIPAM10-PEG10-PNIPAM10 (50 %) and PDEA20-PEG10-PDEA20 (30 %) were found to be 505.0 ± 7.8, 504.8 ± 30.2 and 323.7 ± 8.0 μg/mL, respectively. Extrapolation of the solubility shown in dilute solution above in section 7.5.2 would suggest PNIPAM10-PEG10-PNIPAM10 would result in a greater progesterone saturation solubility than poloxamer 407. Despite this and the differences in concentration between poloxamer 407 and PNIPAM10-PEG10-PNIPAM10, progesterone saturation solubility was equivalent. The similarity in saturation solubility may be as a result of the molarities of the two solutions, which were approximately 16.5 and 18.2 mM for poloxamer 407 and PNIPAM10-PEG10-PNIPAM10, respectively. With such similar molarities, the hydrophobic volume may be similar within each formulation, allowing for dissolution of similar quantities of progesterone. In addition to this, PDEA20-PEG10-PDEA20 exhibited a similar solubilising power to poloxamer 407 and a greater polymer concentration of 30 % (w/v) and as such was expected to exhibit a greater saturated solubility of progesterone, but this was not observed. The unexpected saturation solubilities were hypothesised to be due to differences in nanostructure and hydrophobic volume of PNIPAM10-PEG10-PNIPAM10 and PDEA20-PEG10-PDEA20 in dilute and concentrated solutions. It is known that poloxamer exists as spherical micelles of approximately 10 nm diameter across a wide range of concentrations, however the nanostructure of the PNIPAM10-PEG10-PNIPAM10 and PDEA20-PEG10-PDEA20 materials at 50 and 30 % (w/v) respectively has never been studied. Literature has shown the nanostructure and symmetry of micellar aggregates formed by surfactants may vary depending on concentration.[55] Asymmetric aggregates have been shown to exhibit a larger volume and as such may increase the solubilisation of drugs.[56] In dilute solution, PNIPAM10-PEG10-PNIPAM10 and

PDEA20-PEG10-PDEA20 were found to form aggregates with hydrodynamic diameters of 69.0 ± 6.5 and 52.7 ± 0.7 nm, respectively, which are significantly larger than the reported approximate 10 nm diameter of poloxamer 407 aggregates. Thus, it is theorised that the aggregates formed by PNIPAM10-PEG10-PNIPAM10 and PDEA20-PEG10-PDEA20, in concentrated solution may be much smaller than in dilute solution, resulting in reduced micelle hydrophobic volume and as a consequence, a reduced progesterone solubility.

Tenofovir disoproxil fumarate is largely excluded from the micelles and can be found in the aqueous solution surrounding the micelles. As such the increase in solubility observed in these polymers at elevated temperatures is attributed solely to the improvement in solubility caused by heat alone (Figure 7.7b). The reduction in solubility seen in the polymer samples is attributed to the decreased volume fraction of water in these mixtures, which agrees with what was seen in dilute solution. Adjusting for the phase volume of water accounts for this depression. The adjusted saturated solubilities for poloxamer 407, PNIPAM10-PEG10-PNIPAM10 and PDEA20-PEG10-PDEA20 were 11946 ± 731, 13688 ± 1731 and 11490 ± 617 µg/mL, respectively. These were not statistically different to the saturated solubility of tenofovir disoproxil fumarate in water which was 12269 ± 394 µg/mL.

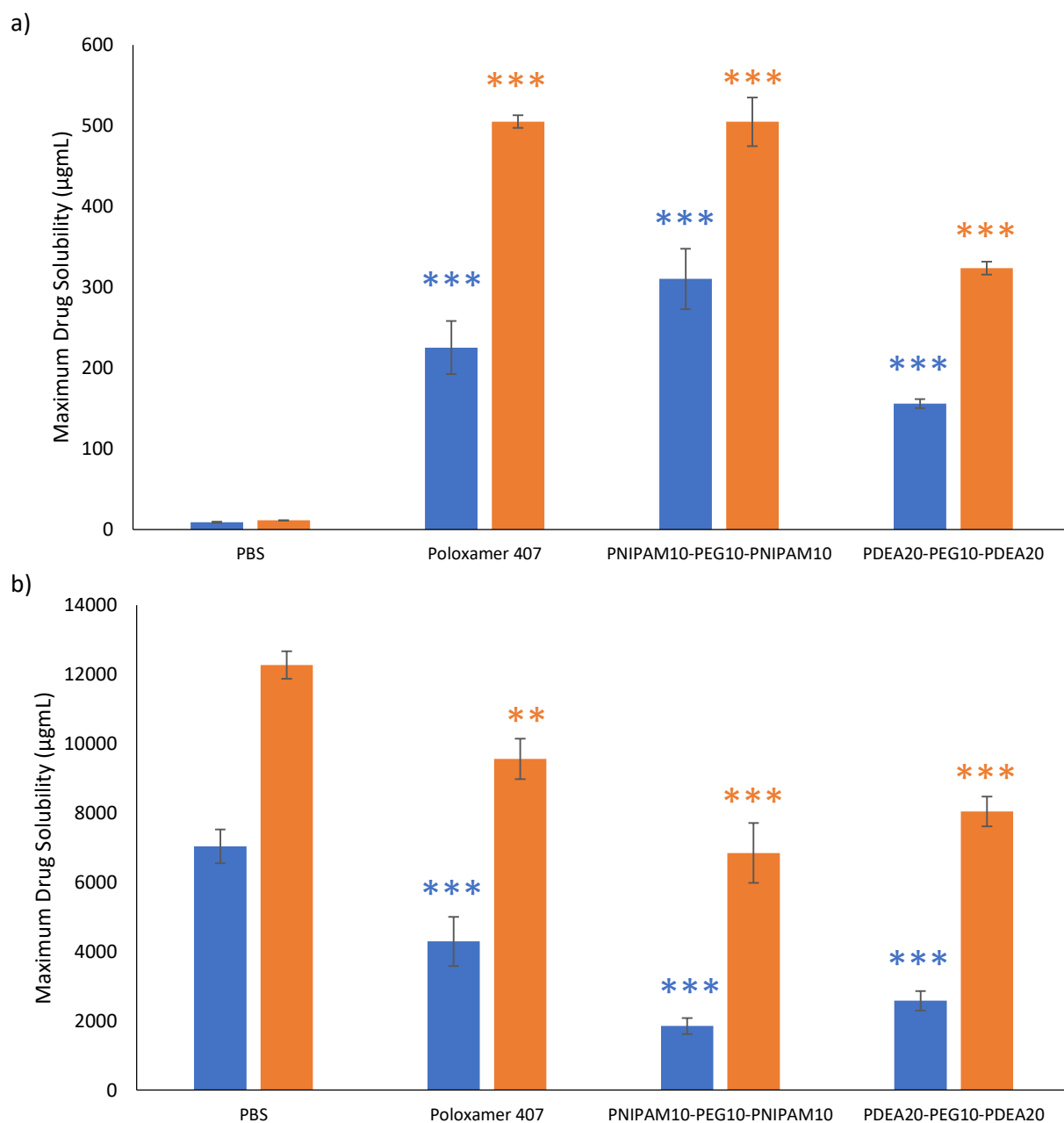Figure 7. 7: The saturated solubility of progesterone (a) and tenofovir disoproxil fumarate (b) in PBS, poloxamer 407 (20 %), PNIPAM10-PEG10-PNIPAM10 (50 %) and PDEA20-PEG10-PDEA20 (30 % in 0.3 M NaCl) at both 25 °C (blue) and 37 °C (orange). Stars represent results which are statistically different to PBS where P < 0.01 for ** and P < 0.001 for ***. Data presented as mean ± standard deviation (n=3).

[7.5.4] Release Studies of Progesterone and Tenofovir Disoproxil Fumarate from the Thermogelling Tri-block Copolymer Aqueous Solutions

The liberation of progesterone (Figure 7.8a and b) and tenofovir disoproxil fumarate (Figure 7.9) from the thermogelling materials (50 µg/mL) across cellulose membrane was investigated at both 25 and 37 °C. Progesterone release from PNIPAM10-PEG10-PNIPAM10 and PDEA20-PEG10-PDEA20 at 25 °C followed Higuchi kinetics (Figure 7.8c) and 100 % of the drug was released after 32 h. The Higuchi model was applied to this release data as it is suitable for describing the release of both sparingly and abundantly soluble therapeutics from planar dosage forms.[57] This model is based on a linear fit to the fractional drug release with the square-root of time.[58] Increasing the temperature to 37 °C retarded the release of progesterone significantly, with 100 % drug liberated only after 144 h. The release profiles of progesterone from PNIPAM10-PEG10-PNIPAM10 and PDEA20-PEG10-PDEA20 at 37 °C did not fit the Higuchi model, but exhibited a good fit to the Korsmeyer-Peppas power law with R^2's of 0.98 and 0.99 respectively (Figure 7.8d). Although, both exhibited extreme exponents of 2.42 and 1.71 designating non-Fickian super case II transport kinetics.[57] This retardation of release from both PNIPAM10-PEG10-PNIPAM10 and PDEA20-PEG10-PDEA20 at 37 °C is attributed to the formation of the gel phase, which provides microphase separated domains in which drug solubilisation may occur, and from which liberation becomes disfavoured, prolonging the release until 144 h. Additionally, polymer entanglements and an increased tortuosity within the samples may contribute to this effect. Progesterone release from poloxamer 407 was equivalent at 25 and 37 °C, where the material is in the gel phase at both temperatures. Both cases gave Higuchi diffusion-controlled release in the first 60 % of the profile (R^2 > 0.98), which is consistent with prior studies of drug delivery across a membrane from poloxamer gels.[59] This behaviour is substantially different than the PNIPAM10-PEG10-PNIPAM10 and PDEA20-PEG10-PDEA20 systems which exhibited clear temperature-dependence on drug release, and a switch from Higuchi kinetics to a non-Fickian release mechanisms. Higuchi kinetics following Fickian diffusion may be rationalised below the Tgel where release of drug is controlled by factors such as partitioning and the viscosity of the medium. Super case II kinetics have been reported for chemically cross-linked PNIPAM hydrogels,[60] where Fickian diffusion is believed to be combined with polymer relaxation and possible swelling effects. The release of progesterone from PNIPAM10-PEG10-PNIPAM10 and PDEA20-PEG10-PDEA20 was significantly slower than poloxamer 407 at 37 °C. For example, at 72 h, 69.5 ± 2.7 % of the entrapped progesterone was delivered from the 20 % (w/v) poloxamer 407 sample, where only 25.3 ± 6.7 and 40.3 ± 4.9 % of the drug had been liberated from PNIPAM10-PEG10-PNIPAM10 and PDEA20-PEG10-PDEA20 respectively (p<0.0001 by one-way ANOVA). This gives the PNIPAM10-PEG10-PNIPAM10 and PDEA20-PEG10-PDEA20 materials an advantage over poloxamer 407 when sustained release of hydrophobic   drugs   is   required.

Figure 7. 8: The release of progesterone at 25 (a) and 37 °C (b) from a 20 % ethanol in water control (blue), Poloxamer 407 (20 %) (orange), PNIPAM10-PEG10-PNIPAM10 (50 %) (grey) and PDEA20-PEG10-PDEA20 (30 % in 0.3 M NaCl) (yellow) and the fit of the release from PNIPAM10-PEG10-PNIPAM10 (grey) and PDEA20-PEG10-PDEA20 (yellow) to the Higuchi model at 25 °C (c) and the Korsmeyer-Peppas power law at 37 °C (d). Data presented at mean ± standard deviation (n=3).

Tenofovir disoproxil fumarate release from the three polymer solutions was equivalent at 25 °C. However, drug release was significantly ($p < 0.05$) enhanced at 37 °C for poloxamer 407 but remained constant in the cases of PNIPAM10-PEG10-PNIPAM10 and PDEA20-PEG10-PDEA20. For example, at 8 h the cumulative release at 25 °C was 58.3 ± 1.5, 64.5 ± 0.8 and 61.0 ± 3.8 % for PNIPAM10-PEG10-PNIPAM10, PDEA20-PEG10-PDEA20 and poloxamer 407, respectively, but 53.8 ± 4.3, 66.2 ± 4.7 and 86.6 ± 5.3 % for the same samples at 37 °C. The Higuchi model was applied to the data and gave $R^2 > 0.98$ in all cases, supporting the principle that the gels act as a matrix controlled release system from which Fickian diffusion occurs.[58] Heat will enhance diffusion out of the matrix when release is purely diffusion controlled as the Stokes-Einstein equation predicts that the diffusion coefficient of a molecule scales linearly with temperature, when viscosity is constant.[61] The control, a solution of tenofovir disoproxil fumarate exhibits this phenomenon. In the poloxamer 407 samples, which are a gel at both temperatures tested, an enhanced release from the gels is attributed to the increased drug diffusion coefficient, despite the increased viscosity of the system. For PNIPAM10-PEG10-PNIPAM10 and PDEA20-PEG10-PDEA20, a phase transition occurs between the two temperatures tested. The identical release rates at 37 °C relative to 25 °C is attributed to the formation of this gel phase, which provides a more tortuous path for liberation to occur where tenofovir is known to be excluded from the micelles, counteracting the increased diffusion coefficient.[58]

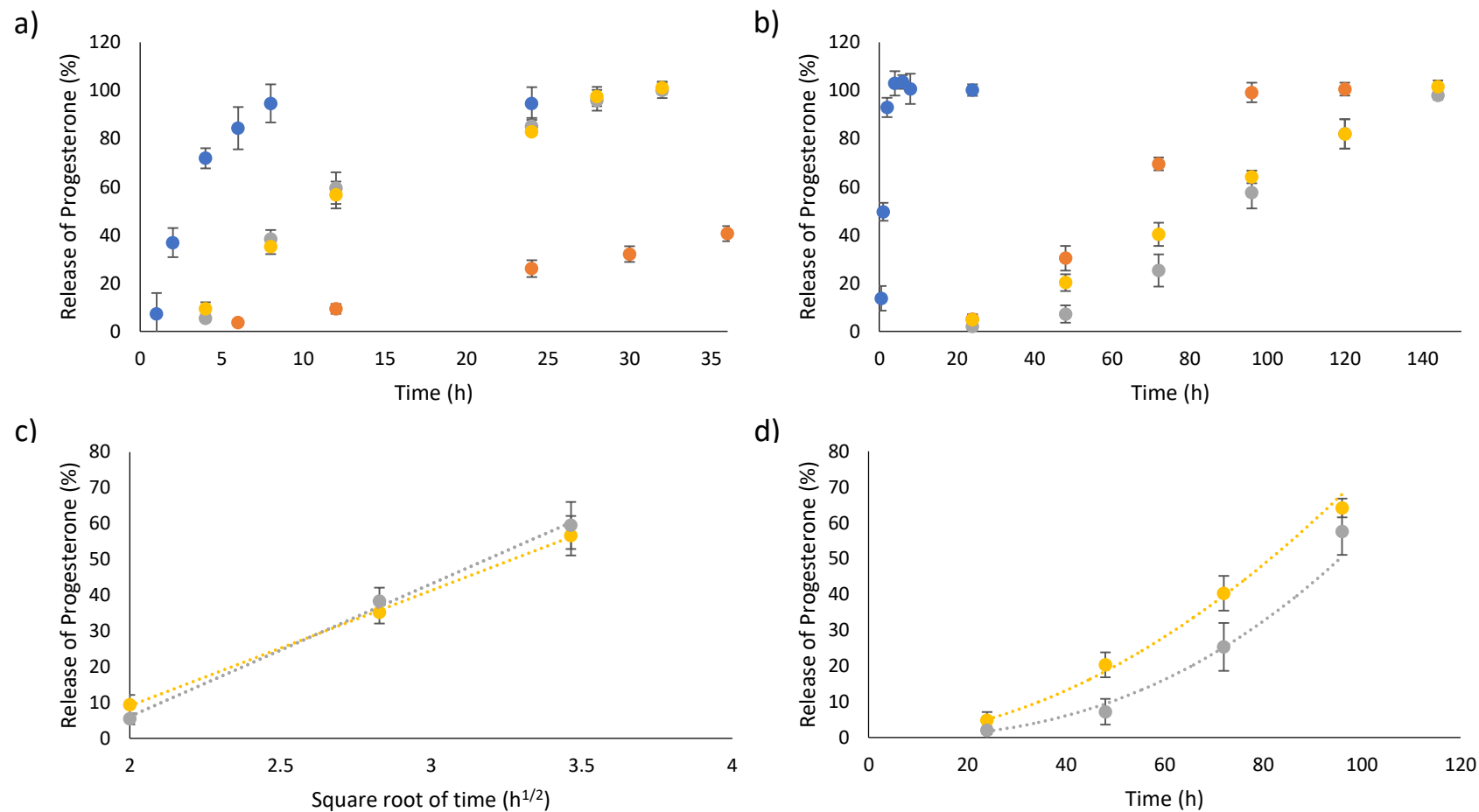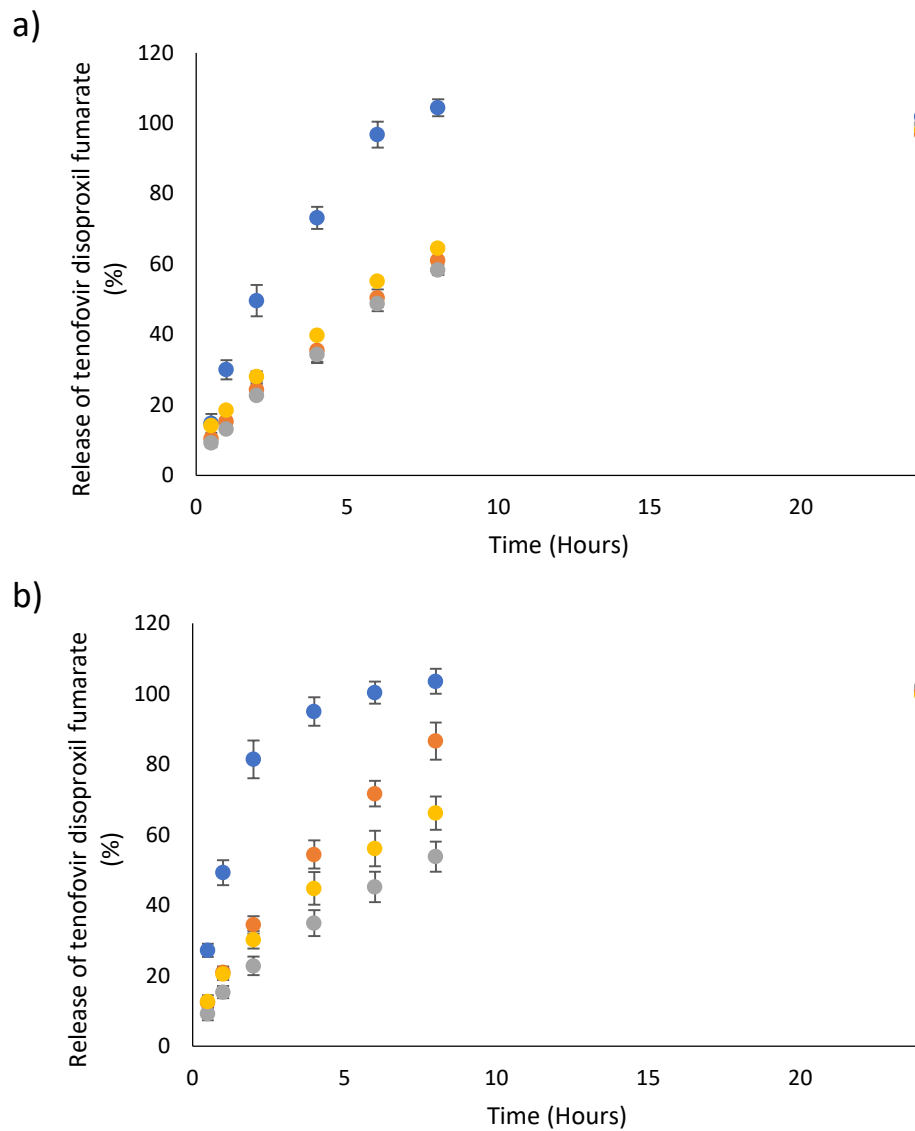Figure 7. 9: The release of tenofovir disoproxil fumarate at 25 (a) and 37 °C (b) from a 20 % ethanol in water control (blue), Poloxamer 407 (20 %) (orange), PNIPAM10-PEG10-PNIPAM10 (50 %) (grey) and PDEA20-PEG10-PDEA20 (30 % in 0.3 M NaCl) (yellow). Data presented at mean ± standard deviation (n=3).

[7.5.4.1] Rheology of the Thermogelling Tri-block Copolymer Solutions with Progesterone or Tenofovir Disoproxil Fumarate

When developing any type of formulation, the effect of active pharmaceutical ingredient on the physical properties on the dosage form must be investigated. In the case of thermogelling dosage forms, the solution to gel transition temperature and the strength of the gel formed may be impacted by the presence of drug. To evaluate this, a single temperature ramp rheology experiment was performed on the formulations with progesterone and tenofovir disoproxil fumarate (Figure 7.13). These single temperature ramps were compared to the those from Chapter 6, where no drug was present. Differences in gelation temperature (G' > G'') and gel strength (G' maximum) are highlighted and discussed below.

The gelation temperatures of poloxamer 407 (20 %), PNIPAM10-PEG10-PNIPAM10 (50 %) and PDEA20-PEG10-PDEA20 (30 % in 0.3 M NaCl) were 24.7 ± 0.3, 35.8 ± 0.2 and 35.8 ± 0.4 °C respectively. In the presence of progesterone, the gelation temperature of poloxamer 407 (20 %) did not significantly vary from 25 °C, which is in agreement with the literature.[30] Whereas the gelation temperature of PNIPAM10-PEG10-PNIPAM10 (50 %) and PDEA20-PEG10-PDEA20 (30 %) were reduced from 35.8 ± 0.4 and 35.8 ± 0.2 to 34.2 and 33.1 °C, respectively. In addition to this, the inclusion of progesterone resulted in a decrease in gel strength for poloxamer 407 (20 %) and PDEA20-PEG10-PDEA20 (30 %) to 10240 and 2361 Pa, while the gel strength of PNIPAM10-PEG10-PNIPAM10 did not vary. In contrast, tenofovir disoproxil fumarate did not alter the gelation temperatures of poloxamer 407 (20 %), PNIPAM10-PEG10-PNIPAM10 (50 %) and PDEA20-PEG10-PDEA20 (30 %). However, the gel strengths were reduced to 9660, 10300 and 2140 Pa, respectively. Regardless of these changes in gelation temperature and gel strength, their suitability for use in healthcare applications would not be adversely affected.

The previously reported DLS experiments confirmed that progesterone drives the formation of micelles below the critical aggregation temperature. This may be as a result of the progesterone binding to the temperature responsive PNIPAM or PDEA arms. As such, progesterone directly impacts the thermodynamics of the micellization process, and as such the temperature at which gelation occurs and the strength of the gel formed. The binding of progesterone may also compete with the polymer chains which bridge between micelles, as described by Semenov (1994). Semenov (1994) described the formation of flower-like micelles from ABA triblock copolymers, which are bridged by unimer chains.[62] In the case of PNIPAM10-PEG10-PNIPAM10 and PDEA20-PEG10-PDEA20, the micelles would be bridged by the central PEG chains of the triblock copolymers. These bridges are expected to strengthen the gel formed. It is suggested that the competition of bridge formation with progesterone-DEA/PNIPAM interaction disfavours bridge formation, which may reduce the gel

strength. For tenofovir disoproxil fumarate, there was no evidence of micellization below the critical transition temperature, and as such tenofovir disoproxil fumarate does not impact the thermodynamics associated with the micellization process. Thus, tenofovir disoproxil fumarate did not alter the transition temperature from solution to gel. The reduction of gel strength shown for the tenofovir disoproxil fumarate containing gels may instead be caused by the packing of the micelle aggregates. Tenofovir disoproxil fumarate is expected to largely reside in the aqueous media surrounding the micelles, which may sterically interfere with packing or increase osmotic pressure between micelles, and in turn reduce the gel strength.[63]
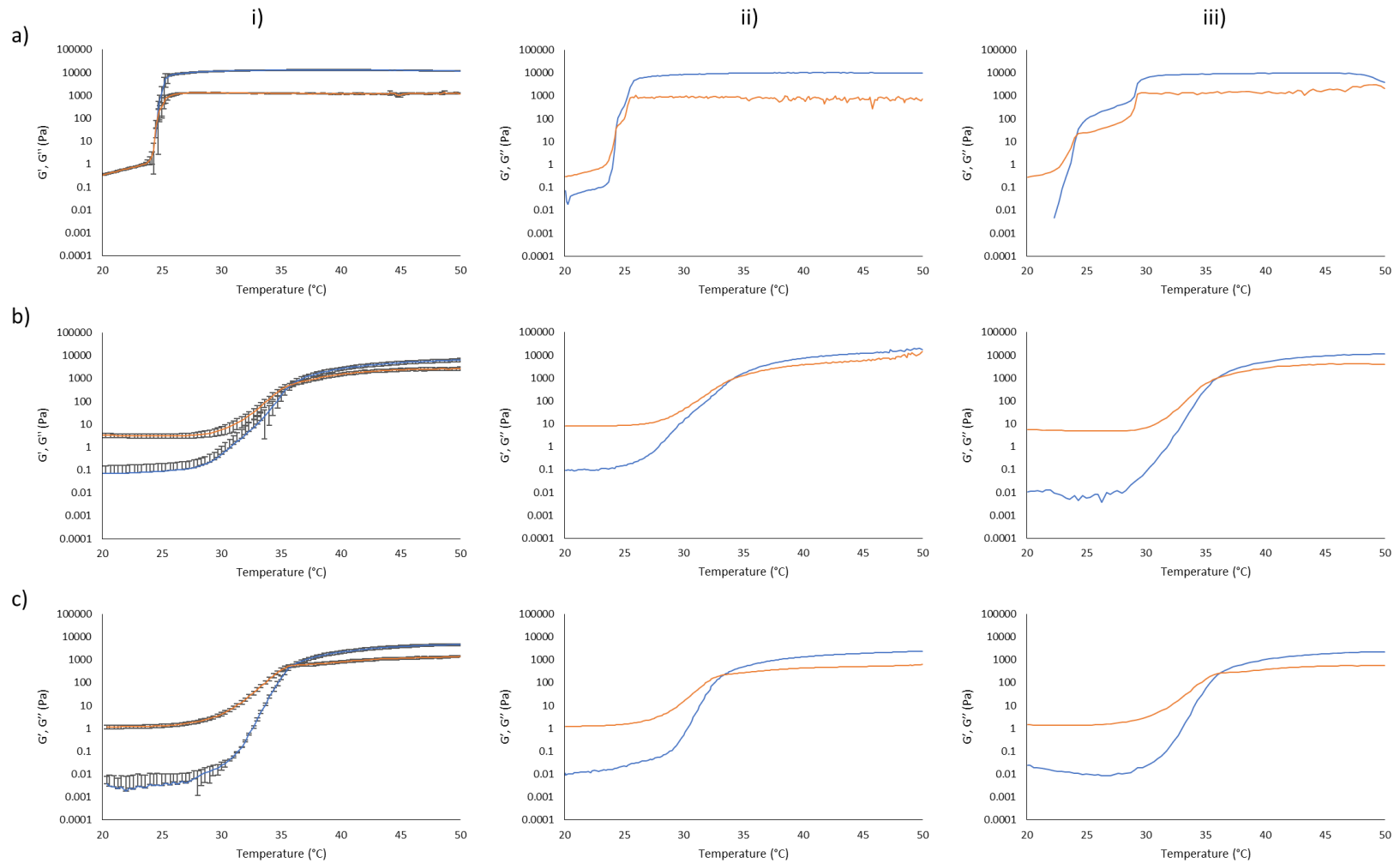
Figure 7. 10: The temperature ramp rheology profiles showing the change in G' (blue) and G'' (orange) for poloxamer 407 (20 %) (a), PNIPAM10-PEG10-PNIPAM10 (50 %) (b) and PDEA20-PEG10-PDEA20 (30% in 0.3 M NaCl) (c) in aqueous solution (i), with 50 µg/mL progesterone (ii) and with 50 µg/mL tenofovir disoproxil fumarate (iii).

[7.6] Conclusions

This chapter has explored the use of poloxamer 407 (20 %), PNIPAM10-PEG10-PNIPAM10 (50 %) and PDEA20-PEG10-PDEA20 (30 % in 0.3 M NaCl) as thermogelling excipients to deliver drugs relevant to vaginal delivery. Progesterone and tenofovir disoproxil fumarate were selected as model hydrophobic and hydrophilic drugs, respectively. The three tri-block copolymers were able to greatly enhance the solubility of progesterone which is most likely as a result of inclusion of the drug into the core of the polymeric micelles. Conversely, the solubility of tenofovir disoproxil fumarate was reduced by the polymers, which is hypothesised to be due to exclusion from the micellar aggregates. The release of the two drugs was evaluated using Franz diffusion cell systems at 25 and 37 °C. The release of progesterone from the poloxamer 407 gels did not vary with an increase in temperature, while tenofovir disoproxil fumarate was liberated rapidly at elevated temperature. PNIPAM10-PEG10-PNIPAM10 and PDEA20-PEG10-PDEA20 however, gave temperature-responsive retardation of release of both drugs at body temperature. The release of progesterone from these gels was sustained over 6 days at 37 °C, while complete release of tenofovir disoproxil fumarate was achieved after 24 h. This effect may be used to achieve controlled delivery of therapeutics or maintaining drugs on bodily surfaces for local effects. Overall, PNIPAM10-PEG10-PNIPAM10 and PDEA20-PEG10-PDEA20 exhibit unique properties as thermogelling materials for drug delivery and may act as advanced materials for future topical therapies.

[7.7] References

1   Human Metabolome Database: Showing metabocard for Progesterone (HMDB0001830), https://hmdb.ca/metabolites/HMDB0001830, (accessed 31 March 2020).

2   CLINICAL PHARMACOLOGY AND BIOPHARMACEUTICS REVIEW(S) APPLICATION NUMBER: 022577Orig1s000, https://www.accessdata.fda.gov/drugsatfda_docs/nda/2012/022577Orig1s000ClinPharmR.pdf, (accessed 31 March 2020).

3   TRUVADA®, https://www.accessdata.fda.gov/drugsatfda_docs/label/2006/021752s005lbl.pdf, (accessed 31 March 2020).

4   N. D. PubChem, Progesterone CID:5994. National Center for Biotechnology Information., https://pubchem.ncbi.nlm.nih.gov/compound/Progesterone., (accessed 31 March 2020).

5   E. K. S. de Melo, T. P. de Araujo, J. W. V. da Silva, S. C. C. Chagas, D. C. G. Bedor, D. P. de Santana and L. B. Leal, *Brazilian J. Pharm. Sci.*, 2017, **53**, 1–5.

6   M. Elmowafy, A. Samy, A. E. Abdelaziz, K. Shalaby, A. Salama, M. A. Raslan and M. A. Abdelgawad, *Beni-Suef Univ. J. Basic Appl. Sci.*, 2017, **6**, 184–191.

7   J. Basso, A. Miranda, S. Nunes, T. Cova, J. Sousa, C. Vitorino and A. Pais, *Gels*, 2018, **4**, 62–73.

8   S. S. Liow, A. A. Karim and X. J. Loh, *MRS Bull.*, 2016, **41**, 557–564.

9   X. J. Loh and J. Li, *Expert Opin. Ther. Pat.*, 2007, **17**, 965–977.

10   M. M. Lübtow, T. Lorson, T. Finger, F. K. Gröber-Becker and R. Luxenhofer, *Macromol. Chem. Phys.*, 2020, **221**, 190–201.

11   Y. Chen, Y. Li, W. Shen, K. Li, L. Yu, Q. Chen and J. Ding, *Sci. Rep.*, 2016, **6**, 1–10.

12   G. Dante, V. Vaccaro and F. Facchinetti, *Facts, views Vis. ObGyn*, 2013, **5**, 66–71.

13   Cyclogest 400mg pessaries - Summary of Product Characteristics (SmPC) - (emc), https://www.medicines.org.uk/emc/product/5569/smpc, (accessed 14 January 2020).

14   Lutigest 100 mg vaginal tablets - Summary of Product Characteristics (SmPC) - (emc), https://www.medicines.org.uk/emc/product/3635/smpc, (accessed 14 January 2020).

15   Crinone 8% Progesterone Vaginal Gel - Summary of Product Characteristics (SmPC) - (emc), https://www.medicines.org.uk/emc/product/1283/smpc, (accessed 8 March 2020).

16   A. L. Haskins, *Proc. Soc. Exp. Biol. Med.*, 1949, **70**, 228–229.

17   J. M. Smith, R. Rastogi, R. S. Teller, P. Srinivasan, P. M. M. Mesquita, U. Nagaraja, J. M. McNicholl, R. M. Hendry, C. T. Dinh, A. Martin, B. C. Herold and P. F. Kiser, *Proc. Natl. Acad. Sci. U. S. A.*, 2013, **110**, 16145–16150.

18   Stribild 150 mg/150 mg/200 mg/245 mg film-coated tablets - Summary of Product Characteristics (SmPC) - (emc), https://www.medicines.org.uk/emc/product/3154/smpc, (accessed 28 January 2020).

19   Lamivudine/Tenofovir disoproxil 300 mg/245 mg Film-coated Tablets - Summary of Product Characteristics (SmPC) - (emc), https://www.medicines.org.uk/emc/product/10500/smpc, (accessed 28 January 2020).

20   Eviplera 200 mg/25 mg/245 mg Film-coated Tablets - Summary of Product Characteristics (SmPC) - (emc), https://www.medicines.org.uk/emc/product/2764/smpc, (accessed 28 January 2020).

21   Delstrigo 100 mg /300 mg /245 mg film-coated tablets - Summary of Product Characteristics (SmPC) - (emc), https://www.medicines.org.uk/emc/product/10500/smpc, (accessed 28 January 2020).

22   Gilead Scienes Ltd, Atripla 600 mg/200 mg/245 mg film coated tablets - Summary of Product Characteristics (SPC) - (eMC), https://www.medicines.org.uk/emc/product/6173/smpc, (accessed 28 January 2020).

23   S. M. Pond and T. N. Tozer, *Clin. Pharmacokinet.*, 1984, **9**, 1–25.

24   K. H. Min, C. K. Rhee, J. Y. Jung and M. W. Suh, *Korean J. Audiol.*, 2012, **16**, 65–70.

25   P. Srinivasan, J. A. Moss, M. Gunawardana, S. A. Churchman, F. Yang, C. T. Dinh, J. M. Mitchell, J. Zhang, R. Fanter, C. S. Miller, I. Butkyavichene, J. M. McNicholl, T. J. Smith, M. M. Baum and J. M. Smith, *PLoS One*, 2016, **11**, 150–159.

26   ClinicalTrials.gov., Safety and Pharmacokinetic Study of HIV Prophylaxis Using Antiretroviral Intravaginal Rings in Healthy Women, https://clinicaltrials.gov/ct2/show/results/NCT02431273?term=tenofovir+intravaginal+ring, (accessed 11 April 2020).

27   A. Agrawal and R. K. Maheshwari, *Asian J. Pharm.*, 2011, **5**, 131–140.

28   E. Ban, M. Park, S. Jeong, T. Kwon, E. H. Kim, K. Jung and A. Kim, *Molecules*, 2017, **22**, 189–196.

29   F. ud Din, D. W. Kim, J. Y. Choi, R. K. Thapa, O. Mustapha, D. S. Kim, Y. K. Oh, S. K. Ku, Y. S. Youn, K. T. Oh, C. S. Yong, J. O. Kim and H. G. Choi, *Acta Biomater.*, 2017, **54**, 239–248.

30   R. Basak and R. Bandyopadhyay, *Langmuir*, 2013, **29**, 4350–4356.

31   B. Q. Y. Chan, H. Cheng, S. S. Liow, Q. Dou, Y. L. Wu, X. J. Loh and Z. Li, *Polymers (Basel).*, 2018, **10**, 89–95.

32   S. Choi and S. W. Kim, *Pharm. Res.*, 2003, **20**, 2008–2010.

33   V. K. Garripelli, R. Namgung, W. J. Kim and S. Jo, *J. Biomater. Sci. Polym. Ed.*, 2012, **23**, 1505–1519.

34   A. Fick, *Ann. Phys.*, 1855, **170**, 59–86.

35   P. Myers, *Chromatographia*, 2014, **77**, 643–643.

36   J. Kestin and J. Yata, *J. Chem. Phys.*, 1968, **49**, 4780–4791.

37   P. Hernandez-Muñoz, R. Gavara and R. J. Hernandez, *J. Memb. Sci.*, 1999, **154**, 195–204.

38   J. Li and D. J. Mooney, *Nat. Rev. Mater.*, 2016, **1**, 10–23.

39   D. Cao, X. Zhang, M. D. Akabar, Y. Luo, H. Wu, X. Ke and T. Ci, *Artif. Cells, Nanomedicine Biotechnol.*, 2019, **47**, 181–191.

40   N. Kamaly, B. Yameen, J. Wu and O. C. Farokhzad, *Chem. Rev.*, 2016, **116**, 2602–2663.

41   M. H. Park, M. K. Joo, B. G. Choi and B. Jeong, *Biodegradable thermogels*, American Chemical Society, 2012, vol. 45.

42   V. M. Shah, D. X. Nguyen, D. A. Rao, R. G. Alany and A. W. G. Alani, in *Temperature-Responsive Polymers*, John Wiley & Sons Ltd, 2018, pp. 313–327.

43   A. J. De Graaf, I. I. Azevedo Próspero Dos Santos, E. H. E. Pieters, D. T. S. Rijkers, C. F. Van Nostrum, T. Vermonden, R. J. Kok, W. E. Hennink and E. Mastrobattista, *J. Control. Release*, 2012, **162**, 582–590.

44   P. Gautam and T. Purvis, *Pharm. Anal. Chem.*, 2017, **03**, 1–11.

45   P. B. Kandagal, D. H. Manjunatha, J. Seetharamappa and S. S. Kalanur, *Anal. Lett.*, 2008, **41**, 561–570.

46   G. Vanhoenacker and P. Sandra, *Anal. Bioanal. Chem.*, 2008, **390**, 245–248.

47   Y. N. Velikhov, I. M. Pritula, V. I. Salo and M. I. Kolybaeva, *Inorg. Mater.*, 2000, **36**, 734–738.

48   Reagent Datasheet Detail: Catalog 10198 - Tenofovir disoproxil fumarate - NIH AIDS Reagent Program, https://www.aidsreagent.org/reagentdetail.cfm?t=antiviral_compounds&id=13, (accessed 22 December 2019).

49   P. Alexandridis and T. Alan Hatton, *Colloids Surfaces A Physicochem. Eng. Asp.*, 1995, **96**, 1–46.

50   A. M. Bodratti and P. Alexandridis, *J. Funct. Biomater.*, 2018, **9**, 1–8.

51   D. A. Chiappetta and A. Sosnik, *Eur. J. Pharm. Biopharm.*, 2007, **66**, 303–317.

52   Y. Lu and K. Park, *Int. J. Pharm.*, 2013, **453**, 198–214.

53   A. R. Tehrani-Bagha and K. Holmberg, *Materials (Basel).*, 2013, **6**, 580–608.

54   F. P. Schwarb, G. Imanidis, E. W. Smith, J. M. Haigh and C. Surber, *Pharm. Res.*, 1999, **16**, 909–915.

55   Y. Hu, L. Ge, J. Han and R. Guo, *Soft Matter*, 2015, **11**, 5624–5631.

56   C. de O. Rangel-Yagui, A. Pessoa and L. C. Tavares, *J. Pharm. Pharm. Sci.*, 2005, **8**, 147–163.

57   M. L. Bruschi, in *Strategies to Modify the Drug Release from Pharmaceutical Systems*, Elsevier, 2015, pp. 63–86.

58   S. Dash, P. N. Murthy, L. Nath and P. Chowdhury, *Acta Pol. Pharm. - Drug Res.*, 2010, **67**, 217–223.

59   G. Dumortier, J. L. Grossiord, F. Agnely and J. C. Chaumeil, *Pharm. Res.*, 2006, **23**, 2709–2728.

60   Y. Danyuo, C. J. Ani, A. A. Salifu, J. D. Obayemi, S. Dozie-Nwachukwu, V. O. Obanawu, U. M. Akpan, O. S. Odusanya, M. Abade-Abugre, F. McBagonluri and W. O. Soboyejo, *Sci. Rep.*, 2019, **9**, 1–14.

61   F. Akomeah, T. Nazir, G. P. Martin and M. B. Brown, *Eur. J. Pharm. Sci.*, 2004, **21**, 337–345.

62   A. N. Semenov, J. F. Joanny and A. R. Khokhlov, *Macromolecules*, 1995, **28**, 1066–1075.

63   Y. M. Kang, G. H. Kim, J. Il Kim, D. Y. Kim, B. N. Lee, S. M. Yoon, J. H. Kim and M. S. Kim, *Biomaterials*, 2011, **32**, 4556–4564.

Chapter Eight: General Conclusions and Future Work

The aim of the work presented in this thesis was to develop novel thermogelling materials and evaluate their use in topical drug delivery formulations. These materials were to be prepared using block copolymers that contain a temperature responsive component which becomes insoluble above a critical temperature, known as a lower critical solution temperature (LCST). When in solution, these materials have been shown to transition from low viscosity state to gel upon surpassing the LCST of the temperature responsive component. However, there are shortcomings of the current materials and thus a need to design new and improved polymers for this application. Thus, the first objective was to develop a computational model which may be used to guide the discovery of novel LCST exhibiting homopolymers which may then be used to develop thermogelling materials. Following this, block copolymers containing an LCST exhibiting component were synthesised by atom-transfer radical polymerisation (ATRP) from PEG macroinitiators. These polymers were then investigated as thermogelling materials using temperature ramp rheology, in order to characterise their gelation temperature and strength. The cytotoxicity of these materials was also evaluated. Using both cytotoxicity and gel strength evaluation, the most promising candidates were selected for further study. The final areas of study involved characterising the gelation properties including gelation time, resistance to shear, recoverability, mucoadhesion and the dissolution and release of therapeutics relevant to vaginal drug delivery, to evaluate the materials in an exemplar topical medicine.

The systematic review of the literature in chapter 2 revealed there is a small number of temperature responsive materials which have been investigated in topical drug delivery, with most studies focussing on Poloxamer 407. Poloxamer 407 exhibits a sharp transition from solution to gel upon an increase in temperature. This transition, however, is heavily concentration dependant. In order achieve a strong gel a minimum concentration of 20 % (w/v) is required, but this exhibits gelation at ca. 25 °C, close to room temperature.[1] Also, it has been found that poloxamer 407 gels exhibit poor residence times, due to shear thinning behaviour, weak mucoadhesion and rapid dissolution.[2] Polymers which exhibit an LCST may also be used to prepare thermogelling materials. The review identified that the most well-studied LCST exhibiting polymer is poly(N-isopropyl acrylamide) (PNIPAM), which transitions at ca. 32 °C. Previous work by Lin and Cheng,[3] Teodorescu et al.[4] and Negru et al.[5] have found PNIPAM and poly(ethylene glycol) (PEG) based block copolymers can transition from solution to gel upon an increase in temperature. These PNIPAM and PEG based materials can form viscous gels (G' > 1 kPa) and thus may be attractive for topical drug delivery. PNIPAM and PEG block copolymers, however, are yet to be exploited in the delivery of drugs to these sites. Four classes of PNIPAM (A) and PEG (B) block copolymers were directly compared by Lin and Cheng.[3] These were diblock (AB), triblock (ABA) and four arm block copolymer and eight arm

block copolymers. Of the four classes of PNIPAM and PEG block copolymer diblock copolymers were found to form the weakest gels. Triblock copolymers were identified as an attractive blueprint as these formed equally strong gels as the four and eight arm block copolymers, while being less expensive to synthesise due to the high cost of star-shaped PEGs. The literature review highlighted that these novel thermogelling materials are rarely compared to poloxamer thermogels. Thus, it is unknown whether novel materials may perform better. Therefore, opportunity was identified for research into novel thermogelling materials for topical drug delivery, aiming to improve upon the properties of poloxamer 407. Furthermore, the tri-block copolymer architecture was identified as the most promising for developing strong gelators.

The work presented in chapter three aimed to develop a multiple linear regression (MLR) quantitative structure property relationship (QSPR) which may be used to guide the development of novel LCST exhibiting polymers with the overall aim of generating novel high-performance thermogelling materials. However, a predictive and generalisable model could not be developed using a dataset of 43 monomers prepared from the literature. Further work to attempt to overcome this may include the development of more sophisticated computational models, including artificial neural networks (ANN). MLR QSPR models do not contain compounds which do not elicit the desired property. This results in the predictions of false positives, meaning in the case of LCSTs, polymers which do not express them in aqueous solution would still be predicted to do so. ANNs, however, can classify the dataset compounds as active or inactive (i.e. express an LCST or do not).[6] Thus, the model would be more likely to accurately predict monomers which may exhibit an LCST. In addition to this, MLR QSPR models are only capable of dealing with simple linear relationships between the predicted variable and the descriptors, which may limit their predictive ability. Comparatively, ANNs can handle more complex non-linear relationships between descriptors and the predictor variable, which may improve the chances of a predictive and generalisable model.[7] ANNs typically require larger datasets than MLR QSPRs, however there are reports of the use of small datasets to build generalizable and predictive models.[8] Therefore, ANNs may be suitable in this case.

The remaining chapters discuss the synthesis, characterisation and development of thermogelling materials based on polymers reported as exhibiting LCSTs from the literature. An iterative selection process was used which included reported non-cytotoxicity, a historic use in drug delivery excipients and the use of Derek by Nexus, a piece of computational software which predicts toxicity based upon the chemical structure. The materials selected were PNIPAM, poly(N,N-diethyl acrylamide) (PDEA), poly(N-vinyl caprolactam) (PNVCl), poly(N-vinyl pyrrolidone) (PVP), poly(2-(N-dimethylamino)ethyl methacrylate) (PDMAEMA) and poly(diethylene glycol methyl ether methacrylate) (PDEGMEMA) which exhibit LCSTs at 32,[9] 25,[10] 34,[11] 30,[12] 35[13] and 28 °C,[14]

respectively. The LCSTs of these polymers is largely independent of molecular weight, with the exception of PDMAEMA, where the LCST shifts to lower temperatures as the molecular weight is increased.[15] Of these polymers, only PNIPAM, PDEA, PDMAEMA and PDEGMEMA exhibited LCSTs within a physiologically-relevant range, which occurred at ca. 32, 35, 30 and 25 °C, respectively. Thus, these were taken forward for triblock copolymer synthesis.

Triblock copolymers were prepared using atom-transfer radical polymerisation (ATRP) using a bi-functional PEG macroinitiator, described in chapter 4. This resulted in the synthesis of ABA triblock copolymers which contained an LCST-exhibiting A block (i.e. PNIPAM, PDEA, PDMAEMA or PDEGMEMA) and a PEG B block to target number average molecular weights (kDa) of 10-4-10, 20-4-20, 10-10-10 and 20-10-20. All four targeted molecular weights were successfully synthesised for PNIPAM, PDEA, PDMAEMA and PDEGMEMA, as confirmed by gel permeation chromatography and ^{1}H NMR. Of the PNIPAM-PEG-PNIPAM triblock copolymers, the 10-4-10 and 20-4-20 have been reported previously,[5,16] whereas, the remaining PNIPAM-PEG-PNIPAM triblock copolymers prepared in this work have not been investigated. PDMAEMA-PEG-PDMAEMA triblock copolymers, however, have previously been prepared but not to these molecular weights nor studied as thermogelling materials. However, this is the first report of the synthesis of PDEGMEMA-PEG-PDEGMEMA and PDEA-PEG-PDEA triblock copolymers, and the effect of molecular weight on their thermoresponsive behaviour. In addition to this, at the current time this is the first study of its kind to directly compare the effect of the temperature responsive block type on the gelation properties of triblock copolymers. The impact of temperature responsive polymer type and gelation of these types of thermogelling materials is relatively unknown and is often not discussed within the literature. Therefore, the work presented in chapter five discusses the characterisation of the behaviour of these polymers in aqueous solution by rheology, to evaluate thermogelling behaviour followed by DLS and SANS to probe mechanisms of gelation. All materials synthesised in chapter 4 were found to increase in viscosity with an increase in temperature when at 20 % (w/v) concentration, and form aggregates in dilute 10 mg/mL solution. A link was observed where aggregates with larger hydrodynamic radii often formed weaker gels. These larger aggregates were typically formed by polymers prepared using short PEG chains, and these formed viscous fluids rather than gels. Further SANS experimentation found the aggregates formed by polymers with a shorter PEG chain were rod-like aggregates, while those with longer PEG chains were spherical core-shell micelles. Furthermore, increasing the concentration resulted in the evolution of a sticky hard sphere interaction parameter, indicating these aggregates attract at a short distance. This is consistent with a theory of bridging flower-like micelles are described by Semenov.[17] To the best of our knowledge this if the first experimental evidence of this gelation mechanism in thermoresponsive ABA copolymers. Following

this, PNIPAM10-PEG10-PDEA10 and PDEA20-PEG10-PDEA20 were selected for further study as these formed the strongest gels and were found to be non-cytotoxic to human keratinocytes.

Chapters six and seven discuss the development vaginally relevant topicals using the two most promising thermogelling materials, PNIPAM10-PEG10-PNIPAM10 and PDEA20-PEG10-PDEA20. The effect of polymer concentration was investigated to attempt to supress Tgel to lower than 37 °C. In agreement with poloxamer 407, increasing the polymer concentration of either material led to a decrease in gelation temperature and an increase in gel strength. Where poloxamer 407 thermogellation exhibits a strong dependence upon concentration, this effect was weaker in PNIPAM10-PEG10-PNIPAM10 and PDEA20-PEG10-PDEA20 thermogels. This has important implications *in vivo*, where biological fluids may decrease the concentration of the material and thus increase the gelation temperature to above physiological, triggering a reverse gel-sol transition. Following this investigation, the formulations which results in physiologically relevant gelation were 50 % (w/v) PNIPAM10-PEG10-PNIPAM10 and 30 % (w/v) PDEA20-PEG10-PDEA20 in 0.3 M NaCl. In addition to this, the dissolution time and mucoadhesion were evaluated in order to predict rank-order of formulation residence time. The PNIPAM10-PEG10-PNIPAM10 and PDEA20-PEG10-PDEA20 formulations were found to have longer dissolution times (ca. 4 h) than poloxamer 407 (ca. 1 h). Also, these polymers exhibited equivalent or greater mucoadhesion than poloxamer 407 gels. Therefore, the materials prepared in this work may offer significant improvements upon residence time when compared to poloxamer 407 as vaginal drug delivery excipients. In chapter seven, the solubility and release of two vaginally relevant therapeutics, progesterone and tenofovir disoproxil fumarate, were investigated using the two thermogelling materials and poloxamer 407. At elevated temperature, the release of progesterone from the materials prepared in this work was found to be equivalent at 100 % release after ca. 140 h, while poloxamer 407 released 100 % of the progesterone after ca. 100 h. In terms of tenofovir disoproxil fumarate, the release from PNIPAM10-PEG10-PNIPAM10 and PDEA20-PEG10-PDEA20 was found to reach ca. 50 % after 8 h while poloxamer 407 released ca. 80 % over the same time period. Therefore, PNIPAM10-PEG10-PNIPAM10 and PDEA20-PEG10-PDEA20 may exhibit prolonged delivery of drugs relative to poloxamer 407.

Significant progress has been made in this work towards the development of thermogelling materials which improve upon the properties observed by poloxamer 407. The study by Lin and Cheng[3] found an ABA triblock copolymer of PNIPAM (A) and PEG (B) formed a gel equivalent in strength to block copolymers with a central PEG and 4 PNIPAM arms. However, this may not be the case for temperature responsive polymer aside from PNIPAM, and stronger gels may form. Thus, it is proposed that the identified temperature responsive polymers shown above should be used to prepare four arm triblock copolymers, and the strength of their gels compared to the triblock

copolymer counterparts. Unfortunately, the PEGs required to synthesise these four arm block copolymers are often quite costly when compared to the linear PEGs needed for triblock copolymers. If these result in significantly stronger gels, the cost of the PEGs required for four arm block copolymers should be weighed against the strength of the gel formed and the performance with regards to properties such as dissolution time mucoadhesion to justify whether this cost is worth it. In addition to this, the degree of interaction between the polymer aggregates in solution is thought to result in an increase in gel strength. Therefore, it may be possible to strengthen these interactions by enhancing the interaction between the PEG chains at the surface of polymer micelles. This may be performed in a multitude of ways including the addition of thiol groups which may form disulphide bridges[18] or mixing two types of block copolymer, those with negative functionalities on the PEG corona and those with positive functionalities.[19] It is thought the formation of such disulphide bridges or electrostatic interaction may result in the of stronger gels. Regardless of this, two materials have been identified as equivalent or better than poloxamer 407 as thermogelling drug delivery excipients. However, additional work is still required to commercialise these materials as thermogelators for drug delivery. The first problem associated would arise from the synthetic procedure. In this work ATRP was used for synthesis, but this can result in the presence of residual copper catalyst which can cause localised cytotoxic effects.[20] The synthetic route may be replaced by the work presented by Treat el al.[21] on copper-free ATRP, where a photoredox catalyst may be used to enable controlled radical polymerisation. If this method is unsuccessful, either another synthetic procedure must be devised, or an efficient purification protocol must be performed. The United States Environmental Protection Agency (USEPA) states that exposure of copper must be below 0.05 mg/kg/day. Therefore, if ATRP is taken forward as the preferred synthetic route, this residual copper must be quantified using techniques such as Inductively coupled plasma (ICP), in order to ensure exposure would not exceed the limit set by the USEPA.[22]

In the work presented in this thesis, basic cytotoxicity studies were performed to evaluate potential safety risks associated with these materials. Before these materials may be used as drug delivery excipient, much more rigorous safety testing must be performed to mitigate for risks in vivo. The International Pharmaceutical Excipients Council (IPEC) requires additional testing which includes, for example, dermal toxicity, eye and skin irritation, skin sensitization, gene mutation and chromosomal damage before a new excipient may be made available for drug delivery.[23] This is both costly and time consuming, but of paramount importance before any commercialisation.

Following the studies outlined by the IPEC, if these materials continue to be safe, potential applications should be identified and additional model in vivo testing should be performed to evaluate the dosage form retention, efficacy and toxicity. The work presented in this thesis identifies

the PNIPAM10-PEG10-PNIPAM10 and PDEA20-PEG10-PDEA20 materials as possible thermogelling vaginal drug delivery excipients. In particular, these materials may be specifically suited to prevention of sexually transmitted diseases following intravaginal administration, due to their observed mucoadhesion, long dissolution times and resistance to shear forces. The dosage forms may be loaded with pre-exposure prophylaxis medicines such as tenofovir and emtricitabine as well as spermicidal agents, which may prevent the transmission of HIV as well as acting as a contraceptive. Model tests in vivo should be performed using live animals, for example macaques, as previously demonstrated by McConville et al.[24] McConville et al. described the preclinical development of a silicone elastomer vaginal ring which were designed to exhibit a controlled release of the non-nucleoside reverse transcriptase inhibitor UC781. Like the McConville et al. study, two groups of animal participants should be selected, one dosed with the drug loaded formulation and one without drug. Vaginal swabs and smears can be taken as necessary over the course of several hours, days or weeks. These swabs and smears should be used to determine the drug release, formulation dissolution rate and identify any adverse effects that may arise. If these materials are successful in these in vivo studies, further clinical trials would be required for governing bodies such as the FDA to approve their use in medicines. If the thermogels were included as part of a licensed medicine, the number of target sites these materials may be suited to may then be expanded upon. For example, additional medicines could be explored for application to the ocular, buccal or rectal mucosa.

[8.1] References

1   A. Fakhari, M. Corcoran and A. Schwarz, *Heliyon*, 2017, **3**, 2–8.

2   M. A. Abou-Shamat, J. Calvo-Castro, J. L. Stair and M. T. Cook, *Macromol. Chem. Phys.*, 2019, **220**, 18–25.

3   H. H. Lin and Y. L. Cheng, *Macromolecules*, 2001, **34**, 3710–3715.

4   M. Teodorescu, I. Negru, P. O. Stanescu, C. Drghici, A. Lungu and A. Sârbu, *React. Funct. Polym.*, 2010, **70**, 790–797.

5   I. Negru, M. Teodorescu, P. O. Stănescu, C. Drăghici, A. Lungu and A. Sârbu, *Soft Mater.*, 2013, **11**, 149–156.

6   M. K. Gupta, S. Gupta and R. K. Rawal, in *Artificial Neural Network for Drug Design, Delivery and Disposition*, Elsevier Inc., 2016, pp. 153–179.

7   C. Ventura, D. A. R. S. Latino and F. Martins, *Eur. J. Med. Chem.*, 2013, **70**, 831–845.

8   A. Pasini, *J. Thorac. Dis.*, 2015, **7**, 953–960.

9   L. Tavagnacco, E. Zaccarelli and E. Chiessi, *J. Mol. Liq.*, 2020, **297**, 111928.

10   H. Y. Liu and X. X. Zhu, *Polymer (Guildf).*, 1999, **40**, 6985–6990.

11   A. A. Tager, A. P. Safronov, E. A. Berezyuk and I. Y. Galaev, *Colloid Polym. Sci.*, 1994, **272**, 1234–1239.

12   X. Liang, V. Kozlovskaya, C. P. Cox, Y. Wang, M. Saeed and E. Kharlampieva, *J. Polym. Sci. Part A Polym. Chem.*, 2014, **52**, 2725–2737.

13   F. L. Baines, N. C. Billingham and S. P. Armes, *Macromolecules*, 1996, **29**, 3416–3420.

14   L. G. Weaver, R. Stockmann, A. Postma and S. H. Thang, *RSC Adv.*, 2016, **6**, 90923–90933.

15   J. Cai, Y. Yue, D. Rui, Y. Zhang, S. Liu and C. Wu, *Macromolecules*, 2011, **44**, 2050–2057.

16   M. Teodorescu, I. Negru, P. O. Stanescu, C. Drăghici, A. Lungu and A. Sârbu, *React. Funct. Polym.*, 2010, **70**, 790–797.

17   A. N. Semenov, J. F. Joanny and A. R. Khokhlov, *Macromolecules*, 1995, **28**, 1066–1075.

18   L. Sun, J. Liu and H. Zhao, *Polym. Chem.*, 2014, **5**, 6584–6592.

19   J. Z. Wu, D. Bratko, H. W. Blanch and J. M. Prausnitz, *Phys. Rev. E - Stat. Physics, Plasmas, Fluids, Relat. Interdiscip. Top.*, 2000, **62**, 5273–5280.

20   S. Y. Chen, S. T. Liu, W. R. Lin, C. K. Lin and S. M. Huang, *Int. J. Mol. Sci.*, 2019, **20**, 10–20.

21   N. J. Treat, H. Sprafke, J. W. Kramer, P. G. Clark, B. E. Barton, J. Read De Alaniz, B. P. Fors and C. J. Hawker, *J. Am. Chem. Soc.*, 2014, **136**, 16096–16101.

22   EMA, GUIDELINE ON THE SPECIFICATION LIMITS FOR RESIDUES OF METAL CATALYSTS OR METAL REAGENTS, https://www.ema.europa.eu/en/documents/scientific-guideline/guideline-specification-limits-residues-metal-catalysts-metal-reagents_en.pdf, (accessed 14 October 2020).

23   M. Steinberg, J. F. Borzelleca, E. K. Enters, F. K. Kinoshita, A. Loper, D. B. Mitchell, C. B. Tamulinas and M. L. Weiner, *Regul. Toxicol. Pharmacol.*, 1996, **24**, 149–154.

24   C. McConville, J. M. Smith, C. F. McCoy, P. Srinivasan, J. Mitchell, A. Holder, R. A. Otten, S. Butera, G. F. Doncel, D. R. Friend and R. K. Malcolm, *Drug Deliv. Transl. Res.*, 2015, **5**, 27–37.

Appendix

Table A. 1: The 11 descriptors identified with a correlation to the CP greater than an absolute value of 0.4 using the training set from dataset A. Given are their description and correlation to CP.

Descriptor	Description	Correlation to CP
ASA-	Water accessible surface area of all atoms with negative partial charge	-0.44
BCUT_SMR_0	The BCUT descriptors using atomic contribution to molar refractivity (using the Wildman and Crippen SMR method) instead of partial charge	0.41
CASA-	Negative charge weighted surface area	-0.46
dipoleY	The y component of the dipole moment	-0.40
FCASA-	Fractional CASA- calculated as CASA- / ASA	-0.41
pmi1	Principal moment of inertia	-0.43
pmiY	y component of the principal moment of inertia	-0.45
Q_VSA_NEG	Total negative van der Waals surface area	-0.49
Q_VSA_PNEG	Total negative polar van der Waals surface area	-0.50
Q_VSA_POL	Total polar van der Waals surface area	-0.45
weinerPol	Wiener polarity number	-0.46

Table A. 2: The 104 descriptors identified with a correlation to the CP greater than an absolute value of 0.4 using the training set from dataset B. Given are their description and correlation to CP.
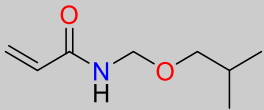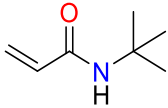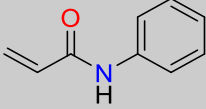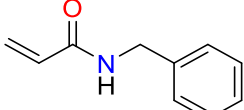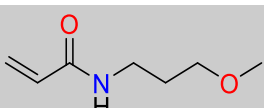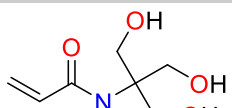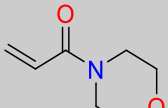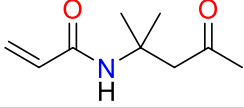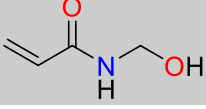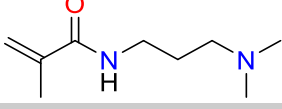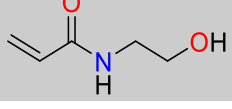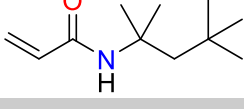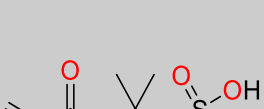
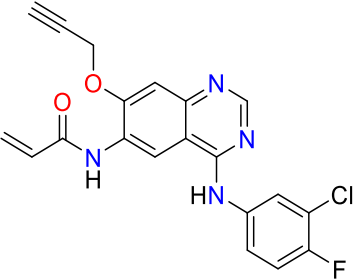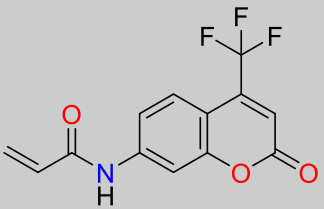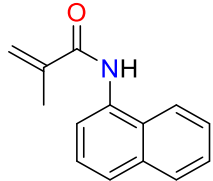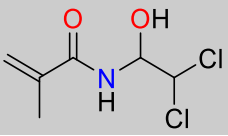| Descriptor	Description	Correlation to CP
AM1_E	The total SCF energy (kcal/mol) calculated using the AM1 Hamiltonian	0.52
AM1_Eele	The electronic energy (kcal/mol) calculated using the AM1 Hamiltonian	0.55
AM1_HF	The heat of formation (kcal/mol) calculated using the AM1 Hamiltonian	0.44
apol	Sum of the atomic polarizabilities	-0.55
ASA	Water accessible surface area calculated using a radius of 1.4 A for the water molecule	-0.51
ASA+	Water accessible surface area of all atoms with positive partial charge	-0.41
a_count	Number of atoms	-0.56
a_heavy	Number of heavy atoms	-0.54
a_hyd	Number of hydrophobic atoms	-0.43
a_IC	Atom information content	-0.54
a_nC	Number of carbon atoms	-0.54
a_nH	Number of hydrogen atoms	-0.53
BCUT_PEOE_0	The BCUT descriptors [Pearlman 1998] are calculated from the eigenvalues of a modified adjacency matrix	0.48
BCUT_SMR_0	The BCUT descriptors using atomic contribution to molar refractivity (using the Wildman and Crippen SMR method) instead of partial charge	0.54

Descriptor	Description	Correlation to CP
bpol	Sum of the absolute value of the difference between atomic polarizabilities of all bonded atoms in the molecule	-0.55
b_count	Number of bonds	-0.55
b_heavy	Number of bonds between heavy atoms	-0.52
b_single	Number of single bonds	-0.55
CASA+	Positive charge weighted surface area	-0.51
CASA-	Negative charge weighted surface area	-0.54
chi0	Atomic connectivity index	-0.56
chi0v	Atomic valence connectivity index	-0.57
chi0v_C	Carbon valence connectivity index	-0.55
chi0_C	Carbon connectivity index	-0.56
chi1	Atomic connectivity index	-0.53
chi1v	Atomic valence connectivity index	-0.53
chi1v_C	Carbon valence connectivity index	-0.44
chi1_C	Carbon connectivity index	-0.44
DCASA	Absolute value of the difference between CASA+ and CASA-	-0.41
diameter	Largest value in the distance matrix	-0.41
dipole	Dipole moment calculated from the partial charges of the molecule	-0.40
E	Value of the potential energy	0.41
FCASA+	Fractional CASA+ calculated as CASA+ / ASA	-0.47
FCASA-	Fractional CASA- calculated as CASA- / ASA	-0.44
GCUT_PEOE_3	Partially equalised electronic orbitals calculated using GCUT	-0.59
GCUT_SLOGP_3	The GCUT descriptors using atomic contribution to logP (using the Wildman and Crippen SlogP method) instead of partial charge	-0.57
GCUT_SMR_0	The GCUT descriptors using atomic contribution to molar refractivity (using the Wildman and Crippen SMR method) instead of partial charge.	0.44
GCUT_SMR_3	The GCUT descriptors using atomic contribution to molar refractivity (using the Wildman and Crippen SMR method) instead of partial charge.	-0.57
h_emd_C	Sum of hydrogen bond donor strengths of carbon atoms	-0.47
h_mr	Molar refractivity using a 4 parameter model based on Hueckel Theory [Labute 2015] with r2 = 0.99, RMSE=0.20 on 1,947 molecules	-0.55
Kier1	First kappa shape index	-0.54
KierA1	First alpha modified shape index	-0.53
lip_acc	The number of O and N atoms	-0.41
MNDO_E	The total SCF energy (kcal/mol) calculated using the MNDO Hamiltonian	0.52
MNDO_Eele	The electronic energy (kcal/mol) calculated using the MNDO Hamiltonian	0.55
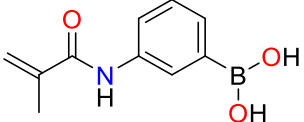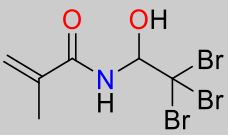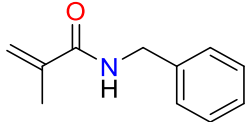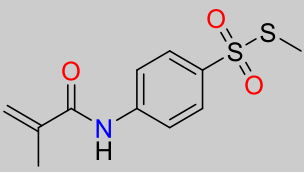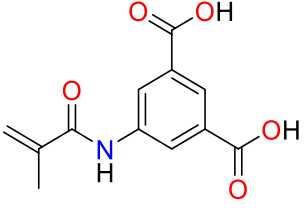
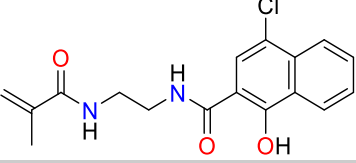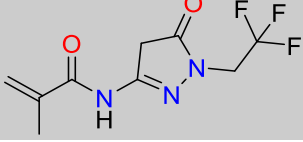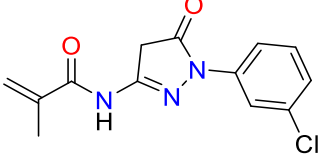| Descriptor	Description	Correlation to CP
MNDO_HF	The heat of formation (kcal/mol) calculated using the MNDO Hamiltonian	0.43
mr	Molecular weight	-0.55
PC+	Total positive partial charge	-0.50
PC-	Total negative partial charge	0.50
PEOE_PC+	Total positive partial charge	-0.45
PEOE_PC-	Total negative partial charge	0.45
PEOE_RPC+	Relative positive partial charge	0.44
PEOE_RPC-	Relative negative partial charge	0.47
PEOE_VSA_HYD	Total hydrophobic van der Waals surface area	-0.50
PEOE_VSA_NEG	Total negative van der Waals surface area	-0.44
petitjean	Value of (diameter - radius) / diameter	-0.45
petitjeanSC	Petitjean graph Shape Coefficient as defined in [Petitjean 1992]: (diameter - radius) / radius.	-0.45
PM3_E	The total SCF energy (kcal/mol) calculated using the PM3 Hamiltonian	0.52
PM3_Eele	The electronic energy (kcal/mol) calculated using the PM3 Hamiltonian	0.55
PM3_HF	The heat of formation (kcal/mol) calculated using the PM3 Hamiltonian	0.47
pmi	Principal moment of inertia	-0.44
pmi1	First diagonal element of diagonalized moment of inertia tensor	-0.54
pmi2	Second diagonal element of diagonalized moment of inertia tensor	-0.42
pmi3	Third diagonal element of diagonalized moment of inertia tensor	-0.43
pmiY	y component of the principal moment of inertia	-0.52
pmiZ	z component of the principal moment of inertia	-0.44
Q_PC+	Total positive partial charge	-0.50
Q_PC-	Total negative partial charge	0.50
Q_RPC+	Relative positive partial charge	0.47
Q_RPC-	Relative negative partial charge	0.63
Q_VSA_NEG	Total negative van der Waals surface area	-0.50
Q_VSA_PNEG	Total negative polar van der Waals surface area	-0.57
Q_VSA_POL	Total polar van der Waals surface area	-0.52
reactive	Indicator of the presence of reactive groups	-0.45
RPC+	Relative positive partial charge	0.47
RPC-	Relative negative partial charge	0.63
SlogP_VSA2	The contribution to logP(o/w) for atom i as calculated in the SlogP descriptor	-0.40
SlogP_VSA9	The contribution to logP(o/w) for atom i as calculated in the SlogP descriptor	-0.45
SMR	Molecular refractivity (including implicit hydrogens)	-0.54
SMR_VSA3	Molecular refractivity (including implicit hydrogens)	-0.49
SMR_VSA7	Molecular refractivity (including implicit hydrogens)	-0.42
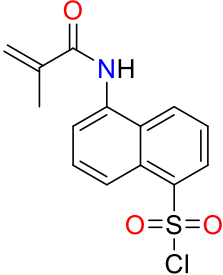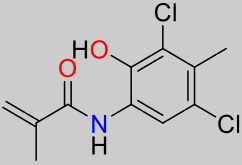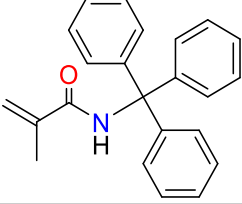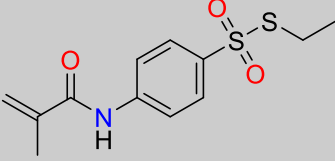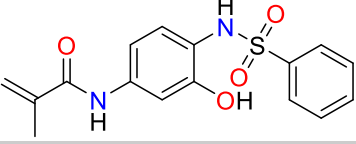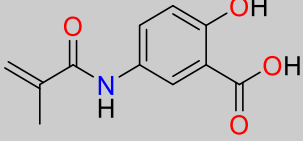
Descriptor	Description	Correlation to CP
std_dim3	Standard dimension 3: the square root of the third largest eigenvalue of the covariance matrix of the atomic coordinates	-0.62
VAdjEq	Vertex adjacency information (equality)	0.56
VAdjMa	Vertex adjacency information (magnitude)	-0.53
VDistMa	If m is the sum of the distance matrix entries then VDistMa is defined to be the sum of log2 m - Dij log2 Dij / m over all i and j	-0.56
vdw_area	Area of van der Waals surface (Å2) calculated using a connection table approximation	-0.56
vdw_vol	van der Waals volume (Å3) calculated using a connection table approximation	-0.56
vol	van der Waals volume calculated using a grid approximation	-0.55
VSA	van der Waals surface area	-0.55
vsa_hyd	Approximation to the sum of VDW surface areas of hydrophobic atoms	-0.44
vsurf_HB6	H-bond donor capacity	-0.42
vsurf_HB7	H-bond donor capacity	-0.43
vsurf_ID7	Hydrophobic integy moment	-0.54
vsurf_ID8	Hydrophobic integy moment	-0.49
vsurf_R	Surface rugosity	-0.55
vsurf_S	Interaction field surface area	-0.52
vsurf_V	Interaction field volume	-0.54
vsurf_W1	Hydrophilic volume	-0.41
vsurf_W6	Hydrophilic volume	-0.41
vsurf_W7	Hydrophilic volume	-0.42
vsurf_Wp1	Polar volume	-0.50
Weight	Molecular weight	-0.54
weinerPath	Wiener path number	-0.50
weinerPol	Wiener polarity number	-0.61
zagreb	Zagreb index	-0.53

Table A. 3: Dataset C consisting of monomers which were identified from Sigma-Aldrich and clustered in order to test the predictability of QSPR model 1-B.

Monomer Name	Monomer Structure
N-(Isobutoxymethyl)acrylamide	
N-(tert-butylacrylamide)	
N-(Phenylacrylamide)	
N-(Benzylacrylamide)	
N-(3-Methoxypropyl)acrylamide	
N-([Tris(hydroxymethyl)methyl]acrylamide)	
4-Acryloylmorpholine	
N-(1,1-Dimethyl-3-oxobutyl)acrylamide	
N-((Hydroxymethyl)acrylamide)	
N-([3-(Dimethylamino)propyl]methacrylamide)	
N-(Hydroxyethyl acrylamide)	
N-(1,1,3,3-Tetramethylbutyl)acrylamide	
2-Acrylamido-2-methyl-1-propanesulfonic acid	

Monomer Name	Monomer Structure
3-(Acrylamido)phenylboronic acid	
N-((2,2,2-tribromo-1-hydroxyethyl)acrylamide)	
4-(Prop-2-enamido)benzoic acid	
(E)-N-(4-((4-nitrophenyl)diazenyl)phenyl)methacrylamide	
4-(Prop-2-enamidomethyl)benzoic acid	
N-(acryloyl-N'-(3,5-dichlorophenyl)urea)	
N-((N-(acrylamido)ethyl)-4-chloro-1-hydroxy-2-naphthamide)	
4-[(3-Bromophenyl)amino]-6-acrylamidoquinazoline	
N-(2,2,2-trichloro-1-(3-M-tolyl-thioureido)-ethyl)-acrylamide)	
N-(2,2,2-TRICHLORO-1-(3-P-TOLYL-THIOUREIDO)-ETHYL)-ACRYLAMIDE	

Monomer Name	Monomer Structure
N-[4-[(3-Chloro-4-fluorophenyl)amino]-7-(2-propyn-1-yloxy)-6-quinazolinyl]-2-propenamide	
7-[4-(Trifluoromethyl)coumarin]acrylamide	
2-METHYL-N-NAPHTHALEN-1-YL-ACRYLAMIDE	
N-(2,2-dichloro-1-hydroxyethyl)-2-methylacrylamide	
3-(Methacryloylamino)phenylboronic acid	
2-methyl-N-(2,2,2-tribromo-1-hydroxyethyl)acrylamide	
N-BENZYLMETHACRYLAMIDE	
4-(2-METHYL-ACRYLOYLAMINO)-BENZENETHIOSULFONIC ACID S-METHYL ESTER	
5-[(2-Methyl-1-oxo-2-propen-1-yl)amino]-1,3-benzenedicarboxylic acid	

Monomer Name	Monomer Structure
5-(2-methyl-acryloylamino)-naphthalene-1-sulfonyl chloride	
N-(3,5-DICHLORO-2-HYDROXY-4-METHYL-PHENYL)-2-METHYL-ACRYLAMIDE	
N-(Triphenylmethyl)methacrylamide	
4-(2-METHYL-ACRYLOYLAMINO)-BENZENETHIOSULFONIC ACID S-ETHYL ESTER	
3'-HYDROXY-4'-(PHENYLSULFONYLAMINO)METHACRYLANILIDE	
2-Hydroxy-5-N-methacrylamidobenzoic acid	
4-CHLORO-1-HYDROXY-N-(N-(METHACRYLAMIDO)ETHYL)-2-NAPHTHAMIDE	
3-(METHACRYLAMIDO)-1-(2,2,2-TRIFLUOROETHYL)-2-PYRAZOLIN-5-ONE	
1-(3-CHLOROPHENYL)-3-METHACRYLAMIDO-2-PYRAZOLIN-5-ONE	

Monomer Name	Monomer Structure

1-ETHYL-7-(METHACRYLAMIDO)-3-PHENYL-2(1H)-QUINOLINONE	
7-[4-(Trifluoromethyl)coumarin]methacrylamide	
N-(1-Naphthyl)-N-phenylmethacrylamide	
N-METHYL-ORTHO-METHACRYLOTOLUIDIDE	
N-ETHYL-PARA-METHACRYLOTOLUIDIDE	
N-ETHYL-META-METHACRYLOTOLUIDIDE	
N-ETHYL-ORTHO-METHACRYLOTOLUIDIDE	
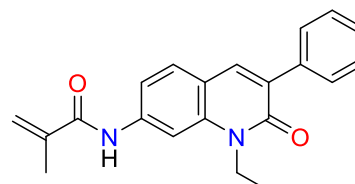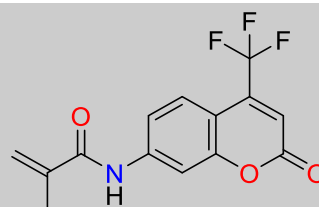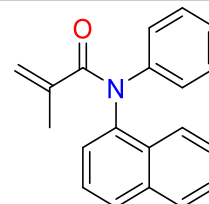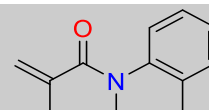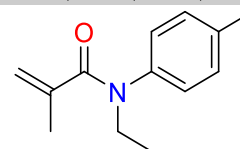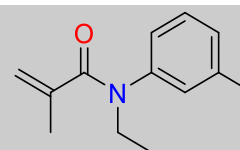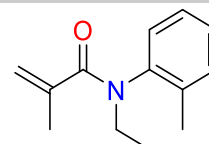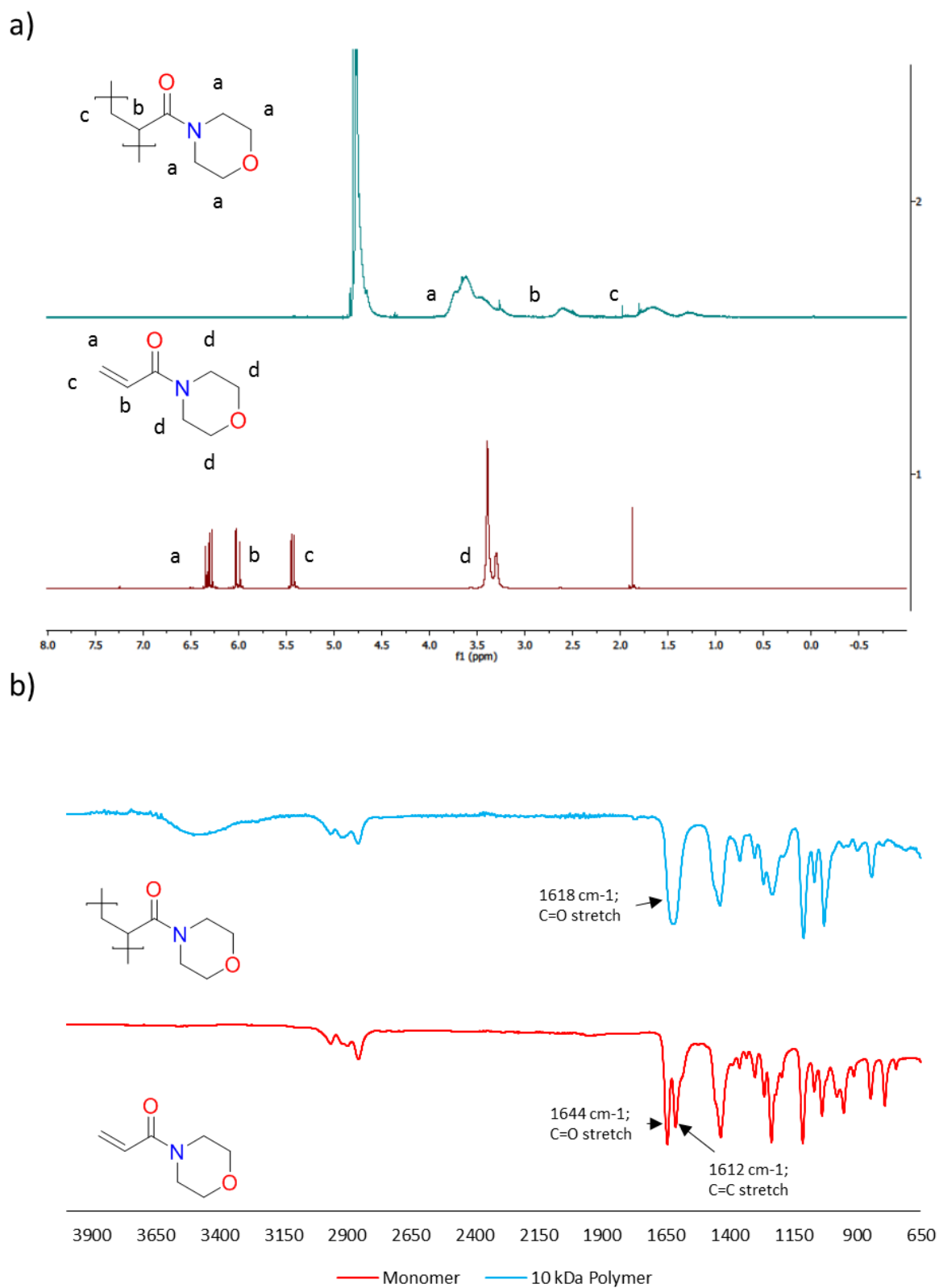
Figure A. 1: The ^{1}H NMR (a) and FTIR (b) spectra of 4-acryloyl morpholine (red) and poly(4-acryloyl morpholine) (blue).

Figure A. 2: The ^{1}H NMR (a) and FTIR (b) spectra of 3-(N-dimethylamino)propyl methacrylamide (red) and poly(3-(N-dimethylamino)propyl methacrylamide) (blue).
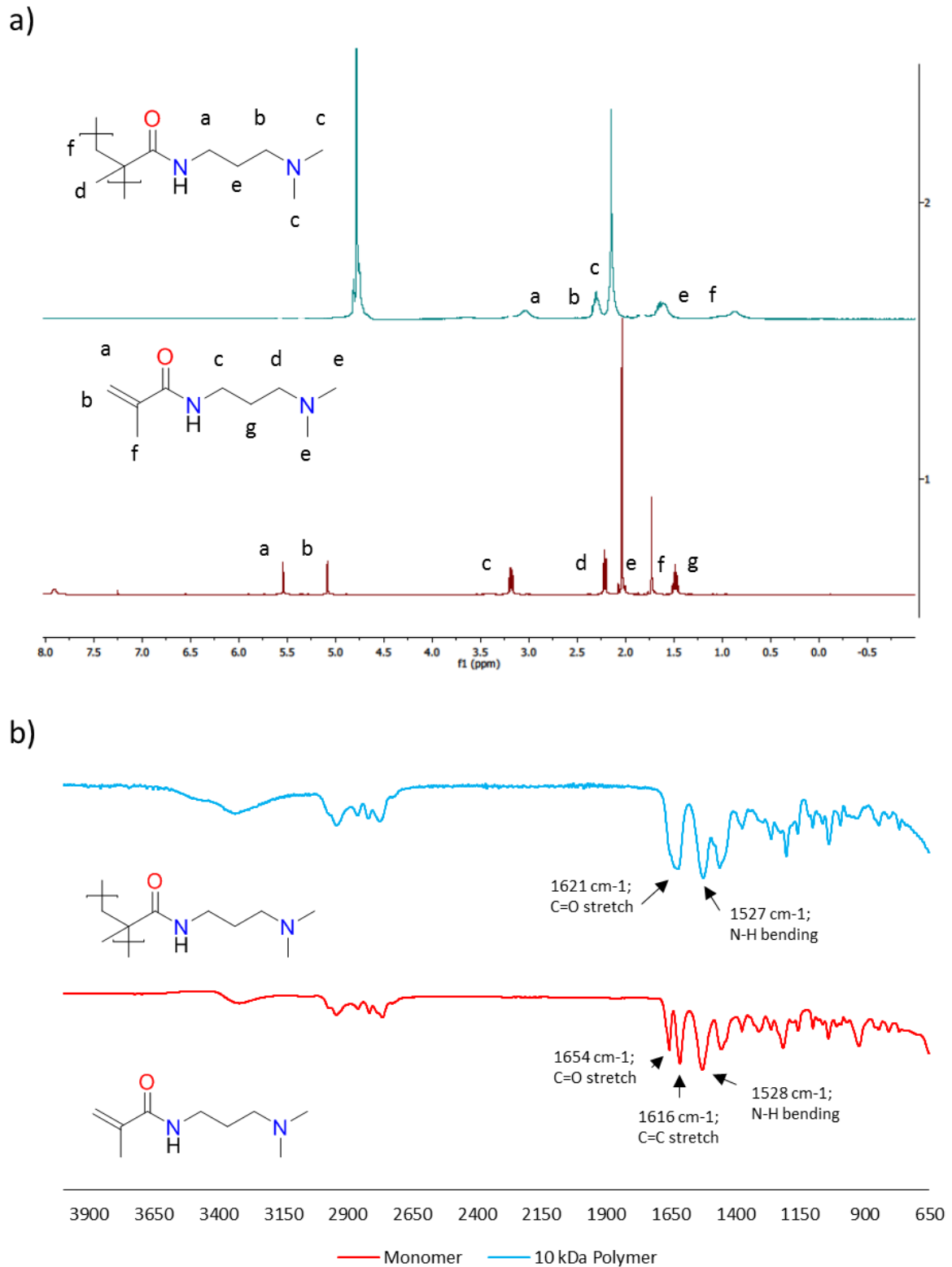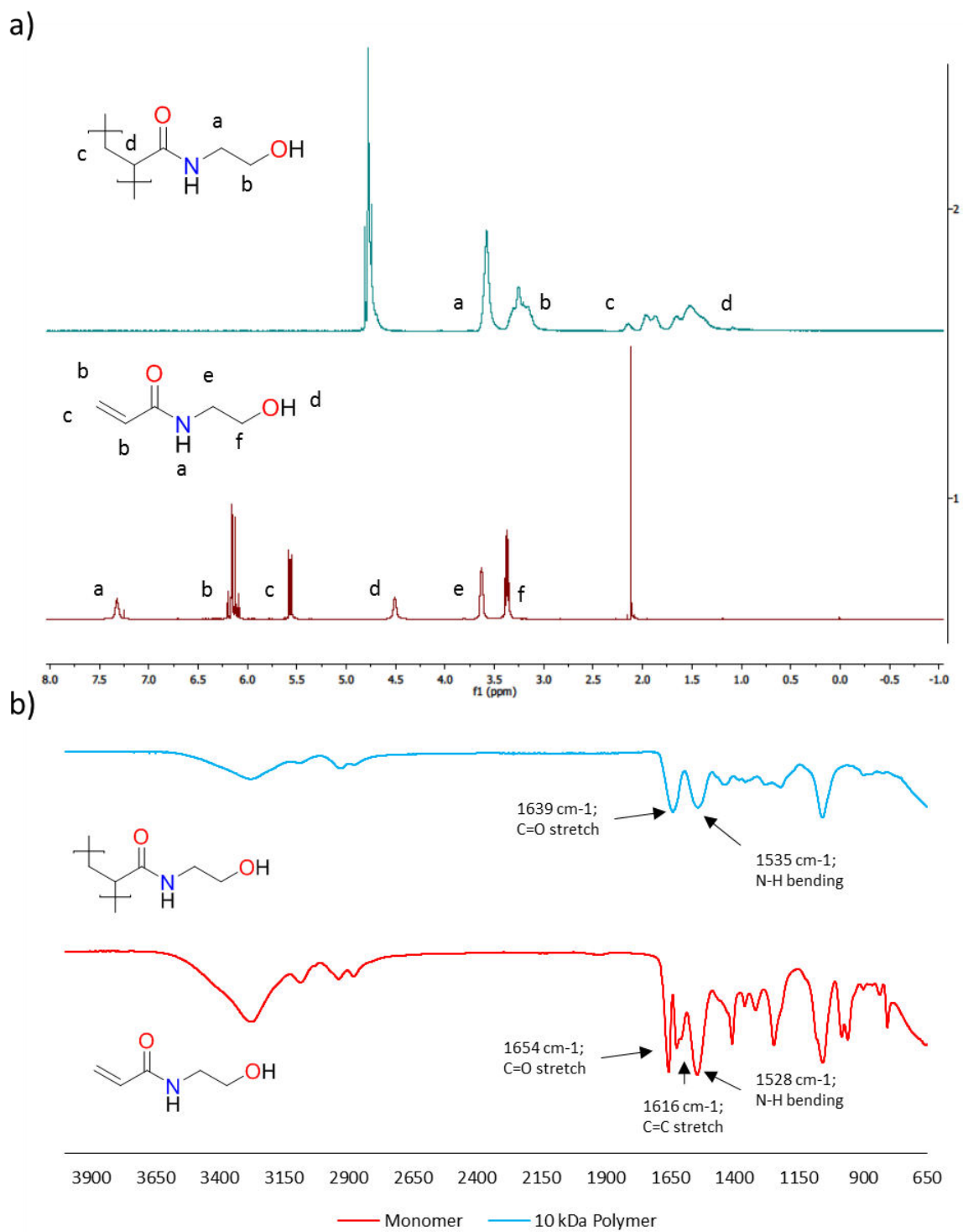
Figure A. 3: The ^{1}H NMR (a) and FTIR (b) spectra of N-hydroxyethyl acrylamide (red) and poly(N-hydroxyethyl acrylamide) (blue).
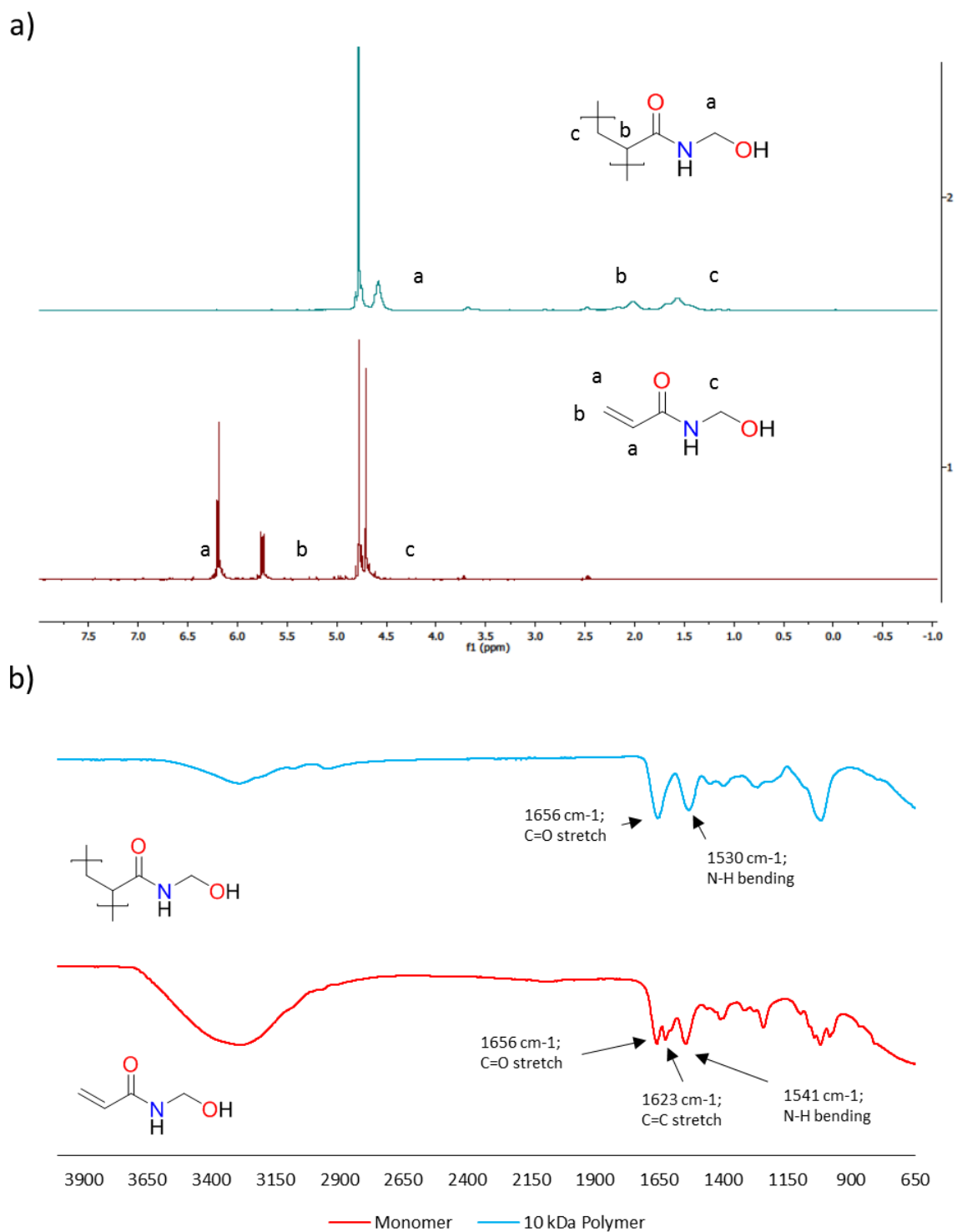
Figure A. 4: The ^{1}H NMR (a) and FTIR (b) spectra of N-hydroxymethyl acrylamide (red) and poly(N-hydroxymethyl acrylamide) (blue).
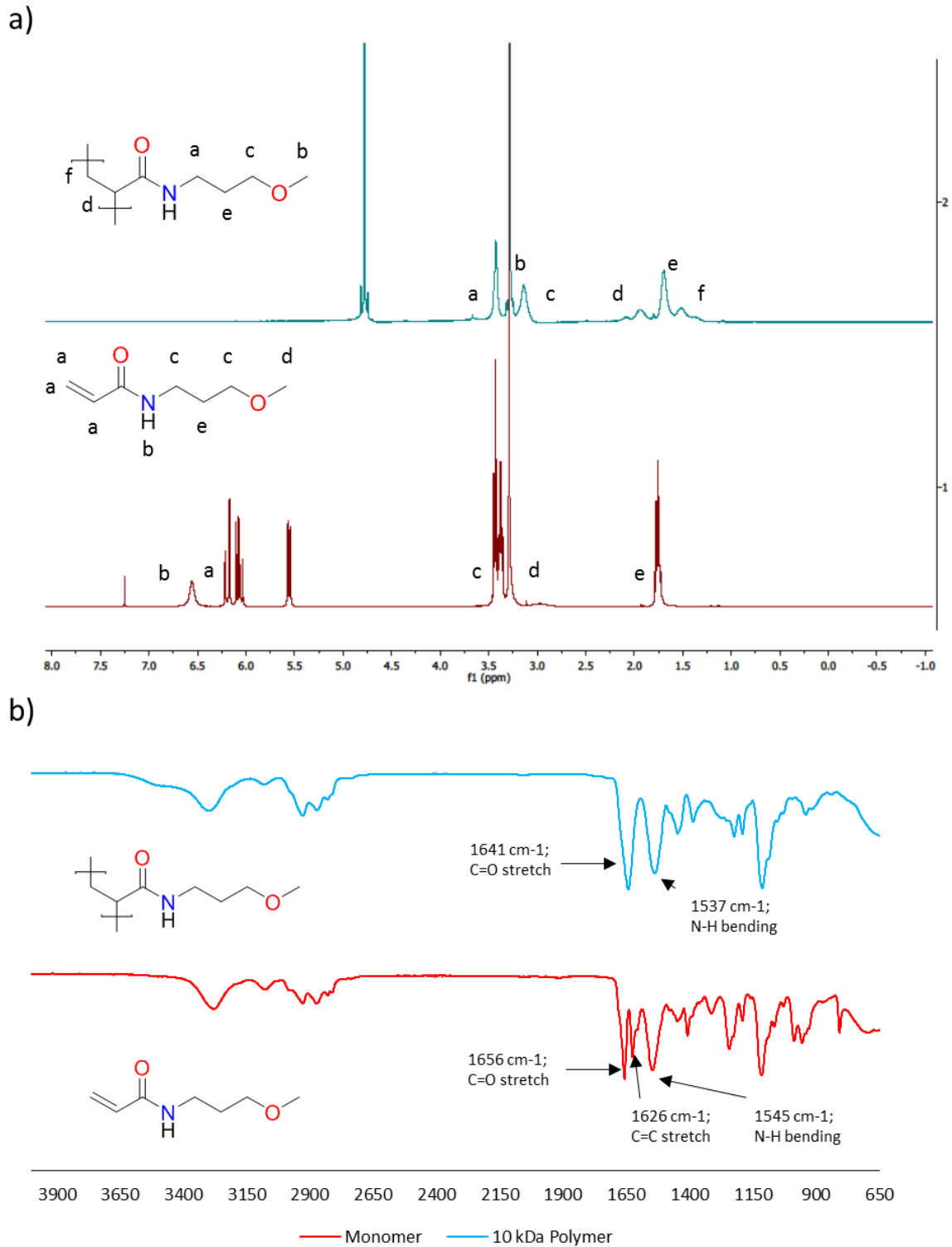
Figure A. 5: The ^{1}H NMR (a) and FTIR (b) spectra of N-(3-Methoxypropyl)acrylamide (red) and poly(N-(3-Methoxypropyl)acrylamide) (blue).
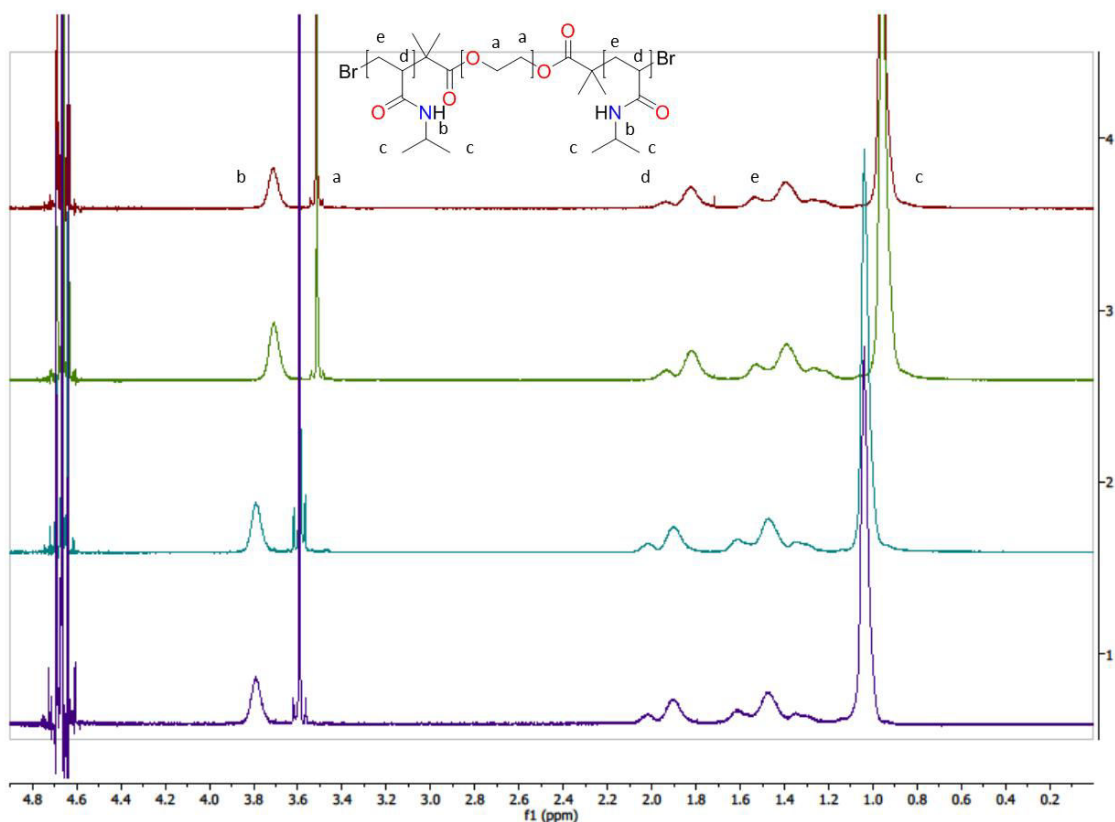
Figure A. 6: The ^{1}H NMR spectra of the PNIPAM tri-block copolymers with architectures of 10-4-10 (red), 20-4-20 (green), 10-10-10 (blue) and 20-10-20 (purple).
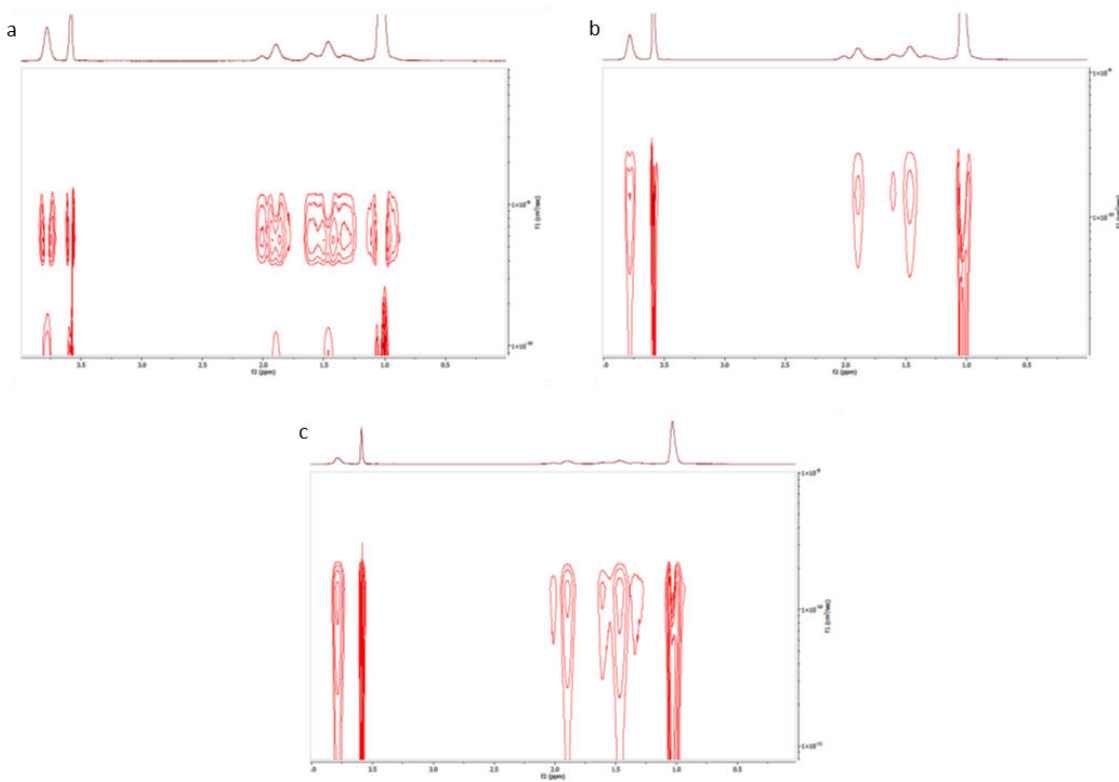
Figure A. 7: The ^{1}H NMR DOSY spectra of the a) 20-4-20, b) 10-10-10 and c) 20-10-20 PNIPAM tri-block copolymers.
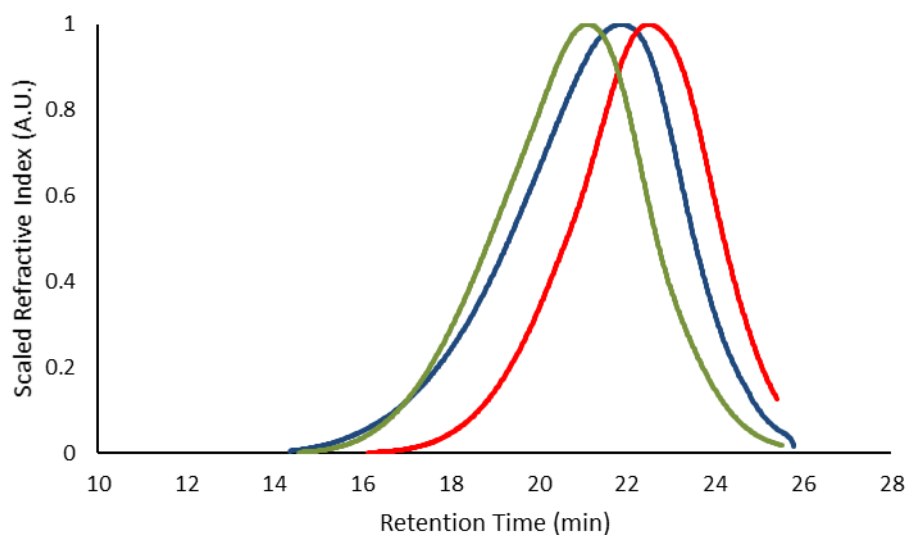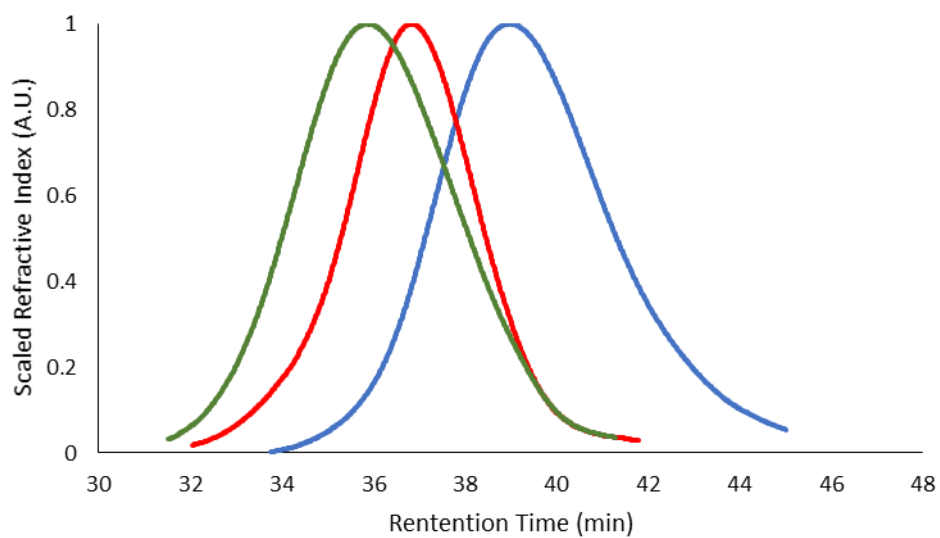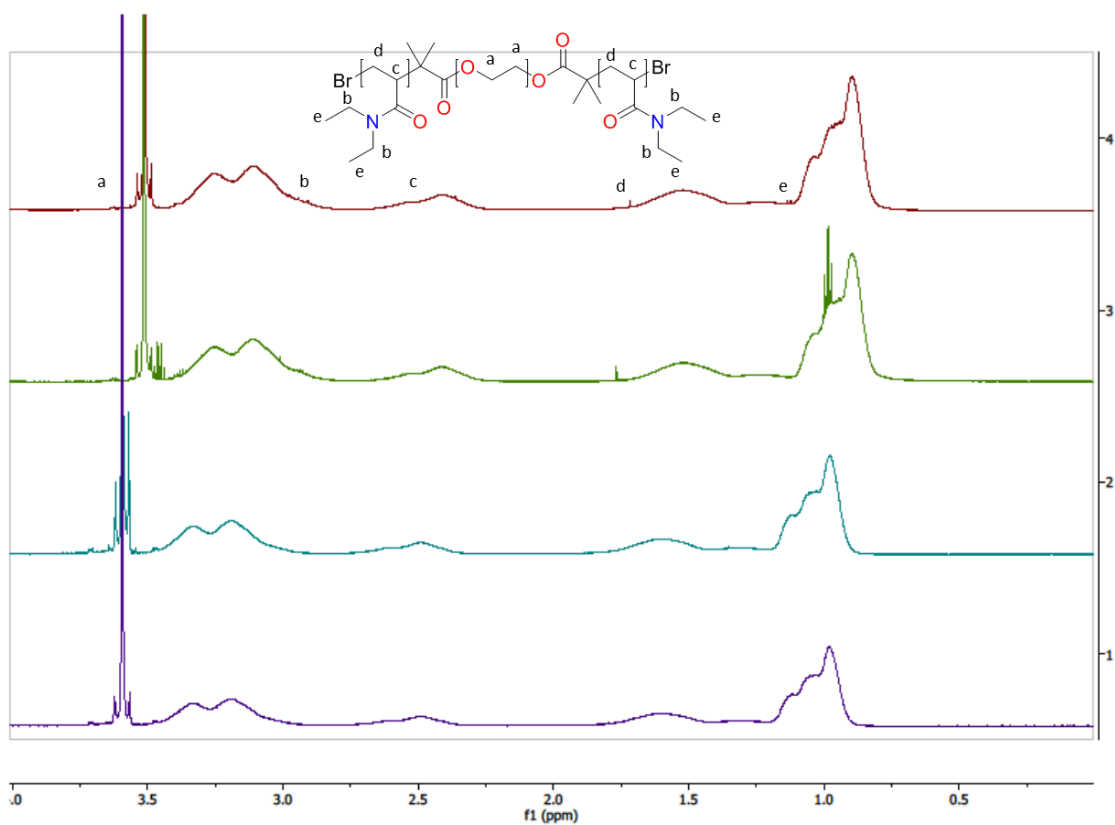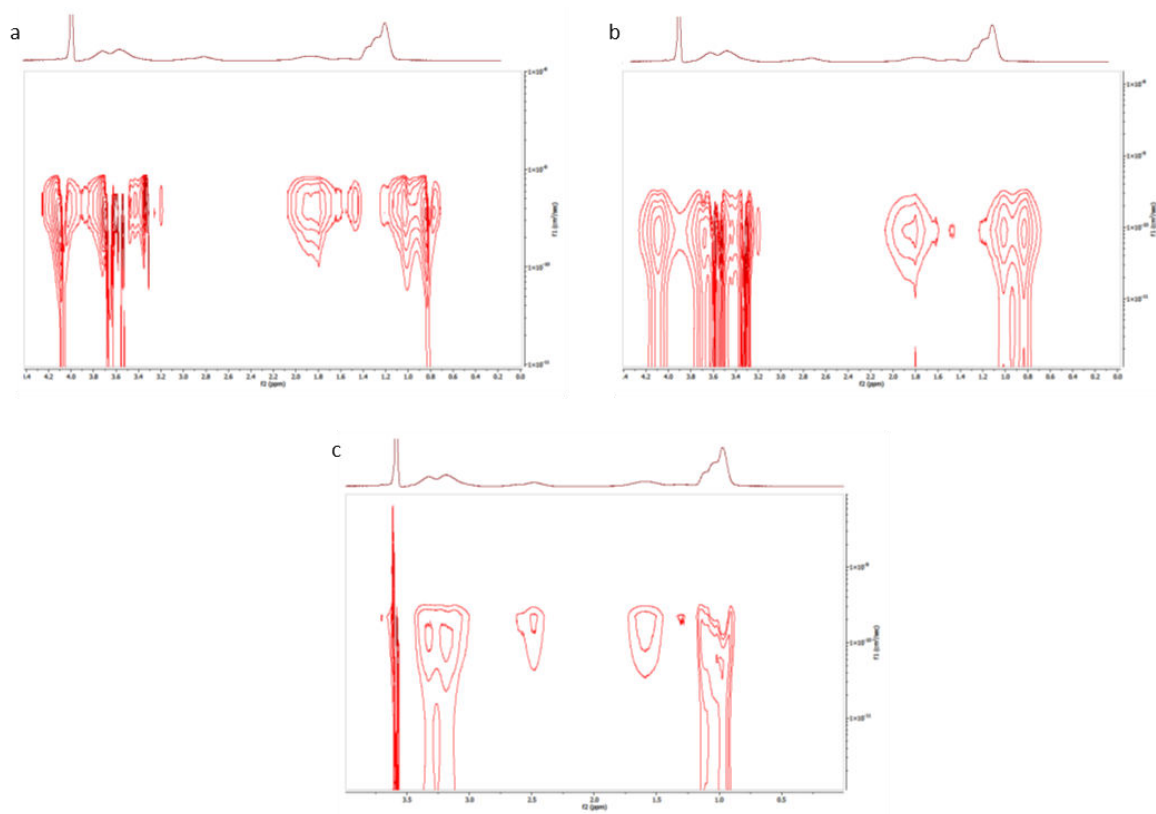
Figure A. 8: The GPC traces of the PNIPAM-PEG-PNIPAM tri-block copolymers with Mns of 20-4-20 (blue), 10-10-10 (red) and 20-10-20 (green).
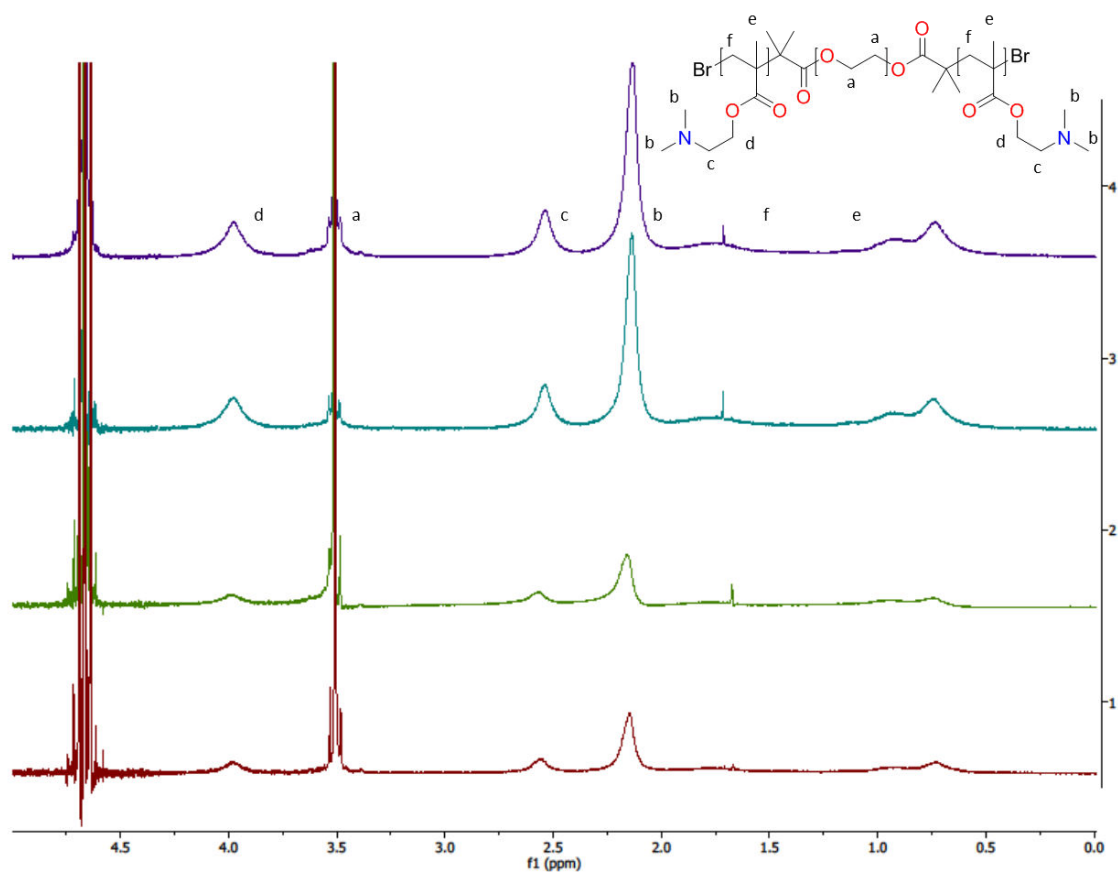
Figure A. 9: The ^{1}H NMR spectra of the PDMAEMA tri-block copolymers with architectures of 10-4-10 (purple), 20-4-20 (blue), 10-10-10 (green) and 20-10-20 (red).
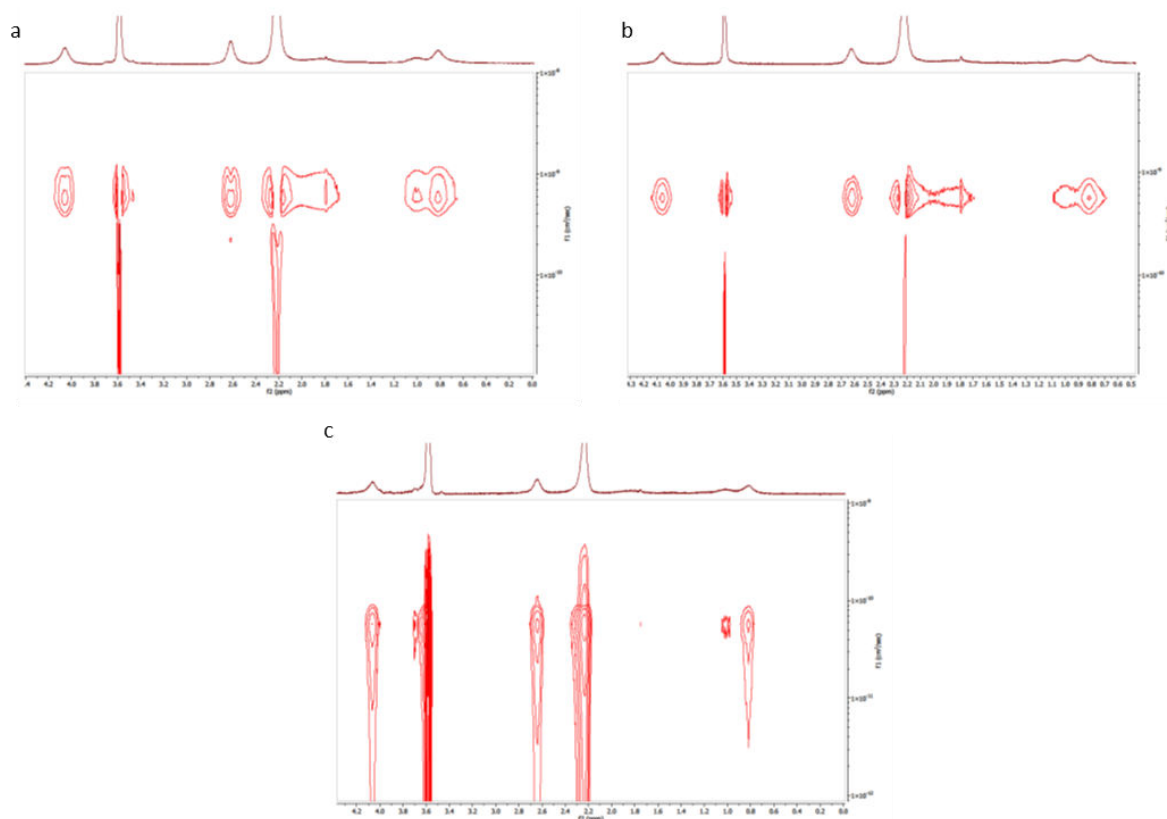
Figure A. 10: The ^{1}H NMR DOSY spectra of the a) 20-4-20, b) 10-10-10 and c) 20-10-20 PDMAEMA tri-block copolymers.
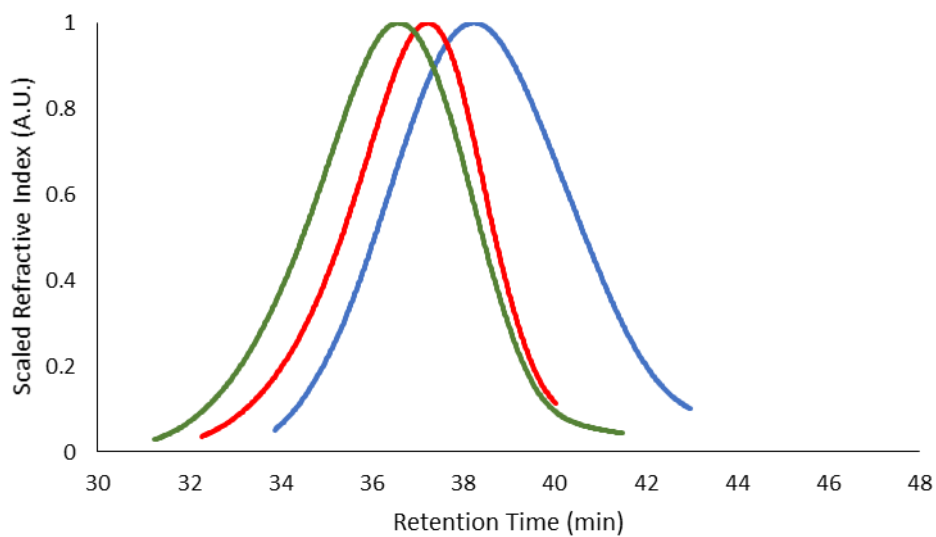

Figure A. 11: The GPC traces of the PDMAEMA-PEG-PDMAEMA tri-block copolymers with Mns of 20-4-20 (blue), 10-10-10 (red) and 20-10-20 (green).

Figure A. 12: The ^{1}H NMR spectra of the PDEA tri-block copolymers with architectures of 10-4-10 (red), 20-4-20 (green), 10-10-10 (blue) and 20-10-20 (purple).

Figure A. 13: The ^{1}H NMR DOSY spectra of the a) 20-4-20, b) 10-10-10 and c) 20-10-20 PDEA tri-block copolymers.

Figure A. 14: The GPC traces of the PDEA-PEG-PDEA tri-block copolymers with Mns of 20-4-20 (blue), 10-10-10 (red) and 20-10-20 (green).
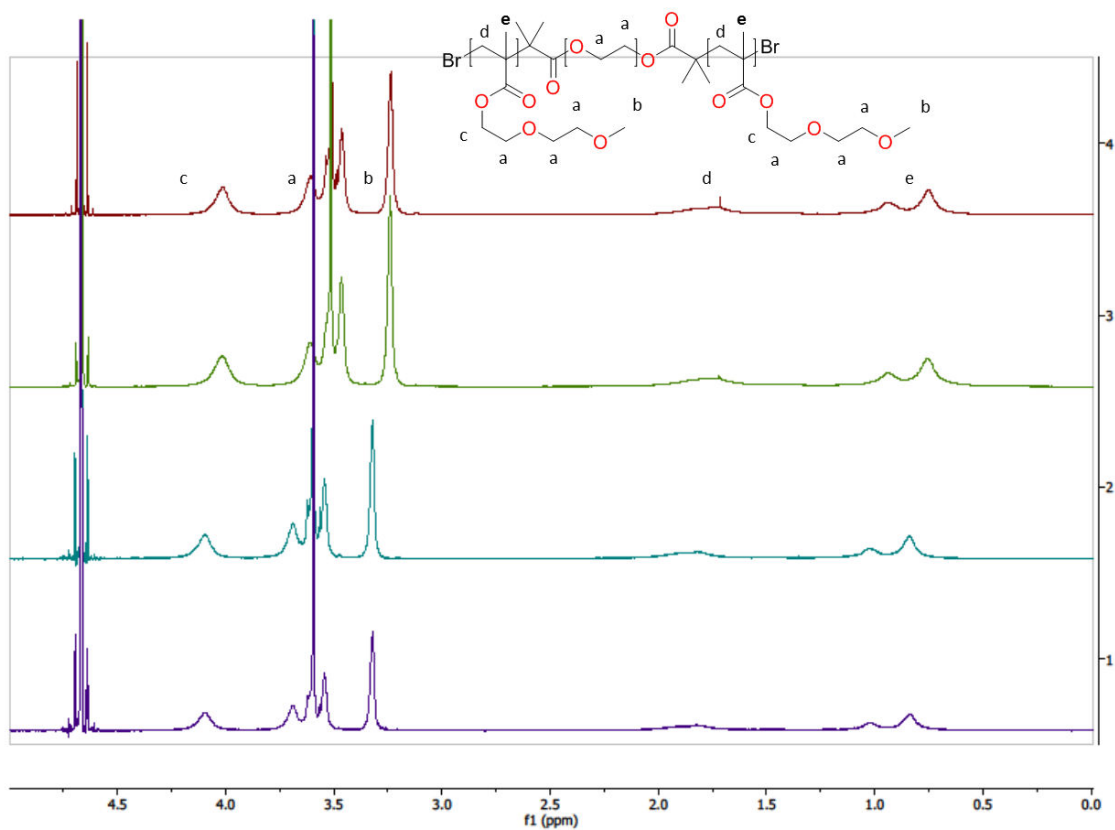
Figure A. 15: The ^{1}H NMR spectra of the PDEGMEMA tri-block copolymers with architectures of 10-4-10 (red), 20-4-20 (green), 10-10-10 (blue) and 20-10-20 (purple).
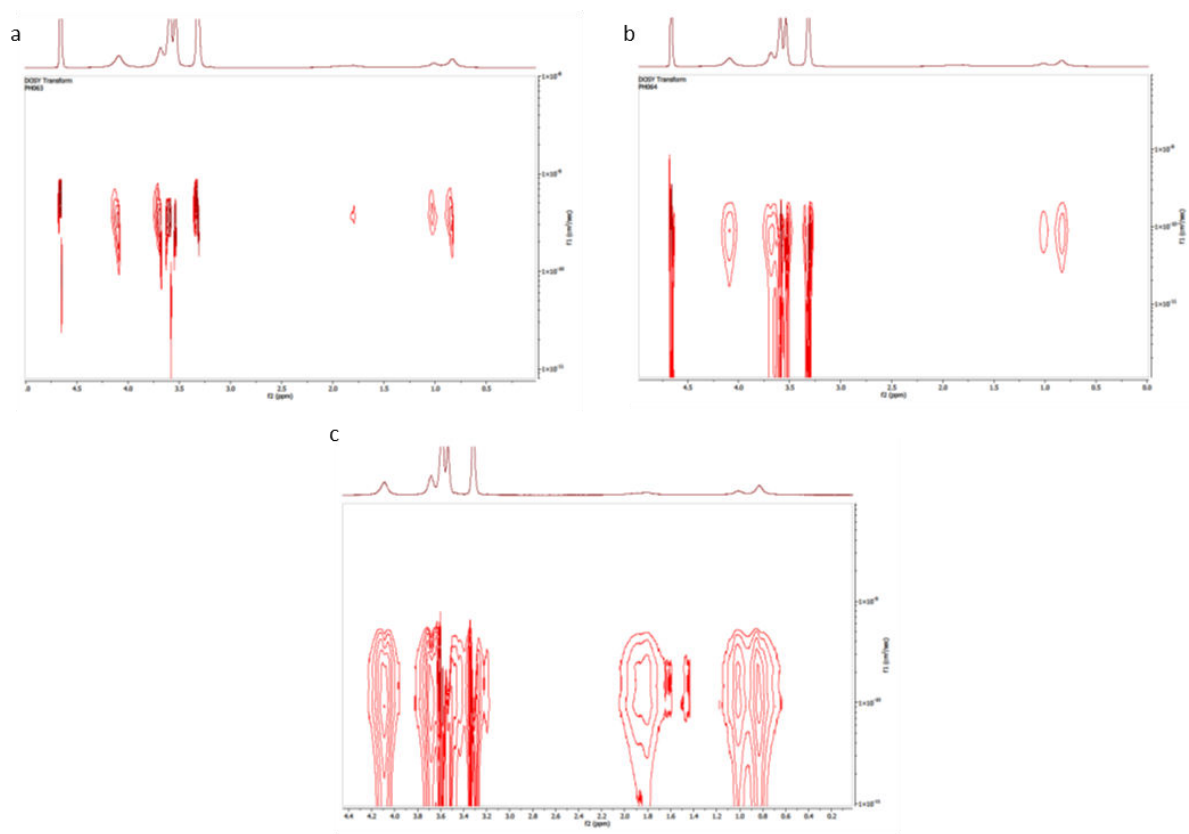
Figure A. 16: The ^{1}H NMR DOSY spectra of the a) 20-4-20, b) 10-10-10 and c) 20-10-20 PDEGMEMA tri-block copolymers.
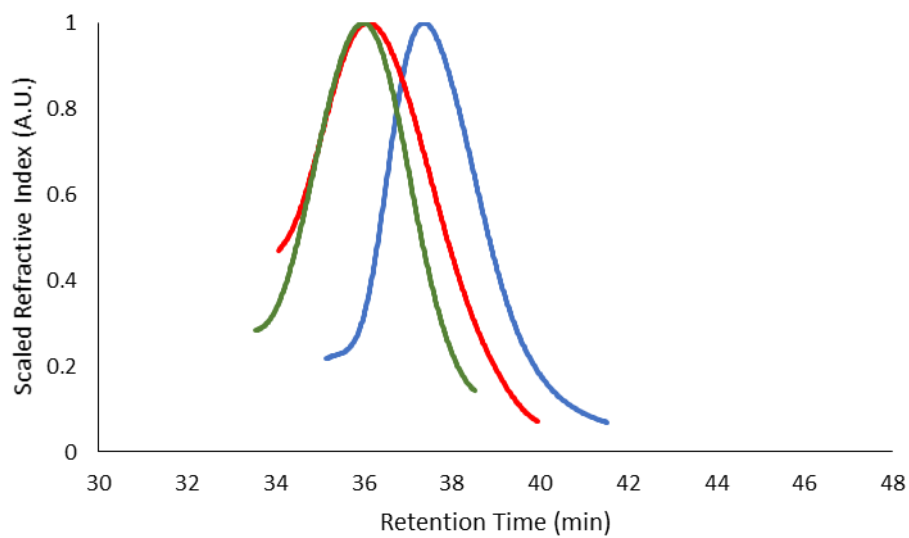

Figure A. 17: The GPC traces of the PDEGMEMA-PEG-PDEGMEMA tri-block copolymers with Mns of

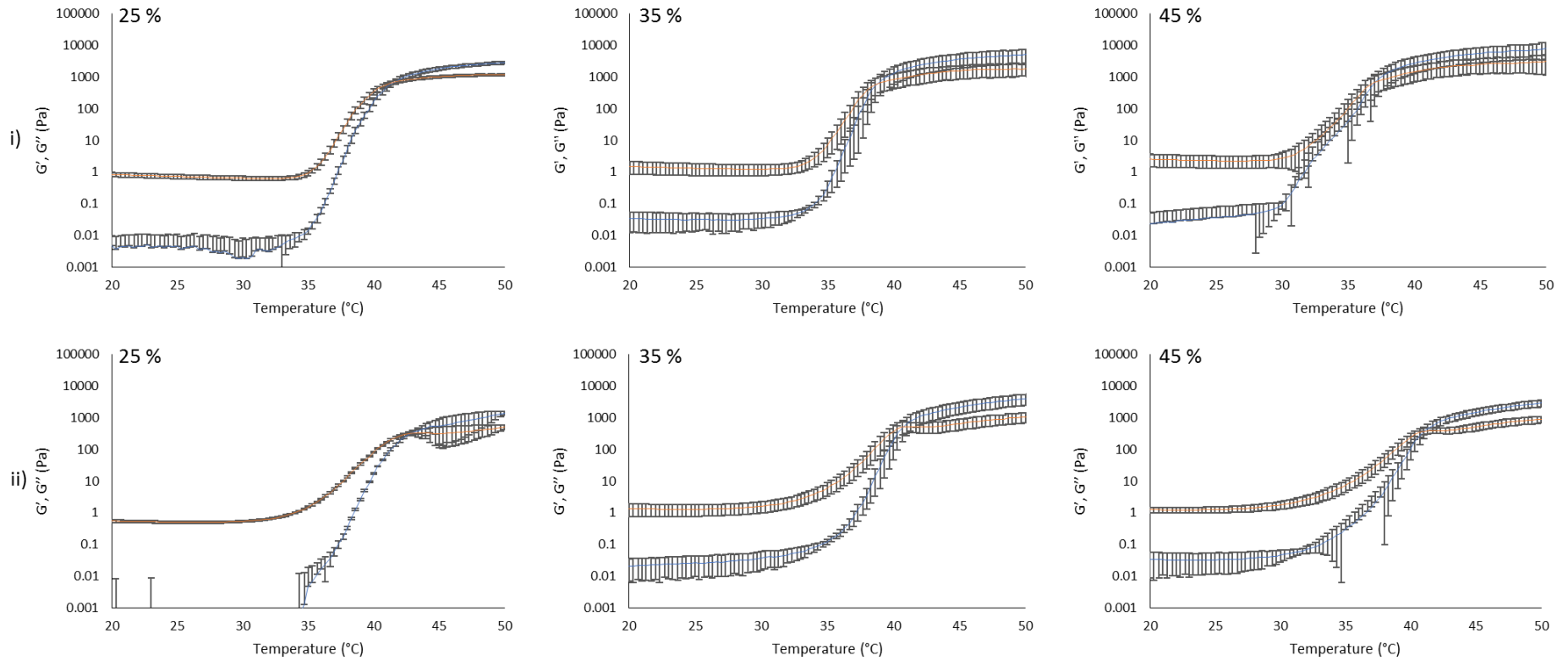20-4-20 (blue), 10-10-10 (red) and 20-10-20 (green).

Figure A. 18: Temperature ramp rheograms of PNIPAM10-PEG10-PNIPAM10 (i) and PDEA20-PEG10-PDEA20 (ii) at 25, 35 and 35 (% w/v)concentration at a fixed shear stress (1 Pa) and frequency (1 Hz). G' is presented as blue, whilst orange corresponds to G''. Data presented as mean ± standard deviation, n = 3.